U.PORTO

UNIVERSIDADE DO PORTO

3.º CICLO D 2025

FMUP
2025

U.PORTO

FM UP FACULDADE DE MEDICINA
UNIVERSIDADE DO PORTO

A Swiss-Knife Nanotechnology Approach to Glioblastoma Treatment

Miguel Diogo de Freitas Horta
TESE DE DOUTORAMENTO APRESENTADA
À FACULDADE DE MEDICINA DA UNIVERSIDADE DO PORTO EM
NEUROCIÊNCIAS

A Swiss-Knife Nanotechnology Approach to Glioblastoma Treatment

Miguel Diogo de Freitas Horta

Miguel Diogo de Freitas Horta

A Swiss-Knife Nanotechnology Approach to Glioblastoma Treatment

Tese de Candidatura ao grau de Doutor em Neurociências – Ramo de Neurociências Experimentais

Programa Doutoral da Faculdade de Medicina da Universidade do Porto

Orientadora: Doutora Raquel Maria Torres Lima; Professora Afiliada da Faculdade de Medicina da Universidade do Porto (FMUP); Instituto de Investigação e Inovação em Saúde (i3S); Instituto de Patologia e Imunologia Molecular da Universidade do Porto (IPATIMUP)

Coorientadora: Doutora Ana Catarina Leite Pereira; Instituto de Investigação e Inovação em Saúde (i3S); Instituto Nacional de Engenharia Biomédica (INEB)

Host Institutions

This work was conducted in the context of the Doctoral Program in Neurosciences – Experimental Neurosciences, from the Faculty of Medicine of the University of Porto (FMUP), Portugal. The Institute for Research and Innovation (i3S), Portugal, and the Institute of Pathology and Molecular Immunology of the University of Porto (IPATIMUP), Portugal, provided the facilities and logistical support for the completion of this thesis project.

Financial Support

This work was supported by Portuguese funds from the FCT – Fundação para a Ciência e Tecnologia, I.P., through the PhD grant 2020.10014.BD, attributed to Miguel Horta.

Publications

This thesis incorporates the research conducted between 2020 and 2025 which culminated in the publication of two peer-reviewed articles: an original research article and a review article. During this period, the work was also presented at national and international conferences in the form of oral and poster communications.

The two articles were integrated within the body of this thesis and are presented, in their published form, in the Appendix section.

ORIGINAL ARTICLE

Miguel Horta, Paula Soares, Bruno Sarmento, Catarina Leite Pereira* and Raquel T. Lima* **(2025)**. *Nanostructured Lipid Carriers for Enhanced Batimastat Delivery Across the Blood-Brain Barrier: An In vitro Study for Glioblastoma Treatment*. Drug Delivery and Translational Research. DOI: https://doi.org/10.1007/s13346-024-01775-8.

*These authors contributed equally to this work.

REVIEW ARTICLE

Miguel Horta, Paula Soares, Catarina Leite Pereira* and Raquel T. Lima* **(2025)**. *Emerging Approaches in Glioblastoma Treatment: Modulating the Extracellular Matrix through Nanotechnology*. Pharmaceutics. DOI: https://doi.org/10.3390/pharmaceutics17020142.

*These authors contributed equally to this work.

Acknowledgements

The end of a PhD is a weird experience. Looking back at the tens of thousands of (mostly nocturnal) hours spent pursuing this very moment, I can't help but feel a melancholic bliss, that bittersweet sentiment of finality. It has been a period of, I hope visible, growth, both scientific and personal, maybe even a bit professional. A period full of bottled-up stress, unbottled exhaustion and, most importantly, fun. A period filled with great people that, with my utmost respect, would like to acknowledge.

Inevitably first, my most sincere gratefulness to my supervisor Raquel Lima. Your never-ending resolve in dealing with me and your unwavering support, which at times was likely exasperated, is one of the main reasons I am writing this today. You have been not only a supervisor, but a mentor in every sense of the word, pushing me to overcome the challenges that appeared in front of me, even if those challenges were sometimes placed there by myself. The sheer amount of time, work, will and guidance that you poured into this scientific project (and me) could not be greater. I know that you're moving away from academia, with this probably being, at least for now, the last experience of long-term mentoring you'll have. I hope that our time together ends up being (looking back) as gratifying for you as it has been for me. Thank you for everything.

To my co-supervisor, Catarina Leite Pereira, I extend nothing less than what I wrote above. Due to the heavily nanotechnological nature of this work, we worked very closely together and, as such, I apologize for the more frequent annoyances. You are the other main reason I am finishing writing this thesis today, always pushing me forward, always available for any question, always present, always picking me up if I stumble, and never letting me stay down. Being your first PhD mentee, I know this was a trial by fire. At least I imagine that I've helped you grow your leadership skills, as they'll surely come in handy for when you have a group of your own. The biggest thank you for all you've taught me, both scientifically and personally, much of your advice and feedback will linger with me for a very long time. I really hope this is not the end of our partnership, maybe somewhere down the road. Let's see what happens after this.

I would also like to express my gratitude to Professor Paula Soares. As my first connection at i3S, and my entry doorway to this fantastic experience, I cannot thank you enough. Thank you for taking me in, thank you for pointing me in the right direction and thank you for asking Raquel and Catarina to put up with me. I will never forget your kindness and affection in leadership, your constant caring in knowing how I am doing and how things are going along. Thank you.

To Professor Bruno Sarmento, and in his person the Nanomedicines & Translational Drug Delivery group, I would like to express my most heartfelt gratitude for what effectively was my adoption. You've always made me feel like

a part of the group, and I thoroughly enjoyed all the time I've spent with the whole of NTDD. Since most of the project happened at the NTDD lab, the logistical and material help that you and the group gave me was beyond invaluable to the completion of this work, and all I hope is that I managed to give a bit of myself in return. Thank you for all the help and support.

To all the current and former members of Cancer Signaling & Metabolism, thank you for all the scientific, logistical and personal help that you've provided over these past few years. In particular, to the people I've bothered the most, Elisabete, Joana, Tito, Rui, Lia, Sofia, Mariana and Luís. Also, thank you (and sorry) João, for lending me Catarina's time, focus and energy for what I imagine must have been days at a time.

A huge thank you to every single NTDD member, both here and gone, for thoroughly adopting me as one of your own. I always felt like I really was. Thank you for the daily laughs, convos and companionship that got me through all of this. You all made going back to the lab everyday worth it. I will always cherish all the memories we've created together, and I sincerely hope this won't be the last I see of you guys. Thank you, Helena, for your singing and upbeat nature lifting everyone's spirit. Thank you, Soraia, for all the help you gave me and for showing me the ropes at the beginning. We had met before and I'm sure we will again. Thank you, Paulo, for your camaraderie and for your infectious positiveness and relentlessness. Thank you, Sofias, Barros, Dias and Costa, for all the good talks we've had. Thank you, Diogo, for the constant laughs and good times. Thank you, Margarida and Cláudia, for the (more than I'd like to admit) frequent scientific help. Thank you, Ju, for accompanying me in jesting with people who don't know anything about lipid nanoparticles. Thank you, Sónia, for your contagious happiness, your perpetual smile and all the western blot help. Thank you, Catarina, for your pessimistic cheerfulness, it's a tough line to walk but you do it splendidly. Thank you, Cecília, for all the help you gave me with the endothelial cells. Last but not least, a big thank you to the visiting Italians, for all the, sadly short, good times.

Moving away from my scientific family to the most important person in the world, all of my love and gratitude to my incredible and now wife Inês. Your patience, love, companionship and support mean everything to me. Thank you for putting up with all of what I am, for accepting all the nights that I've spent in the living room laboring away with the laptop, for the motivational words in trying times, for providing the buoyancy necessary to keep afloat, for unconditionally extending a hand when needed, for all the love that you shower me with. Your presence gives me a reason to push further.

To my wonderful mother and father, thank you for your absolute love and support, not only for these past 4 years of PhD, but for all of my 32 years on this earth. I am what I am because of you. To my siblings, Vasquinho, Rita and Marta, thank

you for your love and constant encouragement. To my grandmothers, Linha and Ester, thank you for being unconditionally proud of me. Despite no longer being here, all my love to my grandfathers, Henrique and Lizé, that I know share that proudness. To my aunts and uncles, Nana, Titi, Pedro, António and Xano, thank you for that constant care, love and motivation. To Luís and Susana, thank you for also being part of the family and of my life.

Last but certainly not least, a big thank you to my closest friends, Toni, Nuno, Vasco and Pim. We may not talk every day, but you're always in my heart.

To all others that I did not have the opportunity to include here, thank you very much.

“The important work of moving the world forward
does not wait to be done by perfect men.”

- George Eliot

TABLE OF CONTENTS

LIST OF FIGURES

LIST OF TABLES

LIST OF ABBREVIATIONS

%EE	Encapsulation Efficiency
^{1}H-NMR	Proton Nuclear Magnetic Resonance
2D	Two-Dimensional
3D	Three-Dimensional
5-FU	5-Fluorouracil
ABC	ATP-Binding Cassette
AC-like	Astrocyte-like
ACP	Activatable Cell Penetrating Peptide
AgNP	Silver Nanoparticle
AS1411	Anti-Nucleolin Aptamer
ATP	Adenosine Triphosphate
BBB	Blood-Brain Barrier
BSA	Bovine Serum Albumin
CAF	Cancer-Associated Fibroblast
CAR	Chimeric Antigen Receptor
CCL2	Chemokine (CC Motif) Ligand 2
CD	Cluster of Differentiation
CDK4	Cyclin-Dependent Kinase 4
CDKN2A	Cyclin-Dependent Kinase Inhibitor 2A
Ce6	Chlorine e6
CG-HSANP	Collagenase-Modified Human Serum Albumin Nanoparticle
CHI3L1	Chitinase-3-like Protein 1
CLIO	Cross-Linked Iron Oxide
CNS	Central Nervous System
CSF-1	Colony Stimulating Factor 1

CTX	Chlorotoxin
CXCL1	Chemokine (CXC Motif) Ligand 1
CypA	Cyclophilin A
ddH_2O	Double Distilled Water
dEGCG	Epigallocatechin-3-Gallate Dimer
DL	Drug Loading
DLS	Dynamic Light Scattering
DMEM	Dulbecco's Modified Eagle's Medium
DMSO	Dimethyl Sulfoxide
DNA	Deoxyribonucleic Acid
DOX	Doxorubicin
DSPE	1,2-Distearoyl-sn-glycero-3-phosphorylethanolamine
DTX	Docetaxel
E8	EEEEEEEE Oligopeptide
EBM-2	Endothelial Basal Medium-2
ECM	Extracellular Matrix
EDB	Extra Domain B
EDC	N-(3-Dimethylaminopropyl)-N′-ethylcarbodiimide Hydrochloride
EGF	Epithelial Growth Factor
EGFR	Epithelial Growth Factor Receptor
ELS	Electrophoretic Light Scattering
EMT	Epithelial-to-Mesenchymal Transition
EPR	Enhanced Permeation and Retention
ERK	Extracellular Signal-Regulated Kinase
FBS	Fetal Bovine Serum
FDA	Food And Drug Administration

fMbat	NLC Mbat functionalized with MMP14cp-PEG-TfP/EGF
fNbat	NLC Nbat functionalized with MMP14cp-PEG-TfP/EGF
GAS1	Growth Arrest-Specific Protein 1
GB	Glioblastoma
GDNF	Glial Cell Line-Derived Neurotrophic Factor
GLI2	GLI Family Zinc Finger 2
GM-CSF	Granulocyte-Macrophage Colony-Stimulating Factor
GPC	Gel Permeation Chromatography
GSC	Glioma Stem Cells
GSH	Glutathione
H_2O_2	Hydrogen Peroxide
HA	Hyaluronic Acid
HBSS	Hanks' Balanced Salt Solution
HEPES	4-(2-hydroxyethyl)-1-piperazineethanesulfonic Acid
HIF	Hypoxia-Inducible Factor
hiPSC	Human Induced Pluripotent Stem Cell
h-MnO_2	Hollow Manganese Dioxide
HPLC	High Performance Liquid Chromatography
IC50	Half Maximal Inhibitory Concentration
ICT2552	Azademethylcolchicine
IDH	Isocitrate Dehydrogenase
IGF-1	Insulin-like Growth Factor 1
IL	Interleukin
JAG1	Jagged 1
JAM-A	Junctional Adhesion Molecule A
LAT1	L-type Amino Acid Transporter 1

LDLR	Low-Density Lipoprotein Receptor
LFNG	Beta-1,3-N-acetylglucosaminyltransferase Lunatic Fringe
LRP1	Low Density Lipoprotein Receptor-related Protein 1
M	NLC formulation M
Mbat	Batimastat-encapsulating NLC formulation M
MDSC	Myeloid-Derived Suppressor Cells
MES-like	Mesenchymal-like
MGMT	O6-Methylguanine-DNA Methyltransferase
MMP	Matrix Metalloproteinase
MMP14cp	MMP-14-cleavable Peptide
MNP	Magnetic Nanoparticle
MRI	Magnetic Resonance Imaging
MW	Molecular Weight
N	NLC formulation N
Nbat	Batimastat-encapsulating NLC formulation N
NEC	Not Elsewhere Classified
NF1	Neurofibromin
NF-κB	Nuclear Factor Kappa-Light-Chain-Enhancer of Activated B Cells
NHS	N-Hydroxysuccinimide
NIRF	Near-Infrared Fluorescence
NK	Natural Killer
NLC	Nanostructured Lipid Carrier
NOS	Not Otherwise Specified
NOTCH3	Neurogenic Locus Notch Homolog Protein 3
NP	Nanoparticle

NPC-like	Neural Progenitor-like
NRP-1	Neuropilin-1
NVU	Neurovascular Unit
NW	Nanoworm
OCT4	Octamer-Binding Transcription Factor 4
OPC-like	Oligodendrocyte Progenitor-like
PBS	Phosphate Buffered Saline
PCL	Polycaprolactone
PD	Programmed Cell Death Protein
PDGF	Platelet-Derived Growth Factor
PDGFRA	Platelet-Derived Growth Factor Receptor A
PDI	Polydispersity Index
PD-L1	Programmed Death-Ligand 1
PEG	Polyethylene Glycol
PET	Positron Emission Tomography
P-gp	P-glycoprotein
PI3K	Phosphatidylinositol 3-kinase
PLA	Polylactic Acid
PLGA	Poly(Lactic-Co-Glycolic Acid)
PTEN	Phosphatase and Tensin Homolog
PTX	Paclitaxel
R8	RRRRRRRR Oligopeptide
RES	Reticuloendothelial System
RIPA	Radioimmunoprecipitation Assay
ROS	Reactive Oxygen Species
RT	Radiotherapy

SDS	Sodium Dodecyl Sulfate
SEC	Size Exclusion Chromatography
SFD-1	Stromal Cell-Derived Factor 1
siRNA	Small Interfering Ribonucleic Acid
SMO	Smoothened
SOX2	Sex Determining Region Y Box 2
SS	Disulfide Bonds
TAM	Tumor-Associated Macrophage
TCEP	Tris(2-carboxyethyl)phosphine Hydrochloride
TCGA	The Cancer Genome Atlas
TEER	Transendothelial Electrical Resistance
TEM	Transmission Electron Microscopy
TERT	Telomerase Reverse Transcriptase
TfP	Transferrin-mimicking Peptide
TGF-β	Transforming Growth Factor Beta
TME	Tumor Microenvironment
TMZ	Temozolomide
TN-C	Tenascin-C
TNF	Tumor Necrosis Factor
TP53	Tumor Protein P53
TTFields	Tumor Treating Fields
VEGF	Vascular Endothelial Growth Factor
VP	Verteporfin
WHO	World Health Organization
YAP	Yes-Associated Protein
ZO-1	Tight Junction Protein 1

ABSTRACT

Glioblastoma (GB) remains a highly aggressive brain tumor with a median survival of only 15 months under the current standard of care. Its lethality stems from multiple factors, including its ability to manipulate the surrounding extracellular matrix (ECM). A key mechanism underlying this manipulation is the overexpression of matrix metalloproteinases (MMPs), particularly MMP-2, MMP-9 and MMP-14, which play a crucial role in ECM remodeling. This dysregulation of MMPs facilitates tumor invasion, angiogenesis, and metastasis, contributing significantly to GB's aggressive behavior and making it one of the most challenging cancers to treat effectively.

This thesis presents an innovative nanotechnology-based approach to address the challenges in GB treatment, focusing on overcoming the blood-brain barrier (BBB) and modulating the ECM of the GB tumor microenvironment (TME). The study developed a multifunctional nanostructured lipid carrier (NLC) designed to locally deliver batimastat, a potent MMP inhibitor, and functionalized with a dual-targeting strategy aiming to: i) facilitate nanoparticle (NP) BBB-crossing, owing to a custom-made construct with a transferrin-mimicking peptide (TfP) terminus, ii) promote the construct's removal at the GB TME, through the construct's MMP-14 cleavable peptide (MMP14cp) terminus, thus exposing the NP´s epidermal growth factor (EGF) moieties and iii) entrap the NP within the GB TME due to its EGF receptor overexpression. Our research started with the successful synthesis and characterization of the targeting molecular construct MMP14cp-PEG-TfP, confirmed using proton nuclear magnetic resonance and gel-permeation chromatography, followed by the optimization of two NLC formulations (fMbat and fNbat), shown to display adequate physicochemical properties for brain delivery. Both functionalized NLCs were shown to be stable in different media, maintaining their average sizes of 300 nm, and highly negative zeta potentials (< –25 mV). Batimastat was efficiently encapsulated within these NLCs, with drug loadings of 0.42 µg/mg, and their surface was functionalized, with the designed construct and EGF, with approximately 90% efficiency. *In vitro* studies demonstrated enhanced BBB permeation of functionalized fMbat compared to its non-functionalized counterpart, while batimastat-loaded NLCs significantly inhibited MMP-2 activity in GB cell lines in comparison with unloaded formulations, indicating their potential to modulate the tumor ECM.

Overall, our "Swiss-knife" approach for GB treatment, combining targeted drug delivery, BBB penetration, and ECM modulation, offers a versatile platform for delivering therapeutic agents to brain tumors, potentially improving treatment efficacy and patient outcomes. Future research directions include *in vivo* studies to validate the system's safety and efficacy, as well as exploration of additional therapeutic payloads. This study's comprehensive approach, which addresses multiple challenges in GB treatment simultaneously, represents a significant advancement in the field of nanomedicine for brain cancer therapy and paves the way for more effective therapies in the future.

Keywords

Glioblastoma (GB); Extracellular Matrix (ECM); Nanostructured Lipid Carrier (NLC); Matrix Metalloproteinase (MMP); Batimastat; Blood-Brain Barrier (BBB)

RESUMO

O glioblastoma (GB) é o tipo mais comum de tumor cerebral maligno, caracterizado pela sua elevada agressividade, tendo atualmente uma média de sobrevivência de apenas 15 meses sob terapêutica padrão. A elevada mortalidade no GB está relacionada com múltiplos fatores, um dos quais a sua capacidade de remodelar a matriz extracelular (ECM) do microambiente tumoral (TME). Esta capacidade de remodelação advém, maioritariamente, da sobre expressão de metaloproteinases de matriz (MMPs), particularmente das MMP-2, MMP-9 e MMP-14, pelas células tumorais. Esta sobre expressão promove a invasão tumoral, a angiogénese e o processo metastático, contribuindo para o comportamento altamente agressivo do GB e tornando-o num dos cancros mais difíceis de tratar de forma eficaz.

Assim, esta tese teve como objetivo, o desenvolvimento de um sistema de libertação baseado em nanotecnologia que pretende, de forma inovadora, combater os desafios atuais no tratamento do GB, nomeadamente a passagem pela barreira hematoencefálica (BBB) e a remodelação da ECM do tumor. Assim, neste projeto, desenvolvemos uma partícula lipídica nanoestruturada (NLC) carregada com batimastat, um potente inibidor de MMPs, e modificada com uma estratégia de dupla funcionalização, contendo o fator de crescimento epidérmico (EGF) e um conjugado molecular bi-funcional clivável. Este último, é formado a partir de uma molécula de polietileno glicol (PEG) e delimitado nas suas extremidades por um péptido clivável pela MMP-14 (MMP14cp) e outro que imita funcionalmente a transferrina (TfP). Esta estratégia de dupla funcionalização tem como objetivo facilitar a passagem das nanopartículas (NPs) pela BBB, através do recetor da TfP, e remover o conjugado molecular, através da clivagem pela MMP14cp, quando as NPs se aproximam do tumor, expondo assim as moléculas de EGF à superfície da partícula, tirando partido da anormal expressão de EGF no tumor para manter as NPs no TME e permitir a libertação local do batimastat. Inicialmente, este trabalho focou-se na síntese do conjugado molecular (MMP14cp-PEG-TfP) através de duas reações químicas sequenciais. A eficiência de ambas as conjugações foram quantificadas e validadas por ressonância magnética nuclear e cromatografia de permeação em gel. De seguida, duas formulações de NLCs (fMbat e fNbat) foram otimizadas e caracterizadas, demonstrando propriedades físico-químicas adequadas para terapias direcionadas ao cérebro. Ambas as formulações de NLC funcionalizadas demonstraram ser estáveis em diferentes meios fisiológicos, apresentando tamanhos médios de aproximadamente 300 nm e uma carga superficial negativa (< –25 mV). As NLCs foram eficazmente carregadas com batimastat (0.42 μg/mg) e a sua superfície foi modificada com o conjugado e moléculas de EGF, com uma eficiência de funcionalização de aproximadamente 90%.

Os ensaios *in vitro* demonstraram que as NPs fMbat funcionalizadas eram capazes de atravessar a BBB de forma significativamente mais eficaz do que as

suas homólogas não funcionalizada. Para além disso, em linhas celulares de GB, as NLCs que continham batimastat inibiram a atividade de MMP-2 de forma mais eficiente quando comparadas com as formulações vazias, evidenciando o seu potencial para remodelar a ECM do tumor.

Em resumo, a nossa estratégia polivalente de “canivete suíço” para terapia do GB, que combina a entrega direcionada de fármacos com um transporte mais eficiente através da BBB e com a remodelação da ECM, oferece uma plataforma versátil para a entrega controlada e direcionada de fármacos em tumores cerebrais, tendo potencial para aumentar a eficácia dos tratamentos e melhorar o prognóstico dos pacientes com GB. A abordagem abrangente deste trabalho, que encara simultaneamente vários desafios no tratamento do GB, representa um avanço significativo na aplicação da nanomedicina como terapia para tumores cerebrais, potencialmente abrindo caminho para tratamentos mais eficazes no futuro.

Palavras-chave

Glioblastoma (GB); Matriz Extracelular (ECM); Partícula Lipídica Nanoestruturada (NLC); Metaloproteinase de Matriz (MMP); Batimastat; Barreira Hematoencefálica (BBB)

CHAPTER I

INTRODUCTION

This chapter was based on the review article *"Emerging Approaches in Glioblastoma Treatment: Modulating the Extracellular Matrix through Nanotechnology*" (Annex I) published in Pharmaceutics (2025).

CHAPTER I – INTRODUCTION

1.1. Glioblastoma

1.1.1. Epidemiology and classification

Glioblastoma (GB) is the most aggressive and highly malignant brain tumor in adults presenting a poor prognosis. Its incidence varies depending on the population studied, mostly ranging from 3 to 4.5 per 100,000 people annually [1-3], accounting for approximately 50% of all malignant central nervous system (CNS) tumors [4]. GB shows a slight male predominance, with a male to female ratio of about 1.6:1 [5]. Although the incidence increases with age, it can occur across all adult age groups [1]. While CNS tumors are common in children, according to the most recent World Health Organization (WHO) guidelines, GB is no longer a possible diagnosis in this age group; instead, it is considered a diffuse pediatric glioma [6].

As our knowledge of GB improves, so do our methods for diagnosing, classifying, and treating the disease [7]. Recent changes in tumor classification, driven by new insights from molecular profiling, have significantly influenced how to diagnose and treat GB, highlighting the clinical importance of these advancements (**Figure 1**) [8]. Under the most recent 2021 WHO classification of tumors of the CNS, which has significantly redefined GB, GB is strictly defined as an isocitrate dehydrogenase (*IDH*)-wildtype, WHO grade 4, tumor. This reclassification emphasizes the distinct biological behavior and more favorable prognosis of *IDH*-mutant tumors compared to their *IDH*-wildtype counterparts [1, 6, 9, 10]. Furthermore, for the diagnosis of GB (*IDH*-wildtype WHO grade 4) it is now required at least one of the following criteria: i) microvascular proliferation or necrosis on histological examination; ii) telomerase reverse transcriptase (*TERT*) gene promoter mutations; iii) epithelial growth factor (EGF) receptor (*EGFR*) gene amplification; iv) combined gain of chromosome 7 and loss of chromosome 10 (+7/-10) [11]. This integrated approach, combining histological and molecular features, provides a more accurate and clinically relevant diagnosis. Notably, this new classification no longer allows for the use of "not otherwise specified" (NOS) in GB diagnosis, further underscoring the importance of molecular testing in modern neuro-oncology [12]. Moreover, the “not elsewhere classified” (NEC) designation is now used when a tumor does not meet the specific GB criteria but still appears to be a diffuse astrocytic glioma without *IDH* mutation [13].

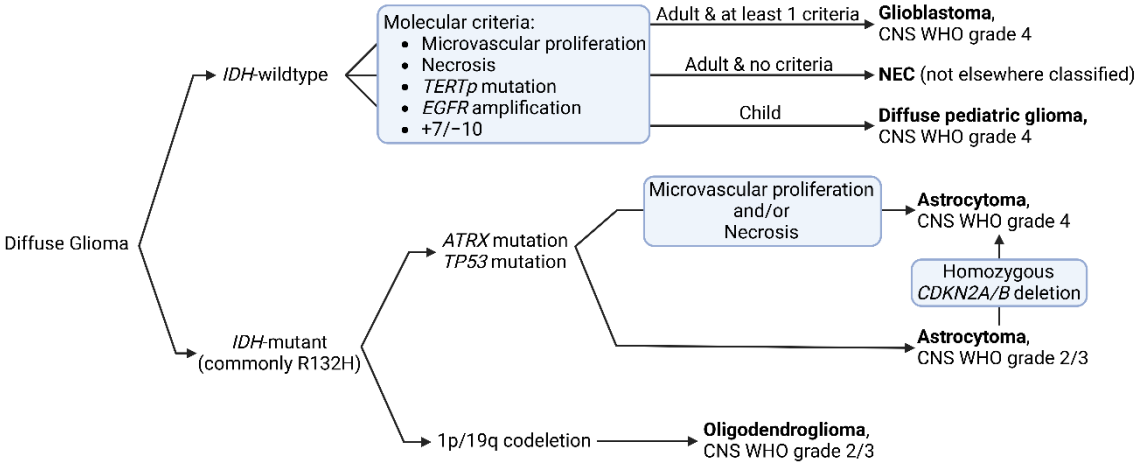

Figure 1. *Glioma classification according to the WHO 2021 classification. CNS WHO grades: 1) Generally indolent tumors with favorable prognosis, 2) Low-grade tumors with potential for recurrence, 3) Malignant tumors with increased mitotic activity, 4) Highly malignant tumors with rapid progression.*

The prognosis for GB remains poor, with median survival varying based on molecular subtypes, which are defined by different transcription profiles [14]. The mesenchymal subtype is characterized by extensive necrosis and inflammation, exhibiting transcription profiles similar to mesenchymal tissues. The proneural subtype, considered milder, is characterized by the expression of genes involved in neurogenesis and oligodendrocyte development. The classical subtype, in between, shows features similar to astrocytes, hence the "classical" name reflecting typical GB characteristics [15]. The mesenchymal subtype has the worst prognosis, with a median survival of about 11.5 months, followed by the classical subtype at 14.7 months, and the proneural subtype at 17.0 months [16]. These survival differences highlight the clinical relevance of molecular subtyping in GB, which will be discussed in more detail later. Although there are several risk factors for GB, exposure to high-dose ionizing radiation and certain rare genetic conditions (e.g., Lynch syndrome, Neurofibromatosis type 1, Li-Fraumeni syndrome) have been associated with increased incidence [17, 18]. However, the majority of GB cases occur sporadically without any known risk factors [19]. Anatomically, GBs are typically supratentorial, with rare cases in the cerebellum or spine [20, 21]. They most commonly affect the frontal and temporal lobes, followed by the parietal and occipital lobes, with a slight preference for the right hemisphere [22]. Tumor location can significantly impact surgical resection and, consequently, patient outcomes [23, 24].

1.1.2. Current treatment options

1.1.2.1. First-line – Stupp protocol

The “Stupp protocol”, introduced in 2005, is the standard of care for treating newly diagnosed GB cases [25]. Named after the Swiss oncologist Roger Stupp, this treatment regimen improved survival outcomes for GB patients compared to previous approaches. The protocol consists of maximal safe surgical resection followed by two main phases, concurrent chemoradiotherapy followed by adjuvant chemotherapy. During the first phase, patients receive radiotherapy (RT) with a total dose of 60 Gy, delivered in 30 fractions of 2 Gy each over 6 weeks (5 days per week). Simultaneously, patients take oral temozolomide (TMZ), an alkylating chemotherapy agent, at a dose of 75 mg/m2 of body surface area, daily, seven days a week throughout the RT period. During the second phase, after a 4-week break once completing RT, patients undergo six cycles of TMZ monotherapy. Each cycle lasts 28 days, with TMZ taken for the first 5 days at a dose of 150-200 mg/m2 [26].

The Stupp protocol demonstrated an improvement in survival compared to RT alone. In the original study, the median overall survival increased from 12.1 months with RT alone to 14.6 months with the combined approach. More importantly, the 2-year survival rate improved from 10.4% to 26.5% [27]. Despite these improvements, the prognosis for GB remains poor. Nevertheless, this protocol is most effective in patients under 70 years of age, with good performance status, and whose tumors exhibit O^6-methylguanine-DNA methyltransferase (*MGMT*) promoter methylation, a biomarker associated with better TMZ treatment response [28]. Moreover, side effects of the Stupp protocol can be significant, with the most common being fatigue, nausea and myelosuppression and the most severe complications including neutropenia, thrombocytopenia, lymphopenia, and increased risk of opportunistic infections. To reduce infection risks, patients with these complications often receive antibiotic prophylaxis during treatment [29]. While the Stupp protocol remains the backbone standard of care for GB, ongoing research seeks to further improve patient outcomes.

1.1.2.2. Second-line treatments

Following Stupp protocol failure, with frequent tumor relapse, there is no universally accepted standard for second-line treatment. The management of recurrent GB remains a therapeutic challenge, with several strategies being explored.

Tumor reoperation: Surgical resection may be considered for some patients with recurrent GB, particularly those with large, symptomatic tumors or those causing significant mass effect. However, the benefit of reoperation remains controversial

and is highly dependent on patient selection. Factors such as tumor location, timing of reoperation, extent of resection, and the patient's overall health condition play crucial roles in determining the suitability for the procedure [30-32].

Reirradiation: For certain patients, reirradiation may be an option. It can be delivered through various techniques, including stereotactic radiosurgery, hypofractionated stereotactic RT, conventionally fractioned external RT or brachytherapy. Similarly to reoperation, the decision to reirradiate depends on factors such as the time since initial radiation, tumor volume, and location. When radiation techniques are carefully selected based on the above factors, treatments generally carry a low toxicity risk, while adhering to recommended cumulative dose limits for brain tissue (100-110 Gy). Nevertheless, patient outcomes remain limited, with median overall survivals rarely exceeds 12 months [33-35].

TMZ rechallenge: For patients who initially responded well to TMZ treatment and have a prolonged treatment-free interval, TMZ rechallenge may be considered. Different dosing schedules have been explored, such as dose-intense (3 weeks on/1 week off, 1 week on/1 week off, among others) or metronomic regimens. However, among the various studies conducted, overall patient survival rarely surpasses 12 months. Notably, a study conducted by Weller and colleagues, the DIRECTOR trial, demonstrated that only *MGMT* promoter-methylated recurrent GBs responded to TMZ rechallenge [36-40].

Nitrosoureas: Carmustine, lomustine, nimustine and fotemustine are highly lipophilic [thus blood-brain barrier (BBB) permeable], DNA alkylating agents that were commonly used as first-line GB treatment before the establishment of the Stupp protocol. Various studies have demonstrated the limited efficacy of these nitrosoureas in recurrent GB, with median overall survival very rarely surpassing 12 months. Additionally, the toxicity profile of these agents, especially their hematological effects, restricts their combination with other therapies and hinders their broader use in clinical practice [41-44].

Bevacizumab: Being a Food and Drug Administration (FDA)-approved anti-angiogenic antibody, bevacizumab has often been employed as a strategy combined with other agents, such as irinotecan or lomustine. While it has been shown to improve progression-free survival, impact on overall survival is still debated [45-48]. Nevertheless, recent research has indicated that high vascular endothelial growth factor (VEGF)-A expression is associated with improved progression-free survival in recurrent GB patients treated with bevacizumab, suggesting potential for a therapeutic improvement through biomarker-guided treatment selection [49].

Regorafenib: This multi-kinase inhibitor has shown potential benefits, particularly in the REGOMA trial, conducted by Lombardi and colleagues, where an improved overall patient survival compared to lomustine treatment in recurrent GB was

observed. However, due to its relatively recent introduction in clinical practice (2020), data on its efficacy in GB is still sparse. More comprehensive characterization and identification of key molecular markers of regorafenib responsiveness on GB is needed for a definitive assessment [50-52].

Other tyrosine kinase inhibitors (TKI): Drugs such as cabozantinib, dasatinib, and entrectinib have been or are being evaluated in clinical trials for recurrent GB, particularly in molecularly selected patient populations. These small-molecule inhibitors target specific tyrosine kinase receptors that are often overexpressed or mutated in GB. While several TKIs have shown potential in preclinical studies and early-phase clinical trials, their efficacy as monotherapies has been limited, mainly due to a lack of tumor specificity and poor BBB permeability. Current research focuses on improving drug delivery, developing combination strategies and identifying biomarkers to predict treatment response [53-55].

Immunotherapy: Over the last decade, immunotherapy, particularly checkpoint inhibitors, has emerged as a potential therapy for GB. While its efficacy has been limited in unselected GB populations, research continues to address its potential in patient specific subgroups [56-59].

Tumor Treating Fields (TTFields): This device-based therapy has emerged as a promising second-line treatment option in clinical practice. It delivers alternating electric fields to tumor sites, promoting cancer cell death by disrupting microtubule alignment during cell division [60-62]. TTFields have demonstrated safety and efficacy in clinical trials, leading to FDA approval for GB and malignant pleural mesothelioma. As TTFields continue to show promise, ongoing clinical trials are exploring its use in lung, ovarian, pancreatic, and other cancers, signaling a growing integration of this innovative approach into standard cancer care protocols [63].

GB treatment goals in the recurrent setting are often palliative, aiming to improve or maintain quality of life while potentially extending survival. The choice of second-line treatments for recurrent GB is highly individualized, depending on various factors, including the patient's age, performance status, tumor molecular profile, response to initial therapy, and time to recurrence [64]. Despite the availability of the referred options, the prognosis for recurrent GB remains poor, with median overall survival typically ranging from 6 to 12 months in a clinical setting, with a very modest increase to approximately 15 months for clinical trial participants [65-68]. This underscores the urgent need for more effective therapies and highlights the importance of ongoing research in this challenging cancer type.

1.1.3. GB and its microenvironment – cellular and molecular features

Adding to its own cellular and molecular features, GB is characterized by a complex and dynamic tumor microenvironment (TME) that plays a crucial role in tumor progression, invasion, and therapy resistance [69]. The TME is composed of various cellular and molecular components (**Figure 2**) that intricately interact to support tumor growth and promote immune evasion [70]. These interactions are key to understanding the mechanisms of GB progression and therapy resistance. As such, gaining a deeper understanding of the TME is essential for developing effective therapeutic strategies.

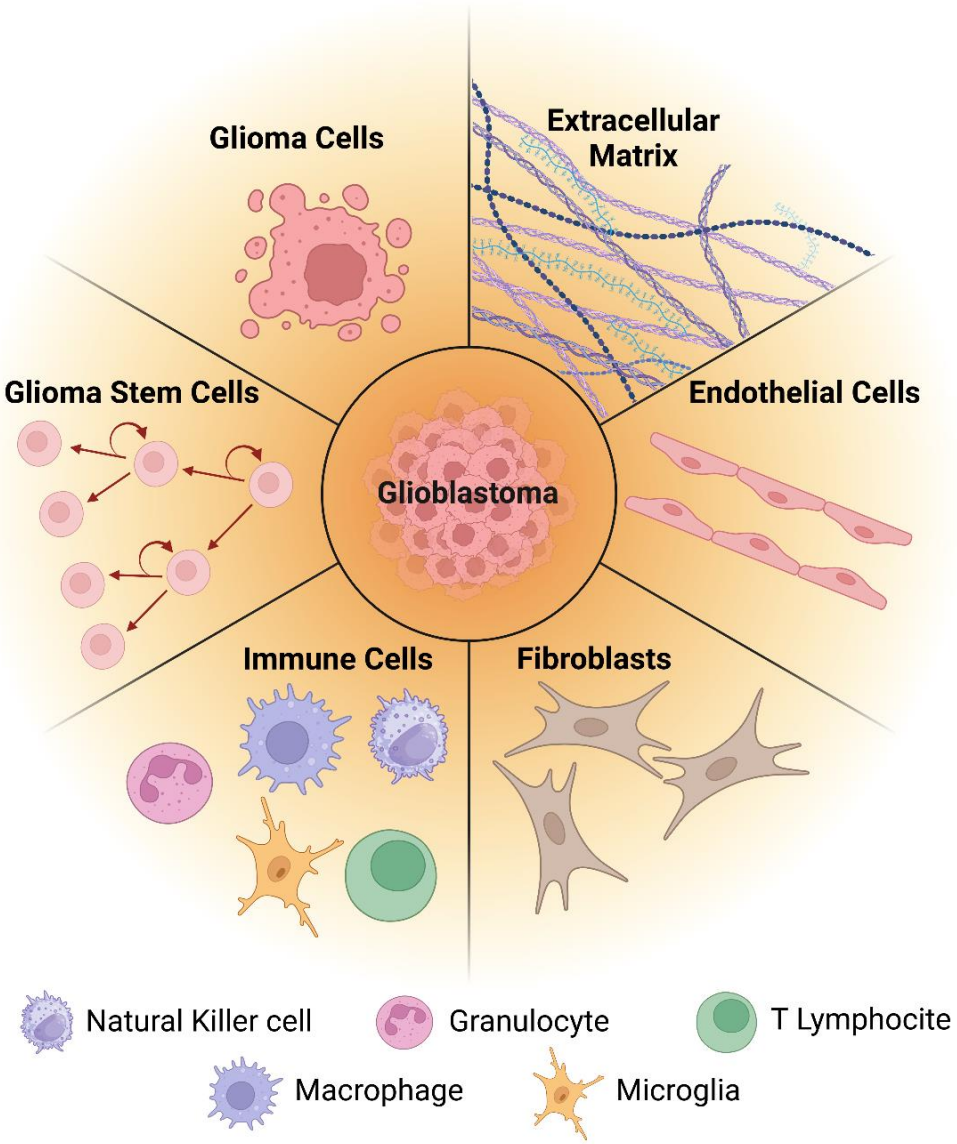

Figure 2. *Cellular and non-cellular components of GB and its microenvironment.*

1.1.3.1. Glioma cells

The primary cellular component of GB tumors consists of malignant glial cells, which exhibit significant inter- and intra-tumoral heterogeneity [71]. This heterogeneity was classified into the previously referred three molecular subtypes: classical, mesenchymal and proneural, based on transcriptomic analyses from The Cancer Genome Atlas (TCGA) [72]. A fourth one was initially proposed, the neural subtype, but later excluded as it was based on a misidentification caused by cellular cross contamination [16].

The classical subtype is the least common of GB tumors, accounting for approximately 20% of all GBs [73]. It is characterized by *EGFR* amplification in nearly all tumors (97%), and some harboring *EGFR* mutations [74, 75]. Consistent genetic alterations included chromosome 7 amplification paired with chromosome 10 loss and focal 9p21.3 homozygous deletion targeting cyclin-dependent kinase inhibitor 2A (*CDKN2A*), which mostly co-occur with *EGFR* amplification [15]. Notably, tumor protein p53 (*TP53*) mutations are rare in the classical subtype despite being the most frequently mutated gene in GB overall [76]. Furthermore, the transcriptomic analyses showed an overexpression of Sonic-hedgehog [smoothened (SMO), growth arrest-specific protein 1 (GAS1) and GLI family zinc finger 2 (GLI2)] and Notch pathway [neurogenic locus notch homolog protein 3 (NOTCH3), jagged 1 (JAG1) and beta-1,3-N-acetylglucosaminyltransferase lunatic fringe (LFNG)] agents, along with high expression of the neural precursor marker nestin [77, 78]. Patients with the classical subtype benefit from aggressive RT and chemotherapy [78].

The prevalence of the mesenchymal subtype ranges from 30% to 50% of all GB tumors, depending on the population studied and the molecular classification methods used [73, 79]. It frequently exhibits neurofibromin (*NF1*) mutations, and deletions at 17q11.2, often co-occurring with phosphatase and tensin homolog (*PTEN*) mutations phosphatidylinositol 3-kinase (PI3K)/AKT pathway enrichment [15, 80]. Mesenchymal markers such as chitinase-3-like protein 1 (CHI3L1) and proto-oncogene tyrosine kinase MET are highly expressed, along with astrocytic markers like cluster of differentiation (CD) 44 and proto-oncogene tyrosine kinase MER, indicating potential epithelial-to-mesenchymal transition (EMT) [15]. Gene expression analysis revealed activation of tumor necrosis factor (TNF) and nuclear factor kappa-light-chain-enhancer of activated B cells (NF-κB) pathways, correlating with extensive necrosis and inflammatory infiltrates characteristic of this subtype [74, 78]. Clinically, while responsive to aggressive RT and chemotherapy, patients with mesenchymal GB have the worst prognosis among all GB subtypes [14].

The proneural subtype, slightly less common than the mesenchymal subtype, accounts for approximately a third of GB tumors [73]. It is characterized by distinct genetic alterations, primarily involving the platelet-derived growth factor receptor

A (*PDGFRA*) gene [78]. This subtype was associated with a gene expression profile linked to oligodendrocyte development and neurogenesis, reflecting its unique biological characteristics. The proneural subtype was also characterized by frequent *TP53* mutations and loss of heterozygosity [15]. Clinically, patients with this subtype generally have a better prognosis compared to those with other subtypes, particularly in younger populations [14, 76, 77, 80].

A more recent perspective on GB heterogeneity suggests that genetic factors alone do not fully account for the diverse glioma cell composition observed within these tumors. An international team of researchers proposed that somatic mutations play a crucial role in shaping tumor's cellular landscape by selectively promoting certain cellular states over others [81]. This process results in a dynamic equilibrium of different cell populations within the tumor, contributing to its heterogeneous nature. Neftel *et al.* conducted a computational analysis that identified gene signatures converging into four recurring cellular states across multiple GB tumors [81]. These states were present in varying combinations of two to four in each patient, again denoting the heterogeneity of GB, being classified as: astrocyte-like (AC-like), mesenchymal-like (MES-like), oligodendrocyte progenitor-like (OPC-like), and neural progenitor-like (NPC-like). OPC-like states were enriched in tumors with *PDGFRA* alterations, NPC-like states in those with cyclin-dependent kinase 4 (*CDK4*) alterations, and AC-like states in tumors with *EGFR* alterations. MES-like states were characterized by *NF1* alterations, extensive immune cell infiltration, and hypoxic conditions [81]. These cellular states aligned with the TCGA subtypes and corroborated findings from other studies suggesting that genomic aberrations alone do not fully explain GB heterogeneity [77, 82]. Regardless, the heterogeneity of GB cell subtypes has significant clinical implications, with recent studies demonstrating that specific cellular compositions of tumors directly impact patient survival outcomes [83].

1.1.3.2. Glioma stem cells

A particularly concerning aspect of GB tumors is the presence of glioma stem cells (GSCs) in its TME, a subpopulation with self-renewal capacity that is thought to drive tumor initiation, recurrence, and therapy resistance [84]. Importantly, GSCs are now understood to represent a functional state rather than a distinct cell lineage [85]. This concept has been further supported by evidence showing that GB cells can dynamically acquire or lose stem-like characteristics in response to TME signals [86]. GSCs share features with normal neural stem cells, including stem cell marker expression such as nestin, sex determining region Y box 2 (SOX2), and CD133, as well as multi-lineage differentiation potential [85]. However, opposite to their normal counterpart, GSCs exhibit aberrant signaling pathway activation, enhancing survival, proliferation, and apoptosis resistance. These alterations confer GSCs a distinct advantage,

enabling them to survive conventional therapies and contribute to tumor relapse, making them critical targets for developing more effective GB treatments [87]. In fact, evidence suggests that GSCs are more resistant to chemotherapy and RT than the bulk of tumor cells [85]. They possess enhanced deoxyribonucleic acid (DNA) repair mechanisms, activated survival pathways, and overexpress drug efflux transporters such as ATP-binding cassette (ABC) proteins [88]. Furthermore, GSCs often reside in specialized niches within the TME, which are characterized by hypoxia and supportive stromal cells. The niches provide protective signals that promote GSC survival and maintenance, further shielding them from therapeutic interventions [89]. GSC metabolism is regulated by several key signaling pathways, including Notch, Hedgehog and Wnt. These pathways, essential for normal stem cell maintenance, are often dysregulated in cancer. Furthermore, transcription factors, such as, SOX2, octamer-binding transcription factor 4 (OCT4) and c-Myc, are essential for maintaining GSC pluripotency and proliferative capacity [90]. While GSCs are certainly influenced by TME cues, studies have also emphasized the reciprocal relationship between GSCs and their microenvironment, supporting and promoting glioma progression [91]. On the one hand, TME-derived cytokines such as interleukin (IL)-6 and transforming growth factor beta (TGF-β) enhance GSC self-renewal and survival [92]. On the other hand, GSCs have been shown to secrete factors that modulate the surrounding immune landscape, creating an immunosuppressive environment conducive to tumor growth. For example, GSCs can induce tumor-associated macrophages (TAMs) to adopt an M2-like phenotype, which suppresses immune responses and promotes tumor development [93]. This intricate interaction between GSCs and their microenvironment underscores the complexity of GB biology and highlights potential targets for therapeutic intervention.

1.1.3.3. Immune cells

The immune component of GB represents approximately 50% of the tumor's cellularity [94]. As previously mentioned, TAMs, which are differentiated from the resident microglia and peripheral monocytes, account for 30% of the tumor mass. These TAMs tend to adopt an M2 anti-inflammatory phenotype and have been shown to suppress $CD8^+$ T cell activity, thereby promoting immune evasion [95]. TAMs are recruited by glioma-cell-derived factors, such as colony stimulating factor 1 (CSF-1), glial cell line-derived neurotrophic factor (GDNF), chemokine (CC motif) ligand 2 (CCL2), stromal cell-derived factor 1 (SFD-1), chemokine (CXC motif) ligand 1 (CXCL1), EGF and granulocyte-macrophage colony-stimulating factor (GM-CSF) [96]. Once in the TME, TAMs secrete a range of molecules, including anti-inflammatory cytokines (IL4, IL10, TGF-β), angiogenesis factors (VEGF, IL8), and pro-tumorigenic growth factors [insulin-like growth factor 1 (IGF-1), EGF and platelet-derived growth factor (PDGF)]. These molecules significantly influence the GB TME and contribute to tumor progression

and therapy resistance, ultimately leading to poorer prognosis for GB patients [94].

Another cell type within the GB TME is myeloid-derived suppressor cells (MDSCs), a diverse population of myeloid progenitor and precursor cells, including macrophages, granulocytes, and dendritic cells at various stages of differentiation [97]. Similar to TAMs, MDSCs impair the function of various T cell subsets, including natural killer T (NK) cells and cytotoxic T lymphocytes [98]. MDSCs also deplete essential amino acids from the TME, such as L-Arginine, and enhance the production of reactive oxygen species (ROS), in order to suppress T-cell activation and function, thereby contributing to the immune evasion of tumors. These changes in the TME create an unfavorable environment for T cells, leading to reduced immune responses against the tumor [99, 100].

Lastly, NK cells, which are important to innate antitumor immunity through antigen-independent immune surveillance, were found to be the least abundant immune cell type in GB. Furthermore, their immune cytolytic activity is suppressed by major histocompatibility complex class I molecules expressed on GB cells [101].

1.1.3.4. Fibroblasts

Recent research has shed new light on the presence and significance of cancer-associated fibroblasts (CAFs) in GB, revealing their role in shaping the TME [102]. Being the primary ECM producers, CAFs contribute significantly to the remodeling of the ECM in GB, promoting tumor growth and invasion. Their abundance correlates with higher tumor grades and activation of ECM remodeling pathways [102]. CAFs also secrete pro-tumorigenic factors, including fibronectin, which plays a critical role in promoting GB cell migration and invasion, thereby enhancing the tumor's aggressive nature [102]. Furthermore, CAFs have been shown to promote resistance to TMZ, through the secretion of CCL2, which activates the extracellular signal-regulated kinases (ERK) 1/2 signaling pathway in GB cells [103]. Interestingly, CAFs exhibit subtype-specific effects in GB [104]. They are more abundant in the mesenchymal subtype compared to other subtypes, while proneural GB cells appear to be more responsive to CAF signaling in terms of migratory and invasive behaviors. This heterogeneity in CAF distribution and influence across GB subtypes adds another layer of complexity to the TME [102]. CAFs have been shown to suppress anti-cancer immune responses in various cancers, highlighting their role in contributing to the immunosuppressive environment characteristic of GB [105].

1.1.3.5. Endothelial cells

While not a part of the GB per se, endothelial cells, that encompass the perivascular niche, have been shown to be key components in the tumor's aggressiveness, since angiogenesis is one of the hallmarks of GB recurrence, proliferation, and invasion [106]. In the GB TME, newly formed blood vessels are structurally fragile and prone to rupture, leading to a compromised BBB. This disruption causes an increased vascular permeability and edema, altering immune responses and the boundary between tumor and normal brain tissue, thus facilitating tumor invasiveness and presents challenges for effective treatment delivery [107].

The recruitment of endothelial cells to the GB site occurs through several mechanisms. Neoangiogenesis is the primary process, where GB cells secrete high levels of pro-angiogenic factors, particularly VEGF, stimulating the formation of new blood vessels from the sprouting of pre-existing ones. This process involves endothelial cell proliferation and migration towards the tumor [108]. Additionally, GBs recruit bone marrow-derived endothelial progenitor cells through vasculogenesis, which then differentiate into endothelial cells within the TME [109]. Lastly, GSCs also have the potential to transdifferentiate into endothelial cells, or to simply assemble into tubular-like structures mimicking blood vessels, further contributing to tumor vasculature [110].

Endothelial cells' contribution to tumor progression is multifaceted. By forming new blood vessels, they ensure a steady supply of nutrients and oxygen to the rapidly growing tumor, while enabling invasion through the vasculature [109]. Endothelial cells also create a specialized niche that promotes the self-renewal of GSCs by expressing NOTCH ligands that activate Notch signaling in adjacent GSCs, supporting their maintenance and proliferation [111]. Furthermore, endothelial cells facilitate bidirectional communication within the TME, exchanging extracellular vesicles with tumor cells, which can, in turn, promote angiogenesis, suppress the immune system, and confer drug resistance [108].

1.1.3.6. Extracellular Matrix

The non-cellular component of the GB TME is the extracellular matrix (ECM). The brain has an unique ECM composition, which accounts for approximately 20% of its volume [112]. It is comprised of various components, including, but not limited to: collagen IV; glycoproteins, such as fibronectin, laminins and tenascins; glycosaminoglycans, such as hyaluronic acid (HA); proteoglycans, such as the lectican family, phosphacan and neuron-glial antigen 2 [113]. While sharing many components with the normal brain, the ECM of GB exhibits distinct characteristics that influence tumor behavior. Besides the fact that GB cells overexpress various ECM components, including HA, brevican, tenascin-C (TN-C), fibronectin, they

also show increased expression of specific integrins and receptors, which promote cell adhesion, migration, and invasion [114].

Notably, HA levels correlate with tumor malignancy, both increasing in parallel. HA, along with fibronectin, has been shown to promote the invasiveness of GB cells [115, 116]. GB ECM is more condensed and less flexible compared to normal brain tissue due to overexpression of these ECM components, potentially hindering the diffusion of therapeutic agents and neuroactive molecules [117]. The tumor also induces altered protein synthesis in surrounding normal tissues, promoting ECM degradation at the invasive front while increasing ECM component production in nearby areas [118, 119]. GB cells can actively migrate along blood vessels or axons through ECM interactions [120].

Research has revealed ECM-driven signals that shape tumor phenotypes and influence metabolic activity [121]. Moreover, the GB ECM is deficient in aggrecan, contains oncofetal proteins, and shows elevated levels of matrix metalloproteinases (MMPs), which increases ECM modulation, invasion, and angiogenesis [119, 122]. The ECM's significant role in cell survival, proliferation, and differentiation processes makes it an attractive target for novel therapeutic approaches, which could be particularly valuable given GB's poor response to conventional treatments.

1.2. Emerging therapeutic alternatives for GB – the advantages of nanotechnology

As previously stated, the current standard of care for GB, which includes both the Stupp protocol and second-line options, has shown limited efficacy in significantly extending long-term survival for patients. This has led researchers to explore alternative therapeutic and diagnostic approaches to overcome the challenges posed by GB's aggressive nature and its strong ability to develop resistance to conventional treatments [123].

One area of intense investigation has been immunotherapy, which aims to direct the patient's own immune system to target and eliminate tumor cells [124]. Currently, various immunotherapeutic strategies are being explored, including checkpoint inhibitors, cancer vaccines, and adoptive cell therapies like chimeric antigen receptor (CAR) T-cells. Despite the success of some of these approaches in other cancer types, their efficacy in GB so far has been limited, mostly due to the immunosuppressive nature of the brain TME and the BBB's restrictive properties, which will be discussed later [125]. Another approach involves targeting specific molecular pathways that are dysregulated in GB. For this, researchers have been developing inhibitors for key signaling molecules involved in GB tumor growth and survival, such as EGFR, VEGF and PI3K/AKT pathway components [126]. Additionally, the potential of oncolytic virotherapy, using

genetically modified viruses to selectively target and destroy cancer cells while sparing healthy tissue, is currently being explored [127]. Novel physical treatment modalities are also being investigated, such as focused ultrasound techniques for targeted drug delivery or tumor ablation [128].

Nanotechnology has emerged as a particularly promising field to address the challenges of GB, offering innovative solutions across multiple fronts. Advanced nanosystems have shown potential for enhancing diagnosis, drug delivery, and even theranostic applications, potentially overcoming many obstacles associated with brain tumor management. These nanoparticle (NP)-based approaches can offer improved penetration across the BBB, targeted delivery to tumor cells, and enhanced imaging capabilities, while minimizing toxicity to healthy tissue, presenting versatile tools for revolutionizing GB detection, treatment, and monitoring (**Figure 3**) [129].

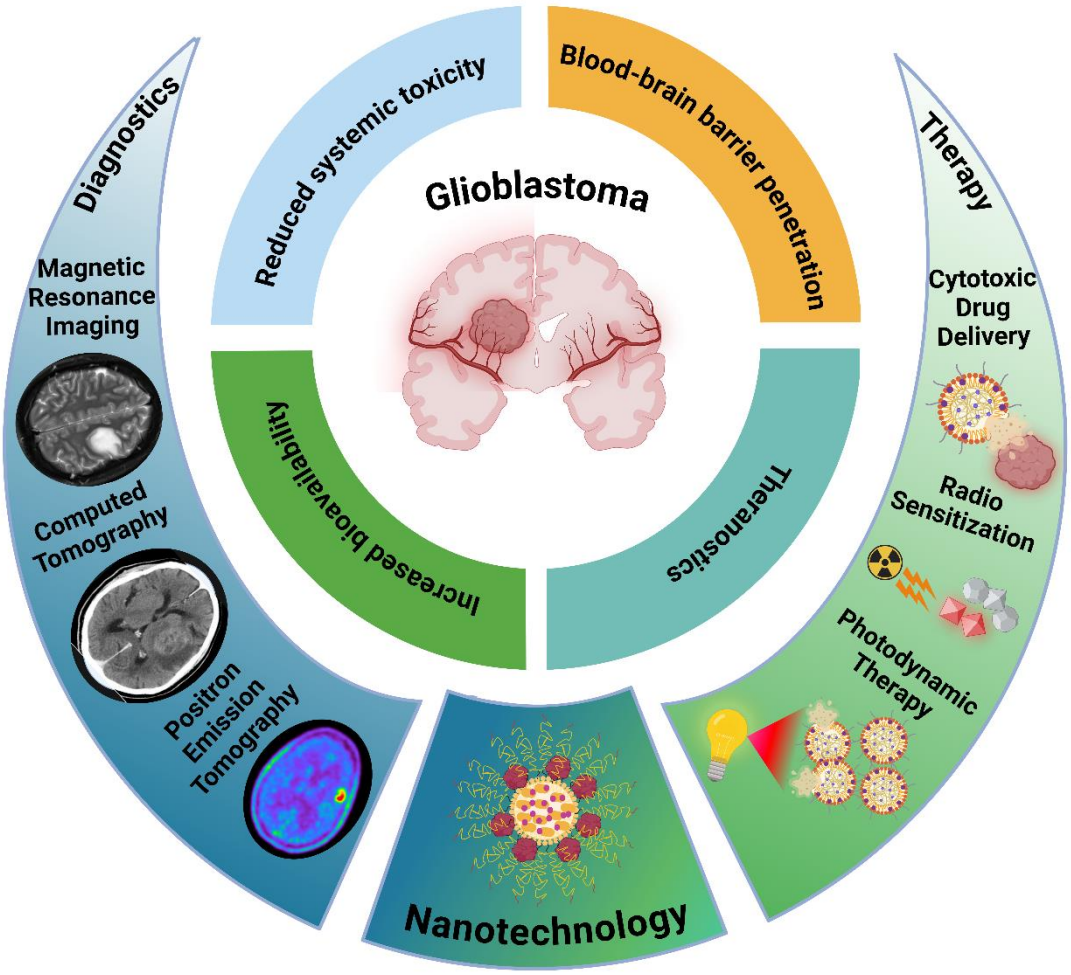

Figure 3. *Nanotechnology benefits and examples of approaches in GB diagnostics and therapy. The brain images included in this figure were adapted from Gue, R. et al [8], Mărginean, L. et al. [130] and Manzarbeitia-Arroba, B. et al. [131], and available under the Creative Commons Attribution (CC BY) license.*

Nanocarriers can be engineered to encapsulate various therapeutic agents, including chemotherapy drugs, small molecule inhibitors, nucleic acids for gene therapy, and even combinations of multiple agents for synergistic effects [132]. Their sizes typically range from 10 to 200 nm, with smaller sizes (10-50 nm) facilitating enhanced tumor penetration, cellular uptake and TME diffusion, while larger sizes (100-200 nm) promote prolonged circulation, better retention at the tumor site, and reduced clearance through renal filtration [133]. Furthermore, the surface of NPs can be modified with targeting ligands to facilitate transport across the BBB and to increase their specificity for GB cells [134]. As research in this area continues to evolve, nanotechnology-based approaches may offer new hope for improving the treatment outcomes for GB patients.

Despite all advances in this field, only a limited number of liposomal strategies have reached clinical trials in GB or other high grade gliomas, following a path similar to what was achieved in other cancers [135]. Among the main candidates studied, Caelyx™, a pegylated liposomal formulation of doxorubicin (DOX), underwent several phase I/II clinical trials, either alone or in a combination therapy (with TMZ, tamoxifen, RT or a combination of these) [136-140]. However, these trials' main conclusion was that the liposomal formulation did not show clinical benefits. More recently, a liposomal formulation of irinotecan (nal-IRI) was tested in two clinical trials, one as single agent and the other combined with TMZ; however both trials ended due to lack of activity [141, 142]. A new phase I clinical trial at the Johns Hopkins University (NCT05768919) is currently recruiting patients to assess the efficacy of liposomal curcumin in combination with RT and TMZ; no study results have been released yet.

While nanotechnology offers promising advantages for GB treatment, its potential non-specific toxicity, both systemically and in brain tissue, remains a critical consideration. Ongoing research focuses on optimizing NP biocompatibility and biodegradability while minimizing inflammatory responses, aiming to optimize the balance between therapeutic efficacy and safety [143, 144]. The limited efficacy observed thus far with these clinical trials suggests that, while NP-based systems can improve drug delivery, further optimization in formulation and the development of new targeting strategies are necessary to enhance their clinical effectiveness in GB treatment.

1.2.1. Overcoming BBB challenges with nanotechnology

The BBB is a crucial physiological interface that plays a vital role in maintaining the balance between the circulatory system and the CNS, while simultaneously posing a significant challenge for the delivery of therapeutic agents to the brain [134, 145].

The complex architecture of the BBB is formed, primarily, by specialized endothelial cells that line the cerebral capillaries, which are distinctively characterized by the presence of tight junctions, specialized protein structures that completely seal the spaces between adjacent cells, creating a highly selective barrier [146]. These tight junctions are composed of transmembrane proteins such as occludin, claudins (particularly claudin-5), and junctional adhesion molecules, such as junctional adhesion molecule A (JAM-A) [147-149]. These proteins are anchored to the endothelial cell membrane by scaffolding proteins, such as tight junction protein 1 (ZO-1) [150].

Surrounding the endothelial cells are several other cellular components that contribute to the BBB's integrity and function, together forming a structure known as the neurovascular unit (NVU) [151]. Astrocytes extend their end-feet to ensheathe the capillaries, providing biochemical support to the endothelial cells, while microglia perform localized immune surveillance, having a significant role in neuroinflammation and innate immunity [152, 153]. Pericytes, contractile cells embedded within the capillary basement membrane, play a crucial role in maintaining BBB integrity, aiding its angiogenesis and microvascular stability [154]. Furthermore, neurons present a very close and important relation with the brain vasculature. Beyond oxygen and glucose delivery, neurovascular coupling plays a role in proteostasis, neuroimmune trafficking, waste clearance, brain temperature regulation, and hippocampal neurogenesis [151].

The BBB serves as a highly sophisticated gatekeeper, carefully controlling the passage of substances between the blood and the brain, achieving this regulation through multiple mechanisms. Passive diffusion permits very small molecules to pass through the BBB comparatively easily, whether they are lipophilic (pinocytosis) or hydrophilic (paracellular pathway) [155, 156]. Some require active transportation, and the BBB contains numerous specialized transport proteins, such as the solute carrier family, that facilitate the movement of essential nutrients, ions, and other small molecules across the barrier [157, 158]. Charged molecules may utilize the unspecific adsorptive transcytosis mechanism, wherein vesicles are formed due to the electrostatic interaction of the cationic molecule and the negative endothelial cell membrane [159]. Larger molecules, such as proteins and molecular complexes, need to be transported through receptor-mediated transcytosis. With this mechanism, specific ligands bind to receptors on endothelial cells, such as transferrin and insulin receptors, triggering the transport of molecules across the BBB [160]. Furthermore, the BBB is also capable of removing potentially harmful substances from the CNS back into the bloodstream through energy-dependent efflux pumps, such as P-glycoprotein (P-gp) and breast cancer resistance protein [161].

The integrity and proper functioning of the BBB is essential for normal brain function. Disruption or dysfunction of the BBB has been implicated in various neurological disorders and neurodegenerative diseases [162]. For example,

changes in BBB permeability can contribute to the progression of conditions such as Alzheimer's disease, multiple sclerosis, and certain brain tumors [163, 164].

The BBB presents a significant challenge in drug delivery to the brain, as many therapeutic compounds cannot easily cross this barrier. This has led to extensive research into nanotechnological methods for bypassing or modulating the BBB to improve drug delivery to the CNS [129]. These methods, some of which will be more thoroughly explored in the following sections, mainly exploit the receptor-mediated BBB transcytosis mechanism through several receptors, such as the transferrin receptor [144, 165], insulin receptor [166], low density lipoprotein receptor [167], leptin receptor [168], nicotine acetylcholine receptor [169], diphtheria toxin receptor [168], scavenger receptor [170, 171], glucose transporter [172], and glutathione transporter [170], among others.

1.2.1.1. BBB in vitro models

The need to evaluate the complex interaction between developed strategies and the BBB and has led to the development of various *in vitro* models to study its properties and interaction with different nanosystems under normal and pathological conditions [173].

Two-dimensional (2D) models are popular for their simplicity, reliability, and affordability [174], being particularly useful in the initial screening and developmental phases of drug research. Their simplest form are monolayer models, which typically involve growing endothelial cells, such as hCMEC/D3, in a transwell chamber, which separates the luminal and abluminal sides, allowing for the study of solute exchange [175]. While cost-effective and scalable, monolayer models lack the complexity of the *in vivo* BBB, often resulting in lower transendothelial electrical resistance (TEER), a measure of membrane integrity, and higher paracellular permeability than observed *in vivo* [176]. To better mimic the BBB's multicellular environment, co-culture models incorporate additional cell types such as astrocytes and pericytes. These models have shown improved barrier functions and tightness compared to monoculture models [177]. Three-dimensional (3D) models, such as organoids, aim to more closely replicate the complexity of the BBB by self-organizing into the proper structural architecture of the barrier similar to what can be observed *in vivo* [174]. Microfluidic BBB models utilize miniaturized devices with microchannels to culture cells under flow conditions, incorporating shear stress to mimic blood flow, which can regulate the expression of tight junction proteins and transporters [178]. These models offer several advantages, such as requiring smaller volumes of reagents and cells, making them more cost-effective for high-throughput screening, and allowing for precise control of flow rates and shear stress [179]. Chip-based models, often referred to as "organ-on-a-chip" or more specifically "BBB-on-a-chip," are advanced microfluidic systems that aim to recreate the structure and function of

the BBB on a smaller scale [180]. These models typically consist of multiple chambers connected by microchannels, allowing for the co-culture of different cell types under flow conditions, offering the ability to integrate sensors for real-time monitoring of barrier function and cellular responses [181]. Despite their clear advantages over 2D models, their increased complexity in setup and maintenance leads to higher costs due to specialized equipment and material, lower throughput for drug screening, and lower reproducibility between laboratories [182, 183]. To overcome limitations in cell sourcing, human induced pluripotent stem cell (hiPSC)-based models have been developed, which aim to more accurately represent the human BBB *in vivo* [184]. However, differentiating and characterizing these cells to ensure they accurately represent mature BBB endothelial cells remains a significant challenge [185].

1.2.2. Exploring the ECM as therapeutic target in GB

Once the challenge of crossing the BBB is no longer an issue and GB becomes the target, initial nanotechnological approaches predominantly focused on directly targeting glioma cells with cytotoxic agents. However, there is growing recognition of the ECM as a critical factor in tumor progression and malignancy [114], as previously discussed. Consequently, researchers are developing novel therapeutic strategies that specifically target the ECM in GB. These exploit the ubiquitous presence of ECM components within the TME, and thus offer significant advantages compared to targeting the glioma cells themselves. These ECM-focused strategies, often investigated in preclinical settings, include the inhibition of matrix-degrading metalloproteinases and integrins, ECM stiffening and degradation [186, 187]. Additionally, targeting structural ECM molecules can enhance other treatment modalities, such as immunotherapy, by increasing the infiltration of immune cells [188, 189]. Nanotechnology approaches interacting with the GB ECM can be categorized into the following classes, as exemplified in **Figure 4**: i) Targeting ECM components: NPs designed to directly interact with or modify the ECM structural elements; ii) ECM-responsive NPs: NPs designed to respond to specific ECM characteristics or changes; iii) Enhancing ECM degradation: NPs that facilitate the breakdown of ECM components to enhance drug penetration or disrupt tumor structure; iv) Preventing ECM degradation: NPs that inhibit matrix-degrading enzymes like metalloproteinases to maintain ECM integrity and limit tumor invasion.

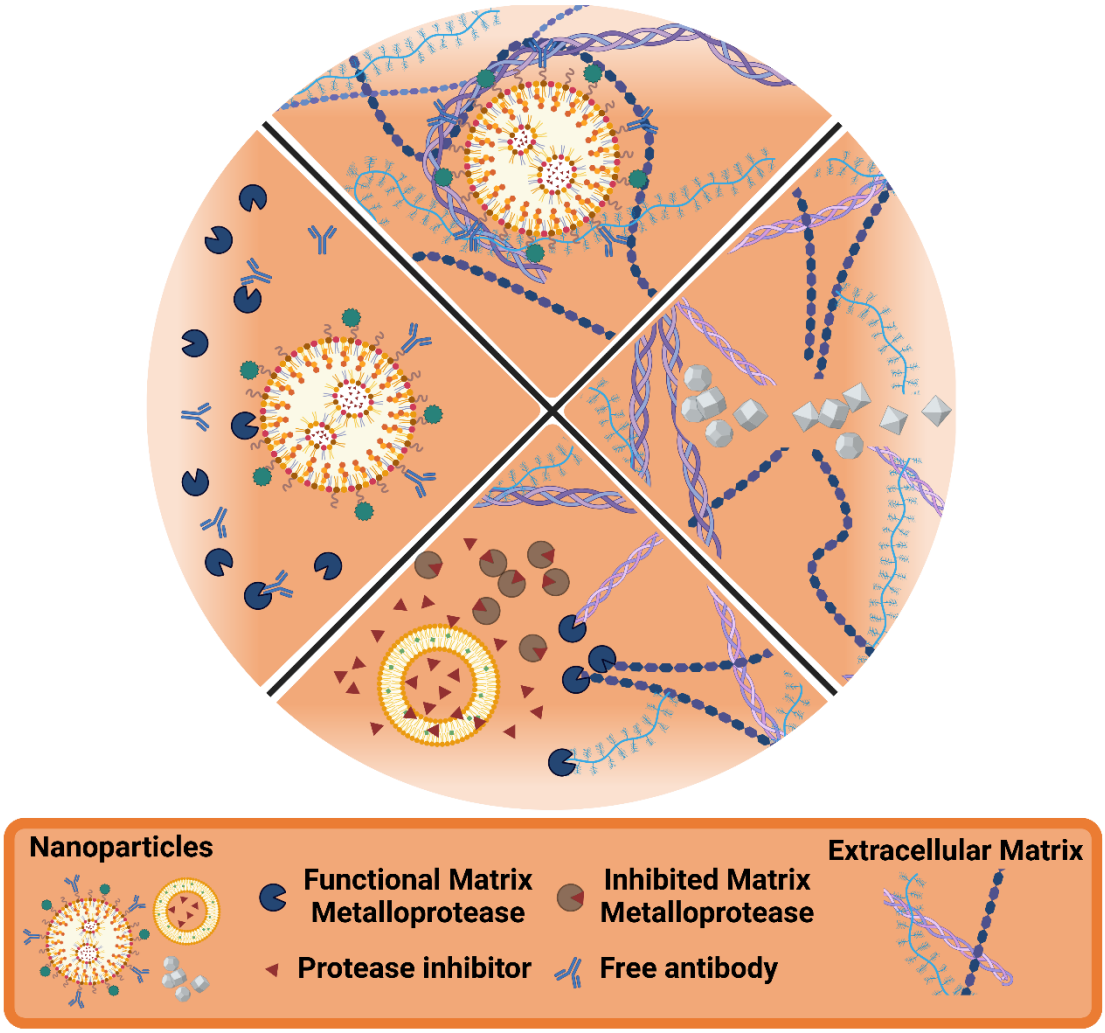

Figure 4. *Nanotechnology strategies interacting with the ECM. Top: NPs targeting the ECM; Left: NPs responding to ECM cues (e.g., increased MMP concentration in the TME); Right: NPs degrading the ECM; Bottom: NPs preventing ECM degradation.*

Table 1 summarizes the various nanotechnology strategies discussed in this section, highlighting their approach, key features and potential applications in GB treatment. This overview provides a comprehensive snapshot of the diverse nanotechnology approaches being explored to reprogram the GB ECM.

Table 1. *Overview of nanotechnology approaches for modulating the ECM in GB.*

Strategy	Approach	Key Features	Outcome	Reference
Targeting ECM components	Fibronectin-targeted liposomal Nanoplatform	Functionalized with EDB-specific aptide to deliver CypA siRNA	Improved cellular uptake and CypA silencing in GB cells; reduced tumor growth and increased survival rates *in vivo*	[190]
	CREKA-micelle NPs	Targets fibrin deposits in GB	Enhanced tumor homing; potential for targeted drug delivery	[191]
	Ft-PLA-PTX dual-targeting peptide system	Targets TN-C and NRP-1	Enhanced internalization in glioma cells and penetration in 3D spheroids; Increased median survival compared to saline	[192]
	PL3-functionalized iron oxide nanoworms and silver NPs	Targets TN-C and NRP-1	Increased GB targeting; increased survival rates in glioma-bearing mice	[193]
	PL1-functionalized silver NPs	Targets fibronectin EDB and TN-C	Strong binding to targets and facilitated cellular uptake	[194]
	MMP-14 targeting dual-modality imaging agent	Combines NIRF dye and PET radionuclide	Enhanced tumor specificity and imaging contrast for GB detection; potential for preoperative planning and real-time surgical guidance	[195]
	VEGF-targeting iron oxide magnetic NPs	Coated with cross-linked BSA and functionalized with anti-VEGF antibodies	Improved tumor visualization using MRI; sustained contrast for 24 hours post-injection	[196]
ECM-responsive NPs	CLIO-ICT NPs	MMP-14-activated prodrug release system	Selective targeting of GB cells and GSCs; disrupted tumor blood vessels; induced apoptosis and reduced GSC populations; real-time tumor response monitoring via MRI	[197]
	Activatable cell-penetrating peptide-modified NPs	MMP-2 and MMP-9 responsive design	Enhanced internalization and targeted PTX delivery within GB microenvironment; improved penetration in 3D GB spheroids; increased survival rates compared to conventional PTX formulations	[186]
	Activatable peptide dual-functionalized NPs	Angiopep-2 and cell penetrating peptide functionalization activatable by MMP-2	Improved glioma localization and therapeutic efficacy; Prolonged survival compared to conventional drug delivery systems	[198]

Table 1. *Overview of nanotechnology approaches for modulating the ECM in GB (cont.).*

	MMP-2-activated NPs with bispecific antibodies	Combines immunotherapy with ferroptosis induction	Targeted B7-H3 and CD3; crossed BBB; accumulated in GB tissue; released cargo upon MMP-2 cleavage; activated T-cells and induced cytokine release	[199]
	pH-responsive DOX-loaded liposomes	Incorporates pH-sensitive peptide trigger	pH-triggered drug release; specific targeting of GB cells under acidic conditions; anti-tumor activity and anti-angiogenic effects	[200]
	Chitosan-based pH-responsive gold NPs	Functionalized with anti-nucleolin aptamer (AS1411)	Enhanced drug release in acidic environments; dual-drug delivery (5-FU and DOX); induced greater cell death than single-drug formulations	[201]
	Acid-cleavable angiopep-2 functionalized NPs	Dual-surface tailored PLGA and PEG based NPs	Brain-targeting in circulation; transformed into GB-accumulating after BBB crossing; enhanced cell uptake and cytotoxicity; improved BBB permeability	[202]
	GB-targeted dextran/dendrimer dual-NP nanogel system	*In situ* nanogel formation by dual-NP system with pH- and MMP-9-sensitive linker	*In situ* nanogel formation; Prolonged drug retention; Enhanced tumor penetration; Delayed GB growth; Improved survival	[203]
	Hypoxia-responsive liposomal system	Stepwise targeting and drug release	Crossed BBB; targeted GB cells; released cargo in hypoxic conditions; synergistic inhibition of GB cell growth and pluripotency	[204]
	Hollow manganese dioxide nanosystem	pH-responsive design	Alleviated tumor hypoxia; enabled targeted drug delivery, imaging, and TME modulation; enhanced photodynamic therapy efficacy	[205]
	Redox-sensitive HA-curcumin conjugate nanocarriers	GSH-responsive disulfide bonds	Rapid drug release in high GSH environments; enhanced curcumin solubility and stability; superior cytotoxicity and cellular uptake in GB cells	[206]
Enhancing ECM degradation	Hyaluronidase-expressing oncolytic adenovirus	Targets HA-rich ECM; increases tumor-infiltrating $CD8^+$ T cells and macrophages	Prolonged survival in GB models; potential combination with anti-PD-1 therapies for enhanced efficacy	[207]
	Collagenase-modified human serum albumin NPs	Loaded with gemcitabine; improved tumor spheroid penetration	Overcame limitations of gemcitabine's short half-life; enhanced drug delivery efficacy and induced higher levels of nuclear fragmentation and ROS generation	[208]
Preventing ECM degradation	PLGA NPs functionalized with chlorotoxin	Targets MMP-2 and chloride channels overexpressed in GB cells; delivers morusin	Effectively crossed BBB; induced apoptosis and ROS generation in GB cells with low toxicity to normal cells	[209]
	Amphiphilic peptide NPs	Conjugated with MMP-9 inhibiting peptide; brain-targeting ligand included	Efficiently inhibited MMP-9 activity; demonstrated low toxicity while crossing the BBB	[210]

1.2.2.1. Targeting ECM components

As previously mentioned, ECM components are ubiquitously distributed throughout the tumor parenchyma, making them a more consistent and accessible target compared to heterogeneous tumor cell populations (**Figure 5**) [188].

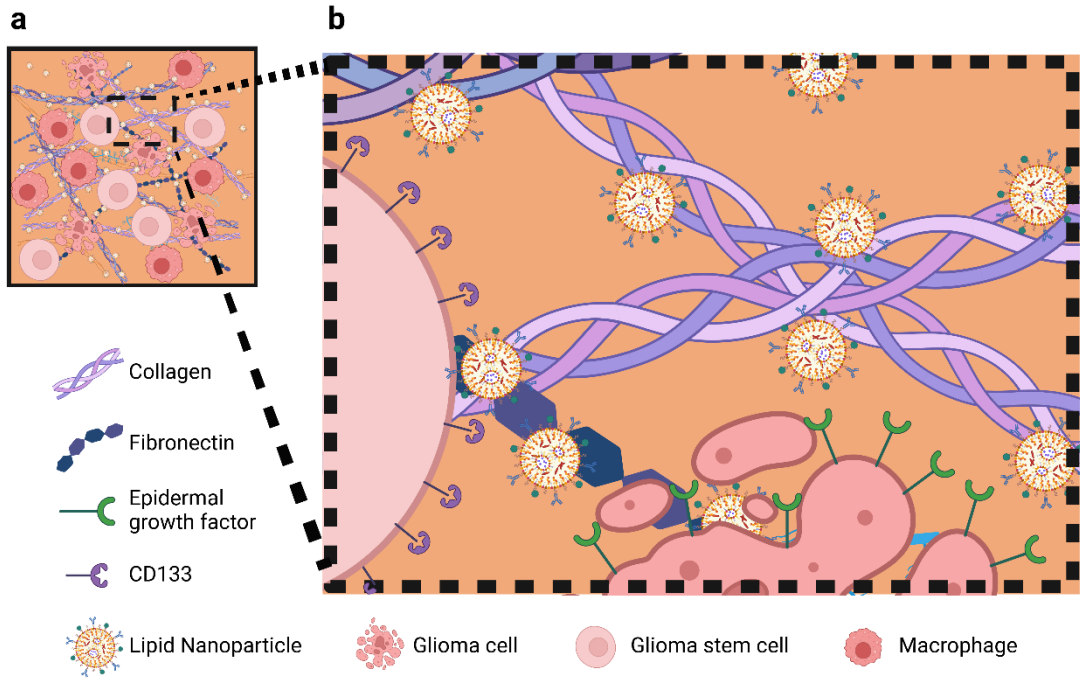

Figure 5. *ECM targeting nanotechnology strategy. a) Schematic overview illustrating NPs interacting with ECM components to locally exert their effect. b) Detailed depiction of NPs avoiding cell receptors and specifically targeting ECM proteins such as collagen and fibronectin.*

Among these components, the extra domain B (EDB) of fibronectin has emerged as a highly promising target for cancer therapy, particularly in aggressive solid tumors such as GB [211]. This specific domain is prominently present in the perivascular space of many aggressive tumors, making it an excellent marker for tumor-associated blood vessels [212]. Its unique overexpression pattern in the TME, coupled with its absence in normal adult tissues, makes EDB a selective target for nanotechnological strategies [213]. Saw *et al.* developed a GB therapy using a fibronectin-targeted liposomal nanoplatform functionalized with an EDB-specific aptide to deliver cyclophilin A (CypA) small interfering ribonucleic acid (siRNA). *In vitro* studies showed improved cellular uptake and CypA silencing in GB cells compared to non-targeted liposomes while in non-orthotopic GB-xenografted mice this targeted system reduced tumor growth and increased survival rates [190].

Previous studies have demonstrated that GB is characterized by a leaky and hemorrhagic vasculature, which promotes thrombosis and fibrin accumulation [191]. This feature, absent in normal tissues, is hypothesized to result from the

increased permeability in GB, allowing plasma proteins to infiltrate the tumor tissue, where fibrinogen is transformed into fibrin through the action of pro-coagulant factors [214]. Therefore, fibrin deposition in the ECM, a feature of both primary and metastatic brain tumors, could be a promising target for therapeutic intervention.

Taking this into consideration, Chung and colleagues developed peptide-functionalized CREKA-micelle NPs to target fibrin deposits in GB [215]. In an orthotopic mouse model of GB, both targeted and non-targeted micelles accumulated at the tumor site due to the enhanced permeability and retention (EPR) effect. However, CREKA-micelles showed enhanced tumor homing within one hour, indicating active fibrin targeting. Biodistribution studies revealed micelle accumulation in the liver and kidneys, suggesting clearance through renal filtration and the reticuloendothelial system. Importantly, no cytotoxicity or tissue damage was observed, supporting the NP system's safety [191].

Another promising ECM target in GB for tumor-specific therapy is TN-C, a glycoprotein with certain splice isoforms uniquely expressed in tumors. Clinical trials have evaluated radiolabeled antibodies targeting TN-C domains A1 and D for glioma and lymphoma therapy [216].

Instead of antibodies, Kang *et al.* developed a dual-targeting peptide system, Ft-PLA-PTX, which combines paclitaxel (PTX) with polylactic acid (PLA) NPs. The peptide Ft targets TN-C and neuropilin-1 (NRP-1), enhancing internalization in U-87 glioma and HUVEC cells, as well as penetration in 3D glioma spheroids. *In vivo* studies in U-87 glioma-bearing mice showed significant accumulation of Ft-PLA-PTX at tumor sites, leading to higher cytotoxicity and apoptosis rates than single-targeted NPs. Treatment resulted in a 269% increase in median survival compared to saline, outperforming Taxol® and other formulations, indicating the effectiveness of this dual-targeting approach [192].

Lingasamy *et al.* studied the targeting of the same ECM molecules TN-C and NRP-1 using an 8-amino acid homing peptide, PL3, to enhance NP delivery to GB and prostate carcinoma. They found that PL3 effectively binds to both targets and functionalizing iron oxide nanoworms (NWs) and silver NPs (AgNPs) with PL3 significantly improved their targeting ability in nude mice models, achieving an eight-fold increase in GB targeting compared to untargeted NPs. Notably, PL3-guided NWs increased survival rates in glioma-bearing mice, while untargeted particles had no therapeutic effect. Furthermore, advanced imaging confirmed the accumulation of PL3-coated NPs in TN-C and NRP-1 positive areas in clinical tumor samples, suggesting potential for future clinical applications [193]. Following their work with PL3, the authors investigated PL1, which targets the ECM components fibronectin EDB and TN-C. The PL1-functionalized AgNPs exhibited strong binding to these targets and facilitated cellular uptake in U-87 cells via a macropinocytosis-like process. The binding affinity of PL1 was

quantified, supporting its potential for delivering therapeutic agents intracellularly [194].

MMPs are key players in the ECM remodeling process that contributes to GB progression [217]. These zinc-dependent enzymes, essential for normal physiological processes, can contribute for malignancy when their regulation is disrupted [218]. In GB, several MMPs are overexpressed, with MMP-2 and MMP-9 being the most extensively studied [219-221]. These secreted gelatinases break down key ECM components like collagens, elastin, and fibronectin, creating space for tumor cell migration and invasion [222]. Additionally, they promote the release of pro-angiogenic factors such as VEGF, enhancing tumor resource availability and facilitating GB infiltration through newly formed blood vessels [223].

Another MMP found overexpressed in GB is the membrane-anchored MMP-14 (also known as MT1-MMP) [224]. It shares similar proteolytic, angiogenic, and immunomodulatory capabilities with the secreted gelatinases and can activate pro-MMP-2, further contributing to GB invasiveness [195, 197]. MMP-14's influence extends beyond ECM degradation, regulating numerous plasma membrane-anchored and extracellular proteins, thereby impacting both intercellular and cell-matrix communication [225]. In the GB TME, both cancer and stromal cells engage with the ECM through various adhesive structures [225]. This interaction often results in aggressive infiltration of adjacent brain tissue, including areas crucial for survival. To facilitate invasion, glioma cells secrete proteolytic enzymes that degrade the ECM and mediate the invasion process and research has revealed that specific MMPs not only promote glioma cell invasion but also alter tumor cell behavior and stimulate cancer progression [118, 226]. As the invasive nature of GB significantly contributes to its high mortality rate and poor prognosis, making it a critical area of study, understanding the complex interplay of various MMPs, in particular MMP-14, in GB is essential [224]. This deeper comprehension could lead to the development of new prognostic and predictive markers, improving patient outcomes. Moreover, exploring MMP interactions may pave the way for novel targeted therapies designed to counteract the invasive nature of GB.

Taking into consideration that MMP-14 is differentially expressed in GB, compared to normal tissues, Kasten *et al.* developed a dual-modality imaging agent targeting the membrane protease. Their peptide probe combines a near-infrared fluorescence (NIRF) dye linked to a quencher that is activated upon cleavage by MMP-14, and an MMP-14-binding peptide attached to a radionuclide chelate for positron emission tomography (PET). This approach enhanced tumor specificity and imaging contrast, as the NIRF signal activates only in the presence of MMP-14. *In vitro* and *in vivo* studies demonstrated the probe's efficacy in detecting GB in cultured cell lines and patient-derived xenograft models, showing favorable tumor-to-background ratios. PET imaging confirmed significant

localization of the probe in orthotopic GB models, and blocking experiments verified its specific targeting of MMP-14-expressing cells. Their strategy seemed to be effective for imaging GBs, providing valuable insights for both preoperative planning and real-time surgical guidance [195].

Finally, in terms of vascularization, GB stands out as one of the most highly angiogenic tumors, with VEGF playing a central role in this process [227]. The formation of new blood vessels in GB is driven by both hypoxia-dependent and independent mechanisms, leading to the development of unique vessels [109]. This angiogenic potential of GB is further enhanced by GSCs, which secrete significantly higher levels of VEGF compared to non-stem glioma cells [228]. Conditioned media from these stem cells have been shown to strongly enhance endothelial cell functions crucial for angiogenesis, including migration, proliferation, and tube formation. This heightened angiogenic activity, primarily driven by VEGF and exacerbated by GSCs, is a major contributor to the aggressive nature of GB, presenting both challenges and opportunities for therapeutic interventions targeting the tumor vasculature [229]. Taking advantage of the enhanced accumulation of VEGF in the ECM of GB tumors, Abakumov *et al.* developed iron oxide magnetic NPs (MNPs) targeting VEGF for enhanced GB imaging [196]. The MNPs were coated with cross-linked bovine serum albumin (BSA) to improve biocompatibility and stability, then functionalized with monoclonal antibodies against VEGF, allowing specific binding to VEGF-positive GB cells. This targeted approach im-proved tumor visualization using magnetic resonance imaging (MRI), addressing limitations of existing contrast agents in specificity and retention [230]. *In vitro* studies confirmed the NPs' stability and cytocompatibility, while *in vivo* experiments in orthotopic C6-xenografted rat models demonstrated superior imaging of tumors and vasculature compared to non-targeted controls, with sustained contrast for 24 hours post-injection [196].

1.2.2.2. ECM-responsive NPs

The ECM provides essential mechanical and biochemical cues through its interactions with cell receptors, allowing it to function as both a structural scaffold and a regulator of cellular behaviors such as adhesion, proliferation, and differentiation [231]. The composition and architecture vary between tissue types, influenced by various factors including the cell type present, mechanical forces, and the availability of nutrients and oxygen in the local microenvironment. This dynamic nature of the ECM reflects changes in tissue status and disease conditions, with GB being no exception [232]. Nanosystems can be designed to modulate their effect once in contact with TME conditional changes, such as the increased presence of secreted and membrane MMPs, the acidic environment and the lack of oxygenation (**Figure 6**).

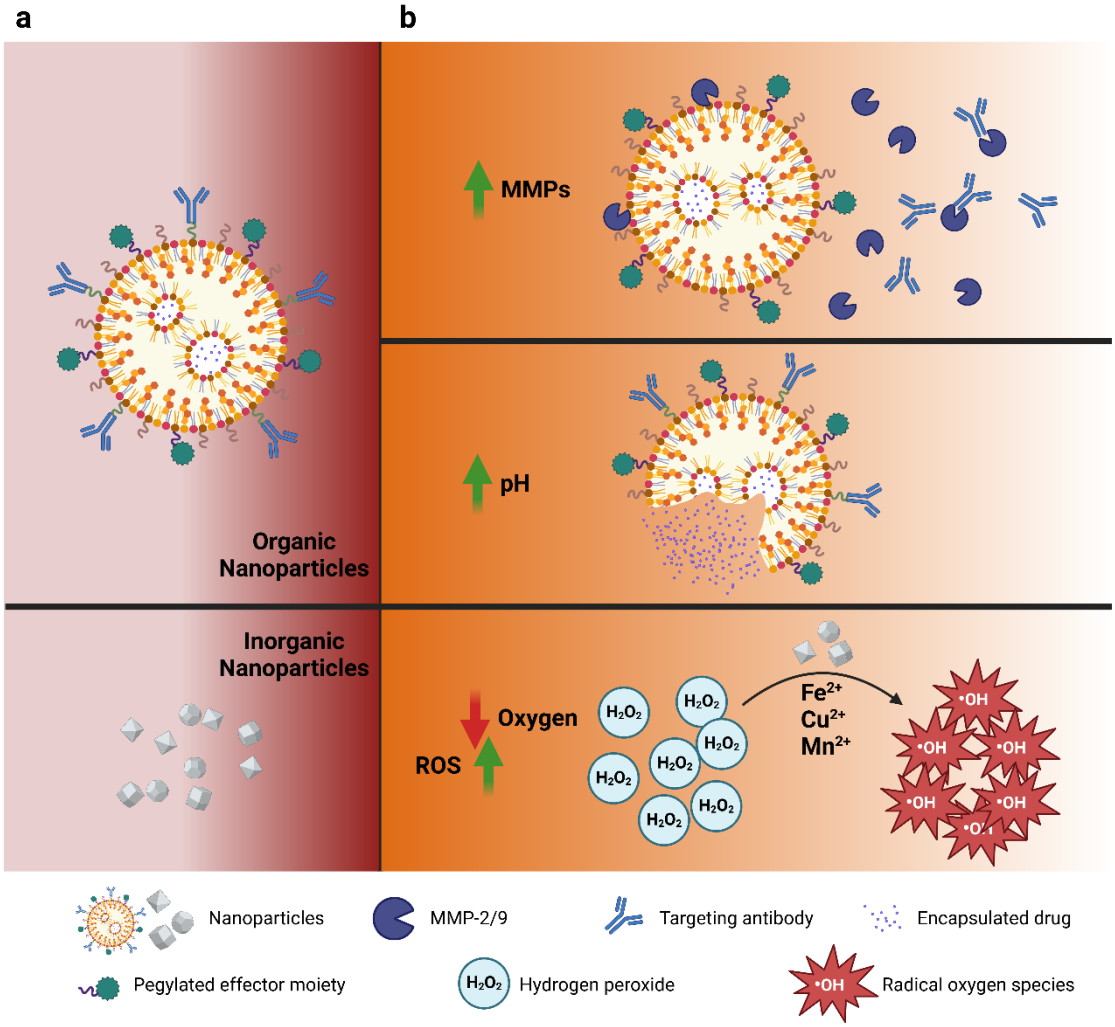

Figure 6. *Utilizing ECM physicochemical cues as a nanotechnological strategy. a) NPs in circulation. b) NPs upon sensing TME conditional alterations. From top to bottom, an increase in secreted and membrane matrix metalloproteases, an increase in acidity, an increase in hypoxia accompanied by an increase in ROS.*

As previously mentioned, MMP-14 is a proteolytic enzyme highly overexpressed in GBs and has been already applied as a microenvironment cue in GB therapy by Mohanty *et al.* Their work focused on creating a theranostic approach using cross-linked iron oxide NPs, named CLIO-ICT, which combined therapeutic and diagnostic functions to target GB and GSCs. These NPs consisted of cross-linked iron oxide particles conjugated to an azademethylcolchicine (ICT2552)-peptide prodrug that released the active drug upon cleavage by MMP-14. The study demonstrated that CLIO-ICT selectively targets GB cells and GSCs, disrupting tumor blood vessels and significantly inducing apoptosis while reducing GSC populations. *In vivo* experiments in orthotopic xenografted mice revealed that CLIO-ICT, especially when combined with TMZ, improved survival rates and reduced tumor growth compared to TMZ alone. Additionally, the dual functionality of CLIO-ICT allowed for real-time tumor response monitoring via MRI. [197].

In a similar direction, Gu and colleagues developed NPs that utilize the upregulated expression of MMP-2 and MMP-9 in GB [217, 233]. These NPs were modified with an activatable cell-penetrating peptide, which is specifically cleaved by MMP-2 and MMP-9, enhancing internalization and enabling targeted PTX delivery within the GB microenvironment. After confirming successful conjugation of the peptide to polyethylene glycol-polycaprolactone (PEG-PCL) NPs, *in vitro* studies showed significantly increased cellular uptake in GB cells and enhanced penetration in 3D GB spheroids. *In vivo* studies in intracranial GB xenograft models indicated that the peptide-modified NPs accumulated in tumor tissues, leading to improved survival rates compared to conventional PTX formulations [186].

A similar strategy in the utilization of activatable cell penetrating peptides, Gao *et al.* developed a molecular construct comprised by 2 oligopeptides, EEEEEEEE (E8) and RRRRRRRR (R8), linked by an MMP-2-cleavable amino acid sequence [198]. Once in circulation, the E8 covers the cationic R8 through electrostatic forces, shielding R8's penetration capability. In this study, the authors developed dual-modified PEG-PCL NPs loaded with the chemotherapeutic docetaxel (DTX), incorporating angiopep-2, a known low density lipoprotein receptor-related protein 1 (LRP1) ligand and BBB penetration enhancer, and the E8R8 peptidic conjugate, an activatable cell penetrating peptide (ACP). *In vitro* studies demonstrated that ACP-modified NPs showed enhanced cellular uptake in GB cells, which could be inhibited by an MMP-2 inhibitor, confirming the MMP-2-dependent activation mechanism. The DTX-loaded dual-modified nanosystem exhibited superior anti-GB effects both *in vitro* and *in vivo* when compared to single-modified NPs or free DTX. Overall, the dual-modified nanosystem showed improved GB targeting and penetration, leading to enhanced therapeutic efficacy, evidencing the success of promising ECM-cue responsiveness strategy [198].

More recently, Fan and colleagues engineered MMP-2-activated NPs that combine immunotherapy with ferroptosis induction for GB treatment [199]. These complex NPs consist of bispecific antibodies targeting B7-H3 (associated with poor prognosis in GB) and CD3, along with a dimer of epigallocatechin-3-gallate (dEGCG) linked to hyaluronic acid via an MMP-2-cleavable sequence. dEGCG, on its own, has been shown to provide a myriad of antitumor effects, mainly associated to its production of intracellular ROS, and subsequent induction of oxidative damage [234]. This design allowed the NPs to cross the BBB, accumulate in GB tissue, and release their cargo upon MMP-2 cleavage. *In vitro* studies showed effective targeting of GB cells, T-cell activation, and cytokine release, leading to enhanced anti-tumor effects. In a mouse orthotopic U-87 GB xenograft model, the NPs demonstrated significantly higher intracranial accumulation compared to free antibodies or non-targeted formulations. Notably, the treatments resulted in 50% of mice surviving longer than 56 days, indicating

a promising strategy for GB therapy that leverages both immune activation and ferroptosis [199].

In addition to MMP-responsiveness, tumor acidosis is a well-studied characteristic of most TMEs [235]. Rapidly proliferating tumor cells often deplete their own oxygen supply, leading to hypoxia. where cells are unable to generate adenosine triphosphate (ATP) through oxidative phosphorylation. In response, the hypoxia-inducible factor (HIF) pathway shifts cellular metabolism towards anaerobic glycolysis, commonly referred to as the Warburg effect, allowing the tumor cells to continue ATP production despite the lack of oxygen. This metabolic adaptation results in the accumulation of lactate and protons as byproducts of fermentation, which alter not only the intracellular pH, but, once expelled, contribute to the characteristic acidification of the TME [94].

To take advantage of the acidic TME in GB, Zhao *et al.* developed a DOX-loaded liposome that responds to the surrounding pH by incorporating a conjugated peptide, which consists of a cell-penetrating sequence and a pH-sensitive trigger. The liposomes were produced through the common thin-film hydration method followed by the less common remote loading technique of DOX. *In vitro* experiments showed pH-triggered drug release and specific targeting of C6 and U-87 GB cells under acidic conditions caused by the peptide modification. *In vivo* experiments in C6 subcutaneous and U-87 orthotopic tumor-bearing mice demonstrated significant anti-tumor activity and antiangiogenic effects, indicating the liposomes' potential for targeted drug delivery and vascular modulation [200].

In a simpler approach, Sathiyaseelan *et al.* utilized chitosan as the pH-responsive component in anti-nucleolin aptamer (AS1411)-functionalized gold NPs, biosynthesized from *Gynura procumbens*, and loaded with both 5-fluorouracil (5-FU) and DOX. Chitosan, a cationic polysaccharide, becomes soluble at acidic pH, enhancing the release of its cargo in such environments. The study demonstrated higher drug release rates under acidic conditions that mimic the GB TME. *In vitro* experiments on LN229 GB cells showed that the dual-drug-loaded NPs induced greater cell death than single-drug formulations, primarily through G0/G1 phase cell cycle arrest, with transmission electron microscopy (TEM) confirming their internalization in cell organelles [201].

More recently, our group has described an elegant functionalization design that utilizes an acid-cleavable angiopep-2 to functionally create two different nanosystems, a brain-targeting NP while in circulation, that transforms into a GB-accumulating NP after BBB crossing [202]. In that sense, poly(lactic-co-glycolic acid) (PLGA) and PEG based NPs were designed to deliver DTX to GB tumors. The polymeric NPs were dual-surface tailored with two key features: i) a brain-targeted acid-responsive angiopep-2 moiety that triggers a structural rearrangement within BBB endosomal vesicles, and ii) an L-histidine moiety that provides preferential accumulation into GB cells after BBB crossing. The

angiopep-2 peptide targets the low-density lipoprotein receptor (LDLR) overexpressed on the BBB, while L-histidine targets the L-type amino acid transporter 1 (LAT1) overexpressed in GB cells. It is important to note that PEG molecules with different molecular weight (MW) were used to create two levels of NP surface decoration, avoiding inter-steric hindrance. *In vitro* studies using tumor invasive margin patient cells showed that the stimuli-responsive multifunctional nanosystem effectively targeted GB cells, enhancing cell uptake by twelve-fold and inducing three times higher cytotoxicity in both 2D and 3D cell models compared to non-targeting formulations. *In vitro* BBB permeability was assessed with a hCMEC/D3 transwell model, with the nanosystem demonstrating a three-fold increased BBB permeability. An *in vivo* biodistribution trial confirmed a three-fold improvement of NP accumulation in the brain. The antitumor efficacy was validated in GB orthotopic models following both intratumoral and intravenous administration, with the median survival and number of long-term survivors increasing by 50% compared to control groups. The acid-cleavable properties of the NPs ensure that the long-length PEG-angiopep-2 separates from the main structure after encountering the acidic pH of endosomes during BBB trafficking. This facilitates endosomal escape and NP expulsion towards the brain. Subsequently, the shorter PEG-L-histidine becomes exposed on the NP surface due to steric deprotection, allowing for GB cell targeting. This study represented the first time that a multi-ligand functionalized NP system was proposed to sequentially target the BBB and GB through the exploitation of a BBB-responsive transport mechanism [202].

Another pH-responsive strategy, proposed by Dosta *et al.*, was the simultaneous use of MMP-responsiveness to create a dual-sensitive nanosystem [203]. These authors produced the nanosystem Dual-NP, composed of an oxidized dextran NP surrounded by smaller DOX-loaded dendrimer NPs. Both are initially linked by a dual-responsive linker (MMP and pH) engineered to quickly disassemble within the TME so that, upon disassembly, the system triggers the *in situ* formation of nanogels through a Schiff base reaction, which in turn enhances the retention of Dual-NP, allowing for the gradual release of small DOX-conjugated dendrimer NPs over time. The authors demonstrated the efficacy of this system in both 3D spheroid models and an orthotopic GB mouse model (GL261). The Dual-NPs showed a deep penetration into the spheroids, being detectable at the tumor site for up to 6 days after a single intratumoral injection in the mouse model. This prolonged presence resulted in a significant tumor growth delay and an increased overall survival compared to untreated controls or DOX-conjugated dendritic NPs alone [203].

Furthermore, as previously noted, hypoxia is a prevalent feature in cancer. The tumor TME often stimulates neoangiogenesis, resulting in the development of aberrant and inefficient blood vessels. This process, paradoxically, intensifies the hypoxic conditions within the tumor. These irregular vessels restrict the delivery

of oxygen, drugs, and immune cells, making tumors more resistant to treatment. Hypoxia also induces significant changes in tumor cells, activating pathways such as the previously mentioned HIF pathway, which enables cell adaptation, promoting invasion, therapy resistance, and immune evasion [236]. This is particularly relevant in GB, one of the most hypoxic tumors [237]. Very recently, Qi and colleagues developed a hypoxia-responsive liposomal system (AMVY@NPs) for GB treatment, designed for stepwise targeting and drug release. This system includes a polymetronidazole core that encapsulates the Yes-associated protein (YAP) inhibitor verteporfin (VP), a cationic lipid layer that adsorbs siRNA targeting YAP (siYAP), and an outer coating with the targeting peptide angiopep-2. The NPs are engineered to cross the BBB, specifically target GB cells, and release their cargo in response to the hypoxic TME. *In vitro* and *in vivo* studies demonstrated that AMVY@NPs effectively released siYAP and VP under hypoxic conditions, leading to synergistic inhibition of GB cell growth and pluripotency. In an orthotopic U-87 xenograft mouse model, these NPs significantly inhibited tumor growth and improved survival without noticeable adverse effects [204].

TME hypoxia and acidosis are linked to ROS creation by the oxidative stress [238]. In GB, elevated ROS levels are a hallmark of the TME, promoting tumor progression, therapy resistance, genomic instability, and invasion [239]. While therapies such as radiation aim to exploit ROS-induced cell death, GB cells often resist by enhancing antioxidant defenses [240]. Considering this, Yang *et al.* developed a hollow manganese dioxide (h-MnO_2) nanosystem aimed at alleviating tumor hypoxia by degrading endogenous hydrogen peroxide (H_2O_2) into oxygen and water. The pH-responsive MnO_2 breaks down in the acidic TME. This nanosystem, produced via a silica template method and functionalized with PEG for stability, enables targeted drug delivery, imaging, and TME modulation. It efficiently loaded chlorine e6 (Ce6), a photodynamic agent, and DOX, releasing them in the TME while generating Mn2+ ions to enhance MRI contrast. By producing oxygen, the system improves photodynamic therapy efficacy, which relies on oxygen to generate ROS. *In vivo* studies confirmed effective accumulation of Ce6/DOX-loaded NPs in tumors and kidneys, demonstrating synergistic effects of chemotherapy and photodynamic therapy in reducing tumor mass [205].

Finally, regarding ECM-responsiveness, the interaction between glutathione (GSH) and disulfide bonds (SS) has been exploited [241]. This interaction relies on two characteristics: i) there is a steep GSH gradient between the extracellular environment (micromolar) and the intracellular tumor environment (millimolar), and ii) SS bonds can be cleaved by GSH. Therefore, drug delivery systems that incorporate SS bonds can rapidly release their therapeutic agents inside target cells, significantly improving drug efficacy [206, 242].

This was explored by Tian *et al.*, who developed a redox-sensitive nanocarrier system for targeted curcumin delivery to GB cells by conjugating HA with curcumin via disulfide bonds. This system takes advantage of the high glutathione levels in TMEs, where GSH can cleave disulfide bonds, leading to rapid drug release inside target cells. Their work explored how the MW of HA affects the properties and performance of nanocarriers. The HA-curcumin conjugates formed nanoscale micelles, enhancing curcumin's solubility and stability. Low (50 kDa) and medium (200-500 kDa) MW HA-based micelles showed GSH sensitivity and superior cytotoxicity and cellular uptake in G422 mouse GB cells compared to high MW micelles or free curcumin, indicating their effectiveness for intracellular drug delivery [206].

1.2.2.3. Enhancing ECM degradation

The GB ECM, as previously discussed, is notably dense and complex, being comprised of overexpressed components, including HA, specific collagens, laminin, TN-C, fibronectin, among others (Figure 2). These excessive ECM components make the TME more compact and less flexible, hindering the diffusion of therapeutic agents [243]. Additionally, this dense physical barrier, impedes both T cell infiltration and drug or nanosystem penetration, contributing to immunosuppression and drug resistance [244]. Recent studies suggest that breaking down the tumor ECM or inhibiting its formation can enhance the penetration and accumulation of nanotherapeutics, thereby improving the efficacy of nanomedicines [187]. One approach to address this issue involves degrading key ECM components, which loosens the ECM structure and increases tumor tissue permeability, allowing immune cells to better migrate and infiltrate the tumor [245].

To optimize ECM degradation strategy by targeting the most abundant components of GB ECM, Kiyokawa and colleagues investigated the role of HA degradation in enhancing the effect of oncolytic adenovirus immunotherapy for GB [207]. They used ICOVIR17, a hyaluronidase-expressing oncolytic adenovirus, to target the HA-rich ECM. In murine orthotopic GB models, ICOVIR17 increased tumor-infiltrating $CD8^+$ T cells and macrophages, leading to prolonged animal survival compared to the control virus ICOVIR15 (no hyaluronidase). ICOVIR17 also upregulated programmed cell death protein (PD)-ligand 1 (PD-L1) expression on GB cells and macrophages. *In vitro* experiments showed that high MW HA inhibited adenovirus-induced NF-kB signaling in macrophages, linking HA degradation to macrophage activation. Combining ICOVIR17 with anti-PD-1 antibody therapy further extended survival in GB mice models, with some animals achieving long-term remission. Mechanistic studies revealed that $CD4^+$ T cells, $CD8^+$ T cells, and macrophages all contributed to the efficacy of the combination therapy. This treatment induced pro-inflammatory

tumor-associated macrophages and enhanced tumor-specific T cell cytotoxicity both locally and systemically [207].

Similarly, Shukla *et al.* addressed ECM as barrier to NP penetration through the functionalization of human serum albumin NPs (HSANPs) with collagenase. These collagenase-modified NPs were loaded with gemcitabine (CG-HSANPs) to overcome the limitations of its short half-life and dose-dependent side effects. *In vitro*, CG-HSANPs demonstrated comparable cytotoxicity with uncoated NPs or free drug but exhibited improved tumor spheroid penetration. Also, CG-HSANPs induced higher levels of nuclear fragmentation, ROS generation, and mitochondrial membrane potential disruption compared to the native drug emphasizing the importance of ECM degradation in enhancing drug delivery efficacy [208].

1.2.2.4. Preventing ECM degradation

The invasive nature of GB is closely associated to its ECM, which facilitates tumor cell migration and invasion [225]. Given the important role of MMPs in GB, various therapies targeting their inhibition have been attempted [246-248]. Several synthetic MMP inhibitors were shown to decrease MMP activity, such as the hydroxamate-based batimastat and marimastat, which bind the MMPs' zinc atom and effectively suppress their functionality [220, 249-252]. However, clinical studies have failed to demonstrate significant impact of these molecules on patient progression-free and overall survival. This was attributed to the molecules' low aqueous solubility and potential side effects [222, 253-255]. As a result, research focusing on MMPs and ECM remodeling as actively targeted therapeutic strategies has been relatively limited [256]. Despite these past challenges, recent strategies have sought innovative ways to target MMPs. While traditional hydroxamate-based MMP inhibitors faced clinical setbacks, nanotechnology offers a promising alternative. By improving solubility and minimizing side effects, fields where NPs excel, nanosystems have the potential to reinvigorate these inhibitors and enable more effective ECM-targeted therapies.

The scorpion venom-derived chlorotoxin (CTX) is a more modern and less synthetic alternative for the old hydroxamate-based MMP inhibitors [257] and has demonstrated active targeting of GB cells [258]. Agarwal *et al.* functionalized PLGA NPs with CTX (with high affinity for MMP-2 and chloride channels overexpressed in GB cells) to deliver morusin, a chemotherapeutic agent with poor bioavailability. These CTX-functionalized NPs (PLGA-MOR-CTX) effectively crossed the BBB and presented anti-cancer effects in U-87 and GI-1 human GB cell lines through apoptosis induction, ROS generation, and MMP inhibition, with low toxicity to normal neuronal cells [209].

Islam and colleagues synthesized amphiphilic peptides containing a brain-targeting ligand (HAIYPRH or CKAPETALC) conjugated with an MMP-9 inhibiting peptide (CTTHWGFTLC), linked by glycine spacers and conjugated to cholesterol at the N-terminus [210]. The amphiphilic peptide-cholesterol (c-GGGCTTHWGFTLCHAIYPRH) formed NPs able to cross an *in vitro* BBB hCMEC/D3 transwell model while showing low toxicity in HeLa cells. The authors also demonstrated an efficient inhibition of MMP-9 activity in an acellular *in vitro* setting [210].

CHAPTER II

AIM

CHAPTER II – AIM

GB remains one of the deadliest cancers, with a notably low survival rate relative to its prevalence. Despite being extensively studied, therapeutic options for GB have stagnated over the past two decades. More recently, potential therapeutical strategies have emerged, many relying on nanotechnology, bringing new hope to GB patients. However, their impact on overall survival remains limited.

GBs overexpress MMPs, particularly the secreted gelatinases MMP-2 and MMP-9, as well as the transmembrane MMP-14. This overexpression enhances the tumor's ability to remodel the surrounding ECM, facilitating its invasion and spread. Moreover, despite its inter- and intra-tumor heterogeneity, most GB tumors overexpress the EGF receptor, contributing to their survival, proliferation and aggressive behavior.

Based on the above, the **MAIN AIM** of this work was to develop a multifunctional “Swiss-knife” therapeutical approach for GB through the design of a novel nanotechnological tool that enables:

i) to enhance BBB crossing;

ii) to entrap and accumulate NPs at the tumor site;

iii) to locally inhibit MMP activity, thus suppressing tumor invasiveness.

To achieve this aim, the following tasks were pursued:

1) Creation of a cleavable molecular construct, through sequential Michael addition and carbodiimide chemical reactions, followed by its purification and characterization. This construct, designed to specifically target the BBB and GB microenvironment, was comprised of a transferrin-mimicking peptide (TfP), PEG and an MMP-14-cleavable peptide (MMP14cp);
2) Production and characterization of nanostructured lipid carriers (NLCs) loaded with batimastat, a potent MMP inhibitor, by the ultrasonicator-assisted hot homogenization technique;
3) Dual functionalization and characterization of batimastat-loaded NLCs with EGF and the construct (TfP-PEG-MMP14cp) through carbodiimide chemistry;
4) *In vitro* cytotoxicity assessment of the developed nanosystem on physiologically relevant cell lines: NHA (normal human astrocytes); U-87, U-251 and T98G (GB cell lines); hCMEC/D3 (human cerebral microvascular endothelial cell line); and HEPG2 (hepatocellular carcinoma cell line);
5) *In vitro* BBB permeability assessment of the developed nanosystem with an hCMEC/D3 transwell model;
6) *In vitro* MMP inhibitory capacity assessment of the developed nanosystem through zymographies of the secretomes of astrocytic and GB cell lines (NHA, U-87, U-251, T98G).

CHAPTER III

MATERIALS AND METHODS

This chapter was based on the methods of the original article *“Nanostructured lipid carriers for enhanced batimastat delivery across the blood–brain barrier: an in vitro study for glioblastoma treatment*” (Annex II) published in Drug Delivery and Translational Research (2025).

CHAPTER III – MATERIALS AND METHODS

3.1. Materials

Gelucire® 44/14 and Compritol® 888 ATO were bought from Gattefossé (Lyon, France). Miglyol® 810N was acquired from CREMER OLEO (Hamburg, Germany), 1,2-Distearoyl-sn-glycero-3-phosphorylethanolamine (DSPE) from Tokyo Chemical Industry (Zwijndrecht, Belgium), and Tween® 80 from Avantor (Easton, Pennsylvania). TfP (THRPPMWSPVWPC) and MMP14cp (SGRIGFLRTA) were synthesized by Genscript Biotech (Rijswijk, Netherlands). N-(3-Dimethylaminopropyl)-N′-ethylcarbodiimide hydrochloride (EDC), N-Hydroxysuccinimide (NHS), Tris(2-carboxyethyl)phosphine hydrochloride (TCEP), 4-(2-hydroxyethyl)-1-piperazineethanesulfonic acid (HEPES) and batimastat were bought from Sigma-Aldrich (Strasbourg, France). Maleimide-PEG-COOH with 10 kDa was received from RuixiBiotech (Shaanxi, China). The micro-BCA™ protein assay kits and the Spectrum™ Spectra/Por™ 3 RC Dialysis Membrane Tubing 3.5 kDa were bought from ThermoFisher Scientific (Porto Salvo, Portugal). DC™ protein assay kits were acquired from Bio-Rad (California, USA) and cOmplete™, Mini, EDTA-free Protease Inhibitor Cocktail from Roche (Basel, Switzerland). The primary antibodies anti-EGFR [EGF Receptor (D38B1) XP® Rabbit mAb #4267] and anti-TfR [Transferrin Receptor/CD71 (D7G9X) XP® Rabbit mAb #13113] were purchased from Cell Signaling Technology (Massachusetts, USA). The secondary antibody anti-rabbit [Amersham ECL Mouse IgG, HRP-linked whole Ab (sheep)] was acquired from Cytiva (Massachusetts, USA). The NHA and T98G cell lines were purchased from ATCC® (Virginia, USA) and the U-87 cell line from Biochrom (Berlin, Germany). The U-251 cell line was kindly provided by the Cell Bank of IPATIMUP (Porto, Portugal) and the hCMEC/D3 cells were purchased from Cedarlane (Burlington, Canada).

3.2. Functionalization construct synthesis

The molecular construct synthesis here optimized was adapted from carbodiimide and maleimide-cysteine reactions previously published by our group [202]. We first started by the PEG-TfP conjugation, where TfP and Maleimide-PEG-COOH conjugation was conducted through a thioether bond between TfP's cysteine and the PEG's maleimide moiety with a Michael addition reaction [259]. First, TfP and TCEP (1:10 molar ratio) were left to react at room temperature for 1 h. Then, a freshly prepared PEG solution was added (1:1 molar ratio of PEG:TfP), and the resulting mixture was left overnight at 4 °C. The TfP-PEG-COOH solution was then diluted 1:50 (v/v) to 5 mL in distilled water and purified through dialysis in a 3.5 kDa membrane for 24 h, with a sink volume of 5 L of distilled water and water changes at 2, 4 and 8 h. The purified TfP-PEG-

COOH was thereafter subjected to carbodiimide chemistry with EDC and NHS [260, 261]. Briefly, the polymer-peptide molecule, EDC and NHS were mixed at a 1:10:10 molar ratio, respectively, and left to react for 1 h. Then, MMP14cp was added (1:1 molar ratio to TfP-PEG) and left to react overnight at 4 °C. The final molecular construct is again purified by dialyzing against 5 L of distilled water in a 3.5 kDa membrane for 24 h with water changes at 2, 4 and 8 h. All reactions occurred with HEPES buffer at pH 7.00.

3.3. Construct conjugation efficiency

PEG-TfP, PEG-MMP14cp and MMP14cp-PEG-TfP conjugation efficiencies were assessed through a micro-BCA™ assay on purified samples following the manufacturer's protocol [262]. Briefly, a 25:24:1 (v/v) ratio of micro-BCA™ reagents A:B:C were combined to create a BCA™ working solution, which was then added to the samples at a 1:1 (v/v) ratio. The resulting mixture was incubated for 2 h at 37 °C and analyzed at 562 nm in a Synergy MX microplate reader (BioTek Instruments Inc., USA).

3.3.1. Proton nuclear magnetic resonance

Proton nuclear magnetic resonance (^{1}H-NMR) measurements were conducted for all samples to validate the different conjugations. The previously prepared samples were frozen overnight at -80 °C and lyophilized over 2 days. Samples were then resuspended in the same volume of deuterium oxide and 700 µL the solutions were transferred to NMR tubes. The samples were then measured in a Bruker Ascend III 400 Hz 9.4 T spectrometer (Bruker Corporation, USA) at room temperature. Chemical shifts are reported in ppm (δ units) and were referenced to the solvent signal.

3.3.2. Gel-permeation chromatography

For qualitative validation of the conjugation success, the MW of the conjugates and pure PEG solutions were calculated by gel permeation chromatography/size exclusion chromatography (GPC/SEC). The analysis was performed using a tri-module system: OMNISEC Reveal, OMNISEC Resolve and OMNISEC Software. Separations were performed at 30 °C in PL aqua gel-OH mixed columns (with porous hydroxy methacrylate polymer). The mobile phase consisted of 0.05 M $NaSO_4$ at a flow rate of 1 mL/min. Samples were filtered through 0.45 µm cellulose acetate filters, and 100 µL of the sample were automatically injected by the autosampler at room temperature. All modules were controlled by the OMNISEC software, which also analyzed sample data.

3.4. NLC synthesis

The lipidic NPs were prepared through an ultrasonicator-assisted hot homogenization technique [263]. Briefly, a lipid phase comprised by Gelucire® 44/14, Compritol® 888 ATO, Miglyol® 810N, DSPE and Tween® 80, and an aqueous phase of double-distilled water were separately heated to 85 °C in a water bath. The latter was then vigorously poured into the former, and the resulting microemulsion was homogenized using a probe-sonicator (VC50 50 W model from Vibra-Cell with a 3 mm probe) at 100% for 15 minutes to obtain a nanodispersion. To synthesize batimastat-encapsulating NLCs, a varied amount of batimastat (dissolved in absolute ethanol at 1 mM) was added to the organic phase during the melting step. All formulations were left to cool down at room temperature and stored at 4 °C. Fluorescent DiO-labeled NLCs were prepared using the same methodology with the addition of 25 µg/mL of DiO (0.5 mg/mL in absolute ethanol) in the organic phase.

For the optimization process, different formulations were tested, regarding the ratio of solid to liquid lipids, amount of surfactant, amount of DSPE, sonicator tip and sonicated volume, as specified in **Table 2**. The best formulations, based on average diameter and polydispersity index (PDI), were selected to proceed with functionalization.

Table 2. *Summary of the iterative optimization process for blank NLCs.*

NLC ID	Gelucire 44/14 (mg)	Compritol 888 ATO (mg)	Miglyol 810N (mg)	Tween 80 (mg)	DSPE (mg)	Solid:Liquid lipid ratio
A	70	6	10	12	2	0.13
B	70	6	10	12	5	0.12
C	70	6	10	12	10	0.12
D	70	6	10	12	15	0.11
F	70	0	10	12	5	0.13
G	70	0	10	12	10	0.13
H	70	0	10	12	15	0.12
J	0	70	10	12	10	0.13
K	70	6	20.25	10	5	0.25
L	70	6	20.25	5	5	0.25
M	70	6	40.5	10	5	0.5
N	70	6	40.5	5	5	0.5

3.5. NP functionalization

NP functionalization with the construct and EGF was achieved with a carbodiimide reaction in a similar manner as described for the construct synthesis [202]. Briefly, the carboxylic acids of both MMP14cp-PEG-TfP and EGF (1:1 molar ratio) were activated with EDC and NHS at a 1:10:10 molar ratio for 1 h, after which the aminated NLCs were added, reacting overnight at 4 °C. The functionalized suspensions were washed with double-distilled water by centrifugation in an Amicon® Ultra 15 mL centrifugal filter at 3600 rpm for 30 minutes. All reactions occurred with HEPES buffer at pH 7.00.

3.6. NLC physicochemical characterization

3.6.1. Average size, PDI and zeta-potential

NLC formulations' average diameter, PDI and zeta-potential were analyzed using dynamic and electrophoretic light scattering (DLS/ELS) (Zetasizer Nano-ZS ZEN3600 with a DTS1060C cuvette and Zetasizer v7.13 software (Malvern Panalytical). All samples were diluted 1:50 (v/v) with distilled water to obtain an appropriate count rate (200,000-400,000 counts per second) and were measured at room temperature. The samples were allowed to rest for 15 seconds between ELS measurements to remove any inter-measurement motility influence. Every formulation was measured three times in sequence.

3.6.2. Surface amine quantification

The quantity of available reactive primary amines at the NP surface was qualitatively evaluated through a fluorescamine assay [264]. Briefly, 100 µL of double-distilled water is inserted into a well of a 96-well plate. Afterwards, 100 µL of the sample and 50 µL of fluorescamine [0.3 mg/mL in dimethyl sulfoxide (DMSO)] is added. After 15 minutes of incubation in the dark, the emitted fluorescence (400/460 nm, excitation/emission) is measured in a Synergy MX microplate reader (BioTek Instruments Inc., USA).

3.6.3. NP morphology

Size and morphology were further analyzed by TEM at the i3S Histology and Electron Microscopy platform, with a JEM-1400 microscope (JEOL, Japan) at an accelerating voltage of 120 kV. Briefly, samples were prepared by pipetting 10 µL of an NLC formulation onto a 300-mesh nickel grid, using uranyl acetate to increase contrast.

3.6.4. Batimastat encapsulation efficiency

Batimastat was quantified by high performance liquid chromatography (HPLC) to assess the encapsulation efficiency (EE%) and drug loading (DL) of the NLCs through a direct method [265]. The NLC formulations were centrifuged in an Amicon® Ultra 15 mL centrifugal filter at 3600 rpm for 30 minutes. The resulting supernatant was discarded, and the pellet was resuspended in DMSO, destroying the NPs and solubilizing batimastat. The chromatography was performed by reverse-phase HPLC in a Hitachi 7000 (Merck, Germany) at a flow rate of 1 mL/min, with a Nova-Pak C18 4 µm column (Waters, USA) as the stationary phase and 50% water 50% acetonitrile as the mobile phase. The analyte was measured at a wavelength of 256 nm and was injected at a volume of 50 µL per sample. The %EE and DL were calculated using **Equation 3.1** and **Equation 3.2**, respectively.

Equation 3.1: $$\%EE = \frac{Recovered\ batimastat\ (mg)}{Total\ batimastat\ (mg)} * 100$$

Equation 3.2: $$DL\ (\mu g/mg) = \frac{Recovered\ batimastat\ (\mu g)}{Total\ lipid\ amount\ (mg)} * 100$$

3.6.5. Surface functionalization efficiency

The functionalization efficiency was quantified by both micro-BCA™, with samples in a 2% sodium dodecyl sulfate (SDS) solution [266], and ^{1}H-NMR, as previously explained for MMP14cp-PEG-TfP conjugation efficiency (Section 3.3). Functionalized NLCs were physicochemically characterized in the exact same manner as their non-functionalized counterparts.

3.6.6. NLC stability

The NLC stability over time was analyzed by DLS/ELS, for up to 2 months, in 5 different physiologically relevant fluids: ddH_2O, 0.09% NaCl, phosphate buffered saline (PBS), Dulbecco's modified Eagle's medium (DMEM) and DMEM supplemented with 10% (v/v) fetal bovine serum (FBS). After producing the NLCs, all formulations were washed by centrifugation in an Amicon® Ultra 15 mL centrifugal filter at 3600 rpm for 30 minutes. Then, the pellets were resuspended in each of the previously referred fluids at the same NP concentration as the original formulations. All samples were stored at 4 °C, and a 20 µL aliquot was removed at 0, 3, 7, 14, 21, 28, 35 and 45 days. The aliquots were diluted 1:50 (v/v) with distilled water to obtain an appropriate count rate (200,000-400,000

counts per second) and were measured in the Zetasizer at room temperature. The samples were allowed to rest for 15 seconds between ELS measurements to remove any inter-measurement motility influence. Every formulation was measured three times in sequence.

3.7. Cell culturing

The GB cell lines, U-87, U-251 and T98G and the non-tumor astrocytic cell line NHA were routinely maintained in DMEM high-glucose (4.5 g/L) with stable glutamine and sodium pyruvate, supplemented with Gibco™ heat-inactivated FBS 10% (v/v), penicillin–streptomycin (1% v/v) and amphotericin B (0.5% v/v). hCMEC/D3 cells were cultured in endothelial basal medium-2 (EBM-2) supplemented with FBS (5% v/v), penicillin–streptomycin (1% v/v), hydrocortisone (1.4 µM), ascorbic acid (5 µg/mL), chemically defined lipid concentrate (1% v/v), 4-(2-hydroxyethyl)−1-piperazineethanesulphonic acid (10 mM) and basic fibroblast growth factor (1 ng/mL). This last supplement was added extemporaneously in the culture medium. Cells were maintained in a humidified incubator at 37 °C with 5% CO_2 and 95% relative humidity. Cell culture medium was changed every 2 to 3 days, depending on cell confluence.

3.8. Cell viability assays

Cells (5×10^3/well) were plated on a 96-well transparent plate and allowed to adhere for 24 h at 37 °C. Cells were then treated for 24, 48 or 72 h with supplemented media (untreated control), free batimastat in concentrations ranging from 0 to 100 nM, or NLC formulations at concentrations equivalent to batimastat at 0 to 100 nM. To evaluate cell response to the treatments, PrestoBlue™ cell viability assay was conducted as previously described by our group [267]. Briefly, cells were washed three times with the non-supplemented media and then incubated with PrestoBlue™ reagent diluted in supplemented medium (10% v/v) for 45 minutes at 37 °C in the dark. Fluorescence was then measured at 560 nm and 590 nm excitation and emission wavelengths in a SpectraMax iD3 multi-detection microplate reader (Molecular Devices, USA) in five technical replicates, excluding the background.

3.9. BBB permeability assay

The methodology for establishing an *in vitro* BBB model was adapted from a previously published protocol [175]. Prior to cell seeding, 24-well Transwell inserts were treated with 50 µL of rat tail collagen type I solution (50 µg/mL in 20 mM acetic acid) for 1 h at 37 °C, followed by two PBS washes. hCMEC/D3 cells

were plated onto the apical chamber of the inserts at a density of 7.5×10^3 cells per well in 400 µL of EBM-2 medium and the basolateral chamber was filled with 1 mL of medium. The model was incubated at 37 °C for 8 days, with media replacement every 48 h. By day 8, the hCMEC/D3 cells formed a confluent monolayer, at which point the permeability study was initiated. The integrity of the cellular barrier was assessed every 48 h by measuring the TEER using a Millicell ERS-2 endothelial Volt-Ohm meter (Merck Millipore, USA). The resistance of a cell-free insert in the same conditions was subtracted from each measurement to obtain the true TEER value. The permeability assay was conducted in the apical-to-basolateral direction, as DiO-labeled NPs, either functionalized or unfunctionalized, suspended in Hanks' balanced salt solution (HBSS, 400 µL at 600 µg/mL) were introduced to the apical compartment. The experiment was performed at 37 °C in an orbital shaker incubator set to 100 rpm. At specific time points (1, 4, 12 and 24 h), 200 µL aliquots were collected from the basolateral chamber and replaced with 200 µL of pre-heated HBSS. The fluorescence intensity of these samples was quantified using a SpectraMax iD3 multi-detection microplate reader (Molecular Devices, USA) at excitation and emission wavelengths of 471 nm and 511 nm, respectively. All experiments were conducted in triplicate.

3.10. Collection of conditioned media

Cells (3×10^5/well) were plated on a 6-well transparent plate, with 3 mL of supplemented medium, and allowed to adhere for 48 h at 37 °C. Cells were then treated for 24, 48 or 72 h with 1.5 mL of non-supplemented media (untreated control), NLC formulations at a concentration equivalent to 50 nM of batimastat, or free batimastat (50 nM), after which the media was collected. Following a centrifugation at 13,000 rpm for 10 minutes, the pellet was discarded, and the supernatant concentrated ten-fold by centrifugation at 3500 rpm for 10 minutes, at 4 °C, in an Amicon® Ultra 4 mL centrifugal filter (30 kDa MW cutoff). The conditioned media (secretomes) were then stored at −80 °C.

3.11. Gelatin zymography

Total protein content of each secretome was quantified with a DC™ protein assay kit. 15 µg of protein was mixed with sample loading buffer [10% SDS, 4% sucrose and 0.03% bromophenol blue in 0.5 M Tris-HCl pH 6.8] at a 2:1 (v/v) ratio. Separation was achieved through electrophoresis with a 10% polyacrylamide gel, containing 0.1% gelatin as substrate, at 80 V for 2 h, as previously described [268, 269]. The gels were then washed twice with 2% Triton X-100 for 30 minutes to remove the SDS, washed with ddH_2O, and further incubated for 16 h at 37 °C with MMP substrate buffer (10 mM $CaCl_2$, 0.5% NaN_2 in 50 mM Tris-HCL pH 7.5).

Lastly, the gels were stained with Coomassie Blue for 30 minutes and destained until the bands were clear. Gel images and band density calculations were obtained with a GS-900 Calibrated Densitometer and the Image Lab 6.1 software (Bio-Rad, USA).

3.12. Preparation of protein cell lysates

Cells (3×10^5/well) were plated on a 6-well transparent plate with 3 mL of supplemented medium and allowed to adhere for 48 h at 37 °C. Before lysate collection, radioimmunoprecipitation assay (RIPA) lysis buffer was prepared by supplementation with cOmplete™, Mini, EDTA-free Protease Inhibitor Cocktail (1:6, v/v). Once cells were confluent, the plate was placed on ice, the culture medium removed, and cells washed twice with cold PBS. 100 µL of cold supplemented RIPA lysis buffer was added to the cells, which were then kept on ice for 10 minutes, swirling the plate occasionally. The cell monolayer was then scraped with a cell scraper, and the lysate was collected. Samples were centrifuged at 14000 g for 15 minutes to remove debris, and the supernatant was collected. The lysates were then either utilized or stored at -20 °C until further analysis.

3.13. Western Blot

Total protein content of cell lysates was determined using the DC™ protein assay kit. 10 µg of protein was mixed with 4x Laemmli Sample Buffer at a 3:1 (v/v) ratio and 10% (v/v) of 1 M dithiothreitol. Protein separation was achieved through electrophoresis with a 7.5% polyacrylamide gel at 30 mA for 2.5 h and gels were transferred to nitrocellulose membranes overnight with 30 V at 4 °C [270]. The membranes were then blocked in 4% Milk with 0.1% TBS-Tween at room temperature for 1 hour, followed by incubation with the primary antibody, anti-EGFR or anti-TfR, diluted 1:1000 in 4% milk with 0.1% TBS-Tween overnight at 4 °C. The membranes were then washed in TBS-Tween 0.1% 5 times for 5 minutes each. Subsequently, they were incubated with anti-rabbit secondary HRP-linked antibody diluted 1:5000 in 4% Milk with 0.1% TBS-Tween for 1 hour at room temperature, followed by another set of washes in TBS-Tween 0.1%. For signal detection, membranes were incubated in the dark with H_2O_2:luminol 1:1 (v/v) for 2 minutes. Chemiluminescence was detected and captured on a ChemiDoc.

3.14. Statistical analysis

The results are presented as the mean ± standard deviation from at least three independent experiments. Statistical analyses were conducted using a one-way analysis of variance (ANOVA) followed by Holm-Sidak's multiple comparison test or Kruskal–Wallis test followed by Dunn's post hoc test to compare the experimental groups. Differences were deemed statistically significant at $*p < 0.05$, $**p < 0.01$, $***p < 0.005$ or $****p < 0.001$. All statistical analyses were carried out using GraphPad Prism 8.0.1 software (GraphPad Software, USA).

CHAPTER IV

RESULTS AND DISCUSSION

This chapter was based on the results and discussion of the original article *“Nanostructured lipid carriers for enhanced batimastat delivery across the blood–brain barrier: an in vitro study for glioblastoma treatment*” (Annex II) published in Drug Delivery and Translational Research (2025).

CHAPTER IV – RESULTS AND DISCUSSION

4.1. Chemical synthesis of the targeting molecular construct

The molecular construct, MMP14cp-PEG-TfP, was designed to provide a cleavable moiety in its link to the NP, MMP14cp, and to permeate the BBB, through its TfP moiety. Binding both peptides, the COOH-PEG-maleimide molecule was designed to have a MW of 13 kDa, in order to conceal the functionalization of EGF, which has a lower MW (6.4 kDa). First, the PEG-maleimide was chemically conjugated with the cysteine-terminated TfP (**Figure 7a**) following a common thiol-maleimide click chemistry. The addition of TCEP, a reducing agent, ensured that no disulfide bridge cross-linking was present between the peptides. The conjugation's efficiency, assayed through micro-BCA™, was 66 ± 20%, presenting a high variability between replicates. As the room temperature under which the reactions occurred was not controlled, its variability could have led to different rates of maleimide hydrolysis, which degrades the maleimide and prevents its reaction with thiols [271]. Nonetheless, this efficiency was considered to be acceptable since its upper limit was very close to other optimized thiol-maleimide reactions described in the literature, between 70% to 90% [202, 271]. Additionally, GPC analysis showed a reproducible increase in MWs after the conjugation reaction, consistent with the expected peptide MW of 1.6 kDa (**Figure 7b**). To further confirm the conjugation, an ^{1}H-NMR analysis was conducted on both the reagents and the dialyzed conjugate (**Figure 7c**). The NMR chemical shifts between δ = 2.9 ppm and 3.1 ppm, which are attributed to a carbon linked to another carbon and to an aromatic ring [272, 273], exhibited low intensity in the pure PEG sample and high intensity in the dialyzed conjugate. This indicates the presence of the peptide's amino acid side chains in the final product (conjugate). Before proceeding with the full construct conjugation, the PEG-MMP14cp bound was also characterized, following a typical NHS-assisted carbodiimide reaction strategy. The conjugation efficiency could not be assessed with micro-BCA™ due to the unexpected interference of undialyzed NHS, which reacted colorimetrically with the assay's copper-based agents. Nevertheless, similarly to PEG-TfP, GPC analysis of the conjugate showed a MW increase compared to the pure polymer, consistent with the MMP14cp's MW of 1.1 kDa (**Figure 7b**). Additionally, ^{1}H-NMR analysis of the dialyzed conjugate showed an increase in chemical shift at an identical δ = 2.9-3.1 ppm, suggesting the presence of the aromatic rings of MMP14cp in the final product (**Figure 7c**). The final construct was prepared following the same reaction procedure using PEG-TfP instead of PEG. The conjugation efficiency, assessed using micro-BCA™, was 81 ± 4%, which is at the reported upper limits of carbodiimide chemistry [202, 274, 275]. GPC analysis showed an increase in MW consistent with the presence of both peptides, totaling a MW of 2.7 kDa (**Figure**

7b). The analysis of the ^{1}H-NMR spectra of the dialyzed conjugate indicated the previously stated presence of histidine, tryptophan and phenylalanine residues in the molecular construct, evidenced by the increased chemical shift at δ = 2.9-3.1 ppm (**Figure 7c**).

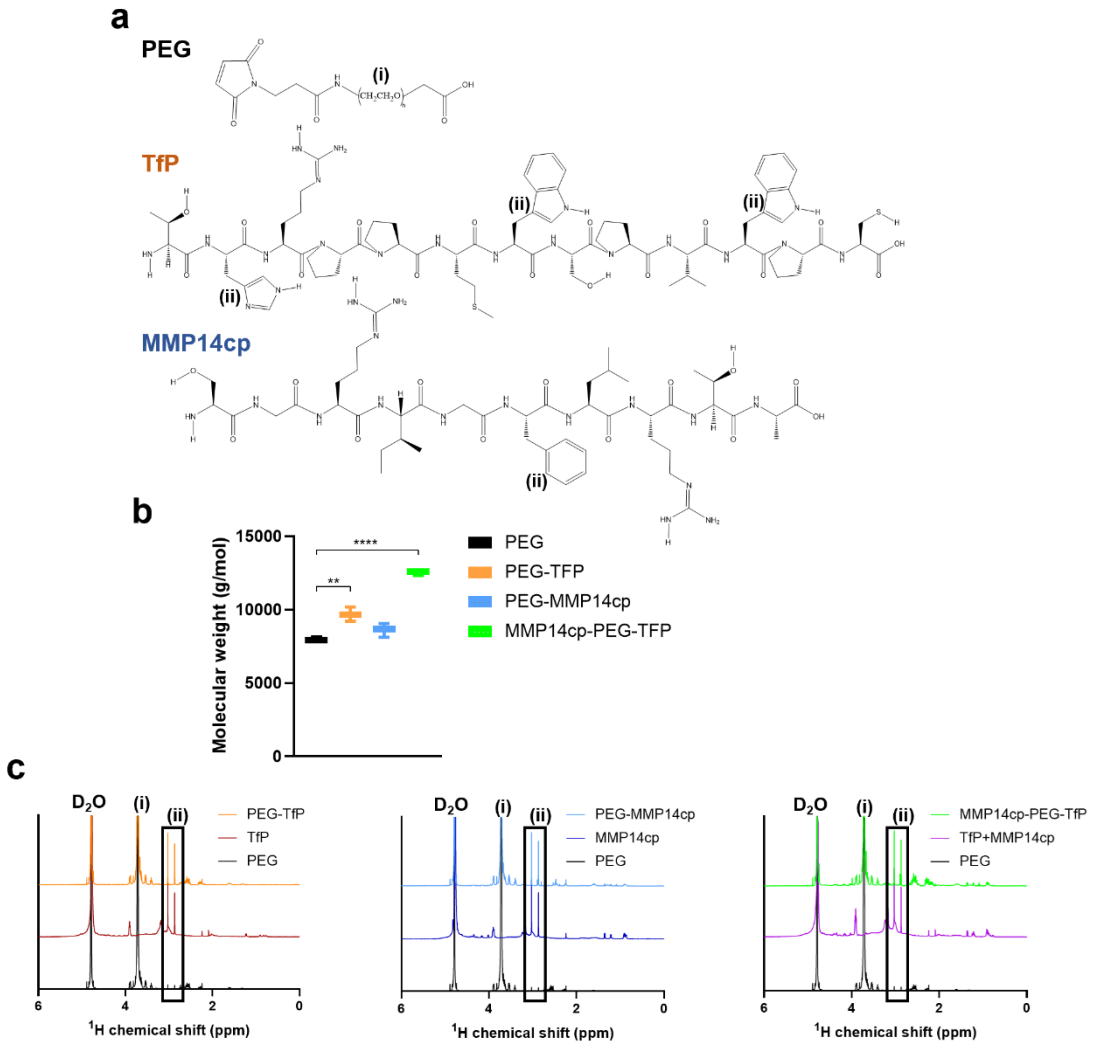

Figure 7. *Conjugation and characterization of the molecular construct for NP functionalization. a) Chemical structure of PEG, TfP and MMP14cp. b) MW of MMP14cp-PEG-TfP reaction steps, determined by GPC analysis. Results are expressed as mean ± SD of 3 independent experiments. **p < 0.005, ****p < 0.0001. c) ^{1}H-NMR spectra of PEG, peptide(s) and purified PEG-peptide(s) for the molecular construct conjugations, PEG-TfP, PEG-MMP14cp and MMP14cp-PEG-TfP. Experiments were conducted in triplicate. D_2O – deuterium oxide, (i) C–C-O at 4.7 ppm, (ii) C–C-C-aromatic ring at 2.9–3.1 ppm.*

4.2. Nanostructured Lipid Carrier (NLC) production and characterization

All NLC formulations were synthesized following an ultrasound-assisted hot homogenization technique [263]. The hydrophilic and hydrophobic NLC components were first separately heated up to 85 °C (**Figure 8i**). After approximately 5 minutes, both the aqueous and organic phases were vigorously mixed, creating a microemulsion, and posteriorly sonicated, resulting in the tested nanosuspensions (**Figure 8ii**). Blank NLC formulations were functionalized, through carbodiimide chemistry, with EGF and MMP14cp-PEG-TfP at a 1:1 molar ratio (**Figure 8iii**). All versions of the developed formulations were finished with a centrifugal wash, where the removed liquid, containing all unincorporated moieties, was replaced with fresh ddH_2O (**Figure 8iv**).

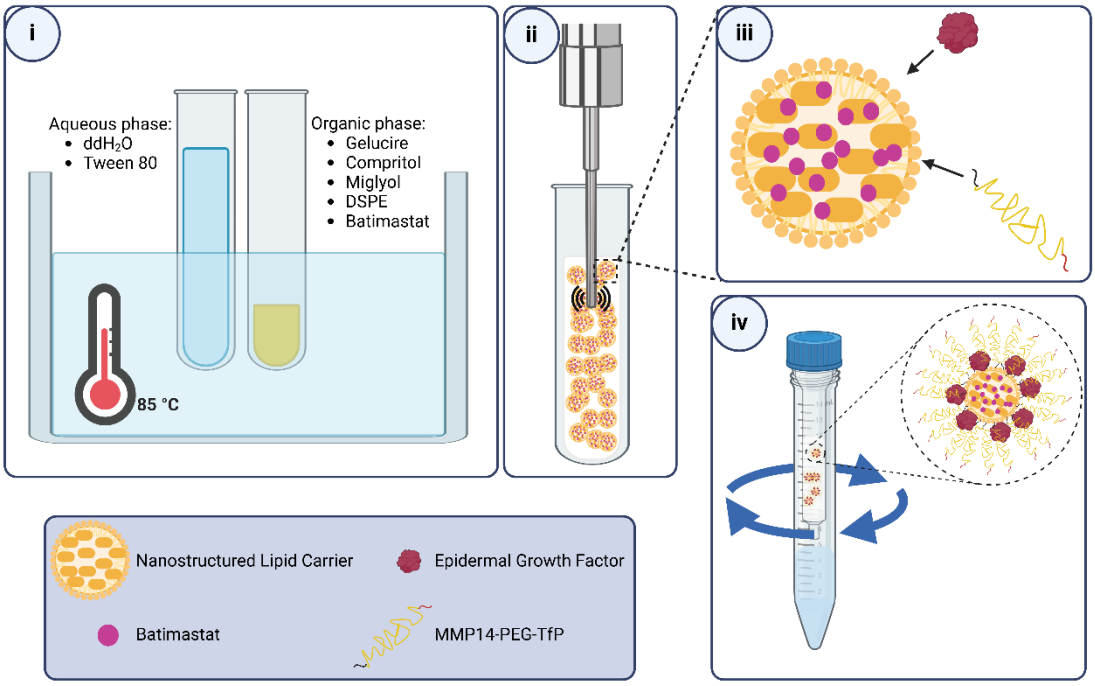

Figure 8. *Batimastat-loaded EGF/MMP14cp-PEG-TfP-functionalized NLC production methodology. (i) Melting; (ii) Sonication; (iii); Functionalization; (iv) Centrifugation wash.*

Table 3. *Physicochemical characterization of the iterative optimization process for blank NLCs.*

Formulation ID	Gelucire 44/14 (mg)	Compritol 888 ATO (mg)	Miglyol 810N (mg)	Tween 80 (mg)	DSPE (mg)	Solid:Liquid lipid ratio	Average diameter (nm)	Polydispersity Index	Zeta potential (mV)	Surface amines (RFU)
A	70	6	10	12	2	0.13	179 ± 59	0.260 ± 0.018	−19.7 ± 1.3	2412 ± 330
B	70	6	10	12	5	0.12	311 ± 77	0.277 ± 0.033	−19.6 ± 2.2	1606 ± 452
C	70	6	10	12	10	0.12	209 ± 35	0.286 ± 0.030	−18.9 ± 1.9	2059 ± 189
D	70	6	10	12	15	0.11	218 ± 123	0.280 ± 0.095	−20.6 ± 0.9	2514 ± 357
F	70	0	10	12	5	0.13	313 ± 240	0.300 ± 0.179	−20.1 ± 2.0	3293 ± 770
G	70	0	10	12	10	0.13	376 ± 277	0.440 ± 0.195	−18.8 ± 6.2	4504 ± 531
H	70	0	10	12	15	0.12	144 ± 45	0.313 ± 0.189	−25.6 ± 3.8	4468 ± 1602
J	0	70	10	12	10	0.13	223 ± 27	0.321 ± 0.047	−18.3 ± 0.9	1144 ± 8
K	70	6	20.25	10	5	0.25	217 ± 57	0.284 ± 0.052	−21.0 ± 2.0	2282 ± 234
L	70	6	20.25	5	5	0.25	324 ± 130	0.312 ± 0.134	−22.9 ± 4.2	520 ± 13
M	**70**	**6**	**40.5**	**10**	**5**	**0.5**	**160 ± 46**	**0.147 ± 0.040**	**−20.6 ± 1.8**	**6078 ± 1203**
N	**70**	**6**	**40.5**	**5**	**5**	**0.5**	**191 ± 39**	**0.125 ± 0.039**	**−20.3 ± 2.4**	**6769 ± 543**

NPs were characterized regarding their average diameter, PDI and zeta-potential, assessed with a Zetasizer, and relative surface amines, evaluated by fluorescamine assay. Results are represented as the mean ± SD of at least 3 independent characterizations. Formulations in bold were selected for functionalization.

4.2.1. Blank NLC optimization

During initial optimization, different combinations and quantities of solid and liquid lipids, surfactant, and the phospholipid DSPE (required for further functionalization) were tested, as depicted in **Table 3**. Ideal benchmarks for average diameter and PDI were chosen as 200 nm, considered to be the standard for blood-to-brain delivery, and <0.2, respectively, to maximize efficient load delivery potential [276, 277]. Zeta potential was optimized to be distant from neutral, as neutral dispersions tend to aggregate due to Wan-der-Walls hydrophobic interactions [278]. Surface amine concentration was intended to be as high as possible, in order to achieve comprehensive functionalization. Considering this, the NLC formulations chosen to continue this work were formulation **M** and formulation **N**.

4.2.2. Batimastat encapsulation

To encapsulate batimastat, 100 µL of this inhibitor (1 mM) dissolved in absolute ethanol were added to the melted lipidic phase prior to sonication (**Figure 8i**). This quantity was chosen to balance batimastat's high inhibitory potential (IC50 described as being between 4-10 nM for most MMPs), and the need to minimize the amount of ethanol introduced to the production process [279, 280]. Evaluation of the encapsulation efficiency and drug loading followed a direct method and were carried out by HPLC. Results showed that both formulations presented an equal capacity for batimastat encapsulation, of 30.5% for Mbat and 30.4% for Nbat. We were also able to observe that an additional 20% of batimastat was lost during the functionalization process, as the formulations fMbat and fNbat presented efficiencies of 10.1% and 10.2%, respectively. These values correspond to a drug loading of 0.42 µg/mg, which is equivalent to 1000 times the reported IC50 of batimastat (**Figure 9a**) [279]. Nasoudi *et al.* reported 4-5000 greater drug loading percentages in polymeric NPs than our lipidic ones but did not provide encapsulation efficiency data [281], while Zhang *et al.* managed to encapsulate 56.72%, without specifying the method used, of the similar compound marimastat in liposomes [282]. In our work, despite the relatively low encapsulation efficiency, the amount of encapsulated drug is enough to provide a biological effect, accordingly to previously reported data [279]. Moreover, regarding physicochemical characteristics, the batimastat-encapsulating formulations showed no significant difference compared to empty NLCs, maintaining the behavior between all formulations (**Figure 9b**).

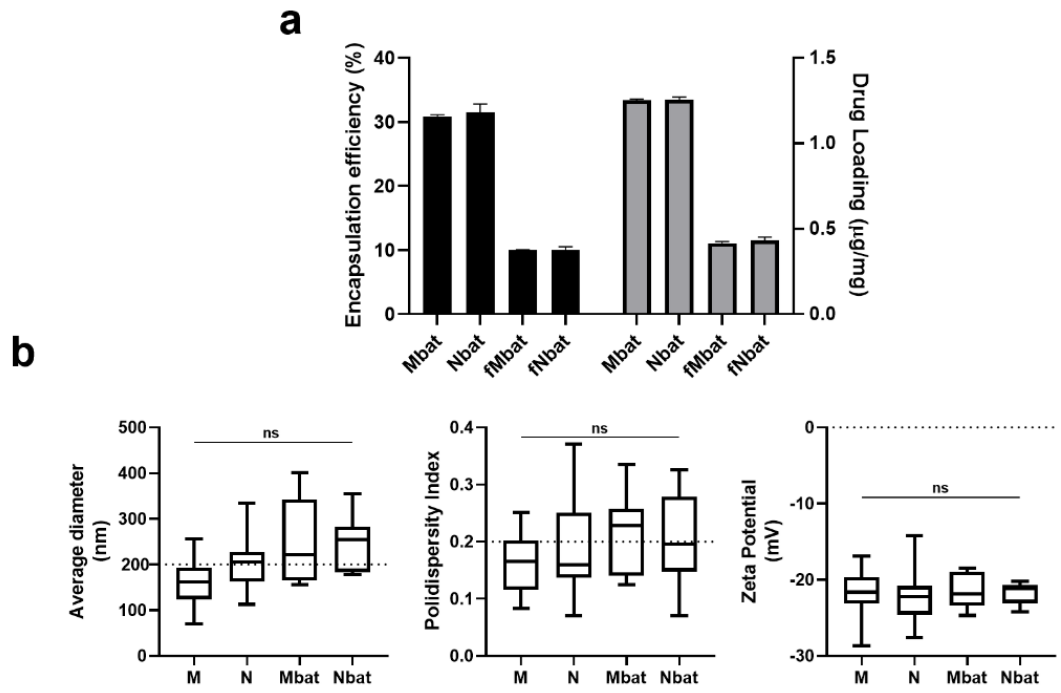

Figure 9. *Encapsulation of batimastat and its effect on the physicochemical characteristics of the NPs. a) Encapsulation efficiency and drug loading of formulations M, N and their functionalized variants, fM and fN, as assessed through the direct method using HPLC. Results are represented as the mean ± SD of 3 independent experiments. b) Physicochemical characteristics of empty formulations (M and N) and NLCs loaded with batimastat (Mbat and Nbat), determined with a Zetasizer. Results are shown as the mean ± SD of at least 5 independent characterizations. Dotted lines represent ideal characteristic benchmarks for NP brain delivery, average size below 200 nm and PDI below 0.2.*

4.2.3. Nanosystem functionalization

NLC functionalization was obtained through the previously described carbodiimide strategy, conjugating the DSPE amines on the NLC surface to the carboxylic terminus of both the molecular construct and EGF (**Figure 8iii**) [283]. As shown in **Figure 10a** and **Figure 10b**, physicochemical characteristics were assayed in a Zetasizer for all possible functionalizations, carried out on both formulations with (Mbat and Nbat) and without batimastat (M and N). Results showed that the average sizes varied significantly between different functionalizations (**Figure 10a**), albeit there were no significant alterations to the non-functionalized suspensions. The PDIs mostly remained slightly above 0.2, indicating almost monodisperse formulations [276]. Most importantly, however, all zeta-potentials were altered, becoming more negative, evidencing that the functionalization had an impact on NP surface charge (**Figure 10b**) [165, 284]. As the zeta-potential is a characterization of the interface between the NP and the surrounding fluid, a change in this interface is expected to induce an alteration in electrical potential [285]. In a previous study, Han *et al.* demonstrated a similar decrease in zeta-potential upon functionalizing their NLCs with transferrin [284].

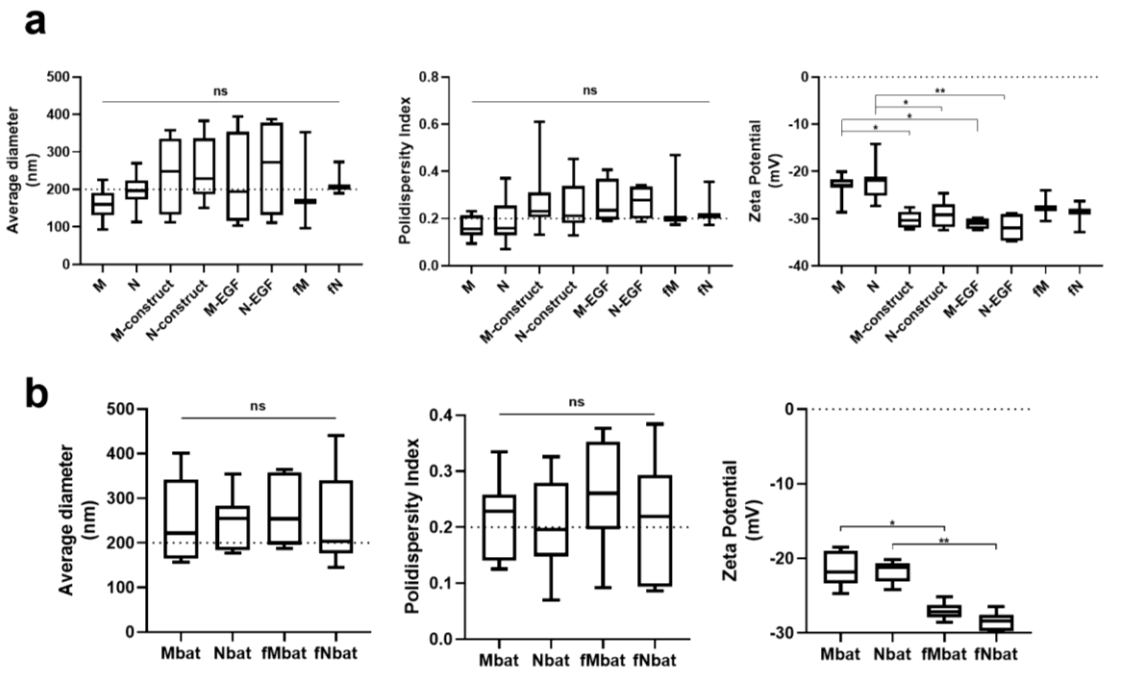

Figure 10. *Functionalization of EGF and MMP14cp-PEG-TfP and its effect on the physicochemical properties of the NPs. All dotted lines represent ideal property benchmarks for NP brain delivery, average size below 200 nm and PDI below 0.2. a) Physicochemical characteristics of empty NLC formulations at different functionalization stages, as measured in a Zetasizer. Results are represented as the mean ± SD of at least 3 independent experiments. *p < 0.05, **p < 0.01. M-construct and N-construct – formulations M and N functionalized with the molecular construct; M-EGF and N-EGF – formulations M and N functionalized with EGF; fM and fN – formulations M and N functionalized with both the construct and EGF; Mbat, Nbat, fMbat and fNbat – formulations M and N encapsulating batimastat and their functionalized variants. b) Physicochemical characteristics of batimastat-encapsulating NLCs before and after functionalization. Results are shown as the mean ± SD of at least 3 independent experiments. *p < 0.05.*

More specifically, our group has previously reported that functionalization of lipidic NPs with the same transferrin peptide here utilized provoked a small decrease in zeta-potential [165]. The efficiency of the functionalization procedure was assessed through a modification of the previously described micro-BCA™ technique, where the addition of a 2% SDS solution was used to mask the lipids' colorimetric influence [266]. The efficiency of fMbat, 85 ± 15%, was expectedly lower than that of fNbat, 92 ± 6%, as the first contained a higher amount of surfactant, resulting in less accessible surface compared to the second. A direct comparison with data reported in the literature is complex owing to the multiple parameters involved, such as the lipids and surfactants utilized, their ratios, the conjugation reaction itself, the molecules being attached, among others. Kebebe *et al.* successfully conjugated cyclic-RGD tumor-targeting peptides to the surface of a gamboic acid-loaded NLC, with the help of EDC/NHS, at a near 100% efficiency [260]. In another study, Du and Li utilized carbodiimide chemistry in an optimization process to functionalize an NLC containing DNA and doxorubicin with bombesin, achieving between 85% to 95% conjugation efficiencies [286]. More recently, a similar conjugation to the one used in this study was conducted

by Teixeira *et al.*, achieving 95% functionalization efficiency in a carbodiimide bond between lactoferrin and stearic acid present in NLCs [287]. Overall, our degree of functionalization is mostly in the range of those described in the aforementioned studies.

4.2.4. Morphological features of the NLCs

Previously synthesized and characterized NLC formulations were further analyzed for morphology using TEM at all stages of encapsulation and functionalization (**Figure 11**). The TEM images revealed that the NPs were generally spherical but displayed slight distortions. This was probably due to the accumulation of smaller NPs around them, which pressed against the inherently labile nature of the lipidic matrices. The formulations tended to aggregate under vacuum but seemed homogenous. Interestingly, two different populations were observed, a larger one with sizes of approximately 300 nm and a smaller one with diameters below 100 nm. The possibility of such a bimodal size distribution occurring has been stated in a comprehensive review by the NLC's inventor Professor R. H. Müller [288]. The presence of these smaller NPs can explain the lower-than-expected encapsulation efficiencies previously detected, as their small diameter may result in their removal during the centrifugation washing procedure.

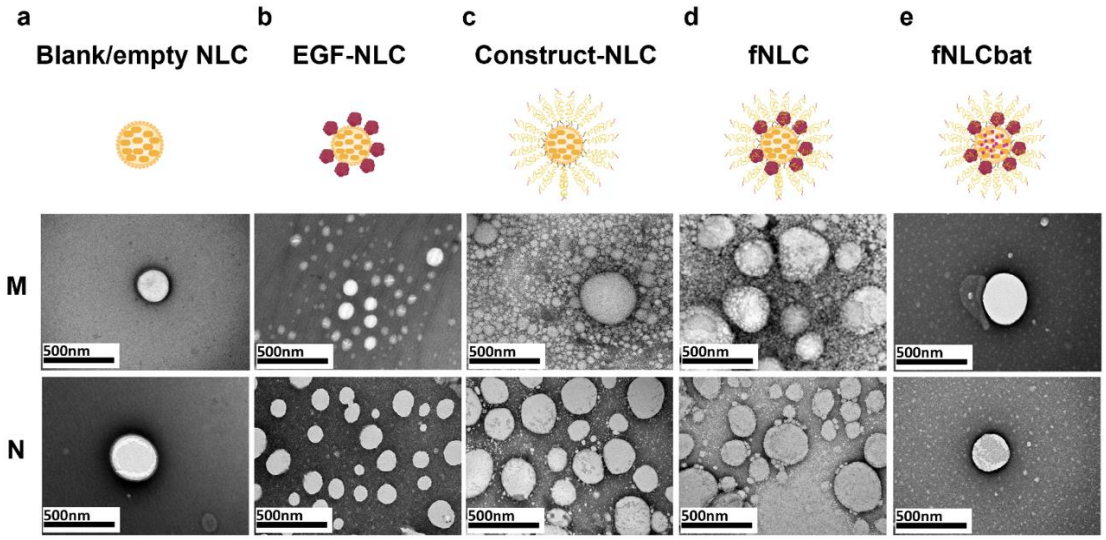

Figure 11. *TEM images of NLC formulations M and N on the different production steps. a) Initial NLCs. b) Construct-functionalized empty NLCs. c) EGF-functionalized empty NLCs. d) Empty NLCs functionalized with both EGF and MMP14cp-PEG-TfP. e) Batimastat-encapsulating construct/EGF-functionalized NLCs.*

4.2.5. NLC stability

The NLC formulations exhibited a good storage stability in terms of particle size, PDI, and zeta-potential over a 30-day storage period at 4 °C (**Figure 12**). The initial average particle size ranged from 200 nm to 350 nm, which is close to the optimal range for BBB-crossing NLCs [276, 277]. Excluding the Nbat formulation, particle size showed minimal variation, with a relative deviation consistently below 15%, reflecting good batch uniformity and stability during storage. Although the percentual PDI values appeared highly variable, due to their small absolute values, they remained consistently low, starting between 0.1 and 0.2, and staying below 0.3 throughout the storage period. This suggests that the NLC formulations maintained their homogeneous nature with no significant particle aggregation or size alterations. Similarly, zeta-potential measurements exhibited robust stability characteristics, maintaining a negative charge of -25 to -30 mV with negligible variation. This magnitude of zeta-potential is considered optimal for maintaining electrostatic repulsion between particles, thereby preventing aggregation and ensuring physical stability [289].

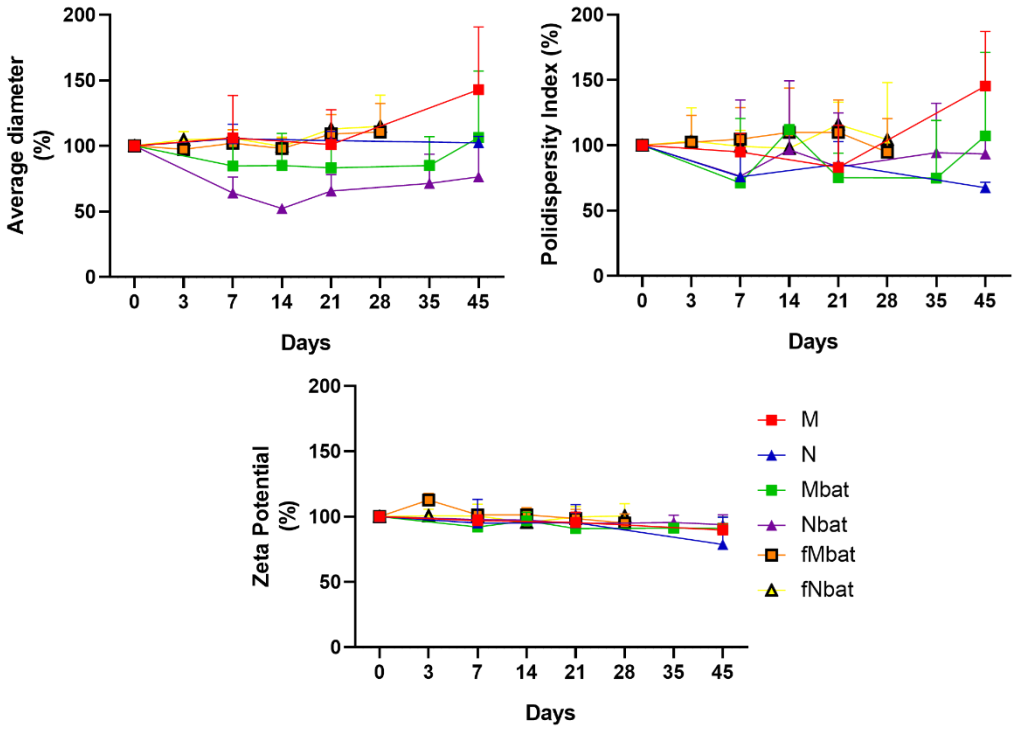

Figure 12. *Physicochemical stability of NLC suspensions M, N, Mbat, Nbat, fMbat and fNbat when stored at 4 °C. All NLC properties were measured periodically with a Zetasizer, for up to 45 days. Results are represented as the mean ± SD of 3 independent experiments.*

The complete formulations, fMbat and fNbat, were also further assessed for stability in different physiologically relevant fluids, including 0.09% NaCl, PBS, DMEM and DMEM supplemented with 10% FBS. Both formulations were found to be stable over 28 days. As shown in **Figure 13**, the formulations presented no variation in zeta-potential, regardless of the fluid. While diameter measurements remained largely consistent, a slight increase in size (although not statistically significant) was observed starting in the third week. Lastly, the PDI values were, again, varying by less than 0.05 units between each assessed timepoint. Overall, the developed NLC formulations exhibited suitable physicochemical characteristics for potential pharmaceutical applications, with promising stability under normal storage conditions. The maintenance of critical quality attributes over the studied period indicates successful formulation development and appropriate selection of lipid matrices, stabilizers and surface chemistry.

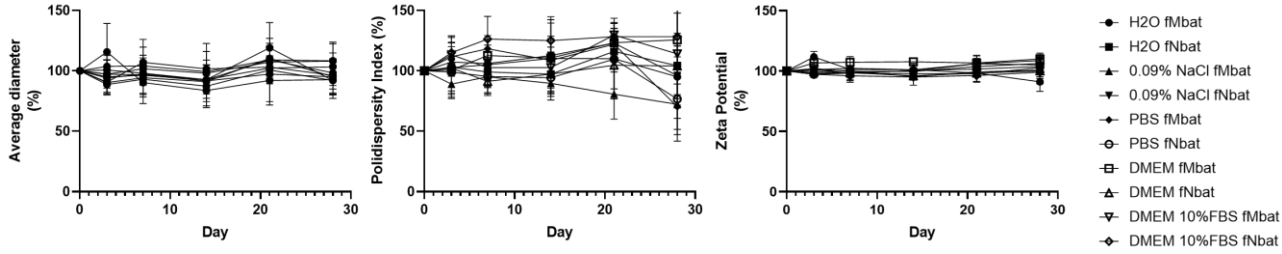

Figure 13. *Physicochemical stability of NLC suspensions fMbat and fNbat in H_2O, 0.09% NaCl, PBS, DMEM and DMEM supplemented with 10% FBS, stored at 4 °C. All NLC physicochemical properties were measured with a Zetasizer, for up to 4 weeks. Results represent the ratio, in percentage, between each measurement and its starting timepoint and are presented as the mean ± SD of 3 independent experiments.*

4.3. *In vitro* permeability across the BBB of DiO-labeled NPs

To assess the ability of the NLCs to permeate through the BBB, a highly hampering therapeutical barrier, we employed a widely recognized *in vitro* model, previously established by our team [165, 175, 202]. This model, which utilizes a monolayer of the hCMEC/D3 cell line, offers several benefits compared to alternative *in vitro* BBB models, including: i) the consistent preservation of BBB-specific characteristics across multiple passages; ii) ease of maintenance and cost-effective reproduction; and iii) the capability to form functional barriers featuring essential tight junction proteins [290]. Moreover, these endothelial cells overexpress the transferrin receptor, the mediator of our NPs' BBB crossing (**Figure 14a**). This model allows for the *in vitro* evaluation of NP permeability across a simulated BBB environment under controlled laboratory conditions [174].

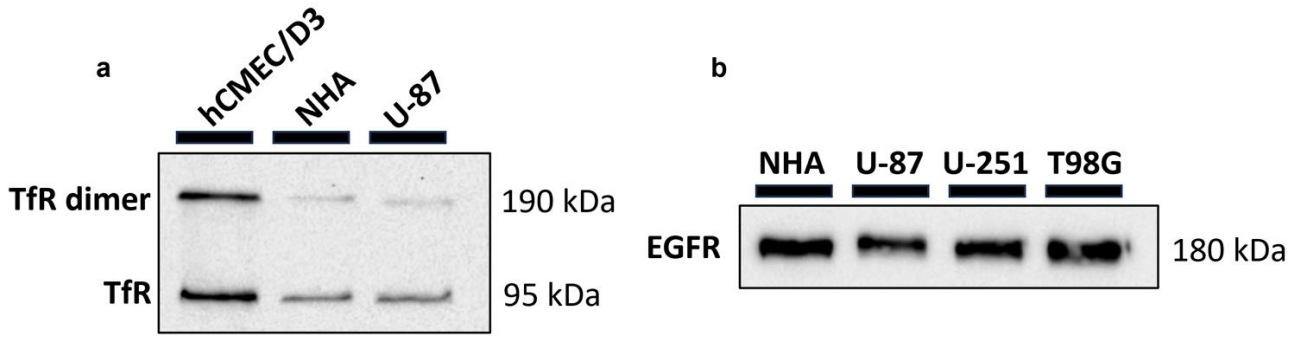

Figure 14. *Expression of EGFR and TfR in astrocytic, GB and endothelial cell lines evaluated by Western blot. a) TfR expression in hCMEC/D3, NHA and U-87 cell lysates (10 µg of total protein). b) EGFR expression in NHA, U-87, U-251 and T98G cell lysate (25 µg of total protein).*

Prior to the permeability assays, the NLCs were labeled with DiO, a highly lipophilic fluorescent dye, to allow their measurement [291]. The previously assessed physicochemical characteristics of average size, PDI and zeta-potential were again measured for the fluorescent NLCs, in order to guarantee that the addition of DiO would not alter the final NP properties. As shown in **Figure 15a**, no statistically significant alterations were observed.

As expected, due to the surface functionalization with the transferrin-mimicking peptide-terminated molecular constructs, we observed a significant increase in permeability of the fMbat formulation. Indeed, in the following 24 hours, the permeated mass nearly tripled (**Figure 15b**). In contrast, the functionalization presented no effect on fNbat, which was unexpected. Given its higher functionalization efficiency, resulting from lower surfactant surface coverage, the fNbat was expected to be more permeable [292]. One limitation of using peptide quantification to assess the functionalization efficiency of a dual-functionalized NP is that this technique can not differentiate between the two molecules being measured. Therefore, despite its higher efficiency, formulation fNbat might actually have a lower amount of the molecular construct on its surface compared to fMbat. Another possibility is that a higher surface coverage of such long molecules might have a deleterious effect due to steric hindrance, contrary to the expected beneficial impact [293]. Interestingly, the unfunctionalized Mbat formulation demonstrated superior permeability compared to the fNbat formulation. This unexpected result is likely attributed to the higher surfactant content in Mbat, which may enhance the NP's interaction with the cellular membranes of the BBB endothelium.

Overall, our results align with existing reports on NPs coopting the transferrin pathway for brain delivery [292, 294]. Moura *et al.*, utilizing the same transferrin-mimicking peptide on a lipid nanocapsule, described a similar increase in permeability from 0% to 3% [165]. In a similar study, Gomes and colleagues,

using the same peptide, showed a three-fold increase in interaction between solid lipid NPs and hCMEC/D3 cells [295].

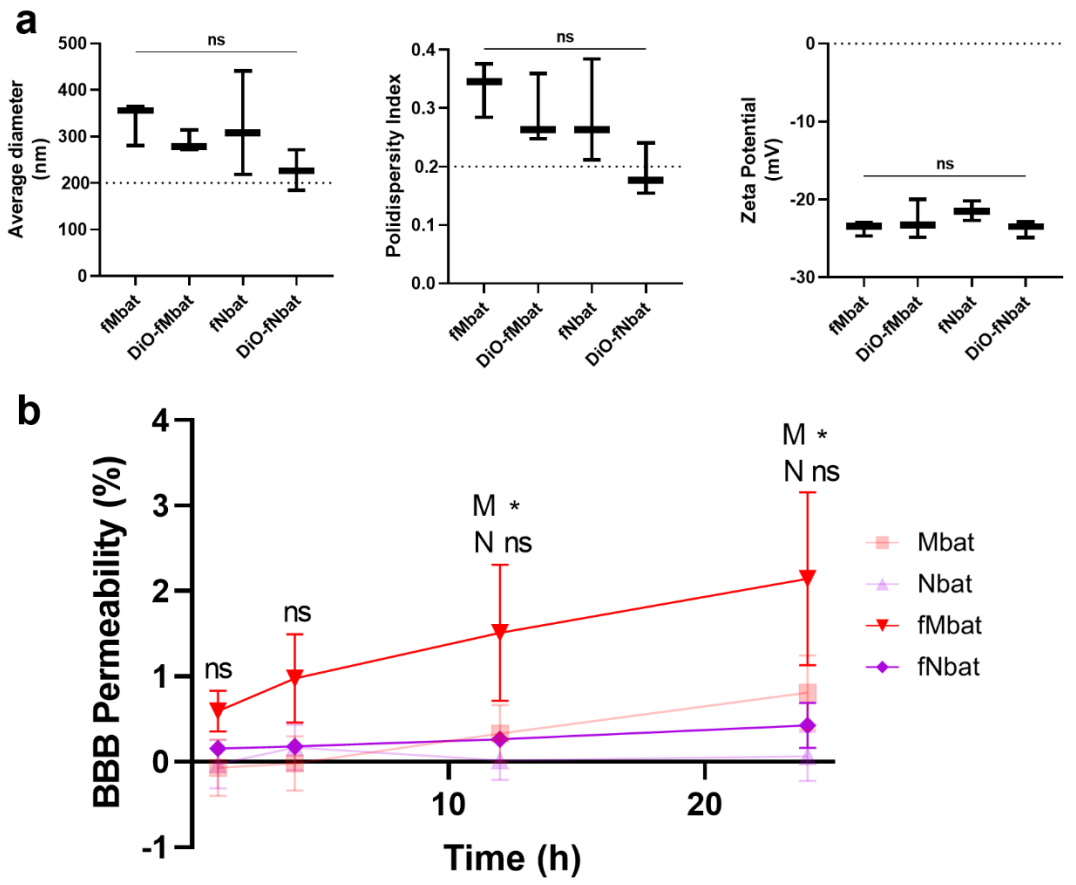

Figure 15. *BBB permeability of DiO-labeled functionalized NLC formulations compared to unfunctionalized DiO-NLCs and their physicochemical characterization. a) Physicochemical characteristics of functionalized formulations fMbat and fNbat produced with and without DiO, measured with a Zetasizer. Results are shown as the mean ± SD of 3 independent characterizations and the dotted lines represent ideal characteristic benchmarks for BBB crossing, average size below 200 nm and PDI below 0.2. b) Assessment of DiO-labeled NP transport across an in vitro BBB Transwell model over 24 h. Results are expressed as the percentage of NP mass that traversed a hCMEC/D3 endothelial cell monolayer to the basolateral compartment, relative to the initial NP mass in the apical chamber. Values represent the mean ± SD of 3 independent experiments. Statistical comparisons were made between each experimental group and the non-functionalized NP control counterpart. *p < 0.05.*

4.4. NLC cytotoxicity assessment

To evaluate the cytotoxicity of the developed NLCs, the heterogeneous nature of GB was considered, and various cell lines were used to represent distinct molecular and genetic profiles [296-300]. As such, the widely utilized cell lines U-87, U-251, and T98G were selected to screen the efficacy of our nano-based approach to GB. In addition to the above, normal human astrocytes (NHA) were used to mimic a healthy glia and serve as a critical control to evaluate the NP's selectivity and potential off-target effects [301].

As shown in **Figure 14b**, all the aforementioned cell lines exhibit elevated expression levels of the EGF receptor, which serves as the target for our NPs to accumulate within the TME. To further assess the cytotoxicity of the accumulation of NPs in non-brain tissue, which frequently occurs in an *in vivo* setting, we conducted viability assays on the endothelial hCMEC/D3 cell line, as a model for the BBB, and HEPG2 cells, as a model of hepatotoxicity [290, 302].

Cell viability was evaluated after treatment of all the cells lines with fMbat, fNbat or free batimastat at concentrations ranging from 0 to 100 nM for 24, 48 or 72 hours (**Figure 16**).

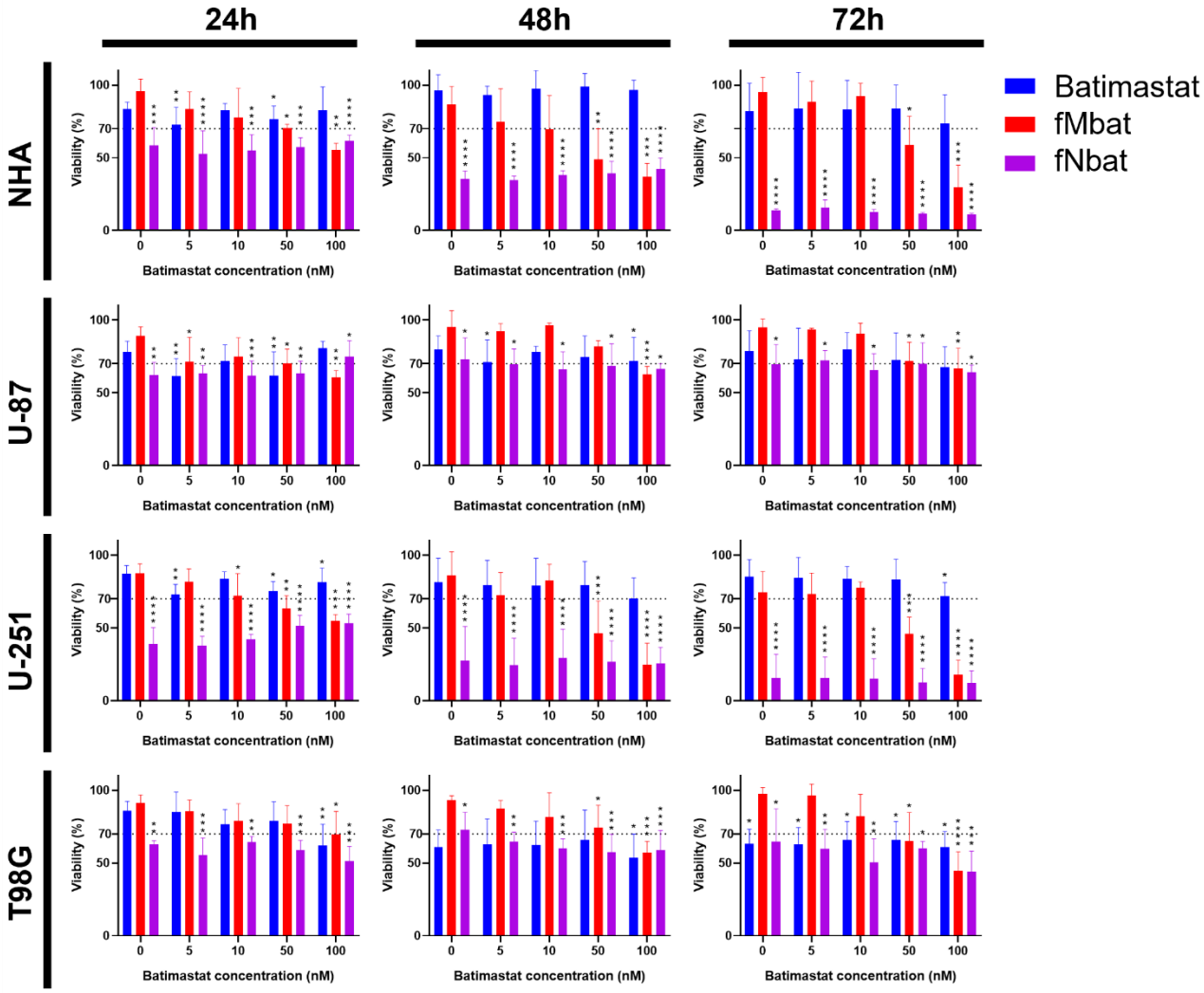

Figure 16. *Evaluation of the cell viability of NHA, U-87, U-251 and T98G cell lines following treatment with free batimastat, batimastat-loaded functionalized NLC M (fMbat) or batimastat-loaded functionalized NLC N (fNbat). Concentrations of 0 nM represent treatments with the empty NLCs fM and fN. Viability was analyzed with PrestoBlue™ assay at 24, 48 or 72 h and is represented as a percentage relative to cells treated with culture medium (untreated control). Results represent the mean ± SD of at least 3 independent experiments. The dotted line represents 70% of cell viability, the cytotoxicity benchmark referenced by the ISO 10993–5 (in vitro cytotoxicity test standardization for medical devices). Statistical comparisons were conducted between each experimental group and the untreated control. *p < 0.05, **p < 0.01, ***p < 0.005, ****p < 0.001.*

Free batimastat showed no significant effect on cell viability at increasing concentration across all cell lines and treatment durations, suggesting that any cytotoxicity present is likely due to the vehicle and not batimastat itself. This is consistent with previous studies reporting similar findings in various cell types and viability assays [303-306]. Regarding the NP formulations, fNbat induced a significant decrease in cell viability across all timepoints and concentrations in all cell lines, except in U-87. With the fMbat formulation, the NHA cell line showed a decrease in viability only at the highest concentrations, particularly at the 72-hour timepoint. In contrast, the U-87 cell line, which appeared more resistant than the others (as observed with fNbat), presented a slight decrease in viability initially, which became less noticeable over time. Moreover, fMbat appeared to have a more pronounced cytotoxic effect on the U-251 cell line than on the others cell lines, with a significant decrease in viability at concentrations above 5 nM. For the T98G cell line, fMbat induced a progressive, albeit small, increase in toxicity as concentrations increased.

Lastly, the cytotoxicity profiles of fMbat and fNbat were evaluated in non-brain tissues, using liver HEPG2 cells and endothelial hCMEC/D3 cells. In HEPG2 cells, both formulations demonstrated a generally safe profile, with fNbat exhibiting a minor increase in cytotoxicity at 72 hours (**Figure 17a**). The endothelial hCMEC/D3 cells, however, showed different responses to the two formulations. fNbat displayed cytotoxicity starting at 48 hours, which became more pronounced at 72 hours, particularly at the 100 nM concentration. In contrast, fMbat maintained a safe profile up to 72 hours, at which point some cytotoxic effects were observed (**Figure 17b**). These results suggest that fMbat has a more favorable safety profile in non-brain tissues compared to fNbat.

The observed difference in cytotoxicity between the two formulations may be attributed to their surfactant content. fMbat contains twice the amount of surfactant compared to fNbat, which likely contributes to its increased stability. The lower surfactant content in fNbat may have led to faster degradation and potential destabilization of cell membranes. Despite the formulations differing only in surfactant amount and having a small disparity in functionalization efficiency, the substantial difference in cytotoxicity between the two formulations was unexpected. Based on these results, fMbat appears to be the better candidate for our therapeutic approach, as it demonstrated lower cytotoxicity, particularly in NHA cells, suggesting a potentially reduced risk of side effects. Nevertheless, while both formulations were designed to target GB cells, their effect on astrocytes became significant at higher concentrations and this cannot be ignored. As such, to combine both a low cytotoxicity and a high MMP inhibitory potential, the 50 nM concentration of batimastat, which is ten-fold higher than its reported IC50 [279], was chosen to continue the *in vitro* assays.

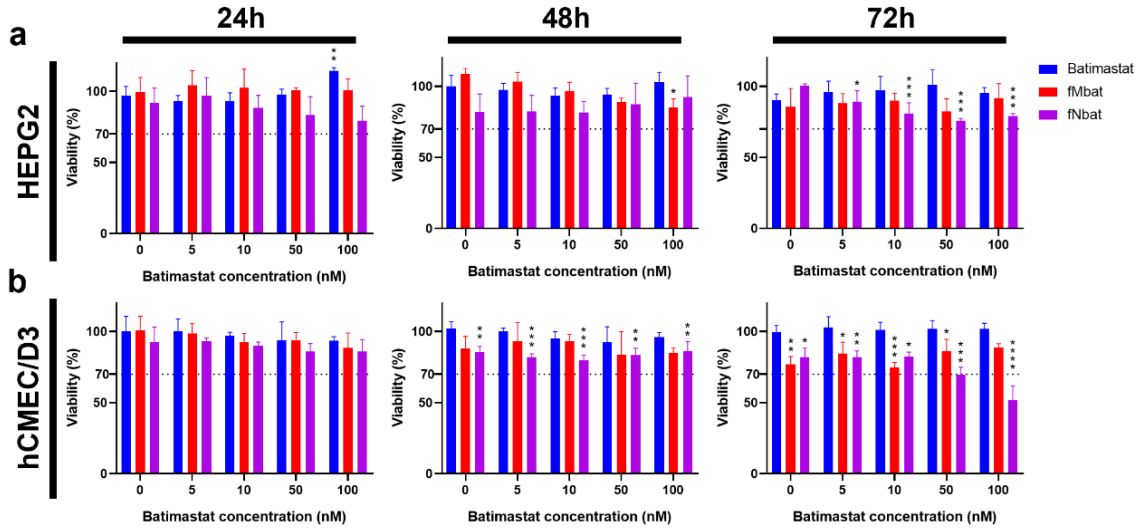

Figure 17. *Evaluation of cell viability of a) HEPG2 and b) hCMEC/D3 cell lines following treatment with free batimastat, batimastat-loaded functionalized NLC M (fMbat) or batimastat-loaded functionalized NLC N (fNbat). Viability was analyzed with PrestoBlue™ assay at 24, 48 or 72 hours and is represented as a percentage relative to cells treated with culture medium (untreated control). Results represent the mean ± SD of 3 independent experiments. Dotted lines represent 70% of cell viability, the cytotoxicity benchmark referenced by the ISO 10993-5 (in vitro cytotoxicity test standardization for medical devices). Statistical comparisons were conducted between each experimental group and the untreated control. *p<0.05, **p<0.01, ***p<0.005, ****p<0.001.*

4.5. NLC MMP inhibitory potential evaluation

The potential of the batimastat-loaded NPs to inhibit MMP activity was examined via gel zymography using the secretome of all cell lines tested. Initially, the basal levels of active MMPs, MMP-2 and MMP-9, were assessed in all 4 cell lines. Although several studies have shown MMP expression on each of these cell lines [297], to the best of our knowledge, none of them presented a simultaneous comparative zymography between all the different cell types and GB cell lines. Nevertheless, some comparisons have determined the relative gelatinase secretion profile between some of them. Bao and colleagues reported that, as expected, U-87 cells secrete both MMP-2 and MMP-9 in much higher amounts than NHA cells [307]. In a different study, Liu *et al.* compared the U-251 and T98G cell lines, demonstrating that T98G cells produce MMP-2 at a higher concentration when compared to U-251. Despite that, the U-251 cells secrete MMP-9 at much higher amounts, with analysis of T98G secretome staying below their zymography sensitivity limit [308]. More recently, Ferreira *et al.* compared the effects of cyclooxygenase inhibitors on U-251, U-87 and T98G cell lines, albeit only performing zymographies of the last two. They demonstrated that, despite having similar pro-MMP-2 activities, U-87 cells have much larger MMP-2 concentrations than T98G cells. Again, the authors were unable to detect any MMP-9 activity [309]. Lastly, Souza *et al.* were able to compare the U-87 and U-251 cell lines, finding that U-87 secretes much more active MMP-2 than U-251.

Interestingly, they were also unable to observe any MMP-9 activity [310]. Therefore, from the available data in the literature, the order of active MMP-2 secretors is U-87 > T98G > U-251 > NHA, and U-251 is, seemingly, the only cell line capable of secreting active MMP-9 in measurable quantities. Our results further support these findings (**Figure 18a**). As expected, the NHA cell line presented an MMP-2 activity (62 kDa [311]) four-fold lower than the U-87 cell line, while the U-251 cell line was only 20% lower than U-87. Unexpectedly, T98G cells presented similar MMP activity to U-87 cells. Additionally, and also contrary to the literature, this cell line was the one with the most noticeable activity of MMP-9 (82 kDa [311]), as opposed to U-251. These discrepancies could be attributed to inherent variability in cell line behavior [312], potentially influenced by factors such as differences in experimental conditions, culture protocols, or intrinsic cellular heterogeneity.

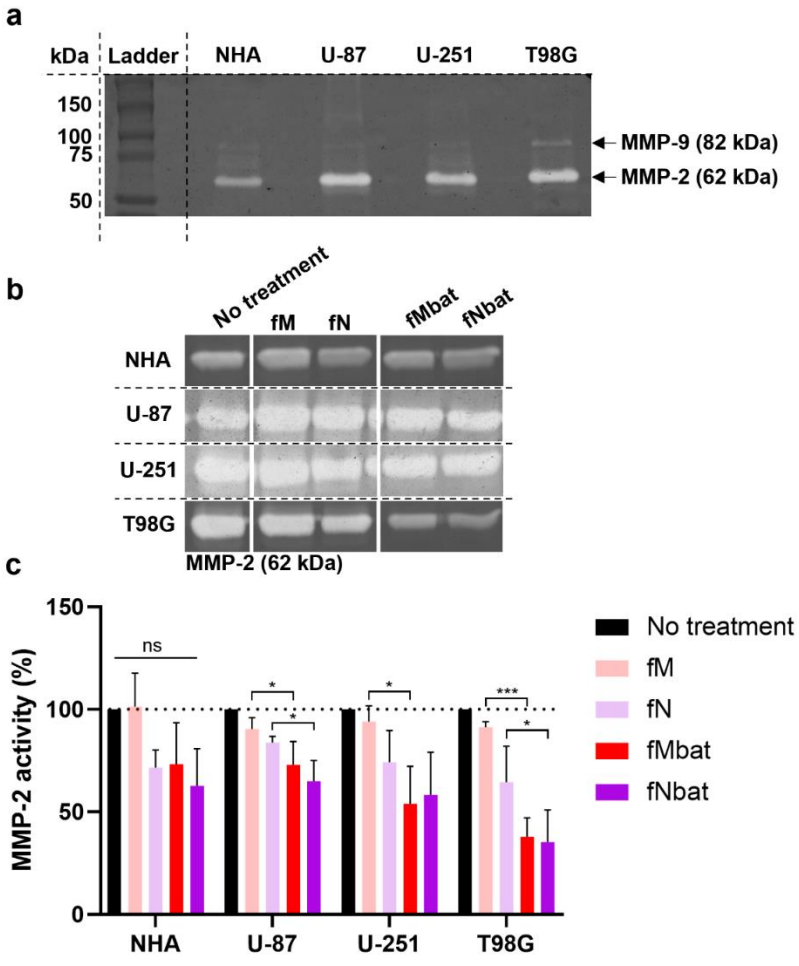

Figure 18. *Assessment of MMP-2 and MMP-9 activity and their inhibition by the NPs on NHA, U-87, U-251 and T98G cell lines, evaluated by gelatin zymography. a) Relative gelatinase activity between the concentrated secretomes. b) MMP-2 activity on concentrated secretomes collected from all the cell lines following treatment with complete media (positive control), empty functionalized NLCs, fM and fN, and batimastat-loaded functionalized NLCs, fMbat and fNbat. c) Densitometry analysis of the gel bands in (b). Density is shown as a percentage relative to the untreated control. The results represent the mean ± SD of 3 independent experiments. Statistical comparisons were made between each experimental group and the empty NP counterpart. *p < 0.05, ***p < 0.005.*

Regarding the effect of the developed NLC formulations on these cell lines (**Figure 18b** and **Figure 18c**), we observed that the unloaded fN formulation led to an overall MMP-2 inhibition in all cell lines: 25% for NHA, 14% for U-87, 19% for U-251 and 41% for T98G. This inhibition could be due to the previously observed cytotoxicity, which may lead to increased cell death and a higher presence of non-proteolytic proteins in the secretomes. As all samples were normalized for total protein content, the secretomes contained a relatively lower percentage of MMPs. In contrast, the batimastat-loaded fMbat formulations achieved a higher MMP-2 inhibition of: 32% in NHA, 11% in U-87, 27% in U-251 and 62% in T98G. Although, this increased efficacy could be associated with higher drug loadings, the fact that the encapsulation efficiency of fMbat and fNbat formulations was nearly identical might indicate that the enhanced effect of the fMbat formulation is more likely due to its improved stability and controlled release. [313]. We could also observe that the NHA and U-87 cell lines showed the least effect of the NLC formulations. For U-87, the higher overall MMP activity may dilute the effect that this concentration of batimastat can provide. To overcome this limitation, the NPs would need to be loaded with a higher amount of the inhibitor, as the 50 nM utilized was evidently not enough to overcome the MMP activity and an increase in NLC concentration is impractical due to the consequent increase in cytotoxicity. Regarding NHA, while literature on batimastat's effect is scarce, Ulasov and colleagues showed that marimastat, a similar compound, presented an MMP inhibitory and growth inhibiting effect on U-87 and U-251 but did not affect NHA cells [314]. Similarly, Alves *et al.* found that batimastat had the same inhibiting effect on models of hematological tumors, which could indicate that it may also possess the same lower efficiency on the NHA cell line [315].

Interestingly, T98G appears to have a particularly high sensitivity to batimastat. Since, to the best of our knowledge, there are no previous studies on batimastat's effect on T98G cells, this is a promising avenue for further mechanistic research. It is, however, important to note that the MMP activity profile of T98G cells observed in this work was slightly different from the previously reported behaviors [308, 309].

CHAPTER V
GENERAL DISCUSSION

CHAPTER V – GENERAL DISCUSSION

The current state of GB therapy remains a significant challenge in oncology. Despite considerable research, progress in treatment has been disappointingly slow, with no palpable evolution since the establishment, back in 2005, of the standard of care – the Stupp protocol [27]. This protocol, which combines radiation therapy with concurrent daily TMZ chemotherapy after maximal safe surgical resection, followed by six cycles of adjuvant TMZ, has resulted in poor outcomes with an average overall survival of approximately 15 months [1], highlighting the complexity of this particular form of brain cancer.

As outlined in Chapter I, there is growing interest in exploring alternative therapeutic strategies that focus on modulating the TME rather than solely relying on traditional cytotoxic approaches [144]. One such strategy involves preventing the degradation of the ECM to hinder tumor growth, which may present several advantages when compared with conventional chemotherapy. First, it targets the tumor's physical environment directly, reducing the risk of drug resistance, a common problem in GB treatment [316]. Second, by focusing on the ECM, this strategy often presents fewer systemic side effects compared to cytotoxic chemotherapies [317]. In GB, in particular, the ECM plays an important role in promoting tumor cell invasion and survival through its degradation and modulation by the overexpression of MMPs [297]. The pivotal role of MMPs in GB makes them attractive therapeutic targets to potentially prevent tumor invasion and progression. The use of MMP inhibitors in cancer therapy is not new, with studies dating back to the end of the previous century. Initially, hydroxamate-based MMP inhibitors, such as batimastat and marimastat, showed promising results. For example, in patients with malignant ascites, batimastat was well absorbed via the intraperitoneal route with approximately half of the patients showing a reduction in weight and abdominal girth, indicating less aggressive ascites [248]. In another clinical trial, interpleural administration of batimastat in patients with malignant pleural effusions resulted in 16 out of 18 patients requiring significantly fewer aspirations in the 3 months after treatment compared to the 3 months before, with 7 requiring no further aspiration due to a considerably lower fluid buildup in the pleural cavity [318]. In contrast, marimastat, did not show improvement in median survival in GB patients as a single agent [246], but increased progression free survival to 29% when combined with TMZ [247]. Nevertheless, numerous issues, including cell death, fibrosis, bleeding, weight loss, poor aqueous solubility, limited bioavailability and severe musculoskeletal toxicity, have decreased the therapeutic impact of these drugs and interest on their development [319, 320]. This underscored the need for more targeted, innovative approaches to MMP inhibition in GB therapy.

Nanotechnology offers an innovative solution for the delivery of drugs with severe systemic toxicity and solubility issues. By encapsulating hydrophobic drugs within

lipidic matrixes it is possible to improve solubility, protect drugs from degradation and enable targeted delivery to tumor tissues, while reducing systemic exposure and associated side effects [321]. NP-based systems also promote controlled release mechanism, maintaining therapeutic levels over time, minimizing administration frequency and toxicity risks [322].

Motivated by nanotechnology's potential to revive abandoned and overlooked drugs, and recognizing the limitations of conventional chemotherapeutic approaches, we took inspiration from a Swiss-knife's versatile capabilities and developed a multifunctional tunable nanosystem that is able to overcome the physical limitations posed by BBB crossing to specifically deliver batimastat into the GB TME. This multifunctionality emerged from the functionalization with a novel molecular construct of our own design, developed to address 3 GB critical challenges: i) BBB crossing; ii) NP entrapment and accumulation specifically within the GB TME, and iii) Inhibition of MMP activity to suppress tumor invasiveness.

Functionalization of NPs is crucial for enhancing their effectiveness in biomedical applications, especially in cancer treatment, offering targeted drug delivery, reducing side effects and improving treatment efficacy [323]. Functionalizing moieties can be tailored to carry various molecules, including drugs [324-326] and imaging agents [327, 328], making them versatile tools for both diagnosis and treatment [329]. Functionalization also allows for better tumor targeting, enhanced permeation through biological barriers, and improved cellular uptake, among others [330-332]. In the context of GB, effective nanosystem functionalization must serve at least two purposes: bypassing the BBB and targeting tumor cells. Research has focused on these dual actions mainly through surface co-modification of NPs, with a common strategy being functionalization with transferrin, for BBB transcytosis, and cell-penetrating peptides, for entry into GB cells [333, 334]. Alternative strategies have also explored dual functionalization with several other molecules, including cRGD, p-hydroxybenzoic acid, multiple cell-penetrating peptides, antibodies, EGF-targeting peptides, folic acid, aptamers, and angiopep-2 [335-342]. While this dual-functionalization approach has been shown to enhance the bioavailability of nanosystems in the brain, it also doubles the potential for non-specific binding and associated side effects due to the presence of multiple targeting moieties [343]. Furthermore, once the NPs cross the BBB, the BBB-targeting functionalization becomes ineffective and may hinder the NP's therapeutic efficacy [202]. To address these challenges, it is advantageous for a NP to present a single active targeting moiety, which can be achieved through TME-mediated structural rearrangement. As such, the functionalization strategy employed in this work, particularly the customized construct that incorporates GB TME-sensitive cues (high local concentration of transmembrane MMP-14),

represents a significant innovation in GB targeting approaches. Previously, nanosystems incorporating MMP-14-sensitivity, such as the one described by Mohanty *et al.* [197], limited themselves to targeting GB cells, overlooking the importance, and hindrance, of the BBB. This strategy, however, proposes a multifunctional NP system that sequentially targets both the BBB and GB by exploiting TME-mediated structural rearrangement (specifically, the unshielding of a sterically hindered molecule). The closest attempted strategy to this nanosystem was described by Martins *et al.* [202], who utilized a pH-dependent uncovering of histidine to achieve a similar goal. However, their pH-mediated structural rearrangement occurs during BBB transcytosis rather than within the GB TME, potentially leading to non-specific binding in healthy brain parenchyma.

Although the designed construct represents the most pioneering part of this work, the nanosystem's core itself, namely the choice of NLC, its composition, and production methodology, were also carefully tailored to positively impact GB therapy. Indeed, NLCs offer unique practical benefits when compared to other particle types. These nanocarriers offer superior drug loading capacity compared to other lipidic NPs [288]. Their imperfect crystal structure, resulting from the blend of solid and liquid lipids, creates more space for drug molecules, making them particularly suitable for the highly lipophilic drugs often used in GB treatment [344]. While polymeric NPs can also be functionalized for targeted delivery and provide controlled release, NLCs typically exhibit better biocompatibility since their composition includes *"generally recognized as safe"* lipids and surfactants, reducing the risk of toxicity associated with some synthetic polymers [345]. Also, inorganic NPs, such as iron, gold or silica-based, excel in specific applications, particularly imaging [346]. However, they lack the versatility that NLCs can accommodate, with very limited drug delivery capabilities. Moreover, the fact that many inorganic NPs contain heavy metals, raises significant concerns regarding tissue bioaccumulation through NP degradation [346, 347]. In this work, the NLCs, produced by ultrasonicator-assisted hot homogenization, were composed of: Gelucire® 44/14, a solid lipid to form the NP matrix; Compritol® 888 ATO, a high melting point lipid to destabilize the matrix and increase drug loading; Miglyol® 810N, a liquid lipid to create liquid pockets within the matrix and increase the destabilization; DSPE, for the presence of amines on the NP surface needed for functionalization; and Tween® 80, a surfactant to stabilize the NP. Different NLCs can be produced through various techniques, including high-pressure homogenization [348], microemulsion [349], emulsification-solvent evaporation [350] or diffusion [351]. The ultrasonicator-assisted hot homogenization [263], used in this study, stands out as a superior method for NLC production, combining the benefits of high-temperature processing (avoidance of organic solvents) and the efficiency of ultrasonic energy (more efficient size reduction, resulting in smaller and more uniform NPs) [352]. Another factor taken into consideration for the choice of production methodology was its scalability. Heating techniques are

amenable to large-scale production, making them suitable for industrial applications, as they avoid the incorporation of organic solvents, removing the need for difficult and costly washing processes [353]. Still, this methodology requires the use of high heat, of up to 85 °C, which may be cost intensive. For large-scale production of NLCs, cold high-pressure homogenization would be the optimal methodology, as it avoids the use of organic solvents and high temperatures [344]. However, this approach requires very specific specialized equipment [354].

After the complete production, functionalization and purification process, the two optimized nanoparticle formulations – fMbat and fNbat – presented quasi-monodisperse suspensions of highly negative NPs with sizes of approximately 300 nm and a drug loading 1000-fold higher than batimastat's IC50, challenging the conventional belief that NP sizes above 200 nm limits BBB crossing ability. BBB permeability is crucial for nanosystems targeting GB because it severely limits drug delivery to the brain tumor, naturally preventing over 98% of the described small-molecule drugs and all macromolecular agents from accessing the brain parenchyma [129]. Our data has shown that size did not limit BBB crossing *in vitro,* consistent with other studies reporting that NPs up to 500 nm in size can effectively traverse the BBB, provided they utilize receptor-mediated transport mechanisms [355-357]. In light of these studies, the average size around 300 nm of the NPs developed in this study was not considered a limitation since, by targeting the transferrin receptor, these NPs are expected to facilitate efficient BBB transport despite their relatively larger size. Through our BBB transwell *in vitro* model, we confirmed fMbat as the more promising candidate. This NLC formulation demonstrated the effectiveness of the TfP by tripling the amount of drug that permeated through the membrane over a 24-hour period. Using specifically the same transferrin peptide as used in our study, Gomes *et al.* increased the interaction of brain endothelial cells with lipidic and polymeric NPs by 3- and 4-fold, respectively [295]. Later, the same authors showed a 2-fold increase in P-gp siRNA BBB transport with TfP-functionalized polymeric NPs [175]. More recently, Moura *et al.* functionalized lipid nanocapsules with the TfP peptide, observing a 3-fold BBB permeability increase [165]. With the use of the complete transferrin molecule for the functionalization of curcumin-loaded NLCs, Neves *et al.* showed a small 1.5-fold increase in BBB permeation of curcumin [358], while Pinheiro *et al.* failed to observe any increase in permeability of lipidic NPs due to transferrin [359]. Sharma *et al.* functionalized liposomes with transferrin, observing an increase in BBB transport from 5.4% to approximately 15% [360], afterwards observing a 4-fold increased brain accumulation *in vivo* [361]. Using transferrin-containing gold NPs, Wiley *et al.* demonstrated in mice an increase in particles per brain mm3 ranging from 1.5- to 2-fold, while curiously observing that the highest transferrin content had significantly less brain accumulation than the less concentrated formulations [362]. Overall, NP

functionalization with complete transferrin demonstrates higher variability and inconsistency regarding the permeability results across different studies conferring greater importance to the stability and predictability to the TfP used in this study.

Notably, the encapsulation of batimastat into NLCs has not been previously explored, highlighting the critical relevance and therapeutical potential of this work. Previous encapsulations of batimastat have been limited to two nanosystems: an elastin antibody-conjugated PLA NP for the prevention of abdominal aortic aneurysm progression [281], and a self-assembling formulation, also made of PLA NPs, for the *in situ* creation of extracellular drug depots [265]. Likewise, marimastat, the chemical analog of batimastat, has not received much attention, with: five encapsulations, three thermosensitive liposomes for anti-cancer treatment [282, 363, 364], a pH-sensitive liposome for atherosclerosis [365], and a polymersome for metastatic recurrences [366]; an association with PTX nanocrystals [367]; and a complex with β-casein and HA-PTX prodrug [368]. Other hydroxamate-based compounds, such as ilomastat and prinomastat, have yet to be implemented into nanosystems. In a broader sense, MMP inhibitor nanoencapsulation is, currently, mainly limited to CTX [209, 369-371]. However, as CTX binds to chloride channels, which are ubiquitously expressed on most cell types [372, 373], its treatment may potentially lead to unintended interactions with non-cancerous cells, a problem that does not occur with hydroxamate-based inhibitors.

To prove the feasibility of our proposed nanotechnological strategy, we first demonstrated the biocompatibility of the nanosystem in multiple cell lines, both tumor and non-tumor. This is of particular importance, as our strategy relies on the inhibition of extracellular MMPs without significant cellular interaction. Therefore, no cytotoxicity was expected. Biocompatibility of delivery systems is crucial as it directly impacts the safety and effectiveness of nanomaterial-based treatments [374]. For GB treatment, biocompatibility becomes particularly important due to the challenging nature of targeting brain tumors, as NPs must be designed to safely penetrate the BBB and then interact with tumor cells without causing significant cellular damage while in circulation [375]. The cytotoxicity evaluation carried out in this study, which considered not only the heterogeneity of GB through the use of multiple cell lines as well as the potential non-specific effects in healthy cells, provided a thorough assessment of both the efficacy and safety. fMbat emerged as the more promising candidate for further development, demonstrating lower cytotoxicity, especially in non-tumor cells. These results underscore the importance of careful formulation design in NP-based drug delivery systems for GB treatment. Other studies have already shown, in different cell types, that at the nanomolar concentrations tested in this work, batimastat is not cytotoxic [303, 315, 376]. Also, the lipids and surfactants used in the

preparation of NLCs demonstrated cellular tolerance across various cell lines [377-380]. Research indicates that most cell lines can tolerate lipid-based NPs at high concentrations [381]. For example, Akanda *et al.* showed retinoic acid-loaded NPs, containing stearic acid and poloxamer 188, to be well-tolerated by human prostate adenocarcinoma cells at a 3 mg/ml dose [382]. Similarly, Ghalaei *et al.* created hyaluronic acid-coated NPs with cetyl alcohol, stabilized by polysorbate 80 and containing stearylamine, which showed excellent tolerance by SK-OV-3 cells [383]. Likewise, Parveen *et al.* demonstrated that cetyl alcohol-based NPs stabilized by polyvinyl alcohol and polysorbate 80 were compatible with MCF-7 cells at concentrations up to 2 mg/ml [384]. In the present study. NLC concentrations never exceeded 1.22 mg/mL, which is well within the safety range of biocompatibility studies (< 3 mg/mL) [381].

The final phase of our characterization focused on evaluating the efficacy of our system *in vitro*, through the NLCs' ability to inhibit MMPs. As previously discussed in Chapter I, MMPs facilitate cancer progression through several mechanisms, such as enabling tumor cells to degrade the ECM and breaking down biological barriers, ultimately promoting the spread of tumor cells [254]. In particular, the secreted gelatinases MMP-2 and MMP-9 are instrumental for GB aggressiveness [297, 298]. Through gelatin zymography assays, we were able to confirm the batimastat-loaded NLCs as effective inhibitors of MMP-2 activity. Using this specific inhibitor, Falk *et al.* demonstrated an MMP-2 activity reduction in cardiac transplants from 2271 ± 571 µg/mL in untreated to 259±140 µg/mL in batimastat-treated allografts [385]. Batimastat's effectiveness has been consistently demonstrated across a few experimental models, including vascular smooth muscle cells (completely blocking the activation of MMP-2) [386], hematological cell lines (small reduction in MMP-2 and MMP-9 activity) [315], breast cancer xenografts (completely blocking collagenase activity) [387], and skeletal muscle (reducing MMP enzymatic activity for approximately 40%) [388]. Notably, to the best of our knowledge, our work demonstrated for the first time batimastat inhibition on GB MMP activity, demonstrating its potential as alternative or combined therapeutic strategy in this type of tumor, and others that rely on MMP activity for their progression and metastatic process.

CHAPTER VI

CONCLUDING REMARKS AND FUTURE PERSPECTIVES

CHAPTER VI – CONCLUDING REMARKS AND FUTURE PERSPECTIVES

This thesis presents a novel approach to GB treatment through nanotechnology and ECM modulation. We have successfully developed and characterized a dual-functionalized nanosystem specifically designed for GB-targeted therapy. This system has yielded promising results *in vitro*, demonstrating the ability to effectively cross a BBB model while maintaining limited non-specific cytotoxicity. Importantly, our nanosystem exhibited significant inhibition of MMPs overexpressed in various GB cell lines, a key factor in tumor progression and invasion. These findings not only validate our approach, but also the versatility of the strategy employed combining nanotechnology, ECM modulation, cancer biology, and targeted delivery. This highlights the importance of multidisciplinary efforts in addressing complex medical challenges.

In the broader context of GB research, this work underscores the potential of nanotechnology in overcoming current treatment limitations and paves the way for more targeted and effective therapies.

However, the translation of our nanotechnology-based approach to clinical applications will require further studies. While our findings are encouraging, it is important to acknowledge the limitations of *in vitro* studies and the need for further *in vivo* validation, particularly pertaining to NLC biodistribution and tissue-specific toxicity. The translation of these nanotechnology-based approaches to clinical applications will require extensive preclinical testing and careful consideration of safety and efficacy profiles. Using GB animal models, ideally mice with orthotopic xenografts of human GB cells, would provide valuable insights into the biodistribution, tumor-specific accumulation, and therapeutic potential of these nanocarriers in a complex biological environment.

Further optimization of the NLC formulations may allow to improve stability and enhance drug loading capacity and targeting efficiency. This could involve exploring different lipid compositions, surfactants, or functionalization strategies to improve the nanocarriers' ability to cross the BBB and selectively target GB cells. Most importantly, increasing drug loading would result in administration of smaller dosages and consequently reducing potential side effects. Additionally, a higher batimastat content would facilitate most of the analytical work, as working near the sensitivity limits of equipment, such as HPLC, is extremely challenging and a consistent difficulty during this project.

Taking advantage of the “Swiss-knife-like” versatility of our nanoformulations, investigation of combination therapies presents other promising possibilities. These batimastat-loaded NLCs could be combined with other therapeutic agents, such as chemotherapeutics or immunomodulators, to potentially achieve synergistic effects and overcome drug resistance mechanisms in GB treatment.

Additionally, expanding the range of MMP inhibitors tested within the NLC system could provide valuable comparative data and potentially identify more effective candidates for GB treatment. Batimastat was chosen for this work since the downsides, presented in clinical trials, seemed tailored for nanotechnology improvement, but other inhibitors should prove similarly fruitful.

Furthermore, exploring the effects of these nanocarriers on other components of the TME, such as immune cells and stromal elements, would offer a more comprehensive understanding of their therapeutic potential. Further research should include long-term studies to evaluate the potential development of resistance to MMP inhibition and its impact on tumor progression. Also, given that our approach may lead to tumor encapsulation, it's crucial to investigate whether this could inadvertently promote adaptive responses or alternative invasion mechanisms. Such studies would be instrumental in developing strategies to counteract potential resistance, ultimately enhancing the durability and efficacy of the treatment.

Ultimately, to fully realize the clinical potential of these NPs, future research must focus on scaling up production processes and addressing regulatory requirements, steps that will pave the way for translating our promising *in vitro* results into viable therapeutic options for GB patients. This would include longer stability studies in different physical states (e.g., frozen, lyophilized and suspension), toxicology assessments, and the development of standardized manufacturing processes to ensure consistent and reproducible quality and efficacy of the nanoformulations.

By pursuing these future directions, we can build upon the promising results of this work towards developing more effective, targeted therapies for GB, ultimately improving outcomes for patients facing this challenging disease.

REFERENCES

REFERENCES

1. Grochans, S., et al., *Epidemiology of Glioblastoma Multiforme-Literature Review*. Cancers (Basel), 2022. **14**(10) DOI: 10.3390/cancers14102412.
2. Gittleman, H., et al., *Survivorship in adults with malignant brain and other central nervous system tumor from 2000–2014*. Neuro-Oncology, 2018. **20**(suppl_7): p. vii6-vii16 DOI: 10.1093/neuonc/noy090.
3. Ostrom, Q.T., et al., *CBTRUS Statistical Report: Primary Brain and Other Central Nervous System Tumors Diagnosed in the United States in 2011-2015*. Neuro Oncol, 2018. **20**(suppl_4): p. iv1-iv86 DOI: 10.1093/neuonc/noy131.
4. Reinders, A.N., M. Koshy, and M. Korpics, *The Patterns of Failure and Prognostic Impact of Tumor Location in Patients Undergoing Reirradiation for Glioblastoma*. Cureus, 2024. **16**(9): p. e68820 DOI: 10.7759/cureus.68820.
5. Carrano, A., et al., *Sex-Specific Differences in Glioblastoma*. Cells, 2021. **10**(7): p. 1783
6. Louis, D.N., et al., *The 2021 WHO Classification of Tumors of the Central Nervous System: a summary.* Neuro Oncol, 2021. **23**(8): p. 1231-1251 DOI: 10.1093/neuonc/noab106.
7. Li, S., et al., *Signaling pathways in brain tumors and therapeutic interventions*. Signal Transduction and Targeted Therapy, 2023. **8**(1): p. 8 DOI: 10.1038/s41392-022-01260-z.
8. Gue, R. and D.A. Lakhani, *The 2021 World Health Organization Central Nervous System Tumor Classification: The Spectrum of Diffuse Gliomas*. Biomedicines, 2024. **12**(6): p. 1349
9. Han, S., et al., *IDH mutation in glioma: molecular mechanisms and potential therapeutic targets*. British Journal of Cancer, 2020. **122**(11): p. 1580-1589 DOI: 10.1038/s41416-020-0814-x.
10. Whitfield, B.T. and J.T. Huse, *Classification of adult-type diffuse gliomas: Impact of the World Health Organization 2021 update*. Brain Pathology, 2022. **32**(4): p. e13062 DOI: https://doi.org/10.1111/bpa.13062.
11. Torp, S.H., O. Solheim, and A.J. Skjulsvik, *The WHO 2021 Classification of Central Nervous System tumours: a practical update on what neurosurgeons need to know—a minireview*. Acta Neurochirurgica, 2022. **164**(9): p. 2453-2464 DOI: 10.1007/s00701-022-05301-y.
12. Stoyanov, G.S., et al., *Reclassification of Glioblastoma Multiforme According to the 2021 World Health Organization Classification of Central Nervous System Tumors: A Single Institution Report and Practical Significance*. Cureus, 2022. **14**(2): p. e21822 DOI: 10.7759/cureus.21822.
13. Osborn, A.G., et al., *The 2021 World Health Organization Classification of Tumors of the Central Nervous System: What Neuroradiologists Need to Know*. American Journal of Neuroradiology, 2022 DOI: https://doi.org/10.3174/ajnr.A7462.
14. Colman, H., et al., *A multigene predictor of outcome in glioblastoma*. Neuro Oncol, 2010. **12**(1): p. 49-57 DOI: 10.1093/neuonc/nop007.

15. Verhaak, R.G., et al., *Integrated genomic analysis identifies clinically relevant subtypes of glioblastoma characterized by abnormalities in PDGFRA, IDH1, EGFR, and NF1*. Cancer Cell, 2010. **17**(1): p. 98-110 DOI: 10.1016/j.ccr.2009.12.020.
16. Wang, Q., et al., *Tumor Evolution of Glioma-Intrinsic Gene Expression Subtypes Associates with Immunological Changes in the Microenvironment*. Cancer Cell, 2017. **32**(1): p. 42-56.e6 DOI: 10.1016/j.ccell.2017.06.003.
17. Ostrom, Q.T., et al., *Risk factors for childhood and adult primary brain tumors*. Neuro Oncol, 2019. **21**(11): p. 1357-1375 DOI: 10.1093/neuonc/noz123.
18. Smith, C.J., et al., *Risk factors for glioblastoma are shared by other brain tumor types*. Human & Experimental Toxicology, 2024. **43**: p. 09603271241241796 DOI: 10.1177/09603271241241796.
19. Gunasegaran, B., et al., *Viruses in glioblastoma: an update on evidence and clinical trials*. BJC Reports, 2024. **2**(1): p. 33 DOI: 10.1038/s44276-024-00051-z.
20. Tarev, I. and A. Cekov, *Cerebellar Glioblastoma: A Literature Review and Case Analysis*. Cureus, 2024. **16**(2): p. e55135 DOI: 10.7759/cureus.55135.
21. Alharbi, B., et al., *Primary spinal cord glioblastoma: A rare cause of paraplegia*. Surg Neurol Int, 2022. **13**: p. 160 DOI: 10.25259/sni_135_2022.
22. Valenzuela-Fuenzalida, J.J., et al., *Association between the Anatomical Location of Glioblastoma and Its Evaluation with Clinical Considerations: A Systematic Review and Meta-Analysis*. Journal of Clinical Medicine, 2024. **13**(12): p. 3460
23. De Luca, C., et al., *Regional Development of Glioblastoma: The Anatomical Conundrum of Cancer Biology and Its Surgical Implication*. Cells, 2022. **11**(8) DOI: 10.3390/cells11081349.
24. Fyllingen, E.H., et al., *Survival of glioblastoma in relation to tumor location: a statistical tumor atlas of a population-based cohort*. Acta Neurochirurgica, 2021. **163**(7): p. 1895-1905 DOI: 10.1007/s00701-021-04802-6.
25. Gilard, V., et al., *Diagnosis and Management of Glioblastoma: A Comprehensive Perspective*. Journal of Personalized Medicine, 2021. **11**(4): p. 258
26. Rodgers, L.T., et al., *Glioblastoma Standard of Care: Effects on Tumor Evolution and Reverse Translation in Preclinical Models*. Cancers, 2024. **16**(15): p. 2638
27. Stupp, R., et al., *Radiotherapy plus concomitant and adjuvant temozolomide for glioblastoma*. N Engl J Med, 2005. **352**(10): p. 987-96 DOI: 10.1056/NEJMoa043330.
28. Rong, L., N. Li, and Z. Zhang, *Emerging therapies for glioblastoma: current state and future directions*. J Exp Clin Cancer Res, 2022. **41**(1): p. 142 DOI: 10.1186/s13046-022-02349-7.
29. Jezierzański, M., et al., *Temozolomide (TMZ) in the Treatment of Glioblastoma Multiforme—A Literature Review and Clinical Outcomes*. Current Oncology, 2024. **31**(7): p. 3994-4002

30. Furtak, J., et al., *Survival after reoperation for recurrent glioblastoma multiforme: A prospective study.* Surgical Oncology, 2022. **42**: p. 101771 DOI: https://doi.org/10.1016/j.suronc.2022.101771.
31. González, V., et al., *Analyzing the role of reoperation in recurrent glioblastoma: a 15-year retrospective study in a single institution.* World Journal of Surgical Oncology, 2022. **20**(1): p. 384 DOI: 10.1186/s12957-022-02852-3.
32. Zhao, Y.-H., et al., *A Meta-Analysis of Survival Outcomes Following Reoperation in Recurrent Glioblastoma: Time to Consider the Timing of Reoperation.* Frontiers in Neurology, 2019. **10** DOI: 10.3389/fneur.2019.00286.
33. Minniti, G., et al., *Current status and recent advances in reirradiation of glioblastoma.* Radiat Oncol, 2021. **16**(1): p. 36 DOI: 10.1186/s13014-021-01767-9.
34. Christ, S.M., et al., *Re-irradiation of recurrent IDH-wildtype glioblastoma in the bevacizumab and immunotherapy era: Target delineation, outcomes and patterns of recurrence.* Clinical and Translational Radiation Oncology, 2024. **44**: p. 100697 DOI: https://doi.org/10.1016/j.ctro.2023.100697.
35. García-Cabezas, S., et al., *Re-irradiation for high-grade gliomas: Has anything changed?* World J Clin Oncol, 2021. **12**(9): p. 767-786 DOI: 10.5306/wjco.v12.i9.767.
36. Bosio, A., et al., *Metronomic Temozolomide in Heavily Pretreated Patients With Recurrent Isocitrate Dehydrogenase Wild-type Glioblastoma: A Large Real-Life Mono-Institutional Study.* Clin Oncol (R Coll Radiol), 2023. **35**(5): p. e319-e327 DOI: 10.1016/j.clon.2023.01.012.
37. Brandes, A.A., et al., *Temozolomide 3 weeks on and 1 week off as first-line therapy for recurrent glioblastoma: phase II study from gruppo italiano cooperativo di neuro-oncologia (GICNO).* Br J Cancer, 2006. **95**(9): p. 1155-60 DOI: 10.1038/sj.bjc.6603376.
38. Franceschi, E., et al., *Temozolomide Rechallenge in Recurrent Glioblastoma: When is it Useful?* Future Oncology, 2018. **14**(11): p. 1063-1069 DOI: 10.2217/fon-2017-0681.
39. Weller, M., et al., *MGMT Promoter Methylation Is a Strong Prognostic Biomarker for Benefit from Dose-Intensified Temozolomide Rechallenge in Progressive Glioblastoma: The DIRECTOR Trial.* Clinical Cancer Research, 2015. **21**(9): p. 2057-2064 DOI: 10.1158/1078-0432.Ccr-14-2737.
40. Wick, W., et al., *One week on/one week off: a novel active regimen of temozolomide for recurrent glioblastoma.* Neurology, 2004. **62**(11): p. 2113-5 DOI: 10.1212/01.wnl.0000127617.89363.84.
41. Brandes, A.A., et al., *How effective is BCNU in recurrent glioblastoma in the modern era? A phase II trial.* Neurology, 2004. **63**(7): p. 1281-4 DOI: 10.1212/01.wnl.0000140495.33615.ca.
42. Herrlinger, U., et al., *Lomustine-temozolomide combination therapy versus standard temozolomide therapy in patients with newly diagnosed glioblastoma with methylated MGMT promoter (CeTeG/NOA–09): a randomised, open-label, phase 3 trial.* The

Lancet, 2019. **393**(10172): p. 678-688 DOI: 10.1016/S0140-6736(18)31791-4.
43. Brandes, A.A., et al., *Second-line chemotherapy with irinotecan plus carmustine in glioblastoma recurrent or progressive after first-line temozolomide chemotherapy: a phase II study of the Gruppo Italiano Cooperativo di Neuro-Oncologia (GICNO)*. J Clin Oncol, 2004. **22**(23): p. 4779-86 DOI: 10.1200/jco.2004.06.181.
44. Reithmeier, T., et al., *BCNU for recurrent glioblastoma multiforme: efficacy, toxicity and prognostic factors*. BMC Cancer, 2010. **10**: p. 30 DOI: 10.1186/1471-2407-10-30.
45. You, W.-C., et al., *Re-irradiation combined with bevacizumab for recurrent glioblastoma beyond bevacizumab failure: survival outcomes and prognostic factors*. Scientific Reports, 2023. **13**(1): p. 9442 DOI: 10.1038/s41598-023-36290-2.
46. Ameratunga, M., et al., *Anti-angiogenic therapy for high-grade glioma*. Cochrane Database of Systematic Reviews, 2018(11) DOI: 10.1002/14651858.CD008218.pub4.
47. Fu, M., et al., *Use of Bevacizumab in recurrent glioblastoma: a scoping review and evidence map*. BMC Cancer, 2023. **23**(1): p. 544 DOI: 10.1186/s12885-023-11043-6.
48. Ranchor, R., et al., *3P Bevacizumab plus irinotecan as second-line treatment of glioblastoma: Real-world evidence*. ESMO Open, 2023. **8**(1) DOI: 10.1016/j.esmoop.2023.101015.
49. Alves, B., et al., *High VEGFA Expression Is Associated with Improved Progression-Free Survival after Bevacizumab Treatment in Recurrent Glioblastoma*. Cancers, 2023. **15**(8): p. 2196
50. Chiesa, S., et al., *Clinical and NGS predictors of response to regorafenib in recurrent glioblastoma*. Scientific Reports, 2022. **12**(1): p. 16265 DOI: 10.1038/s41598-022-20417-y.
51. Lombardi, G., et al., *Regorafenib compared with lomustine in patients with relapsed glioblastoma (REGOMA): a multicentre, open-label, randomised, controlled, phase 2 trial*. The Lancet Oncology, 2019. **20**(1): p. 110-119 DOI: 10.1016/S1470-2045(18)30675-2.
52. Mongiardi, M.P., et al., *Regorafenib and glioblastoma: a literature review of preclinical studies, molecular mechanisms and clinical effectiveness*. Expert Rev Mol Med, 2024. **26**: p. e5 DOI: 10.1017/erm.2024.8.
53. Pearson, J.R.D. and T. Regad, *Targeting cellular pathways in glioblastoma multiforme*. Signal Transduct Target Ther, 2017. **2**: p. 17040 DOI: 10.1038/sigtrans.2017.40.
54. Brar, H.K., et al., *Tyrosine Kinase Inhibitors for Glioblastoma Multiforme: Challenges and Opportunities for Drug Delivery*. Pharmaceutics, 2022. **15**(1) DOI: 10.3390/pharmaceutics15010059.
55. Rahban, M., et al., *Characterization of prevalent tyrosine kinase inhibitors and their challenges in glioblastoma treatment*. Frontiers in Chemistry, 2024. **11** DOI: 10.3389/fchem.2023.1325214.

56. Arrieta, V.A., et al., *Immune checkpoint blockade in glioblastoma: from tumor heterogeneity to personalized treatment*. The Journal of Clinical Investigation, 2023. **133**(2) DOI: 10.1172/JCI163447.
57. Ser, M.H., et al., *Immune Checkpoint Inhibitors and Glioblastoma: A Review on Current State and Future Directions*. J Immunother Precis Oncol, 2024. **7**(2): p. 97-110 DOI: 10.36401/jipo-23-34.
58. Wang, H., et al., *Current state of immune checkpoints therapy for glioblastoma*. Heliyon, 2024. **10**(2): p. e24729 DOI: https://doi.org/10.1016/j.heliyon.2024.e24729.
59. Schonfeld, E., et al., *The landscape of immune checkpoint inhibitor clinical trials in glioblastoma: A systematic review*. Neurooncol Adv, 2024. **6**(1): p. vdae174 DOI: 10.1093/noajnl/vdae174.
60. Davis, M.E., *Glioblastoma: Overview of Disease and Treatment*. Clin J Oncol Nurs, 2016. **20**(5 Suppl): p. S2-8 DOI: 10.1188/16.CJON.S1.2-8.
61. Kirson, E.D., et al., *Alternating electric fields arrest cell proliferation in animal tumor models and human brain tumors*. Proc Natl Acad Sci U S A, 2007. **104**(24): p. 10152-7 DOI: 10.1073/pnas.0702916104.
62. Stupp, R., et al., *Tumor Treating Fields (TTFields) – A novel cancer treatment modality: Translating preclinical evidence and engineering into a survival benefit with delayed decline in quality of life*. Annals of Oncology, 2017. **28**: p. v112 DOI: 10.1093/annonc/mdx366.009.
63. Wang, Y., M. Pandey, and M.T. Ballo, *Integration of Tumor-Treating Fields into the Multidisciplinary Management of Patients with Solid Malignancies*. Oncologist, 2019. **24**(12): p. e1426-e1436 DOI: 10.1634/theoncologist.2017-0603.
64. Tan, A.C., et al., *Management of glioblastoma: State of the art and future directions*. CA: A Cancer Journal for Clinicians, 2020. **70**(4): p. 299-312 DOI: https://doi.org/10.3322/caac.21613.
65. Chang, C., et al., *Recurrent Glioblastoma—Molecular Underpinnings and Evolving Treatment Paradigms*. International Journal of Molecular Sciences, 2024. **25**(12): p. 6733
66. Birzu, C., et al., *Recurrent Glioblastoma: From Molecular Landscape to New Treatment Perspectives*. Cancers (Basel), 2020. **13**(1) DOI: 10.3390/cancers13010047.
67. Carpentier, A., et al., *Repeated blood–brain barrier opening with a nine-emitter implantable ultrasound device in combination with carboplatin in recurrent glioblastoma: a phase I/II clinical trial*. Nature Communications, 2024. **15**(1): p. 1650 DOI: 10.1038/s41467-024-45818-7.
68. Ling, A.L., et al., *Clinical trial links oncolytic immunoactivation to survival in glioblastoma*. Nature, 2023. **623**(7985): p. 157-166 DOI: 10.1038/s41586-023-06623-2.
69. Barthel, L., et al., *Glioma: molecular signature and crossroads with tumor microenvironment*. Cancer Metastasis Rev, 2022. **41**(1): p. 53-75 DOI: 10.1007/s10555-021-09997-9.
70. Himes, B.T., et al., *Immunosuppression in Glioblastoma: Current Understanding and Therapeutic Implications*. Front Oncol, 2021. **11**: p. 770561 DOI: 10.3389/fonc.2021.770561.

71. Eisenbarth, D. and Y.A. Wang, *Glioblastoma heterogeneity at single cell resolution*. Oncogene, 2023. **42**(27): p. 2155-2165 DOI: 10.1038/s41388-023-02738-y.
72. Huse, J.T., H.S. Phillips, and C.W. Brennan, *Molecular subclassification of diffuse gliomas: Seeing order in the chaos*. Glia, 2011. **59**(8): p. 1190-1199 DOI: https://doi.org/10.1002/glia.21165.
73. Lin, N., et al., *Prevalence and Clinicopathologic Characteristics of the Molecular Subtypes in Malignant Glioma: A Multi-Institutional Analysis of 941 Cases*. PLOS ONE, 2014. **9**(4): p. e94871 DOI: 10.1371/journal.pone.0094871.
74. Chen, R., et al., *Glioma Subclassifications and Their Clinical Significance*. Neurotherapeutics, 2017. **14**(2): p. 284-297 DOI: 10.1007/s13311-017-0519-x.
75. Rodriguez, S.M.B., et al., *An Overview of EGFR Mechanisms and Their Implications in Targeted Therapies for Glioblastoma*. Int J Mol Sci, 2023. **24**(13) DOI: 10.3390/ijms241311110.
76. Lee, Y.-J., et al., *Gene expression profiling of glioblastoma cell lines depending on TP53 status after tumor-treating fields (TTFields) treatment*. Scientific Reports, 2020. **10**(1): p. 12272 DOI: 10.1038/s41598-020-68473-6.
77. Brennan, Cameron W., et al., *The Somatic Genomic Landscape of Glioblastoma*. Cell, 2013. **155**(2): p. 462-477 DOI: 10.1016/j.cell.2013.09.034.
78. Zhang, P., et al., *Current Opinion on Molecular Characterization for GBM Classification in Guiding Clinical Diagnosis, Prognosis, and Therapy*. Front Mol Biosci, 2020. **7**: p. 562798 DOI: 10.3389/fmolb.2020.562798.
79. Behnan, J., G. Finocchiaro, and G. Hanna, *The landscape of the mesenchymal signature in brain tumours*. Brain, 2019. **142**(4): p. 847-866 DOI: 10.1093/brain/awz044.
80. Azam, Z., S.-S.T. TO, and B.A. Tannous, *Mesenchymal Transformation: The Rosetta Stone of Glioblastoma Pathogenesis and Therapy Resistance*. Advanced Science, 2020. **7**(22): p. 2002015 DOI: https://doi.org/10.1002/advs.202002015.
81. Neftel, C., et al., *An Integrative Model of Cellular States, Plasticity, and Genetics for Glioblastoma*. Cell, 2019. **178**(4): p. 835-849.e21 DOI: 10.1016/j.cell.2019.06.024.
82. Couturier, C.P., et al., *Single-cell RNA-seq reveals that glioblastoma recapitulates a normal neurodevelopmental hierarchy*. Nature Communications, 2020. **11**(1): p. 3406 DOI: 10.1038/s41467-020-17186-5.
83. Nikitin, P.V., et al., *Cell-Population Dynamics in Diffuse Gliomas during Gliomagenesis and Its Impact on Patient Survival*. Cancers (Basel), 2022. **15**(1) DOI: 10.3390/cancers15010145.
84. Gimple, R.C., et al., *Glioblastoma stem cells: lessons from the tumor hierarchy in a lethal cancer*. Genes Dev, 2019. **33**(11-12): p. 591-609 DOI: 10.1101/gad.324301.119.
85. Eckerdt, F. and L.C. Platanias, *Emerging Role of Glioma Stem Cells in Mechanisms of Therapy Resistance*. Cancers, 2023. **15**(13): p. 3458

86. Almairac, F., et al., *ERK-Mediated Loss of miR-199a-3p and Induction of EGR1 Act as a "Toggle Switch" of GBM Cell Dedifferentiation into NANOG- and OCT4-Positive Cells*. Cancer Research, 2020. **80**(16): p. 3236-3250 DOI: 10.1158/0008-5472.Can-19-0855.
87. Ma, D.K., et al., *Adult neural stem cells in the mammalian central nervous system*. Cell Res, 2009. **19**(6): p. 672-82 DOI: 10.1038/cr.2009.56.
88. Eramo, A., et al., *Chemotherapy resistance of glioblastoma stem cells*. Cell Death & Differentiation, 2006. **13**(7): p. 1238-1241 DOI: 10.1038/sj.cdd.4401872.
89. Auffinger, B., et al., *The role of glioma stem cells in chemotherapy resistance and glioblastoma multiforme recurrence*. Expert Rev Neurother, 2015. **15**(7): p. 741-52 DOI: 10.1586/14737175.2015.1051968.
90. Hersh, A.M., et al., *Molecular Pathways and Genomic Landscape of Glioblastoma Stem Cells: Opportunities for Targeted Therapy*. Cancers (Basel), 2022. **14**(15) DOI: 10.3390/cancers14153743.
91. Crivii, C.-B., et al., *Glioblastoma Microenvironment and Cellular Interactions*. Cancers, 2022. **14**(4): p. 1092
92. Liu, S., et al., *Regulatory T cells promote glioma cell stemness through TGF-β–NF-κB–IL6–STAT3 signaling*. Cancer Immunology, Immunotherapy, 2021. **70**(9): p. 2601-2616 DOI: 10.1007/s00262-021-02872-0.
93. Li, X., et al., *Research Progress About Glioma Stem Cells in the Immune Microenvironment of Glioma*. Front Pharmacol, 2021. **12**: p. 750857 DOI: 10.3389/fphar.2021.750857.
94. Sharma, P., et al., *Tumor microenvironment in glioblastoma: Current and emerging concepts*. Neurooncol Adv, 2023. **5**(1): p. vdad009 DOI: 10.1093/noajnl/vdad009.
95. Persico, P., et al., *Checkpoint Inhibitors as High-Grade Gliomas Treatment: State of the Art and Future Perspectives*. J Clin Med, 2021. **10**(7) DOI: 10.3390/jcm10071367.
96. Roesch, S., et al., *When Immune Cells Turn Bad-Tumor-Associated Microglia/Macrophages in Glioma*. Int J Mol Sci, 2018. **19**(2) DOI: 10.3390/ijms19020436.
97. Mi, Y., et al., *The Emerging Role of Myeloid-Derived Suppressor Cells in the Glioma Immune Suppressive Microenvironment*. Frontiers in Immunology, 2020. **11** DOI: 10.3389/fimmu.2020.00737.
98. Alban, T.J., et al., *Glioblastoma Myeloid-Derived Suppressor Cell Subsets Express Differential Macrophage Migration Inhibitory Factor Receptor Profiles That Can Be Targeted to Reduce Immune Suppression*. Front Immunol, 2020. **11**: p. 1191 DOI: 10.3389/fimmu.2020.01191.
99. Veglia, F., E. Sanseviero, and D.I. Gabrilovich, *Myeloid-derived suppressor cells in the era of increasing myeloid cell diversity*. Nature Reviews Immunology, 2021. **21**(8): p. 485-498 DOI: 10.1038/s41577-020-00490-y.
100. Gabrilovich, D.I., *Myeloid-Derived Suppressor Cells*. Cancer Immunology Research, 2017. **5**(1): p. 3-8 DOI: 10.1158/2326-6066.Cir-16-0297.
101. Fares, J., et al., *Advances in NK cell therapy for brain tumors*. npj Precision Oncology, 2023. **7**(1): p. 17 DOI: 10.1038/s41698-023-00356-1.

102. Galbo, P.M., Jr., et al., *Functional Contribution and Clinical Implication of Cancer-Associated Fibroblasts in Glioblastoma*. Clin Cancer Res, 2024. **30**(4): p. 865-876 DOI: 10.1158/1078-0432.Ccr-23-0493.
103. Zuo, M., et al., *Glioma-associated fibroblasts promote glioblastoma resistance to temozolomide through CCL2-CCR2 paracrine signaling*. bioRxiv, 2024: p. 2024.03.05.581575 DOI: 10.1101/2024.03.05.581575.
104. Lootens, T., et al., *Glioblastoma-Associated Mesenchymal Stem/Stromal Cells and Cancer-Associated Fibroblasts: Partners in Crime?* International Journal of Molecular Sciences, 2024. **25**(4): p. 2285
105. Zhang, C., et al., *CAFs orchestrates tumor immune microenvironment—A new target in cancer therapy?* Frontiers in Pharmacology, 2023. **14** DOI: 10.3389/fphar.2023.1113378.
106. Randles, A., et al., *Computational modelling of perivascular-niche dynamics for the optimization of treatment schedules for glioblastoma*. Nat Biomed Eng, 2021. **5**(4): p. 346-359 DOI: 10.1038/s41551-021-00710-3.
107. Ahir, B.K., H.H. Engelhard, and S.S. Lakka, *Tumor Development and Angiogenesis in Adult Brain Tumor: Glioblastoma*. Mol Neurobiol, 2020. **57**(5): p. 2461-2478 DOI: 10.1007/s12035-020-01892-8.
108. Hovis, G., et al., *Understanding the Role of Endothelial Cells in Glioblastoma: Mechanisms and Novel Treatments*. Int J Mol Sci, 2024. **25**(11) DOI: 10.3390/ijms25116118.
109. Pacheco, C., et al., *Glioblastoma Vasculature: From its Critical Role in Tumor Survival to Relevant in Vitro Modelling*. Frontiers in Drug Delivery, 2022. **2** DOI: 10.3389/fddev.2022.823412.
110. Maddison, K., et al., *Characteristics of vasculogenic mimicry and tumour to endothelial transdifferentiation in human glioblastoma: a systematic review*. BMC Cancer, 2023. **23**(1): p. 185 DOI: 10.1186/s12885-023-10659-y.
111. Zhu, T.S., et al., *Endothelial Cells Create a Stem Cell Niche in Glioblastoma by Providing NOTCH Ligands That Nurture Self-Renewal of Cancer Stem-Like Cells*. Cancer Research, 2011. **71**(18): p. 6061-6072 DOI: 10.1158/0008-5472.Can-10-4269.
112. Lam, D., et al., *Tissue-specific extracellular matrix accelerates the formation of neural networks and communities in a neuron-glia co-culture on a multi-electrode array*. Scientific Reports, 2019. **9**(1): p. 4159 DOI: 10.1038/s41598-019-40128-1.
113. Lau, L.W., et al., *Pathophysiology of the brain extracellular matrix: a new target for remyelination*. Nature Reviews Neuroscience, 2013. **14**(10): p. 722-729 DOI: 10.1038/nrn3550.
114. Marino, S., et al., *The Extracellular Matrix in Glioblastomas: A Glance at Its Structural Modifications in Shaping the Tumoral Microenvironment-A Systematic Review*. Cancers (Basel), 2023. **15**(6) DOI: 10.3390/cancers15061879.
115. Safarians, G., et al., *Glioblastoma Spheroid Invasion through Soft, Brain-Like Matrices Depends on Hyaluronic Acid–CD44 Interactions*. Advanced Healthcare Materials, 2023. **12**(14): p. 2203143 DOI: https://doi.org/10.1002/adhm.202203143.

116. Serres, E., et al., *Fibronectin expression in glioblastomas promotes cell cohesion, collective invasion of basement membrane in vitro and orthotopic tumor growth in mice*. Oncogene, 2014. **33**(26): p. 3451-3462 DOI: 10.1038/onc.2013.305.
117. Wang, C., et al., *Matrix Stiffness Modulates Patient-Derived Glioblastoma Cell Fates in Three-Dimensional Hydrogels*. Tissue Eng Part A, 2021. **27**(5-6): p. 390-401 DOI: 10.1089/ten.TEA.2020.0110.
118. Erices, J.I., et al., *Glioblastoma Microenvironment and Invasiveness: New Insights and Therapeutic Targets*. International Journal of Molecular Sciences, 2023. **24**(8): p. 7047
119. Belousov, A., et al., *The Extracellular Matrix and Biocompatible Materials in Glioblastoma Treatment*. Front Bioeng Biotechnol, 2019. **7**: p. 341 DOI: 10.3389/fbioe.2019.00341.
120. Gupta, R.K., et al., *Tumor-specific migration routes of xenotransplanted human glioblastoma cells in mouse brain*. Scientific Reports, 2024. **14**(1): p. 864 DOI: 10.1038/s41598-023-51063-7.
121. Sood, D., et al., *3D extracellular matrix microenvironment in bioengineered tissue models of primary pediatric and adult brain tumors*. Nat Commun, 2019. **10**(1): p. 4529 DOI: 10.1038/s41467-019-12420-1.
122. Ganguly, K., et al., *Biological significance and pathophysiological role of Matrix Metalloproteinases in the Central Nervous System*. International Journal of Biological Macromolecules, 2024. **280**: p. 135967 DOI: https://doi.org/10.1016/j.ijbiomac.2024.135967.
123. White, J., et al., *The tumour microenvironment, treatment resistance and recurrence in glioblastoma*. Journal of Translational Medicine, 2024. **22**(1): p. 540 DOI: 10.1186/s12967-024-05301-9.
124. Raghani, N.R., et al., *Revolutionizing cancer treatment: comprehensive insights into immunotherapeutic strategies*. Medical Oncology, 2024. **41**(2): p. 51 DOI: 10.1007/s12032-023-02280-7.
125. Liu, Y., et al., *Immunotherapy for glioblastoma: current state, challenges, and future perspectives*. Cellular & Molecular Immunology, 2024 DOI: 10.1038/s41423-024-01226-x.
126. Khabibov, M., et al., *Signaling pathways and therapeutic approaches in glioblastoma multiforme (Review)*. Int J Oncol, 2022. **60**(6) DOI: 10.3892/ijo.2022.5359.
127. Hamad, A., et al., *Recent Developments in Glioblastoma Therapy: Oncolytic Viruses and Emerging Future Strategies*. Viruses, 2023. **15**(2) DOI: 10.3390/v15020547.
128. Hersh, A.M., et al., *Applications of Focused Ultrasound for the Treatment of Glioblastoma: A New Frontier*. Cancers (Basel), 2022. **14**(19) DOI: 10.3390/cancers14194920.
129. Wu, D., et al., *The blood–brain barrier: Structure, regulation and drug delivery*. Signal Transduction and Targeted Therapy, 2023. **8**(1): p. 217 DOI: 10.1038/s41392-023-01481-w.
130. Mărginean, L., et al., *CT in the Differentiation of Gliomas from Brain Metastases: The Radiomics Analysis of the Peritumoral Zone*. Brain Sciences, 2022. **12**(1): p. 109

131. Manzarbeitia-Arroba, B., et al., *18F-Fluoroethyl-L Tyrosine Positron Emission Tomography Radiomics in the Differentiation of Treatment-Related Changes from Disease Progression in Patients with Glioblastoma*. Cancers, 2024. **16**(1): p. 195
132. Yusuf, A., et al., *Nanoparticles as Drug Delivery Systems: A Review of the Implication of Nanoparticles' Physicochemical Properties on Responses in Biological Systems*. Polymers, 2023. **15**(7): p. 1596
133. Yu, W., et al., *Size-Tunable Strategies for a Tumor Targeted Drug Delivery System*. ACS Cent Sci, 2020. **6**(2): p. 100-116 DOI: 10.1021/acscentsci.9b01139.
134. Ruiz-Molina, D., et al., *Advances in Preclinical/Clinical Glioblastoma Treatment: Can Nanoparticles Be of Help?* Cancers (Basel), 2022. **14**(19) DOI: 10.3390/cancers14194960.
135. Lai, G., et al., *Progress of nanoparticle drug delivery system for the treatment of glioma*. Frontiers in Bioengineering and Biotechnology, 2024. **12** DOI: 10.3389/fbioe.2024.1403511.
136. Fabel, K., et al., *Long-term stabilization in patients with malignant glioma after treatment with liposomal doxorubicin*. Cancer, 2001. **92**(7): p. 1936-42 DOI: 10.1002/1097-0142(20011001)92:7<1936::aid-cncr1712>3.0.co;2-h.
137. Chua, S.L., et al., *Phase 2 study of temozolomide and Caelyx in patients with recurrent glioblastoma multiforme*. Neuro Oncol, 2004. **6**(1): p. 38-43 DOI: 10.1215/s1152851703000188.
138. Hau, P., et al., *Pegylated liposomal doxorubicin-efficacy in patients with recurrent high-grade glioma*. Cancer, 2004. **100**(6): p. 1199-207 DOI: 10.1002/cncr.20073.
139. Beier, C.P., et al., *RNOP-09: pegylated liposomal doxorubicine and prolonged temozolomide in addition to radiotherapy in newly diagnosed glioblastoma--a phase II study*. BMC Cancer, 2009. **9**: p. 308 DOI: 10.1186/1471-2407-9-308.
140. Ananda, S., et al., *Phase 2 trial of temozolomide and pegylated liposomal doxorubicin in the treatment of patients with glioblastoma multiforme following concurrent radiotherapy and chemotherapy*. J Clin Neurosci, 2011. **18**(11): p. 1444-8 DOI: 10.1016/j.jocn.2011.02.026.
141. Clarke, J.L., et al., *A phase I trial of intravenous liposomal irinotecan in patients with recurrent high-grade gliomas*. Journal of Clinical Oncology, 2015. **33**(15_suppl): p. 2029-2029 DOI: 10.1200/jco.2015.33.15_suppl.2029.
142. Elinzano, H., et al., *Nanoliposomal Irinotecan and Metronomic Temozolomide for Patients With Recurrent Glioblastoma: BrUOG329, A Phase I Brown University Oncology Research Group Trial*. Am J Clin Oncol, 2021. **44**(2): p. 49-52 DOI: 10.1097/coc.0000000000000780.
143. Roque, D., et al., *Nanoparticle-Based Treatment in Glioblastoma*. J Pers Med, 2023. **13**(9) DOI: 10.3390/jpm13091328.
144. Horta, M., et al., *Nanostructured lipid carriers for enhanced batimastat delivery across the blood–brain barrier: an in vitro study for glioblastoma treatment*. Drug Delivery and Translational Research, 2025 DOI: 10.1007/s13346-024-01775-8.

145. Arvanitis, C.D., G.B. Ferraro, and R.K. Jain, *The blood-brain barrier and blood-tumour barrier in brain tumours and metastases*. Nat Rev Cancer, 2020. **20**(1): p. 26-41 DOI: 10.1038/s41568-019-0205-x.
146. Kadry, H., B. Noorani, and L. Cucullo, *A blood–brain barrier overview on structure, function, impairment, and biomarkers of integrity*. Fluids and Barriers of the CNS, 2020. **17**(1): p. 69 DOI: 10.1186/s12987-020-00230-3.
147. Sugiyama, S., et al., *The tight junction protein occludin modulates blood–brain barrier integrity and neurological function after ischemic stroke in mice*. Scientific Reports, 2023. **13**(1): p. 2892 DOI: 10.1038/s41598-023-29894-1.
148. Hashimoto, Y. and M. Campbell, *Tight junction modulation at the blood-brain barrier: Current and future perspectives*. Biochimica et Biophysica Acta (BBA) - Biomembranes, 2020. **1862**(9): p. 183298 DOI: https://doi.org/10.1016/j.bbamem.2020.183298.
149. Stamatovic, S.M., et al., *Junctional proteins of the blood-brain barrier: New insights into function and dysfunction*. Tissue Barriers, 2016. **4**(1): p. e1154641 DOI: 10.1080/21688370.2016.1154641.
150. Zheng, X., B. Ren, and Y. Gao, *Tight junction proteins related to blood-brain barrier and their regulatory signaling pathways in ischemic stroke*. Biomedicine & Pharmacotherapy, 2023. **165**: p. 115272 DOI: https://doi.org/10.1016/j.biopha.2023.115272.
151. Schaeffer, S. and C. Iadecola, *Revisiting the neurovascular unit*. Nature Neuroscience, 2021. **24**(9): p. 1198-1209 DOI: 10.1038/s41593-021-00904-7.
152. Lia, A., et al., *Two decades of astrocytes in neurovascular coupling*. Front Netw Physiol, 2023. **3**: p. 1162757 DOI: 10.3389/fnetp.2023.1162757.
153. Ding, Z., et al., *Emerging Roles of Microglia in Neuro-vascular Unit: Implications of Microglia-Neurons Interactions*. Frontiers in Cellular Neuroscience, 2021. **15** DOI: 10.3389/fncel.2021.706025.
154. Sweeney, M.D., S. Ayyadurai, and B.V. Zlokovic, *Pericytes of the neurovascular unit: key functions and signaling pathways*. Nature Neuroscience, 2016. **19**(6): p. 771-783 DOI: 10.1038/nn.4288.
155. Curley, S.M. and N.C. Cady, *Biologically-Derived Nanomaterials for Targeted Therapeutic Delivery to the Brain*. Science Progress, 2018. **101**(3): p. 273-292 DOI: 10.3184/003685018X15306123582346.
156. Soni, V., et al., *Chapter 14 - Design and Fabrication of Brain-Targeted Drug Delivery*, in *Basic Fundamentals of Drug Delivery*, R.K. Tekade, Editor. 2019, Academic Press. p. 539-593.
157. Zaragozá, R., *Transport of Amino Acids Across the Blood-Brain Barrier*. Frontiers in Physiology, 2020. **11** DOI: 10.3389/fphys.2020.00973.
158. Latif, S. and Y.S. Kang, *Blood-Brain Barrier Solute Carrier Transporters and Motor Neuron Disease*. Pharmaceutics, 2022. **14**(10) DOI: 10.3390/pharmaceutics14102167.
159. Zhu, X., et al., *7 - Brain drug delivery by adsorption-mediated transcytosis*, in *Brain Targeted Drug Delivery System*, H. Gao and X. Gao, Editors. 2019, Academic Press. p. 159-183.

160. Haqqani, A.S., K. Bélanger, and D.B. Stanimirovic, *Receptor-mediated transcytosis for brain delivery of therapeutics: receptor classes and criteria*. Frontiers in Drug Delivery, 2024. **4** DOI: 10.3389/fddev.2024.1360302.
161. Ntafoulis, I., et al., *Drug Repurposing, a Fast-Track Approach to Develop Effective Treatments for Glioblastoma*. Cancers, 2022. **14**(15): p. 3705
162. Profaci, C.P., et al., *The blood-brain barrier in health and disease: Important unanswered questions*. J Exp Med, 2020. **217**(4) DOI: 10.1084/jem.20190062.
163. Sweeney, M.D., A.P. Sagare, and B.V. Zlokovic, *Blood–brain barrier breakdown in Alzheimer disease and other neurodegenerative disorders*. Nature Reviews Neurology, 2018. **14**(3): p. 133-150 DOI: 10.1038/nrneurol.2017.188.
164. Zierfuss, B., C. Larochelle, and A. Prat, *Blood-brain barrier dysfunction in multiple sclerosis: causes, consequences, and potential effects of therapies*. The Lancet Neurology, 2024. **23**(1): p. 95-109 DOI: 10.1016/S1474-4422(23)00377-0.
165. Moura, R.P., et al., *Functionalized retinoic acid lipid nanocapsules promotes a two-front attack on inflammation and lack of demyelination on neurodegenerative disorders*. Journal of Controlled Release, 2023. **358**: p. 43-58 DOI: https://doi.org/10.1016/j.jconrel.2023.04.034.
166. Ulbrich, K., T. Knobloch, and J. Kreuter, *Targeting the insulin receptor: nanoparticles for drug delivery across the blood-brain barrier (BBB)*. J Drug Target, 2011. **19**(2): p. 125-32 DOI: 10.3109/10611861003734001.
167. Zhang, B., et al., *LDLR-mediated peptide-22-conjugated nanoparticles for dual-targeting therapy of brain glioma*. Biomaterials, 2013. **34**(36): p. 9171-82 DOI: 10.1016/j.biomaterials.2013.08.039.
168. Tosi, G., et al., *Can leptin-derived sequence-modified nanoparticles be suitable tools for brain delivery?* Nanomedicine (Lond), 2012. **7**(3): p. 365-82 DOI: 10.2217/nnm.11.98.
169. You, L., et al., *Targeted Brain Delivery of Rabies Virus Glycoprotein 29-Modified Deferoxamine-Loaded Nanoparticles Reverses Functional Deficits in Parkinsonian Mice*. ACS Nano, 2018. **12**(5): p. 4123-4139 DOI: 10.1021/acsnano.7b08172.
170. Gaillard, P.J., et al., *Enhanced brain drug delivery: safely crossing the blood-brain barrier*. Drug Discov Today Technol, 2012. **9**(2): p. e71-e174 DOI: 10.1016/j.ddtec.2011.12.002.
171. Ashizawa, A.T. and D. Steindler, *Et-61 * Novel Lipid Nanoparticles for the Delivery of Nucleic Acids to Glioblastoma*. Neuro-Oncology, 2014. **16**(suppl 5): p. v92-v92 DOI: 10.1093/neuonc/nou255.58.
172. Gromnicova, R., et al., *Glucose-coated gold nanoparticles transfer across human brain endothelium and enter astrocytes in vitro*. PLoS One, 2013. **8**(12): p. e81043 DOI: 10.1371/journal.pone.0081043.
173. Jagtiani, E., et al., *In vitro blood brain barrier models: An overview*. Journal of Controlled Release, 2022. **343**: p. 13-30 DOI: https://doi.org/10.1016/j.jconrel.2022.01.011.

174. Chaulagain, B., et al., *Experimental Models of In Vitro Blood–Brain Barrier for CNS Drug Delivery: An Evolutionary Perspective*. International Journal of Molecular Sciences, 2023. **24**(3): p. 2710
175. Gomes, M.J., et al., *Delivery of siRNA silencing P-gp in peptide-functionalized nanoparticles causes efflux modulation at the blood-brain barrier*. Nanomedicine (Lond), 2017. **12**(12): p. 1385-1399 DOI: 10.2217/nnm-2017-0023.
176. He, Y., et al., *Cell-Culture Models of the Blood–Brain Barrier*. Stroke, 2014. **45**(8): p. 2514-2526 DOI: 10.1161/STROKEAHA.114.005427.
177. Park, J.S., et al., *Establishing Co-Culture Blood–Brain Barrier Models for Different Neurodegeneration Conditions to Understand Its Effect on BBB Integrity*. International Journal of Molecular Sciences, 2023. **24**(6): p. 5283
178. Hajal, C., et al., *Engineered human blood-brain barrier microfluidic model for vascular permeability analyses*. Nat Protoc, 2022. **17**(1): p. 95-128 DOI: 10.1038/s41596-021-00635-w.
179. Andjelkovic, A.V., et al., *Modeling blood-brain barrier pathology in cerebrovascular disease in vitro: current and future paradigms*. Fluids Barriers CNS, 2020. **17**(1): p. 44 DOI: 10.1186/s12987-020-00202-7.
180. Li, M., et al., *Blood–brain barrier microfluidic chips and their applications*. Organs-on-a-Chip, 2023. **5**: p. 100027 DOI: https://doi.org/10.1016/j.ooc.2023.100027.
181. Wang, Y.I., H.E. Abaci, and M.L. Shuler, *Microfluidic blood-brain barrier model provides in vivo-like barrier properties for drug permeability screening*. Biotechnol Bioeng, 2017. **114**(1): p. 184-194 DOI: 10.1002/bit.26045.
182. Cui, B. and S.W. Cho, *Blood-brain barrier-on-a-chip for brain disease modeling and drug testing*. BMB Rep, 2022. **55**(5): p. 213-219 DOI: 10.5483/BMBRep.2022.55.5.043.
183. Cameron, T., et al., *Review of Design Considerations for Brain-on-a-Chip Models*. Micromachines (Basel), 2021. **12**(4) DOI: 10.3390/mi12040441.
184. Ribecco-Lutkiewicz, M., et al., *A novel human induced pluripotent stem cell blood-brain barrier model: Applicability to study antibody-triggered receptor-mediated transcytosis*. Scientific Reports, 2018. **8**(1): p. 1873 DOI: 10.1038/s41598-018-19522-8.
185. Delsing, L., et al., *Models of the blood-brain barrier using iPSC-derived cells*. Molecular and Cellular Neuroscience, 2020. **107**: p. 103533 DOI: https://doi.org/10.1016/j.mcn.2020.103533.
186. Gu, G., et al., *PEG-co-PCL nanoparticles modified with MMP-2/9 activatable low molecular weight protamine for enhanced targeted glioblastoma therapy*. Biomaterials, 2013. **34**(1): p. 196-208 DOI: https://doi.org/10.1016/j.biomaterials.2012.09.044.
187. Xu, X., et al., *Nanomedicine Strategies to Circumvent Intratumor Extracellular Matrix Barriers for Cancer Therapy*. Advanced Healthcare Materials, 2022. **11**(1): p. 2101428 DOI: https://doi.org/10.1002/adhm.202101428.
188. Mohiuddin, E. and H. Wakimoto, *Extracellular matrix in glioblastoma: opportunities for emerging therapeutic approaches*. Am J Cancer Res, 2021. **11**(8): p. 3742-3754

189. Mai, Z., et al., *Modulating extracellular matrix stiffness: a strategic approach to boost cancer immunotherapy.* Cell Death & Disease, 2024. **15**(5): p. 307 DOI: 10.1038/s41419-024-06697-4.
190. Saw, P.E., et al., *Tumor-Associated Fibronectin Targeted Liposomal Nanoplatform for Cyclophilin A siRNA Delivery and Targeted Malignant Glioblastoma Therapy.* Frontiers in Pharmacology, 2018. **9** DOI: 10.3389/fphar.2018.01194.
191. Chung, E.J., et al., *Fibrin-binding, peptide amphiphile micelles for targeting glioblastoma*. Biomaterials, 2014. **35**(4): p. 1249-56 DOI: 10.1016/j.biomaterials.2013.10.064.
192. Kang, T., et al., *Synergistic targeting tenascin C and neuropilin-1 for specific penetration of nanoparticles for anti-glioblastoma treatment.* Biomaterials, 2016. **101**: p. 60-75 DOI: https://doi.org/10.1016/j.biomaterials.2016.05.037.
193. Lingasamy, P., et al., *Tumor-penetrating peptide for systemic targeting of Tenascin-C.* Scientific Reports, 2020. **10**(1): p. 5809 DOI: 10.1038/s41598-020-62760-y.
194. Lingasamy, P., et al., *PL1 Peptide Engages Acidic Surfaces on Tumor-Associated Fibronectin and Tenascin Isoforms to Trigger Cellular Uptake.* Pharmaceutics, 2021. **13**(12) DOI: 10.3390/pharmaceutics13121998.
195. Kasten, B.B., et al., *Targeting MMP-14 for dual PET and fluorescence imaging of glioma in preclinical models.* Eur J Nucl Med Mol Imaging, 2020. **47**(6): p. 1412-1426 DOI: 10.1007/s00259-019-04607-x.
196. Abakumov, M.A., et al., *VEGF-targeted magnetic nanoparticles for MRI visualization of brain tumor.* Nanomedicine: Nanotechnology, Biology and Medicine, 2015. **11**(4): p. 825-833 DOI: https://doi.org/10.1016/j.nano.2014.12.011.
197. Mohanty, S., et al., *A Novel Theranostic Strategy for MMP-14-Expressing Glioblastomas Impacts Survival.* Mol Cancer Ther, 2017. **16**(9): p. 1909-1921 DOI: 10.1158/1535-7163.MCT-17-0022.
198. Gao, H., et al., *Angiopep-2 and Activatable Cell-Penetrating Peptide Dual-Functionalized Nanoparticles for Systemic Glioma-Targeting Delivery.* Molecular Pharmaceutics, 2014. **11**(8): p. 2755-2763 DOI: 10.1021/mp500113p.
199. Fan, R., et al., *Engineering MMP-2 Activated Nanoparticles Carrying B7-H3 Bispecific Antibodies for Ferroptosis-Enhanced Glioblastoma Immunotherapy.* ACS Nano, 2023. **17**(10): p. 9126-9139 DOI: 10.1021/acsnano.2c12217.
200. Zhao, Y., et al., *Tumor-specific pH-responsive peptide-modified pH-sensitive liposomes containing doxorubicin for enhancing glioma targeting and anti-tumor activity.* Journal of Controlled Release, 2016. **222**: p. 56-66 DOI: https://doi.org/10.1016/j.jconrel.2015.12.006.
201. Sathiyaseelan, A., et al., *pH-controlled nucleolin targeted release of dual drug from chitosan-gold based aptamer functionalized nano drug delivery system for improved glioblastoma treatment.* Carbohydrate Polymers, 2021. **262**: p. 117907 DOI: https://doi.org/10.1016/j.carbpol.2021.117907.

202. Martins, C., et al., *Stimuli-Responsive Multifunctional Nanomedicine for Enhanced Glioblastoma Chemotherapy Augments Multistage Blood-to-Brain Trafficking and Tumor Targeting*. Small, 2023. **19**(22): p. e2300029 DOI: 10.1002/smll.202300029.
203. Dosta, P., et al., *Matrix Metalloproteinase- and pH-Sensitive Nanoparticle System Enhances Drug Retention and Penetration in Glioblastoma*. ACS Nano, 2024. **18**(22): p. 14145-14160 DOI: 10.1021/acsnano.3c03409.
204. Qi, J., et al., *Stepwise-targeting and hypoxia-responsive liposome AMVY@NPs carrying siYAP and verteporfin for glioblastoma therapy*. Journal of Nanobiotechnology, 2024. **22**(1): p. 495 DOI: 10.1186/s12951-024-02776-y.
205. Yang, G., et al., *Hollow MnO2 as a tumor-microenvironment-responsive biodegradable nano-platform for combination therapy favoring antitumor immune responses*. Nature Communications, 2017. **8**(1): p. 902 DOI: 10.1038/s41467-017-01050-0.
206. Tian, C., et al., *The effect of the molecular weight of hyaluronic acid on the physicochemical characterization of hyaluronic acid-curcumin conjugates and in vitro evaluation in glioma cells*. Colloids and Surfaces B: Biointerfaces, 2018. **165**: p. 45-55 DOI: https://doi.org/10.1016/j.colsurfb.2018.02.016.
207. Kiyokawa, J., et al., *Modification of Extracellular Matrix Enhances Oncolytic Adenovirus Immunotherapy in Glioblastoma*. Clin Cancer Res, 2021. **27**(3): p. 889-902 DOI: 10.1158/1078-0432.Ccr-20-2400.
208. Shukla, M.K., et al., *Tumor micro-environment targeted collagenase-modified albumin nanoparticles for improved drug delivery*. Journal of Drug Delivery Science and Technology, 2022. **71**: p. 103366 DOI: https://doi.org/10.1016/j.jddst.2022.103366.
209. Agarwal, S., et al., *Chlorotoxin modified morusin–PLGA nanoparticles for targeted glioblastoma therapy*. Journal of Materials Chemistry B, 2019. **7**(39): p. 5896-5919 DOI: 10.1039/C9TB01131E.
210. Islam, Y., et al., *Development of Brain Targeting Peptide Based MMP-9 Inhibiting Nanoparticles for the Treatment of Brain Diseases with Elevated MMP-9 Activity*. Journal of Pharmaceutical Sciences, 2020. **109**(10): p. 3134-3144 DOI: https://doi.org/10.1016/j.xphs.2020.06.021.
211. Ventura, E., et al., *TGF-β induces oncofetal fibronectin that, in turn, modulates TGF-β superfamily signaling in endothelial cells*. Journal of Cell Science, 2018. **131**(1) DOI: 10.1242/jcs.209619.
212. Lui, B.G., et al., *Targeting the tumor vasculature with engineered cystine-knot miniproteins*. Nature Communications, 2020. **11**(1): p. 295 DOI: 10.1038/s41467-019-13948-y.
213. Spaeth, N., et al., *Radioimmunotherapy targeting the extra domain B of fibronectin in C6 rat gliomas: a preliminary study about the therapeutic efficacy of iodine-131-labeled SIP(L19)*. Nuclear Medicine and Biology, 2006. **33**(5): p. 661-666 DOI: https://doi.org/10.1016/j.nucmedbio.2006.05.001.
214. Dzikowski, L., et al., *Fibrinogen in the glioblastoma microenvironment contributes to the invasiveness of brain tumor-initiating cells*. Brain Pathol, 2021. **31**(5): p. e12947 DOI: 10.1111/bpa.12947.

215. Zhang, N., et al., *Recent advances of CREKA peptide-based nanoplatforms in biomedical applications.* Journal of Nanobiotechnology, 2023. **21**(1): p. 77 DOI: 10.1186/s12951-023-01827-0.
216. Brack, S.S., et al., *Tumor-Targeting Properties of Novel Antibodies Specific to the Large Isoform of Tenascin-C.* Clinical Cancer Research, 2006. **12**(10): p. 3200-3208 DOI: 10.1158/1078-0432.Ccr-05-2804.
217. Zhou, W., et al., *Increased expression of MMP-2 and MMP-9 indicates poor prognosis in glioma recurrence.* Biomed Pharmacother, 2019. **118**: p. 109369 DOI: 10.1016/j.biopha.2019.109369.
218. de Almeida, L.G.N., et al., *Matrix Metalloproteinases: From Molecular Mechanisms to Physiology, Pathophysiology, and Pharmacology.* Pharmacological Reviews, 2022. **74**(3): p. 714-770 DOI: 10.1124/pharmrev.121.000349.
219. Ramachandran, R.K., et al., *Expression and prognostic impact of matrix metalloproteinase-2 (MMP-2) in astrocytomas.* PLoS One, 2017. **12**(2): p. e0172234 DOI: 10.1371/journal.pone.0172234.
220. Xue, Q., et al., *High expression of MMP9 in glioma affects cell proliferation and is associated with patient survival rates.* Oncol Lett, 2017. **13**(3): p. 1325-1330 DOI: 10.3892/ol.2017.5567.
221. Rao, J.S., *Molecular mechanisms of glioma invasiveness: the role of proteases.* Nat Rev Cancer, 2003. **3**(7): p. 489-501 DOI: 10.1038/nrc1121.
222. Conlon, G.A. and G.I. Murray, *Recent advances in understanding the roles of matrix metalloproteinases in tumour invasion and metastasis.* J Pathol, 2019. **247**(5): p. 629-640 DOI: 10.1002/path.5225.
223. Munaut, C., et al., *Vascular endothelial growth factor expression correlates with matrix metalloproteinases MT1-MMP, MMP-2 and MMP-9 in human glioblastomas.* Int J Cancer, 2003. **106**(6): p. 848-55 DOI: 10.1002/ijc.11313.
224. Ulasov, I., et al., *The emerging role of MMP14 in brain tumorigenesis and future therapeutics.* Biochimica et Biophysica Acta (BBA) - Reviews on Cancer, 2014. **1846**(1): p. 113-120 DOI: https://doi.org/10.1016/j.bbcan.2014.03.002.
225. Niland, S., A.X. Riscanevo, and J.A. Eble, *Matrix Metalloproteinases Shape the Tumor Microenvironment in Cancer Progression.* Int J Mol Sci, 2021. **23**(1) DOI: 10.3390/ijms23010146.
226. Hatoum, A., R. Mohammed, and O. Zakieh, *The unique invasiveness of glioblastoma and possible drug targets on extracellular matrix.* Cancer Manag Res, 2019. **11**: p. 1843-1855 DOI: 10.2147/CMAR.S186142.
227. Zhang, A.B., et al., *Exploring the Past, Present, and Future of Anti-Angiogenic Therapy in Glioblastoma.* Cancers, 2023. **15**(3): p. 830
228. Codrici, E., et al., *Glioma Stem Cells and Their Microenvironments: Providers of Challenging Therapeutic Targets.* Stem Cells International, 2016. **2016**(1): p. 5728438 DOI: https://doi.org/10.1155/2016/5728438.
229. Reardon, D.A., et al., *A review of VEGF/VEGFR-targeted therapeutics for recurrent glioblastoma.* J Natl Compr Canc Netw, 2011. **9**(4): p. 414-27 DOI: 10.6004/jnccn.2011.0038.

230. Wu, Z., et al., *Advances in magnetic resonance imaging contrast agents for glioblastoma-targeting theranostics*. Regen Biomater, 2021. **8**(6): p. rbab062 DOI: 10.1093/rb/rbab062.
231. Karamanos, N.K., et al., *A guide to the composition and functions of the extracellular matrix*. The FEBS Journal, 2021. **288**(24): p. 6850-6912 DOI: https://doi.org/10.1111/febs.15776.
232. Hogan, K.J., M.R. Perez, and A.G. Mikos, *Extracellular matrix component-derived nanoparticles for drug delivery and tissue engineering*. Journal of Controlled Release, 2023. **360**: p. 888-912 DOI: https://doi.org/10.1016/j.jconrel.2023.07.034.
233. Karimi, N., et al., *Bioinformatic analysis of MMP family members in GBM*. Informatics in Medicine Unlocked, 2023. **39**: p. 101240 DOI: https://doi.org/10.1016/j.imu.2023.101240.
234. Talib, W.H., et al., *Targeting Cancer Hallmarks with Epigallocatechin Gallate (EGCG): Mechanistic Basis and Therapeutic Targets*. Molecules, 2024. **29**(6): p. 1373
235. Bogdanov, A., et al., *Tumor acidity: From hallmark of cancer to target of treatment*. Frontiers in Oncology, 2022. **12** DOI: 10.3389/fonc.2022.979154.
236. Chen, Z., et al., *Hypoxic microenvironment in cancer: molecular mechanisms and therapeutic interventions*. Signal Transduction and Targeted Therapy, 2023. **8**(1): p. 70 DOI: 10.1038/s41392-023-01332-8.
237. Park, J.H. and H.K. Lee, *Current Understanding of Hypoxia in Glioblastoma Multiforme and Its Response to Immunotherapy*. Cancers (Basel), 2022. **14**(5) DOI: 10.3390/cancers14051176.
238. Kuo, C.-L., et al., *Mitochondrial oxidative stress in the tumor microenvironment and cancer immunoescape: foe or friend?* Journal of Biomedical Science, 2022. **29**(1): p. 74 DOI: 10.1186/s12929-022-00859-2.
239. Aggarwal, V., et al., *Role of Reactive Oxygen Species in Cancer Progression: Molecular Mechanisms and Recent Advancements*. Biomolecules, 2019. **9**(11) DOI: 10.3390/biom9110735.
240. Olivier, C., et al., *Drug Resistance in Glioblastoma: The Two Faces of Oxidative Stress*. Front Mol Biosci, 2020. **7**: p. 620677 DOI: 10.3389/fmolb.2020.620677.
241. Ma, W., et al., *Research Progress of Disulfide Bond Based Tumor Microenvironment Targeted Drug Delivery System*. Int J Nanomedicine, 2024. **19**: p. 7547-7566 DOI: 10.2147/ijn.S471734.
242. Li, J., et al., *Redox-sensitive micelles self-assembled from amphiphilic hyaluronic acid-deoxycholic acid conjugates for targeted intracellular delivery of paclitaxel*. Biomaterials, 2012. **33**(7): p. 2310-2320 DOI: https://doi.org/10.1016/j.biomaterials.2011.11.022.
243. Henke, E., R. Nandigama, and S. Ergün, *Extracellular Matrix in the Tumor Microenvironment and Its Impact on Cancer Therapy.* Frontiers in Molecular Biosciences, 2020. **6** DOI: 10.3389/fmolb.2019.00160.
244. Abyaneh, H.S., et al., *Towards extracellular matrix normalization for improved treatment of solid tumors*. Theranostics, 2020. **10**(4): p. 1960-1980 DOI: 10.7150/thno.39995.

245. Zhou, Y., et al., *Overcoming the biological barriers in the tumor microenvironment for improving drug delivery and efficacy*. Journal of Materials Chemistry B, 2020. **8**(31): p. 6765-6781 DOI: 10.1039/D0TB00649A.
246. Levin, V.A., et al., *Randomized, double-blind, placebo-controlled trial of marimastat in glioblastoma multiforme patients following surgery and irradiation*. J Neurooncol, 2006. **78**(3): p. 295-302 DOI: 10.1007/s11060-005-9098-5.
247. Groves, M.D., et al., *Phase II trial of temozolomide plus the matrix metalloproteinase inhibitor, marimastat, in recurrent and progressive glioblastoma multiforme*. J Clin Oncol, 2002. **20**(5): p. 1383-8 DOI: 10.1200/JCO.2002.20.5.1383.
248. Parsons, S.L., S.A. Watson, and R.J. Steele, *Phase I/II trial of batimastat, a matrix metalloproteinase inhibitor, in patients with malignant ascites*. Eur J Surg Oncol, 1997. **23**(6): p. 526-31 DOI: 10.1016/s0748-7983(97)93077-8.
249. Brown, P.D., *Matrix metalloproteinase inhibitors in the treatment of cancer*. Med Oncol, 1997. **14**(1): p. 1-10 DOI: 10.1007/BF02990939.
250. Mannello, F., G. Tonti, and S. Papa, *Matrix metalloproteinase inhibitors as anticancer therapeutics*. Curr Cancer Drug Targets, 2005. **5**(4): p. 285-98 DOI: 10.2174/1568009054064615.
251. Boguszewska-Czubara, A., et al., *Perspectives and New Aspects of Metalloproteinases' Inhibitors in the Therapy of CNS Disorders: From Chemistry to Medicine*. Curr Med Chem, 2019. **26**(18): p. 3208-3224 DOI: 10.2174/0929867325666180514111500.
252. Pijet, B., et al., *The matrix metalloproteinase inhibitor marimastat inhibits seizures in a model of kainic acid-induced status epilepticus*. Sci Rep, 2020. **10**(1): p. 21314 DOI: 10.1038/s41598-020-78341-y.
253. Mentlein, R., K. Hattermann, and J. Held-Feindt, *Lost in disruption: role of proteases in glioma invasion and progression*. Biochim Biophys Acta, 2012. **1825**(2): p. 178-85 DOI: 10.1016/j.bbcan.2011.12.001.
254. Cathcart, J., A. Pulkoski-Gross, and J. Cao, *Targeting Matrix Metalloproteinases in Cancer: Bringing New Life to Old Ideas*. Genes Dis, 2015. **2**(;1): p. 26-34 DOI: 10.1016/j.gendis.2014.12.002.
255. Quesnel, A., G.S. Karagiannis, and P.S. Filippou, *Extracellular proteolysis in glioblastoma progression and therapeutics*. Biochim Biophys Acta Rev Cancer, 2020. **1874**(2): p. 188428 DOI: 10.1016/j.bbcan.2020.188428.
256. Sehedic, D., et al., *Locoregional Confinement and Major Clinical Benefit of (188)Re-Loaded CXCR4-Targeted Nanocarriers in an Orthotopic Human to Mouse Model of Glioblastoma*. Theranostics, 2017. **7**(18): p. 4517-4536 DOI: 10.7150/thno.19403.
257. Fields, G.B., *Mechanisms of Action of Novel Drugs Targeting Angiogenesis-Promoting Matrix Metalloproteinases*. Front Immunol, 2019. **10**: p. 1278 DOI: 10.3389/fimmu.2019.01278.
258. Farkas, S., et al., *Chlorotoxin binds to both matrix metalloproteinase 2 and neuropilin 1*. J Biol Chem, 2023. **299**(9): p. 104998 DOI: 10.1016/j.jbc.2023.104998.

259. Esfandyari-Manesh, M., et al., *S2P peptide-conjugated PLGA-Maleimide-PEG nanoparticles containing Imatinib for targeting drug delivery to atherosclerotic plaques*. Daru, 2020. **28**(1): p. 131-138 DOI: 10.1007/s40199-019-00324-w.
260. Kebebe, D., et al., *Dimeric c(RGD) peptide conjugated nanostructured lipid carriers for efficient delivery of Gambogic acid to breast cancer*. Int J Nanomedicine, 2019. **14**: p. 6179-6195 DOI: 10.2147/IJN.S202424.
261. Gao, L., et al., *Tumor-penetrating Peptide Conjugated and Doxorubicin Loaded T(1)-T(2) Dual Mode MRI Contrast Agents Nanoparticles for Tumor Theranostics*. Theranostics, 2018. **8**(1): p. 92-108 DOI: 10.7150/thno.21074.
262. Smith, P.K., et al., *Measurement of protein using bicinchoninic acid*. Analytical Biochemistry, 1985. **150**(1): p. 76-85 DOI: https://doi.org/10.1016/0003-2697(85)90442-7.
263. Ferreira, M., et al., *Optimization of nanostructured lipid carriers loaded with methotrexate: A tool for inflammatory and cancer therapy*. Int J Pharm, 2015. **492**(1-2): p. 65-72 DOI: 10.1016/j.ijpharm.2015.07.013.
264. Udenfriend, S., et al., *Fluorescamine: A Reagent for Assay of Amino Acids, Peptides, Proteins, and Primary Amines in the Picomole Range*. Science, 1972. **178**(4063): p. 871-872 DOI: doi:10.1126/science.178.4063.871.
265. Cao, Z., et al., *Bioorthogonal in situ assembly of nanomedicines as drug depots for extracellular drug delivery*. Nat Commun, 2022. **13**(1): p. 2038 DOI: 10.1038/s41467-022-29693-8.
266. Morton, R.E. and T.A. Evans, *Modification of the bicinchoninic acid protein assay to eliminate lipid interference in determining lipoprotein protein content*. Analytical Biochemistry, 1992. **204**(2): p. 332-334 DOI: https://doi.org/10.1016/0003-2697(92)90248-6.
267. Peixoto, J., et al., *Using a Dual CRISPR/Cas9 Approach to Gain Insight into the Role of LRP1B in Glioblastoma*. International Journal of Molecular Sciences, 2023. **24**(14): p. 11285 DOI: https://doi.org/10.3390/ijms241411285.
268. Ferreira, L.B., et al., *Osteopontin-a splice variant is overexpressed in papillary thyroid carcinoma and modulates invasive behavior*. Oncotarget, 2016. **7**(32): p. 52003-52016 DOI: 10.18632/oncotarget.10468.
269. Cardoso, A.P., et al., *Macrophages stimulate gastric and colorectal cancer invasion through EGFR Y1086, c-Src, Erk1/2 and Akt phosphorylation and smallGTPase activity*. Oncogene, 2014. **33**(16): p. 2123-2133 DOI: 10.1038/onc.2013.154.
270. Mahmood, T. and P.C. Yang, *Western blot: technique, theory, and trouble shooting*. N Am J Med Sci, 2012. **4**(9): p. 429-34 DOI: 10.4103/1947-2714.100998.
271. Martinez-Jothar, L., et al., *Insights into maleimide-thiol conjugation chemistry: Conditions for efficient surface functionalization of nanoparticles for receptor targeting*. J Control Release, 2018. **282**: p. 101-109 DOI: 10.1016/j.jconrel.2018.03.002.
272. Van Koninckxloo, A., et al., *NMR chemical shift study of the interaction of selected peptides with liposomal and micellar models of apoptotic cells*. J Biol Inorg Chem, 2014. **19**(8): p. 1367-76 DOI: 10.1007/s00775-014-1195-5.

273. Kumar, S., G. Hause, and W.H. Binder, *Thio-Bromo "Click" Reaction Derived Polymer-Peptide Conjugates for Their Self-Assembled Fibrillar Nanostructures*. Macromol Biosci, 2020. **20**(6): p. e2000048 DOI: 10.1002/mabi.202000048.
274. Gurer, F., et al., *Water-based carbodiimide mediated synthesis of polysaccharide-amino acid conjugates: Deprotection, charge and structural analysis*. Carbohydr Polym, 2021. **267**: p. 118226 DOI: 10.1016/j.carbpol.2021.118226.
275. Wickramathilaka, M.P. and B.Y. Tao, *Characterization of covalent crosslinking strategies for synthesizing DNA-based bioconjugates*. J Biol Eng, 2019. **13**(1): p. 63 DOI: 10.1186/s13036-019-0191-2.
276. Danaei, M., et al., *Impact of Particle Size and Polydispersity Index on the Clinical Applications of Lipidic Nanocarrier Systems*. Pharmaceutics, 2018. **10**(2): p. 57
277. Furtado, D., et al., *Overcoming the Blood–Brain Barrier: The Role of Nanomaterials in Treating Neurological Diseases*. Advanced Materials, 2018. **30**(46): p. 1801362 DOI: https://doi.org/10.1002/adma.201801362.
278. Doane, T.L., et al., *Nanoparticle zeta -potentials*. Acc Chem Res, 2012. **45**(3): p. 317-26 DOI: 10.1021/ar200113c.
279. Chang, M., *Matrix metalloproteinase profiling and their roles in disease*. RSC Adv, 2023. **13**(9): p. 6304-6316 DOI: 10.1039/d2ra07005g.
280. Anchan, A., et al., *Melanoma Mediated Disruption of Brain Endothelial Barrier Integrity Is Not Prevented by the Inhibition of Matrix Metalloproteinases and Proteases*. Biosensors (Basel), 2022. **12**(8) DOI: 10.3390/bios12080660.
281. Nosoudi, N., et al., *Prevention of abdominal aortic aneurysm progression by targeted inhibition of matrix metalloproteinase activity with batimastat-loaded nanoparticles*. Circ Res, 2015. **117**(11): p. e80-9 DOI: 10.1161/CIRCRESAHA.115.307207.
282. Zhang, K., et al., *Dual Targeting of Cancer Cells and MMPs with Self-Assembly Hybrid Nanoparticles for Combination Therapy in Combating Cancer*. Pharmaceutics, 2021. **13**(12): p. 1990 DOI: 10.3390/pharmaceutics13121990.
283. Marques, A.C., et al., *Functionalizing nanoparticles with cancer-targeting antibodies: A comparison of strategies*. Journal of Controlled Release, 2020. **320**: p. 180-200 DOI: https://doi.org/10.1016/j.jconrel.2020.01.035.
284. Han, Y., et al., *Transferrin-modified nanostructured lipid carriers as multifunctional nanomedicine for codelivery of DNA and doxorubicin*. Int J Nanomedicine, 2014. **9**: p. 4107-16 DOI: 10.2147/ijn.S67770.
285. Cho, W.-S., et al., *Surface functionalization affects the zeta potential, coronal stability and membranolytic activity of polymeric nanoparticles*. Nanotoxicology, 2014. **8**(2): p. 202-211 DOI: 10.3109/17435390.2013.773465.
286. Du, J. and L. Li, *Which one performs better for targeted lung cancer combination therapy: pre- or post-bombesin-decorated nanostructured lipid carriers?* Drug Deliv, 2016. **23**(5): p. 1799-809 DOI: 10.3109/10717544.2015.1099058.

287. Teixeira, M.I., et al., *Formulation, Characterization, and Cytotoxicity Evaluation of Lactoferrin Functionalized Lipid Nanoparticles for Riluzole Delivery to the Brain*. Pharmaceutics, 2022. **14**(1): p. 185 DOI: 10.3390/pharmaceutics14010185.
288. Muller, R.H., M. Radtke, and S.A. Wissing, *Solid lipid nanoparticles (SLN) and nanostructured lipid carriers (NLC) in cosmetic and dermatological preparations*. Adv Drug Deliv Rev, 2002. **54 Suppl 1**: p. S131-55 DOI: 10.1016/s0169-409x(02)00118-7.
289. Azhar Shekoufeh Bahari, L. and H. Hamishehkar, *The Impact of Variables on Particle Size of Solid Lipid Nanoparticles and Nanostructured Lipid Carriers; A Comparative Literature Review.* Adv Pharm Bull, 2016. **6**(2): p. 143-51 DOI: 10.15171/apb.2016.021.
290. Weksler, B., I.A. Romero, and P.-O. Couraud, *The hCMEC/D3 cell line as a model of the human blood brain barrier*. Fluids and Barriers of the CNS, 2013. **10**(1): p. 16 DOI: 10.1186/2045-8118-10-16.
291. de Barros, D.P.C., et al., *Design of Quercetin-Loaded Natural Oil-Based Nanostructured Lipid Carriers for the Treatment of Bacterial Skin Infections*. Molecules, 2022. **27**(24): p. 8818
292. Thomsen, M.S., et al., *Blood-Brain Barrier Transport of Transferrin Receptor-Targeted Nanoparticles*. Pharmaceutics, 2022. **14**(10) DOI: 10.3390/pharmaceutics14102237.
293. Beard, R., et al., *Chemical biology tools for probing transcytosis at the blood–brain barrier*. Chemical Science, 2019. **10**(46): p. 10772-10778 DOI: 10.1039/C9SC04024B.
294. Johnsen, K.B., et al., *Targeting the transferrin receptor for brain drug delivery*. Progress in Neurobiology, 2019. **181**: p. 101665 DOI: https://doi.org/10.1016/j.pneurobio.2019.101665.
295. Gomes, M.J., et al., *Tailoring Lipid and Polymeric Nanoparticles as siRNA Carriers towards the Blood-Brain Barrier - from Targeting to Safe Administration*. J Neuroimmune Pharmacol, 2017. **12**(1): p. 107-119 DOI: 10.1007/s11481-016-9685-6.
296. Perrin, S.L., et al., *Glioblastoma heterogeneity and the tumour microenvironment: implications for preclinical research and development of new treatments*. Biochem Soc Trans, 2019. **47**(2): p. 625-638 DOI: 10.1042/BST20180444.
297. Hagemann, C., et al., *A complete compilation of matrix metalloproteinase expression in human malignant gliomas*. World J Clin Oncol, 2012. **3**(5): p. 67-79 DOI: 10.5306/wjco.v3.i5.67.
298. Hagemann, C., et al., *Comparative expression pattern of Matrix-Metalloproteinases in human glioblastoma cell-lines and primary cultures*. BMC Res Notes, 2010. **3**: p. 293 DOI: 10.1186/1756-0500-3-293.
299. Li, H., et al., *Differences in Protein Expression between the U251 and U87 Cell Lines*. Turk Neurosurg, 2017. **27**(6): p. 894-903 DOI: 10.5137/1019-5149.JTN.17746-16.1.
300. Motaln, H., et al., *Heterogeneous glioblastoma cell cross-talk promotes phenotype alterations and enhanced drug resistance*. Oncotarget, 2015. **6**(38): p. 40998-1017 DOI: 10.18632/oncotarget.5701.

301. Eldridge, B.N., et al., *Photothermal therapy of glioblastoma multiforme using multiwalled carbon nanotubes optimized for diffusion in extracellular space*. ACS Biomater Sci Eng, 2016. **2**(6): p. 963-976 DOI: 10.1021/acsbiomaterials.6b00052.
302. Vilas-Boas, V. and M. Vinken, *Hepatotoxicity induced by nanomaterials: mechanisms and in vitro models*. Archives of Toxicology, 2021. **95**(1): p. 27-52 DOI: 10.1007/s00204-020-02940-x.
303. Tonn, J.C., et al., *Effect of synthetic matrix-metalloproteinase inhibitors on invasive capacity and proliferation of human malignant gliomas in vitro*. Int J Cancer, 1999. **80**(5): p. 764-72 DOI: 10.1002/(sici)1097-0215(19990301)80:5<764::aid-ijc22>3.0.co;2-j.
304. Layfield, H.J., et al., *Repurposing Cancer Drugs Batimastat and Marimastat to Inhibit the Activity of a Group I Metalloprotease from the Venom of the Western Diamondback Rattlesnake, Crotalus atrox*. Toxins (Basel), 2020. **12**(5): p. 309 DOI: 10.3390/toxins12050309.
305. Jimenez, R.E., et al., *Effect of matrix metalloproteinase inhibition on pancreatic cancer invasion and metastasis: an additive strategy for cancer control*. Ann Surg, 2000. **231**(5): p. 644-54 DOI: 10.1097/00000658-200005000-00004.
306. Tian, K., et al., *p53 modeling as a route to mesothelioma patients stratification and novel therapeutic identification*. J Transl Med, 2018. **16**(1): p. 282 DOI: 10.1186/s12967-018-1650-0.
307. Bao, G., et al., *Glycoprotein non-metastaticmelanoma protein B promotes glioma motility and angiogenesis through the Wnt/β-catenin signaling pathway*. Experimental Biology and Medicine, 2016. **241**(17): p. 1968-1976 DOI: 10.1177/1535370216654224.
308. Liu, Q., et al., *IL-6 promotion of glioblastoma cell invasion and angiogenesis in U251 and T98G cell lines*. Journal of Neuro-Oncology, 2010. **100**(2): p. 165-176 DOI: 10.1007/s11060-010-0158-0.
309. Ferreira, M.T., et al., *Cyclooxygenase Inhibition Alters Proliferative, Migratory, and Invasive Properties of Human Glioblastoma Cells In Vitro*. International Journal of Molecular Sciences, 2021. **22**(9): p. 4297
310. Souza, F.d.C., M.T. Ferreira, and A. Colquhoun, *Influence of Lipoxygenase Inhibition on Glioblastoma Cell Biology*. International Journal of Molecular Sciences, 2020. **21**(21): p. 8395
311. Toth, M., A. Sohail, and R. Fridman, *Assessment of Gelatinases (MMP-2 and MMP-9) by Gelatin Zymography*, in *Metastasis Research Protocols*, M. Dwek, S.A. Brooks, and U. Schumacher, Editors. 2012, Humana Press: Totowa, NJ. p. 121-135.
312. Torsvik, A., et al., *U-251 revisited: genetic drift and phenotypic consequences of long-term cultures of glioblastoma cells*. Cancer Med, 2014. **3**(4): p. 812-24 DOI: 10.1002/cam4.219.
313. Moore, T.L., et al., *Nanoparticle colloidal stability in cell culture media and impact on cellular interactions*. Chemical Society Reviews, 2015. **44**(17): p. 6287-6305 DOI: 10.1039/C4CS00487F.

314. Ulasov, I., et al., *Inhibition of MMP14 potentiates the therapeutic effect of temozolomide and radiation in gliomas*. Cancer Med, 2013. **2**(4): p. 457-67 DOI: 10.1002/cam4.104.
315. Alves, R., et al., *Batimastat Induces Cytotoxic and Cytostatic Effects in In Vitro Models of Hematological Tumors*. International Journal of Molecular Sciences, 2024. **25**(8): p. 4554
316. Dymova, M.A., E.V. Kuligina, and V.A. Richter, *Molecular Mechanisms of Drug Resistance in Glioblastoma*. Int J Mol Sci, 2021. **22**(12) DOI: 10.3390/ijms22126385.
317. Anttila, J.V., et al., *Contrasting the impact of cytotoxic and cytostatic drug therapies on tumour progression*. PLoS Comput Biol, 2019. **15**(11): p. e1007493 DOI: 10.1371/journal.pcbi.1007493.
318. Macaulay, V.M., et al., *Phase I study of intrapleural batimastat (BB-94), a matrix metalloproteinase inhibitor, in the treatment of malignant pleural effusions*. Clin Cancer Res, 1999. **5**(3): p. 513-20
319. Islam, M.T., N.H. Jang, and H.J. Lee, *Natural Products as Regulators against Matrix Metalloproteinases for the Treatment of Cancer*. Biomedicines, 2024. **12**(4): p. 794
320. Overall, C.M. and O. Kleifeld, *Validating matrix metalloproteinases as drug targets and anti-targets for cancer therapy*. Nature Reviews Cancer, 2006. **6**(3): p. 227-239 DOI: 10.1038/nrc1821.
321. Mehta, M., et al., *Lipid-Based Nanoparticles for Drug/Gene Delivery: An Overview of the Production Techniques and Difficulties Encountered in Their Industrial Development*. ACS Materials Au, 2023. **3**(6): p. 600-619 DOI: 10.1021/acsmaterialsau.3c00032.
322. Beloqui, A., et al., *Nanostructured lipid carriers: Promising drug delivery systems for future clinics*. Nanomedicine: Nanotechnology, Biology and Medicine, 2016. **12**(1): p. 143-161 DOI: https://doi.org/10.1016/j.nano.2015.09.004.
323. Wang, B., et al., *Current advance of nanotechnology in diagnosis and treatment for malignant tumors*. Signal Transduction and Targeted Therapy, 2024. **9**(1): p. 200 DOI: 10.1038/s41392-024-01889-y.
324. Oleksa, V., et al., *Doxorubicin-Conjugated Iron Oxide Nanoparticles: Surface Engineering and Biomedical Investigation*. ChemPlusChem, 2020. **85**(6): p. 1156-1163 DOI: https://doi.org/10.1002/cplu.202000360.
325. Kumar, A., et al., *Gold nanoparticles functionalized with therapeutic and targeted peptides for cancer treatment*. Biomaterials, 2012. **33**(4): p. 1180-9 DOI: 10.1016/j.biomaterials.2011.10.058.
326. Al-Obaidy, R., et al., *Targeted delivery of paclitaxel drug using polymer-coated magnetic nanoparticles for fibrosarcoma therapy: in vitro and in vivo studies*. Scientific Reports, 2023. **13**(1): p. 3180 DOI: 10.1038/s41598-023-30221-x.
327. Muthukumar, T., et al., *Carbon nanoparticle from a natural source fabricated for folate receptor targeting, imaging and drug delivery application in A549 lung cancer cells*. European Journal of Pharmaceutics and Biopharmaceutics, 2014. **88**(3): p. 730-736 DOI: https://doi.org/10.1016/j.ejpb.2014.09.011.

328. Paproski, R.J., et al., *Porphyrin Nanodroplets: Sub-micrometer Ultrasound and Photoacoustic Contrast Imaging Agents*. Small, 2016. **12**(3): p. 371-80 DOI: 10.1002/smll.201502450.
329. Raheem, M.A., et al., *Advances in nanoparticles-based approaches in cancer theranostics*. OpenNano, 2023. **12**: p. 100152 DOI: https://doi.org/10.1016/j.onano.2023.100152.
330. Sun, L., et al., *Smart nanoparticles for cancer therapy*. Signal Transduction and Targeted Therapy, 2023. **8**(1): p. 418 DOI: 10.1038/s41392-023-01642-x.
331. Zhou, Z., T. Sun, and C. Jiang, *Recent advances on drug delivery nanocarriers for cerebral disorders*. Biomed Mater, 2021. **16**(2): p. 024104 DOI: 10.1088/1748-605X/abdc97.
332. Miranda, M.A., et al., *Targeted uptake of folic acid-functionalized polymeric nanoparticles loading glycoalkaloidic extract in vitro and in vivo assays*. Colloids and Surfaces B: Biointerfaces, 2020. **192**: p. 111106 DOI: https://doi.org/10.1016/j.colsurfb.2020.111106.
333. Wang, X., et al., *Cell-Penetrating Peptide and Transferrin Co-Modified Liposomes for Targeted Therapy of Glioma*. Molecules, 2019. **24**(19) DOI: 10.3390/molecules24193540.
334. Lakkadwala, S., et al., *Dual functionalized liposomes for efficient co-delivery of anti-cancer chemotherapeutics for the treatment of glioblastoma*. J Control Release, 2019. **307**: p. 247-260 DOI: 10.1016/j.jconrel.2019.06.033.
335. Belhadj, Z., et al., *Multifunctional targeted liposomal drug delivery for efficient glioblastoma treatment*. Oncotarget, 2017. **8**(40): p. 66889-66900 DOI: 10.18632/oncotarget.17976.
336. Jin, Z., et al., *Dual functional nanoparticles efficiently across the blood-brain barrier to combat glioblastoma via simultaneously inhibit the PI3K pathway and NKG2A axis*. J Drug Target, 2021. **29**(3): p. 323-335 DOI: 10.1080/1061186x.2020.1841214.
337. Liu, C., et al., *Enhanced blood-brain-barrier penetrability and tumor-targeting efficiency by peptide-functionalized poly(amidoamine) dendrimer for the therapy of gliomas*. Nanotheranostics, 2019. **3**(4): p. 311-330 DOI: 10.7150/ntno.38954.
338. Gao, J.Q., et al., *Glioma targeting and blood-brain barrier penetration by dual-targeting doxorubincin liposomes*. Biomaterials, 2013. **34**(22): p. 5628-39 DOI: 10.1016/j.biomaterials.2013.03.097.
339. Zhu, X., et al., *Transferrin/aptamer conjugated mesoporous ruthenium nanosystem for redox-controlled and targeted chemo-photodynamic therapy of glioma*. Acta Biomater, 2018. **82**: p. 143-157 DOI: 10.1016/j.actbio.2018.10.012.
340. Chen, C., et al., *Peptide-22 and Cyclic RGD Functionalized Liposomes for Glioma Targeting Drug Delivery Overcoming BBB and BBTB*. ACS Appl Mater Interfaces, 2017. **9**(7): p. 5864-5873 DOI: 10.1021/acsami.6b15831.
341. Zhang, P., et al., *Transferrin-modified c[RGDfK]-paclitaxel loaded hybrid micelle for sequential blood-brain barrier penetration and glioma targeting therapy*. Mol Pharm, 2012. **9**(6): p. 1590-8 DOI: 10.1021/mp200600t.
342. Zhu, Y., et al., *Highly efficacious and specific anti-glioma chemotherapy by tandem nanomicelles co-functionalized with brain tumor-targeting and cell-*

penetrating peptides. J Control Release, 2018. **278**: p. 1-8 DOI: 10.1016/j.jconrel.2018.03.025.
343. Tietjen, G.T., et al., *Focus on Fundamentals: Achieving Effective Nanoparticle Targeting*. Trends Mol Med, 2018. **24**(7): p. 598-606 DOI: 10.1016/j.molmed.2018.05.003.
344. Chauhan, I., et al., *Nanostructured Lipid Carriers: A Groundbreaking Approach for Transdermal Drug Delivery*. Adv Pharm Bull, 2020. **10**(2): p. 150-165 DOI: 10.34172/apb.2020.021.
345. Amiri, F., S. Ziaei Chamgordani, and H. Ghourchian, *An in vitro study for reducing the cytotoxicity and dose dumping risk of remdesivir via entrapment in nanostructured lipid carriers*. Scientific Reports, 2024. **14**(1): p. 19360 DOI: 10.1038/s41598-024-70003-7.
346. Kim, D., et al., *Recent Development of Inorganic Nanoparticles for Biomedical Imaging*. ACS Cent Sci, 2018. **4**(3): p. 324-336 DOI: 10.1021/acscentsci.7b00574.
347. Kolosnjaj-Tabi, J., J. Volatron, and F. Gazeau, *Basic Principles of In Vivo Distribution, Toxicity, and Degradation of Prospective Inorganic Nanoparticles for Imaging*, in *Design and Applications of Nanoparticles in Biomedical Imaging*, J.W.M. Bulte and M.M.J. Modo, Editors. 2017, Springer International Publishing: Cham. p. 9-41.
348. Kasongo, K.W., R.H. Müller, and R.B. Walker, *The use of hot and cold high pressure homogenization to enhance the loading capacity and encapsulation efficiency of nanostructured lipid carriers for the hydrophilic antiretroviral drug, didanosine for potential administration to paediatric patients*. Pharmaceutical Development and Technology, 2012. **17**(3): p. 353-362 DOI: 10.3109/10837450.2010.542163.
349. Cirri, M., et al., *Design, characterization and in vivo evaluation of nanostructured lipid carriers (NLC) as a new drug delivery system for hydrochlorothiazide oral administration in pediatric therapy*. Drug Delivery, 2018. **25**(1): p. 1910-1921 DOI: 10.1080/10717544.2018.1529209.
350. Zhang, T., et al., *Characterization and evaluation of nanostructured lipid carrier as a vehicle for oral delivery of etoposide*. European Journal of Pharmaceutical Sciences, 2011. **43**(3): p. 174-179 DOI: https://doi.org/10.1016/j.ejps.2011.04.005.
351. Hu, F.-Q., et al., *Preparation and characterization of stearic acid nanostructured lipid carriers by solvent diffusion method in an aqueous system*. Colloids and Surfaces B: Biointerfaces, 2005. **45**(3): p. 167-173 DOI: https://doi.org/10.1016/j.colsurfb.2005.08.005.
352. Subroto, E., R. Andoyo, and R. Indiarto, *Solid Lipid Nanoparticles: Review of the Current Research on Encapsulation and Delivery Systems for Active and Antioxidant Compounds*. Antioxidants (Basel), 2023. **12**(3) DOI: 10.3390/antiox12030633.
353. Saha, A., et al., *A facile cost-effective electrolyte-assisted approach and comparative study towards the Greener synthesis of silica nanoparticles*. Nanoscale Adv, 2023. **5**(5): p. 1386-1396 DOI: 10.1039/d2na00872f.
354. Rao, R.R., et al., *Medium and large scale preparation of Nanostructured Lipid Carriers of asenapine maleate: Quality-by-design based optimization,*

production, characterization and performance evaluation. Journal of Drug Delivery Science and Technology, 2022. **71**: p. 103275 DOI: https://doi.org/10.1016/j.jddst.2022.103275.
355. Brown, T.D., et al., *Effect of Nanoparticle Composition, Size, Shape, and Stiffness on Penetration Across the Blood–Brain Barrier*. ACS Biomaterials Science & Engineering, 2020. **6**(9): p. 4916-4928 DOI: 10.1021/acsbiomaterials.0c00743.
356. Key, J., et al., *Soft Discoidal Polymeric Nanoconstructs Resist Macrophage Uptake and Enhance Vascular Targeting in Tumors*. ACS Nano, 2015. **9**(12): p. 11628-11641 DOI: 10.1021/acsnano.5b04866.
357. Tsuji, T., H. Yoshitomi, and J. Usukura, *Endocytic mechanism of transferrin-conjugated nanoparticles and the effects of their size and ligand number on the efficiency of drug delivery*. Microscopy, 2012. **62**(3): p. 341-352 DOI: 10.1093/jmicro/dfs080.
358. Neves, A.R., et al., *Transferrin-functionalized lipid nanoparticles for curcumin brain delivery*. J Biotechnol, 2021. **331**: p. 108-117 DOI: 10.1016/j.jbiotec.2021.03.010.
359. Pinheiro, R.G.R., et al., *Quercetin lipid nanoparticles functionalized with transferrin for Alzheimer's disease*. European Journal of Pharmaceutical Sciences, 2020. **148**: p. 105314 DOI: https://doi.org/10.1016/j.ejps.2020.105314.
360. Sharma, G., et al., *Grafting of Cell-Penetrating Peptide to Receptor-Targeted Liposomes Improves their Transfection Efficiency and Transport across Blood–Brain Barrier Model*. Journal of Pharmaceutical Sciences, 2012. **101**(7): p. 2468-2478 DOI: https://doi.org/10.1002/jps.23152.
361. Sharma, G., et al., *Cell penetrating peptide tethered bi-ligand liposomes for delivery to brain in vivo: Biodistribution and transfection*. Journal of Controlled Release, 2013. **167**(1): p. 1-10 DOI: https://doi.org/10.1016/j.jconrel.2013.01.016.
362. Wiley, D.T., et al., *Transcytosis and brain uptake of transferrin-containing nanoparticles by tuning avidity to transferrin receptor*. Proc Natl Acad Sci U S A, 2013. **110**(21): p. 8662-7 DOI: 10.1073/pnas.1307152110.
363. Lv, Y., et al., *Nanoplatform Assembled from a CD44-Targeted Prodrug and Smart Liposomes for Dual Targeting of Tumor Microenvironment and Cancer Cells*. ACS Nano, 2018. **12**(2): p. 1519-1536 DOI: 10.1021/acsnano.7b08051.
364. Lyu, Y., et al., *Potent delivery of an MMP inhibitor to the tumor microenvironment with thermosensitive liposomes for the suppression of metastasis and angiogenesis*. Signal Transduction and Targeted Therapy, 2019. **4**(1): p. 26 DOI: 10.1038/s41392-019-0054-9.
365. Li, X., et al., *Liposomal codelivery of inflammation inhibitor and collagen protector to the plaque for effective anti-atherosclerosis*. Chinese Chemical Letters, 2023. **34**(1): p. 107483 DOI: https://doi.org/10.1016/j.cclet.2022.04.081.
366. Li, J., et al., *Enzymatically Transformable Polymersome-Based Nanotherapeutics to Eliminate Minimal Relapsable Cancer*. Adv Mater, 2021. **33**(49): p. e2105254 DOI: 10.1002/adma.202105254.

367. Xiao, Q., et al., *A drug-delivering-drug strategy for combined treatment of metastatic breast cancer*. Nanomedicine: Nanotechnology, Biology and Medicine, 2018. **14**(8): p. 2678-2688 DOI: https://doi.org/10.1016/j.nano.2018.06.012.
368. Lv, Y., et al., *Targeting intracellular MMPs efficiently inhibits tumor metastasis and angiogenesis*. Theranostics, 2018. **8**(10): p. 2830-2845 DOI: 10.7150/thno.23209.
369. Dardevet, L., et al., *Chlorotoxin: a helpful natural scorpion peptide to diagnose glioma and fight tumor invasion*. Toxins (Basel), 2015. **7**(4): p. 1079-101 DOI: 10.3390/toxins7041079.
370. Wiranowska, M., *Advances in the use of chitosan and chlorotoxin-functionalized chitosan polymers in drug delivery and detection of glioma – A review*. Carbohydrate Polymer Technologies and Applications, 2024. **7**: p. 100427 DOI: https://doi.org/10.1016/j.carpta.2024.100427.
371. Boltman, T., M. Meyer, and O. Ekpo, *Diagnostic and Therapeutic Approaches for Glioblastoma and Neuroblastoma Cancers Using Chlorotoxin Nanoparticles*. Cancers (Basel), 2023. **15**(13) DOI: 10.3390/cancers15133388.
372. Jentsch, T.J., et al., *Molecular Structure and Physiological Function of Chloride Channels*. Physiological Reviews, 2002. **82**(2): p. 503-568 DOI: 10.1152/physrev.00029.2001.
373. Shrestha, A., et al., *Chlorotoxin and Lung Cancer: A Targeting Perspective for Drug Delivery*. Pharmaceutics, 2022. **14**(12): p. 2613
374. Kyriakides, T.R., et al., *Biocompatibility of nanomaterials and their immunological properties*. Biomed Mater, 2021. **16**(4) DOI: 10.1088/1748-605X/abe5fa.
375. Mukhtar, M., et al., *Nanomaterials for Diagnosis and Treatment of Brain Cancer: Recent Updates*. Chemosensors, 2020. **8**(4): p. 117
376. Woods, N.K. and J. Padmanabhan, *Inhibition of Amyloid Precursor Protein Processing Enhances Gemcitabine-mediated Cytotoxicity in Pancreatic Cancer Cells*. Journal of Biological Chemistry, 2013. **288**(42): p. 30114-30124 DOI: 10.1074/jbc.M113.459255.
377. Jadhav, S.R., et al., *Structural aspects of a self-emulsifying multifunctional amphiphilic excipient: Part I. The case of Gelucire® 44/14*. Journal of Molecular Liquids, 2021. **340**: p. 117172 DOI: https://doi.org/10.1016/j.molliq.2021.117172.
378. Tupinambá Branquinho, R., et al., *Increased Body Exposure to New Anti-Trypanosomal Through Nanoencapsulation*. Scientific Reports, 2017. **7**(1): p. 8429 DOI: 10.1038/s41598-017-08469-x.
379. Marino, M., et al., *An in vitro approach to study the absorption of a new oral formulation of berberine*. PharmaNutrition, 2021. **18**: p. 100279 DOI: https://doi.org/10.1016/j.phanu.2021.100279.
380. Kaur, G. and S.K. Mehta, *Developments of Polysorbate (Tween) based microemulsions: Preclinical drug delivery, toxicity and antimicrobial applications*. International Journal of Pharmaceutics, 2017. **529**(1): p. 134-160 DOI: https://doi.org/10.1016/j.ijpharm.2017.06.059.

381. Dhiman, N., et al., *Lipid Nanoparticles as Carriers for Bioactive Delivery*. Front Chem, 2021. **9**: p. 580118 DOI: 10.3389/fchem.2021.580118.
382. Akanda, M.H., et al., *Delivery of retinoic acid to LNCap human prostate cancer cells using solid lipid nanoparticles*. International Journal of Pharmaceutics, 2015. **493**(1): p. 161-171 DOI: https://doi.org/10.1016/j.ijpharm.2015.07.042.
383. Mohammadi Ghalaei, P., J. Varshosaz, and H. Sadeghi Aliabadi, *Evaluating Cytotoxicity of Hyaluronate Targeted Solid Lipid Nanoparticles of Etoposide on SK-OV-3 Cells*. Journal of Drug Delivery, 2014. **2014**(1): p. 746325 DOI: https://doi.org/10.1155/2014/746325.
384. Parveen, R., et al., *Solid lipid nanoparticles of anticancer drug andrographolide: formulation, in vitro and in vivo studies*. Drug Development and Industrial Pharmacy, 2014. **40**(9): p. 1206-1212 DOI: 10.3109/03639045.2013.810636.
385. Falk, V., et al., *Regulation of matrix metalloproteinases and effect of MMP-inhibition in heart transplant related reperfusion injury*. European Journal of Cardio-Thoracic Surgery, 2002. **22**(1): p. 53-58 DOI: 10.1016/s1010-7940(02)00207-5.
386. Lövdahl, C., J. Thyberg, and A. Hultgårdh-Nilsson, *The Synthetic Metalloproteinase Inhibitor Batimastat Suppresses Injury-Induced Phosphorylation of MAP Kinase ERK1/ERK2 and Phenotypic Modification of Arterial Smooth Muscle Cells in vitro*. Journal of Vascular Research, 2000. **37**(5): p. 345-354 DOI: 10.1159/000025750.
387. Sledge, G.W., Jr., et al., *Effect of Matrix Metalloproteinase Inhibitor Batimastat on Breast Cancer Regrowth and Metastasis in Athymic Mice*. JNCI: Journal of the National Cancer Institute, 1995. **87**(20): p. 1546-1551 DOI: 10.1093/jnci/87.20.1546.
388. Kumar, A., S. Bhatnagar, and A. Kumar, *Matrix metalloproteinase inhibitor batimastat alleviates pathology and improves skeletal muscle function in dystrophin-deficient mdx mice*. Am J Pathol, 2010. **177**(1): p. 248-60 DOI: 10.2353/ajpath.2010.091176.

APPENDIX

APPENDIX

Appendix I

Review article:

Miguel Horta, Paula Soares, Catarina Leite Pereira* and Raquel T. Lima* **(2025)**. *Emerging Approaches in Glioblastoma Treatment: Modulating the Extracellular Matrix through Nanotechnology*. Pharmaceutics. DOI: https://doi.org/10.3390/pharmaceutics17020142.

*These authors contributed equally to this work.

pharmaceutics

MDPI

Review

Emerging Approaches in Glioblastoma Treatment: Modulating the Extracellular Matrix Through Nanotechnology

Miguel Horta [1,2,3], Paula Soares [1,2,3], Catarina Leite Pereira [1,4,*,†] and Raquel T. Lima [1,2,3,*,†]

[1] i3S—Instituto de Investigação e Inovação em Saúde, University of Porto, Rua Alfredo Allen 208, 4200-135 Porto, Portugal; mhorta@i3s.up.pt (M.H.); psoares@ipatimup.pt (P.S.)
[2] IPATIMUP—Instituto de Patologia e Imunologia Molecular, University of Porto, Rua Júlio Amaral de Carvalho 45, 4200-135 Porto, Portugal
[3] FMUP—Faculty of Medicine, University of Porto, Alameda Prof. Hernâni Monteiro, 4200-319 Porto, Portugal
[4] INEB—Instituto Nacional de Engenharia Biomédica, University of Porto, Rua Alfredo Allen 208, 4200-135 Porto, Portugal
* Correspondence: catarina.pereira@i3s.up.pt (C.L.P.); rlima@ipatimup.pt (R.T.L.)
† These authors contributed equally to this work.

Abstract: Glioblastoma's (GB) complex tumor microenvironment (TME) promotes its progression and resistance to therapy. A critical component of TME is the extracellular matrix (ECM), which plays a pivotal role in promoting the tumor's invasive behavior and aggressiveness. Nanotechnology holds significant promise for GB treatment, with the potential to address challenges posed by both the blood-brain barrier and the GB ECM. By enabling targeted delivery of therapeutic and diagnostic agents, nanotechnology offers the prospect of improving treatment efficacy and diagnostic accuracy at the tumor site. This review provides a comprehensive exploration of GB, including its epidemiology, classification, and current treatment strategies, alongside the intricacies of its TME. It highlights nanotechnology-based strategies, focusing on nanoparticle formulations such as liposomes, polymeric nanoparticles, and gold nanoparticles, which have shown promise in GB therapy. Furthermore, it explores how different emerging nanotechnology strategies modulate the ECM to overcome the challenges posed by its high density, which restricts drug distribution within GB tumors. By emphasizing the intersection of nanotechnology and GB ECM, this review underscores an innovative approach to advancing GB treatment. It addresses the limitations of current therapies, identifies new research avenues, and emphasizes the potential of nanotechnology to improve patient outcomes.

Keywords: nanotechnology; nanoparticles; glioblastoma (GB); tumor microenvironment (TME); extracellular matrix (ECM)

Academic Editor: Xiaowei Zeng

Received: 21 December 2024
Revised: 10 January 2025
Accepted: 16 January 2025
Published: 21 January 2025

Citation: Horta, M.; Soares, P.; Leite Pereira, C.; Lima, R.T. Emerging Approaches in Glioblastoma Treatment: Modulating the Extracellular Matrix Through Nanotechnology. *Pharmaceutics* **2025**, *17*, 142. https://doi.org/10.3390/pharmaceutics17020142

1. Glioblastoma: Epidemiology and Classification

Glioblastoma (GB) is the most aggressive and highly malignant brain tumor in adults, presenting a poor prognosis. Its incidence varies depending on the population studied, mostly ranging from 3 to 4.5 per 100,000 people annually [1–3], accounting for approximately 50% of all malignant central nervous system (CNS) tumors [4]. GB shows a slight male predominance, with a male to female ratio of about 1.6:1 [5]. Although the incidence increases with age, it can occur across all adult age groups [1]. While CNS tumors are common in children, according to the most recent World Health Organization (WHO) guidelines, GB is no longer a possible diagnosis in this age group; instead, it is considered a diffuse pediatric glioma [6].

As our knowledge of GB improves, so do our methods for diagnosing, classifying, and treating the disease [7]. Recent changes in tumor classification, driven by new insights from molecular profiling, have significantly influenced how to diagnose and treat GB, highlighting the clinical importance of these advancements (Figure 1) [8]. Under the most recent 2021 WHO classification of tumors of the CNS, which has significantly redefined GB, GB is strictly defined as an isocitrate dehydrogenase (*IDH*)-wildtype, WHO grade 4, tumor. This reclassification emphasizes the distinct biological behavior and more favorable prognosis of *IDH*-mutant tumors compared to their *IDH*-wildtype counterparts [1,6,9,10]. Furthermore, for the diagnosis of GB (*IDH*-wildtype WHO grade 4) at least one of the following criteria is now required: (i) microvascular proliferation or necrosis on histological examination; (ii) telomerase reverse transcriptase (*TERT*) gene promoter mutations; (iii) epithelial growth factor (EGF) receptor (*EGFR*) gene amplification; (iv) combined gain of chromosome 7 and loss of chromosome 10 (+7/−10) [11]. This integrated approach, combining histological and molecular features, provides a more accurate and clinically relevant diagnosis. Notably, this new classification no longer allows for the use of "not otherwise specified" (NOS) in GB diagnosis, further underscoring the importance of molecular testing in modern neuro-oncology [12]. Moreover, the "not elsewhere classified" (NEC) designation is now used when a tumor does not meet the specific GB criteria but still appears to be a diffuse astrocytic glioma without *IDH* mutation [13].

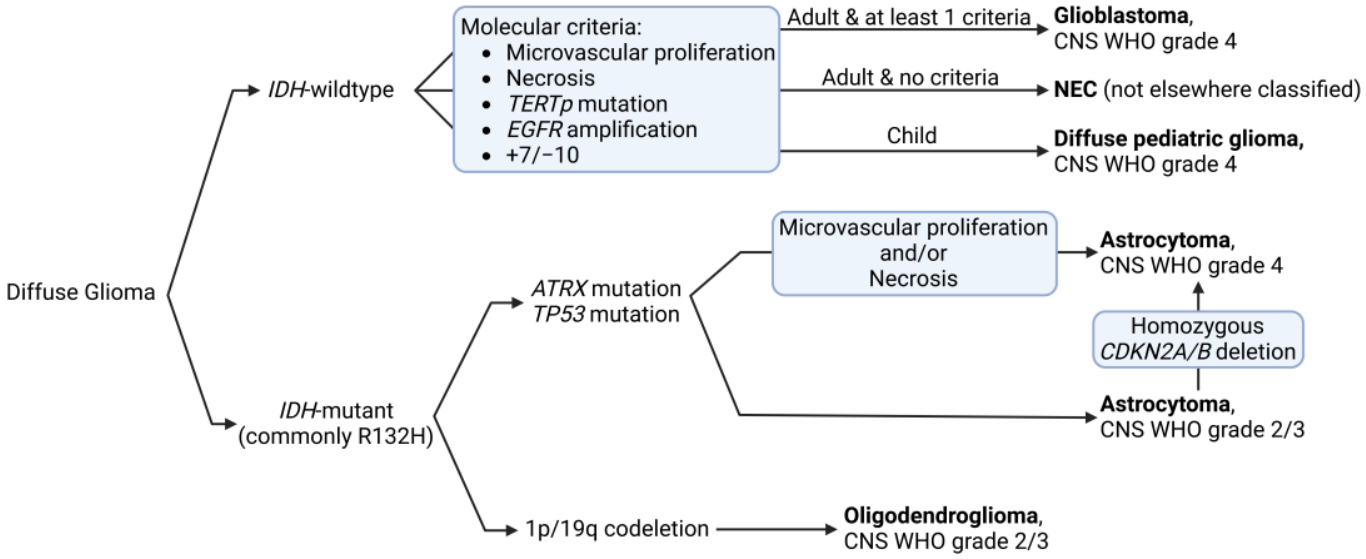

Figure 1. Glioma classification according to the WHO 2021 classification. CNS WHO grades: (1) Generally indolent tumors with favorable prognosis, (2) Low-grade tumors with potential for recurrence, (3) Malignant tumors with increased mitotic activity, (4) Highly malignant tumors with rapid progression.

The prognosis for GB remains poor, with median survival varying based on molecular subtypes, which are defined by different transcription profiles [14]. The mesenchymal subtype is characterized by extensive necrosis and inflammation, exhibiting transcription profiles similar to mesenchymal tissues. The proneural subtype, considered milder, is characterized by the expression of genes involved in neurogenesis and oligodendrocyte development. The classical subtype, in between, shows features similar to astrocytes, hence the "classical" name reflecting typical GB characteristics [15]. The mesenchymal subtype has the worst prognosis, with a median survival of about 11.5 months, followed by the classical subtype at 14.7 months, and the proneural subtype at 17.0 months [16]. These survival differences highlight the clinical relevance of molecular subtyping in GB,

which will be discussed in more detail later. Although there are several risk factors for GB, exposure to high-dose ionizing radiation and certain rare genetic conditions (e.g., Lynch syndrome, Neurofibromatosis type 1, Li-Fraumeni syndrome) have been associated with increased incidence [17,18]. However, the majority of GB cases occur sporadically without any known risk factors [19]. Anatomically, GBs are typically supratentorial, with rare cases in the cerebellum or spine [20,21]. They most commonly affect the frontal and temporal lobes, followed by the parietal and occipital lobes, with a slight preference for the right hemisphere [22]. Tumor location can significantly impact surgical resection and, consequently, patient outcomes [23,24].

2. Current Treatment Options

2.1. First-Line—Stupp Protocol

The "Stupp protocol", introduced in 2005, is the standard of care for treating newly diagnosed GB cases [25]. Named after the Swiss oncologist Roger Stupp, this treatment regimen improved survival outcomes for GB patients compared to previous approaches. The protocol consists of maximal safe surgical resection followed by two main phases, concurrent chemoradiotherapy followed by adjuvant chemotherapy. During the first phase, patients receive radiotherapy (RT) with a total dose of 60 Gy, delivered in 30 fractions of 2 Gy each over 6 weeks (5 days per week). Simultaneously, patients take oral temozolomide (TMZ), an alkylating chemotherapy agent, at a dose of 75 mg/m^2 of body surface area, daily, seven days a week throughout the RT period. During the second phase, after a 4-week break once completing RT, patients undergo six cycles of TMZ monotherapy. Each cycle lasts 28 days, with TMZ taken for the first 5 days at a dose of 150–200 mg/m^2 [26].

The Stupp protocol demonstrated an improvement in survival compared to RT alone. In the original study, the median overall survival increased from 12.1 months with RT alone to 14.6 months with the combined approach. More importantly, the 2-year survival rate improved from 10.4% to 26.5% [27]. Despite these improvements, the prognosis for GB remains poor. Nevertheless, this protocol is most effective in patients under 70 years of age, with good performance status, and whose tumors exhibit methylguanine methyltransferase (*MGMT*) promoter methylation, a biomarker associated with better TMZ treatment response [28]. Moreover, side effects of the Stupp protocol can be significant, with the most common being fatigue, nausea, and myelosuppression, and the most severe complications including neutropenia, thrombocytopenia, lymphopenia, and increased risk of opportunistic infections. To reduce infection risks, patients with these complications often receive antibiotic prophylaxis during treatment [29]. While the Stupp protocol remains the backbone standard of care for GB, ongoing research seeks to further improve patient outcomes.

2.2. Second-Line Treatments

Following Stupp protocol failure, with frequent tumor relapse, there is no universally accepted standard for second-line treatment. The management of recurrent GB remains a therapeutic challenge, with several strategies being explored. Tumor reoperation is considered for patients with large, symptomatic tumors, but its benefits remain controversial and depend on patient selection [30–32]. Another strategy, reirradiation, presents options including stereotactic radiosurgery, hypofractionated stereotactic RT, conventionally fractioned external RT, or brachytherapy. Decision depends on factors such as time since initial radiation and tumor characteristics [33–35]. A third option is a TMZ rechallenge, which is considered for initial responders with prolonged treatment-free intervals. Various dosing schedules have been explored, but overall survival rarely exceeds 12 months [36–40]. Treatment with nitrosoureas, such as carmustine, lomustine, nimustine, and fotemustine, have

also shown limited efficacy in recurrent GB, with median overall survival rarely exceeding 12 months [41–44]. Bevacizumab, a Food and Drug Administration (FDA)-approved anti-angiogenic antibody, has often been employed as a strategy combined with other agents, such as irinotecan or lomustine. While it has been shown to improve progression-free survival, impact on overall survival is still debated [45–48]. Nevertheless, recent research has indicated that high vascular endothelial growth factor (VEGF)-A expression is associated with improved progression-free survival in recurrent GB patients treated with bevacizumab, suggesting potential for a therapeutic improvement through biomarker-guided treatment selection [49]. The multi-kinase inhibitor Regorafenib has shown potential benefits in the REGOMA trial, but more comprehensive data are still needed due to its relatively recent introduction in clinical practice in 2020 [50–52]. Other tyrosine kinase inhibitors, such as cabozantinib, dasatinib, and entrectinib, are currently being evaluated, particularly in molecularly selected populations. However, their efficacy as monotherapies has been limited, mainly due to lack of tumor specificity and poor blood-brain barrier (BBB) permeability [53–55]. Over the last decade, immunotherapy, particularly checkpoint inhibitors, has emerged as a potential therapy for GB. While its efficacy has been limited in unselected GB populations, research continues to address its potential in patient specific subgroups [56–59]. Also, Tumor Treating Fields (TTFields) have emerged as a promising second-line treatment option in clinical practice. This device-based therapy delivers alternating electric fields to tumor sites, promoting cancer cell death by disrupting microtubule alignment during cell division [60–62]. TTFields have demonstrated safety and efficacy in clinical trials, leading to FDA approval for GB and malignant pleural mesothelioma. As TTFields continue to show promise, ongoing clinical trials are exploring its use in lung, ovarian, pancreatic, and other cancers, signaling a growing integration of this innovative approach into standard cancer care protocols [63].

GB treatment goals in the recurrent setting are often palliative, aiming to improve or maintain quality of life while potentially extending survival. The choice of second-line treatments for recurrent GB is highly individualized and depends on various factors, including the patient's age, performance status, tumor molecular profile, response to initial therapy, and time to recurrence [64]. Despite the availability of the referred options, the prognosis for recurrent GB remains poor, with median overall survival typically ranging from 6 to 12 months in a clinical setting, with a very modest increase to approximately 15 months for clinical trial participants [65–68]. This underscores the urgent need for more effective therapies and highlights the importance of ongoing research in this challenging cancer type.

3. Glioblastoma and Its Microenvironment—Cellular and Molecular Features

Adding to its own cellular and molecular features, GB is characterized by a complex and dynamic tumor microenvironment (TME) that plays a crucial role in tumor progression, invasion, and therapy resistance [69]. The TME is composed of various cellular and molecular components (Figure 2) that intricately interact to support tumor growth and promote immune evasion [70]. These interactions are key to understanding the mechanisms of GB progression and therapy resistance. As such, gaining a deeper understanding of the TME is essential for developing effective therapeutic strategies.

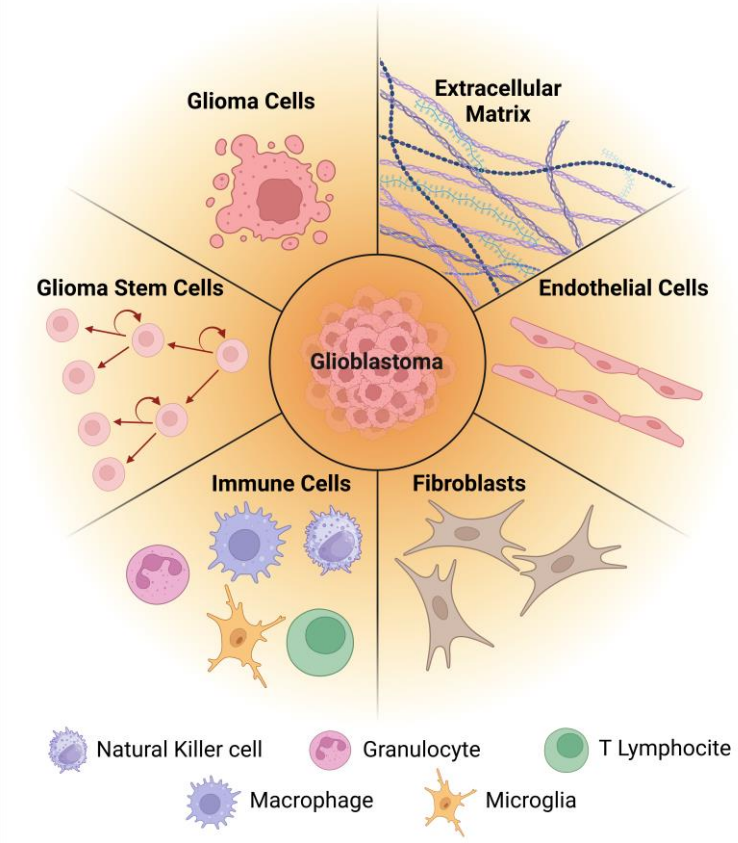

Figure 2. Cellular and non-cellular components of GB and its microenvironment.

3.1. Glioma Cells

The primary cellular component of GB tumors consists of malignant glial cells, which exhibit significant inter- and intra-tumoral heterogeneity [71]. This heterogeneity was classified into the previously referred three molecular subtypes, classical, mesenchymal, and proneural, based on transcriptomic analyses from The Cancer Genome Atlas (TCGA) [72]. A fourth one was initially proposed, the neural subtype, but later excluded as it was based on a misidentification caused by cellular cross contamination [16].

The classical subtype is the least common among GB tumors, accounting for approximately 20% of all GBs [73]. It is characterized by *EGFR* amplification in nearly all tumors (97%), and some harboring *EGFR* mutations [74,75]. Consistent genetic alterations included chromosome 7 amplification paired with chromosome 10 loss and focal 9p21.3 homozygous deletion targeting cyclin-dependent kinase inhibitor 2A (*CDKN2A*), which mostly co-occur with *EGFR* amplification [15]. Notably, tumor protein p53 (*TP53*) mutations are rare in the classical subtype despite being the most frequently mutated gene in GB overall [76]. Furthermore, the transcriptomic analyses showed an overexpression of Sonic-hedgehog (smoothened (SMO), growth arrest-specific protein 1 (GAS1), and GLI family zinc finger 2 (GLI2)) and Notch pathway (neurogenic locus notch homolog protein 3 (NOTCH3), jagged 1 (JAG1), and beta-1,3-*N*-acetylglucosaminyltransferase lunatic fringe (LFNG)) agents, along with high expression of the neural precursor marker nestin [77,78]. Patients with the classical subtype benefit from aggressive RT and chemotherapy [78].

The prevalence of the mesenchymal subtype ranges from 30% to 50% of all GB tumors depending on the population studied and the molecular classification methods used [73,79]. It frequently exhibits neurofibromin (*NF1*) mutations and deletions at 17q11.2 (further affecting NF1 expression), often co-occurring with phosphatase and tensin homolog (*PTEN*) mutations and phosphatidylinositol 3-kinase (PI3K)/AKT pathway enrichment [15,80].

Mesenchymal markers such as chitinase-3-like protein 1 (CHI3L1) and proto-oncogene tyrosine kinase MET are highly expressed, along with astrocytic markers like cluster of differentiation (CD) 44 and proto-oncogene tyrosine kinase MER, indicating potential epithelial-to-mesenchymal transition [15]. Gene expression analysis revealed activation of tumor necrosis factor and nuclear factor kappa-light-chain-enhancer of activated B cells (NF-κB) pathways, correlating with extensive necrosis and inflammatory infiltrates characteristic of this subtype [74,78]. Clinically, while responsive to aggressive RT and chemotherapy, patients with mesenchymal GB have the worst prognosis among all GB subtypes [14].

The proneural subtype, slightly less common than the mesenchymal subtype, accounts for approximately a third of GB tumors [73]. It is characterized by distinct genetic alterations, primarily involving the platelet-derived growth factor receptor A (*PDGFRA*) gene [78]. This subtype was associated with a gene expression profile linked to oligodendrocyte development and neurogenesis, reflecting its unique biological characteristics. The proneural subtype was also characterized by frequent *TP53* mutations and loss of heterozygosity [15]. Clinically, patients with this subtype generally have a better prognosis compared to those with other subtypes, particularly in younger populations [14,76,77,80].

A more recent perspective on GB heterogeneity suggests that genetic factors alone do not fully account for the diverse glioma cell composition observed within these tumors. An international team of researchers proposed that somatic mutations play a crucial role in shaping the tumor's cellular landscape by selectively promoting certain cellular states over others [81]. This process results in a dynamic equilibrium of different cell populations within the tumor, contributing to its heterogeneous nature. Neftel et al. conducted a computational analysis that identified gene signatures converging into four recurring cellular states across multiple GB tumors [81]. These states were present in varying combinations of two to four in each patient, again denoting the heterogeneity of GB, being classified as astrocyte-like (AC-like), mesenchymal-like (MES-like), oligodendrocyte progenitor-like (OPC-like), and neural progenitor-like (NPC-like). OPC-like states were enriched in tumors with *PDGFRA* alterations, NPC-like states in those with cyclin-dependent kinase 4 (*CDK4*) alterations, and AC-like states in tumors with *EGFR* alterations. MES-like states were characterized by *NF1* alterations, extensive immune cell infiltration, and hypoxic conditions [81]. These cellular states aligned with the TCGA subtypes and corroborated findings from other studies suggesting that genomic aberrations alone do not fully explain GB heterogeneity [77,82]. Regardless, the heterogeneity of GB cell subtypes has significant clinical implications, with recent studies demonstrating that specific cellular compositions of tumors directly impact patient survival outcomes [83].

3.2. Glioma Stem Cells

A particularly concerning aspect of GB tumors is the presence of glioma stem cells (GSCs) in its TME, a subpopulation with self-renewal capacity that is thought to drive tumor initiation, recurrence, and therapy resistance [84]. Importantly, GSCs are now understood to represent a functional state rather than a distinct cell lineage [85]. This concept has been further supported by evidence showing that GB cells can dynamically acquire or lose stem-like characteristics in response to TME signals [86]. GSCs share features with normal neural stem cells, including stem cell marker expression such as nestin, sex determining region Y box 2 (SOX2), and CD133, as well as multi-lineage differentiation potential [85]. However, opposite to their normal counterpart, GSCs exhibit aberrant signaling pathway activation, enhancing survival, proliferation, and apoptosis resistance. These alterations confer GSCs a distinct advantage, enabling them to survive conventional therapies and contribute to tumor relapse, making them critical targets for developing more effective GB

treatments [87]. In fact, evidence suggests that GSCs are more resistant to chemotherapy and RT than the bulk of tumor cells [85]. They possess enhanced deoxyribonucleic acid (DNA) repair mechanisms, activated survival pathways, and overexpress drug efflux transporters such as ATP-binding cassette (ABC) proteins [88]. Furthermore, GSCs often reside in specialized niches within the TME, which are characterized by hypoxia and supportive stromal cells. The niches provide protective signals that promote GSCs survival and maintenance, further shielding them from therapeutic interventions [89]. GSCs metabolism is regulated by several key signaling pathways, including Notch, Hedgehog, and Wnt. These pathways, essential for normal stem cell maintenance, are often dysregulated in cancer. Furthermore, transcription factors, such as SOX2, octamer-binding transcription factor 4 (OCT4), and c-Myc, are essential for maintaining GSCs pluripotency and proliferative capacity [90]. While GSCs are certainly influenced by TME cues, studies have also emphasized the reciprocal relationship between GSCs and their microenvironment, supporting and promoting glioma progression [91]. On one hand, TME-derived cytokines such as interleukin (IL)-6 and transforming growth factor beta (TGF-β) enhance GSCs self-renewal and survival [92]. On the other hand, GSCs have been shown to secrete factors that modulate the surrounding immune landscape, creating an immunosuppressive environment conducive to tumor growth. For example, GSCs can induce tumor-associated macrophages (TAMs) to adopt an M2-like phenotype, which suppresses immune responses and promotes tumor development [93]. This intricate interaction between GSCs and their microenvironment underscores the complexity of GB biology and highlights potential targets for therapeutic intervention.

3.3. Immune Cells

The immune component of GB represents approximately 50% of the tumor's cellularity [94]. As previously mentioned, TAMs, which are differentiated from the resident microglia and peripheral monocytes, account for 30% of the tumor mass. These TAMs tend to adopt an M2 anti-inflammatory phenotype and have been shown to suppress $CD8^+$ T cell activity, thereby promoting immune evasion [95]. TAMs are recruited by glioma-cell-derived factors, such as colony stimulating factor 1 (CSF-1), glial cell line-derived neurotrophic factor (GDNF), chemokine (CC motif) ligand 2 (CCL2), stromal cell-derived factor 1 (SFD-1), chemokine (CXC motif) ligand 1 (CXCL1), EGF, and granulocyte-macrophage colony-stimulating factor (GM-CSF) [96]. Once in the TME, TAMs secrete a range of molecules, including anti-inflammatory cytokines (IL4, IL10, TGFβ), angiogenesis factors (VEGF, IL8), and pro-tumorigenic growth factors (insulin-like growth factor 1 (IGF-1), EGF, and platelet-derived growth factor (PDGF)). These molecules significantly influence the GB TME and contribute to tumor progression and therapy resistance, ultimately leading to poorer prognosis for GB patients [94].

Another cell type within the GB TME is myeloid-derived suppressor cells (MDSCs), a diverse population of myeloid progenitor and precursor cells, including macrophages, granulocytes, and dendritic cells at various stages of differentiation [97]. Similar to TAMs, MDSCs impair the function of various T cell subsets, including natural killer T (NK) cells and cytotoxic T lymphocytes [98]. MDSCs also deplete essential amino acids from the TME, such as L-Arginine, and enhance the production of reactive oxygen species (ROS) to suppress T-cell activation and function, thereby contributing to the immune evasion of tumors. These changes in the TME create an unfavorable environment for T cells, leading to reduced immune responses against the tumor [99,100].

Lastly, NK cells, which are important to innate antitumor immunity through antigen-independent immune surveillance, were found to be the least abundant immune cell type in

GB. Furthermore, their immune cytolytic activity is suppressed by major histocompatibility complex class I molecules expressed on GB cells [101].

3.4. Fibroblasts

Recent research has shed new light on the presence and significance of cancer-associated fibroblasts (CAFs) in GB, revealing their role in shaping the TME [102]. Being the primary extracellular matrix (ECM) producers, CAFs contribute significantly to the remodeling of the ECM in GB, promoting tumor growth and invasion. Their abundance correlates with higher tumor grades and activation of ECM remodeling pathways [102]. CAFs also secrete pro-tumorigenic factors, including fibronectin, which plays a critical role in promoting GB cell migration and invasion, thereby enhancing the tumor's aggressive nature [102]. Furthermore, CAFs have been shown to promote resistance to TMZ through the secretion of CCL2, which activates the extracellular signal-regulated kinases (ERK) 1/2 signaling pathway in GB cells [103]. Interestingly, CAFs exhibit subtype-specific effects in GB [104]. They are more abundant in the mesenchymal subtype compared to other subtypes, while proneural GB cells appear to be more responsive to CAF signaling in terms of migratory and invasive behaviors. This heterogeneity in CAF distribution and influence across GB subtypes adds another layer of complexity to the TME [102]. CAFs have been shown to suppress anti-cancer immune responses in various cancers, highlighting their role in contributing to the immunosuppressive environment characteristic of GB [105].

3.5. Endothelial Cells

While not a part of the GB per se, endothelial cells, which encompass the perivascular niche, have been shown to be key components in the tumor's aggressiveness, since angiogenesis is one of the hallmarks of GB recurrence, proliferation, and invasion [106]. In the GB TME, newly formed blood vessels are structurally fragile and prone to rupture, leading to a compromised BBB. This disruption causes an increased vascular permeability and edema, altering immune responses and the boundary between tumor and normal brain tissue, thus facilitating tumor invasiveness and presents challenges for effective treatment delivery [107].

The recruitment of endothelial cells to the GB site occurs through several mechanisms. Neoangiogenesis is the primary process, where GB cells secrete high levels of pro-angiogenic factors, particularly VEGF, stimulating the formation of new blood vessels from the sprouting of pre-existing ones. This process involves endothelial cell proliferation and migration towards the tumor [108]. Additionally, GBs recruit bone marrow-derived endothelial progenitor cells through vasculogenesis, which then differentiate into endothelial cells within the TME [109]. Lastly, GSCs also have the potential to transdifferentiate into endothelial cells, or to simply assemble into tubular-like structures mimicking blood vessels, further contributing to tumor vasculature [110].

Endothelial cells' contribution to tumor progression is multifaceted. By forming new blood vessels, they ensure a steady supply of nutrients and oxygen to the rapidly growing tumor while enabling invasion through the vasculature [109]. Endothelial cells also create a specialized niche that promotes the self-renewal of GSCs by expressing NOTCH ligands that activate Notch signaling in adjacent GSCs, supporting their maintenance and proliferation [111]. Furthermore, endothelial cells facilitate bidirectional communication within the TME, exchanging extracellular vesicles with tumor cells, which can, in turn, promote angiogenesis, suppress the immune system, and confer drug resistance [108].

3.6. Extracellular Matrix

The non-cellular component of the GB TME is the ECM. The brain has an unique ECM composition, which accounts for approximately 20% of its volume [112]. It is comprised

of various components, including, but not limited to: collagen IV; glycoproteins, such as fibronectin, laminins, and tenascins; glycosaminoglycans, such as hyaluronic acid (HA); and proteoglycans, such as the lectican family, phosphacan, and neuron-glial antigen 2 [113]. While sharing many components with the normal brain, the ECM of GB exhibits distinct characteristics that influence tumor behavior. Besides the fact that GB cells overexpress various ECM components, including HA, brevican, tenascin-C (TN-C), and fibronectin, they also show increased expression of specific integrins and receptors, which promote cell adhesion, migration, and invasion [114].

Notably, HA levels correlate with tumor malignancy, both increasing in parallel. HA, along with fibronectin, has been shown to promote the invasiveness of GB cells [115,116]. GB ECM is more condensed and less flexible compared to normal brain tissue due to overexpression of these ECM components, potentially hindering the diffusion of therapeutic agents and neuroactive molecules [117]. The tumor also induces altered protein synthesis in surrounding normal tissues, promoting ECM degradation at the invasive front while increasing ECM component production in nearby areas [118,119]. GB cells can actively migrate along blood vessels or axons through ECM interactions [120].

Research has revealed ECM-driven signals that shape tumor phenotypes and influence metabolic activity [121]. Moreover, the GB ECM is deficient in aggrecan, contains oncofetal proteins, and shows elevated levels of matrix metalloproteinases (MMPs), which increases ECM modulation, invasion, and angiogenesis [119,122]. The ECM's significant role in cell survival, proliferation, and differentiation processes makes it an attractive target for novel therapeutic approaches, which could be particularly valuable given GB's poor response to conventional treatments.

4. Nanotechnology in Glioblastoma

Among multiple alternative approaches to treat GB, nanotechnology has emerged as a particularly promising field to address the challenges posed by this tumor. Nanoparticle (NP)-based drug delivery systems offer the potential to overcome many of the challenges associated with treating brain tumors, including poor drug penetration across the BBB and the need for targeted delivery to tumor cells while minimizing toxicity to healthy tissue (Figure 3) [123].

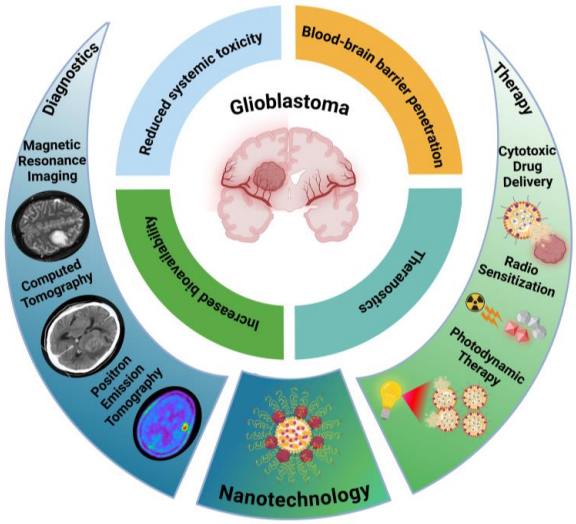

Figure 3. Nanotechnology benefits and examples of approaches in GB diagnostics and therapy. The brain images included in this figure were adapted from Gue, R. et al. [8], Mărginean, L. et al. [124], and Manzarbeitia-Arroba, B. et al. [125], and available under the Creative Commons Attribution (CC BY) license.

Nanocarriers can be engineered to encapsulate various therapeutic agents, including chemotherapy drugs, small molecule inhibitors, nucleic acids for gene therapy, and even combinations of multiple agents for synergistic effects [126]. Their sizes typically range from 10 to 200 nm, with smaller sizes (10–50 nm) facilitating enhanced tumor penetration, cellular uptake, and TME diffusion, while larger sizes (100–200 nm) promote prolonged circulation, better retention at the tumor site, and reduced clearance through renal filtration [127].

Furthermore, the surface of nanoparticles can be modified with targeting ligands to facilitate transport across the BBB and to increase their specificity for GB cells [128]. As research in this area continues to evolve, nanotechnology-based approaches may offer new hope for improving the treatment outcomes for GB patients.

Despite all advances in this field, only a limited number of liposomal strategies have reached clinical trials in GB or other high grade gliomas, following a path similar to what was achieved in other cancers [129]. Among the main candidates studied, Caelyx™, a pegylated liposomal formulation of doxorubicin (DOX), underwent several phase I/II clinical trials, either alone or in a combination therapy (with TMZ, tamoxifen, RT, or a combination of these) [130–134]. However, these trials' main conclusion was that the liposomal formulation did not show clinical benefits. More recently, a liposomal formulation of irinotecan (nal-IRI) was tested in two clinical trials, one as single agent and the other combined with TMZ; however, both trials ended due to lack of activity [135,136]. A new phase I clinical trial at Johns Hopkins University (NCT05768919) is currently recruiting patients to assess the efficacy of liposomal curcumin in combination with radiotherapy and TMZ; no study results have been released yet.

The limited efficacy observed thus far with these clinical trials suggests that while nanoparticle-based systems can improve drug delivery, further optimization in formulation and the development of new targeting strategies are necessary to enhance their clinical effectiveness in GB treatment. While nanotechnology offers promising advantages for GB treatment, its potential non-specific toxicity, both systemically and in brain tissue, remains a critical consideration. Ongoing research focuses on optimizing nanoparticle biocompatibility and biodegradability while minimizing inflammatory responses, aiming to optimize the balance between therapeutic efficacy and safety [137,138].

5. Nanotechnology and the ECM

While initial nanotechnological approaches focused primarily on targeting glioma cells, there is growing recognition of the ECM as a critical factor to tumor progression and malignancy [114], as previously discussed. Consequently, researchers are developing novel therapeutic strategies that specifically target the ECM in GB. These exploit the ubiquitous presence of ECM components within the TME, and thus offer significant advantages compared to targeting the glioma cells themselves. These ECM-focused strategies, often investigated in preclinical settings, include the inhibition of matrix-degrading metalloproteinases and integrins, ECM stiffening, and degradation [139,140]. Additionally, targeting structural ECM molecules can enhance other treatment modalities, such as immunotherapy, by increasing the infiltration of immune cells [141,142]. Nanotechnology approaches interacting with the GB ECM can be categorized into the following classes, as exemplified in Figure 4: (i) ECM as the target: nanoparticles designed to directly interact with or modify the ECM structural components; (ii) ECM-responsive nanoparticles: nanoparticles designed to respond to specific ECM characteristics or changes; (iii) Enhancing ECM degradation: nanoparticles that facilitate the breakdown of ECM components to enhance drug penetration or disrupt tumor structure; (iv) Preventing ECM degradation: nanoparticles that inhibit matrix-degrading enzymes like metalloproteinases to maintain ECM integrity and limit tumor invasion.

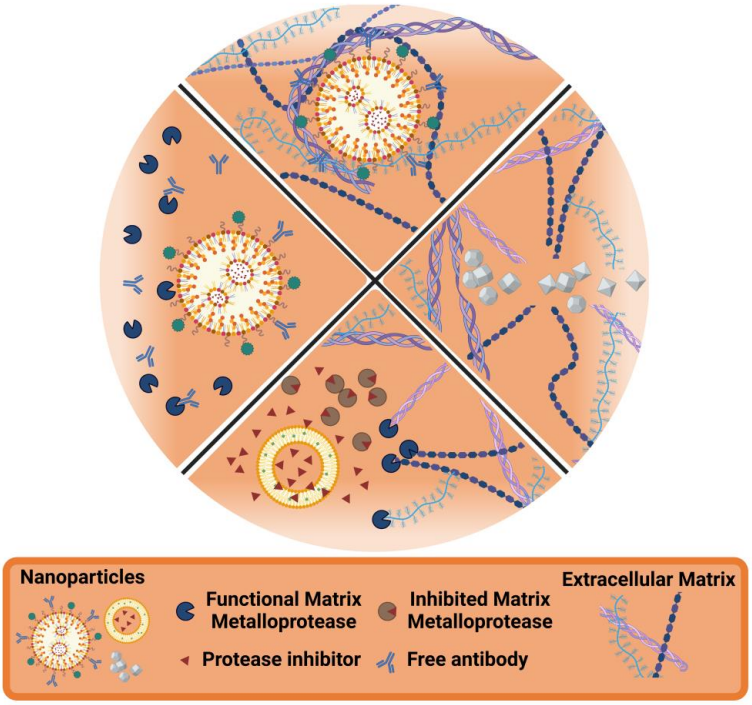

Figure 4. Nanotechnology strategies interacting with the ECM. Top: Nanoparticles targeting the ECM; Left: Nanoparticles responding to ECM cues (e.g., increased MMP concentration in the TME); Right: Nanoparticles degrading the ECM; Bottom: Nanoparticles preventing ECM degradation.

Table 1 summarizes the various nanotechnology strategies discussed in this section, highlighting their approach, key features, and potential applications in GB treatment. This overview provides a comprehensive snapshot of the diverse nanotechnology approaches being explored to reprogram the GB ECM.

Table 1. Overview of nanotechnology approaches for modulating the ECM in GB.

Strategy	Approach	Key Features	Outcome	Ref.
ECM as the target	Fibronectin-targeted liposomal nanoplatform	Functionalized with EDB-specific aptide to deliver CypA siRNA	Improved cellular uptake and CypA silencing in GB cells; reduced tumor growth and increased survival rates in vivo	[143]
	CREKA-micelle nanoparticles	Targets fibrin deposits in GB	Enhanced tumor homing; potential for targeted drug delivery	[144]
	Ft-PLA-PTX dual-targeting peptide system	Targets TN-C and NRP-1	Enhanced internalization in glioma cells and penetration in 3D spheroids; Increased median survival compared to saline	[145]
	PL3-functionalized iron oxide nanoworms and silver nanoparticles	Targets TN-C and NRP-1	Increased GB targeting; increased survival rates in glioma-bearing mice	[146]
	PL1-functionalized silver nanoparticles	Targets fibronectin EDB and TN-C	Strong binding to targets and facilitated cellular uptake	[147]
	MMP-14 targeting dual-modality imaging agent	Combines NIRF dye and PET radionuclide	Enhanced tumor specificity and imaging contrast for GB detection; potential for preoperative planning and real-time surgical guidance	[148]
	VEGF-targeting iron oxide magnetic nanoparticles	Coated with cross-linked BSA and functionalized with anti-VEGF antibodies	Improved tumor visualization using MRI; sustained contrast for 24 h post-injection	[149]

Table 1. *Cont.*

Strategy	Approach	Key Features	Outcome	Ref.
ECM-responsive nanoparticles	CLIO-ICT nanoparticles	MMP-14-activated prodrug release system	Selective targeting of GB cells and GSCs; disrupted tumor blood vessels; induced apoptosis and reduced GSCs populations; real-time tumor response monitoring via MRI	[150]
	Activatable cell-penetrating peptide-modified nanoparticles	MMP-2 and MMP-9 responsive design	Enhanced internalization and targeted PTX delivery within GB microenvironment; improved penetration in 3D GB spheroids; increased survival rates compared to conventional PTX formulations	[139]
	MMP-2-activated nanoparticles with bispecific antibodies	Combines immunotherapy with ferroptosis induction	Targeted B7-H3 and CD3; crossed BBB; accumulated in GB tissue; released cargo upon MMP-2 cleavage; activated T-cells and induced cytokine release	[151]
	pH-responsive DOX-loaded liposomes	Incorporates pH-sensitive peptide trigger	pH-triggered drug release; specific targeting of GB cells under acidic conditions; anti-tumor activity and anti-angiogenic effects	[152]
	Chitosan-based pH-responsive gold nanoparticles	Functionalized with anti-nucleolin aptamer (AS1411)	Enhanced drug release in acidic environments; dual-drug delivery (5-FU and DOX); induced greater cell death than single-drug formulations	[153]
	Acid-cleavable angiopep-2 functionalized nanoparticles	Dual-surface tailored PLGA and PEG based NPs	Brain-targeting in circulation; transformed into GB-accumulating after BBB crossing; enhanced cell uptake and cytotoxicity; improved BBB permeability	[154]
	Hypoxia-responsive liposomal system (AMVY@NPs)	Stepwise targeting and drug release	Crossed BBB; targeted GB cells; released cargo in hypoxic conditions; synergistic inhibition of GB cell growth and pluripotency	[155]
	Hollow manganese dioxide (h-MnO_2) nanosystem	pH-responsive design	Alleviated tumor hypoxia; enabled targeted drug delivery, imaging, and TME modulation; enhanced photodynamic therapy efficacy	[156]
	Redox-sensitive HA-curcumin conjugate nanocarriers	GSH-responsive disulfide bonds	Rapid drug release in high GSH environments; enhanced curcumin solubility and stability; superior cytotoxicity and cellular uptake in GB cells	[157]
Enhancing ECM degradation	Hyaluronidase-expressing oncolytic adenovirus (ICOVIR17)	Targets HA-rich ECM; increases tumor-infiltrating $CD8^+$ T cells and macrophages	Prolonged survival in GB models; potential combination with anti-PD-1 therapies for enhanced efficacy	[158]
	Collagenase-modified human serum albumin nanoparticles (CG-HSANPs)	Loaded with gemcitabine; improved tumor spheroid penetration	Overcame limitations of gemcitabine's short half-life; enhanced drug delivery efficacy and induced higher levels of nuclear fragmentation and ROS generation	[159]

Table 1. *Cont.*

Strategy	Approach	Key Features	Outcome	Ref.
Preventing ECM degradation	PLGA nanoparticles functionalized with chlorotoxin (CTX)	Targets MMP-2 and chloride channels overexpressed in GB cells; delivers morusin	Effectively crossed BBB; induced apoptosis and ROS generation in GB cells with low toxicity to normal cells	[160]
	Amphiphilic peptide nanoparticles	Conjugated with MMP-9 inhibiting peptide; brain-targeting ligand included	Efficiently inhibited MMP-9 activity; demonstrated low toxicity while crossing the BBB	[161]

5.1. ECM as the Target

As previously mentioned, ECM components are ubiquitously distributed throughout the tumor parenchyma, making them a more consistent and accessible target compared to heterogeneous tumor cell populations (Figure 5) [141].

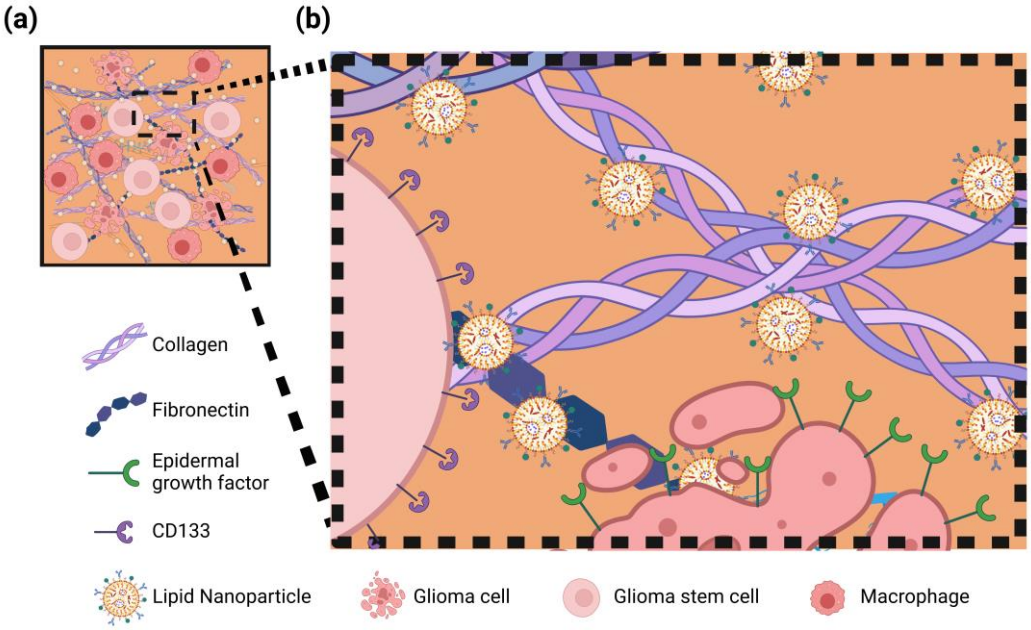

Figure 5. ECM targeting nanotechnology strategy. (**a**) Schematic overview illustrating nanoparticles interacting with ECM components to locally exert their effect; (**b**) Detailed depiction of nanoparticles avoiding cell receptors and specifically targeting ECM proteins such as collagen and fibronectin.

Among these components, the extra domain B (EDB) of fibronectin has emerged as a highly promising target for cancer therapy, particularly in aggressive solid tumors such as GB [162]. This specific domain is prominently present in the perivascular space of many aggressive tumors, making it an excellent marker for tumor-associated blood vessels [163]. Its unique overexpression pattern in the TME, coupled with its absence in normal adult tissues, makes EDB a selective target for nanotechnological strategies [164]. Saw et al. developed a GB therapy using a fibronectin-targeted liposomal nanoplatform functionalized with an EDB-specific aptide to deliver cyclophilin A (CypA), small interfering ribonucleic acid (siRNA). In vitro studies showed improved cellular uptake and CypA silencing in GB cells compared to non-targeted liposomes, while in non-orthotopic GB-xenografted mice, this targeted system reduced tumor growth and increased survival rates [143].

Previous studies have demonstrated that GB is characterized by a leaky and hemorrhagic vasculature, which promotes thrombosis and fibrin accumulation [144]. This feature, absent in normal tissues, is hypothesized to result from the increased permeability in GB,

allowing plasma proteins to infiltrate the tumor tissue, where fibrinogen is transformed into fibrin through the action of pro-coagulant factors [165]. Therefore, fibrin deposition in the ECM, a feature of both primary and metastatic brain tumors, could be a promising target for therapeutic intervention.

Taking this into consideration, Chung et al. [144] developed peptide-functionalized CREKA-micelle nanoparticles to target fibrin deposits in GB [166]. In an orthotopic mouse model of GB, both targeted and non-targeted micelles accumulated at the tumor site due to the enhanced permeability and retention (EPR) effect. However, CREKA-micelles showed enhanced tumor homing within one hour, indicating active fibrin targeting. Biodistribution studies revealed micelle accumulation in the liver and kidneys, suggesting clearance through renal filtration and the reticuloendothelial system. Importantly, no cytotoxicity or tissue damage was observed, supporting the nanoparticle system's safety [144].

Another promising ECM target in GB for tumor-specific therapy is TN-C, a glycoprotein with certain splice isoforms uniquely expressed in tumors. Clinical trials have evaluated radiolabeled antibodies targeting TN-C domains A1 and D for glioma and lymphoma therapy [167].

Instead of antibodies, Kang et al. developed a dual-targeting peptide system, Ft-PLA-PTX, which combines paclitaxel (PTX) with polylactic acid (PLA) nanoparticles. The peptide Ft targets TN-C and neuropilin-1 (NRP-1), enhancing internalization in U87 glioma and HUVEC cells, as well as penetration in 3D glioma spheroids. In vivo studies in U87 glioma-bearing mice showed significant accumulation of Ft-PLA-PTX at tumor sites, leading to higher cytotoxicity and apoptosis rates than single-targeted nanoparticles. Treatment resulted in a 269% increase in median survival compared to saline, outperforming Taxol® and other formulations, indicating the effectiveness of this dual-targeting approach [145].

Lingasamy et al. studied the targeting of the same ECM molecules TN-C and NRP-1 using an 8-amino acid homing peptide, PL3, to enhance nanoparticle delivery to GB and prostate carcinoma. They found that PL3 effectively binds to both targets and functionalizing iron oxide nanoworms (NWs) and silver nanoparticles (AgNPs) with PL3 significantly improved their targeting ability in nude mice models, achieving an eight-fold increase in GB targeting compared to untargeted nanoparticles. Notably, PL3-guided NWs increased survival rates in glioma-bearing mice, while untargeted particles had no therapeutic effect. Furthermore, advanced imaging confirmed the accumulation of PL3-coated nanoparticles in TN-C and NRP-1 positive areas in clinical tumor samples, suggesting potential for future clinical applications [146]. Following their work with PL3, the authors investigated PL1, which targets the ECM components fibronectin EDB and TN-C. The PL1-functionalized AgNPs exhibited strong binding to these targets and facilitated cellular uptake in U87 cells via a macropinocytosis-like process. The binding affinity of PL1 was quantified, supporting its potential for delivering therapeutic agents intracellularly [147].

MMPs are key players in the ECM remodeling process that contributes to GB progression [168]. These zinc-dependent enzymes, essential for normal physiological processes, can contribute to malignancy when their regulation is disrupted [169]. In GB, several MMPs are overexpressed, with MMP-2 and MMP-9 being the most extensively studied [170–172]. These secreted gelatinases break down key ECM components like collagens, elastin, and fibronectin, creating space for tumor cell migration and invasion [173]. Additionally, they promote the release of pro-angiogenic factors such as VEGF, enhancing tumor resource availability and facilitating GB infiltration through newly formed blood vessels [174].

Another MMP found to be overexpressed in GB is the membrane-anchored MMP-14 (also known as MT1-MMP) [175]. It shares similar proteolytic, angiogenic, and immunomodulatory capabilities with the secreted gelatinases and can activate pro-MMP-2, further contributing to GB invasiveness [148,150]. MMP-14's influence extends beyond

ECM degradation, regulating numerous plasma membrane-anchored and extracellular proteins, thereby impacting both intercellular and cell-matrix communication [176]. In the GB TME, both cancer and stromal cells engage with the ECM through various adhesive structures [176]. This interaction often results in aggressive infiltration of adjacent brain tissue, including areas crucial for survival. To facilitate invasion, glioma cells secrete proteolytic enzymes that degrade the ECM and mediate the invasion process, and research has revealed that specific MMPs not only promote glioma cell invasion but also alter tumor cell behavior and stimulate cancer progression [118,177]. As the invasive nature of GB significantly contributes to its high mortality rate and poor prognosis, making it a critical area of study, understanding the complex interplay of various MMPs, in particular MMP-14, in GB is essential [175]. This deeper comprehension could lead to the development of new prognostic and predictive markers, improving patient outcomes. Moreover, exploring MMP interactions may pave the way for novel targeted therapies designed to counteract the invasive nature of GB.

Taking into consideration that MMP-14 is differentially expressed in GB, compared to normal tissues, Kasten et al. developed a dual-modality imaging agent targeting the membrane protease. Their peptide probe combines a near-infrared fluorescence (NIRF) dye linked to a quencher that is activated upon cleavage by MMP-14, and an MMP-14-binding peptide attached to a radionuclide chelate for positron emission tomography (PET). This approach enhanced tumor specificity and imaging contrast, as the NIRF signal activates only in the presence of MMP-14. In vitro and in vivo studies demonstrated the probe's efficacy in detecting GB in cultured cell lines and patient-derived xenograft models, showing favorable tumor-to-background ratios. PET imaging confirmed significant localization of the probe in orthotopic GB models, and blocking experiments verified its specific targeting of MMP-14-expressing cells. Their strategy seemed to be effective for imaging GBs, providing valuable insights for both preoperative planning and real-time surgical guidance [148].

Finally, in terms of vascularization, GB stands out as one of the most highly angiogenic tumors, with VEGF playing a central role in this process [178]. The formation of new blood vessels in GB is driven by both hypoxia-dependent and independent mechanisms, leading to the development of unique vessels [109]. This angiogenic potential of GB is further enhanced by GSCs, which secrete significantly higher levels of VEGF compared to non-stem glioma cells [179]. Conditioned media from these stem cells have been shown to strongly enhance endothelial cell functions crucial for angiogenesis, including migration, proliferation, and tube formation. This heightened angiogenic activity, primarily driven by VEGF and exacerbated by GSCs, is a major contributor to the aggressive nature of GB, presenting both challenges and opportunities for therapeutic interventions targeting the tumor vasculature [180]. Taking advantage of the enhanced accumulation of VEGF in the ECM of GB tumors, Abakumov et al. developed iron oxide magnetic nanoparticles (MNPs) targeting VEGF for enhanced GB imaging [149]. The MNPs were coated with cross-linked bovine serum albumin (BSA) to improve biocompatibility and stability, then functionalized with monoclonal antibodies against VEGF, allowing specific binding to VEGF-positive GB cells. This targeted approach improved tumor visualization using magnetic resonance imaging (MRI), addressing limitations of existing contrast agents in specificity and retention [181]. In vitro studies confirmed the nanoparticles' stability and cytocompatibility, while in vivo experiments in orthotopic C6-xenografted rat models demonstrated superior imaging of tumors and vasculature compared to non-targeted controls, with sustained contrast for 24 h post-injection [149].

5.2. ECM-Responsive Nanoparticles

The ECM provides essential mechanical and biochemical cues through its interactions with cell receptors, allowing it to function as both a structural scaffold and a regulator of cellular behaviors such as adhesion, proliferation, and differentiation [182]. The composition and architecture vary between tissue types, influenced by various factors including the cell type present, mechanical forces, and the availability of nutrients and oxygen in the local microenvironment. This dynamic nature of the ECM reflects changes in tissue status and disease conditions, with GB being no exception [183]. Nanosystems can be designed to modulate their effect once in contact with TME conditional changes, such as the increased presence of secreted and membrane MMPs, the acidic environment, and the lack of oxygenation (Figure 6).

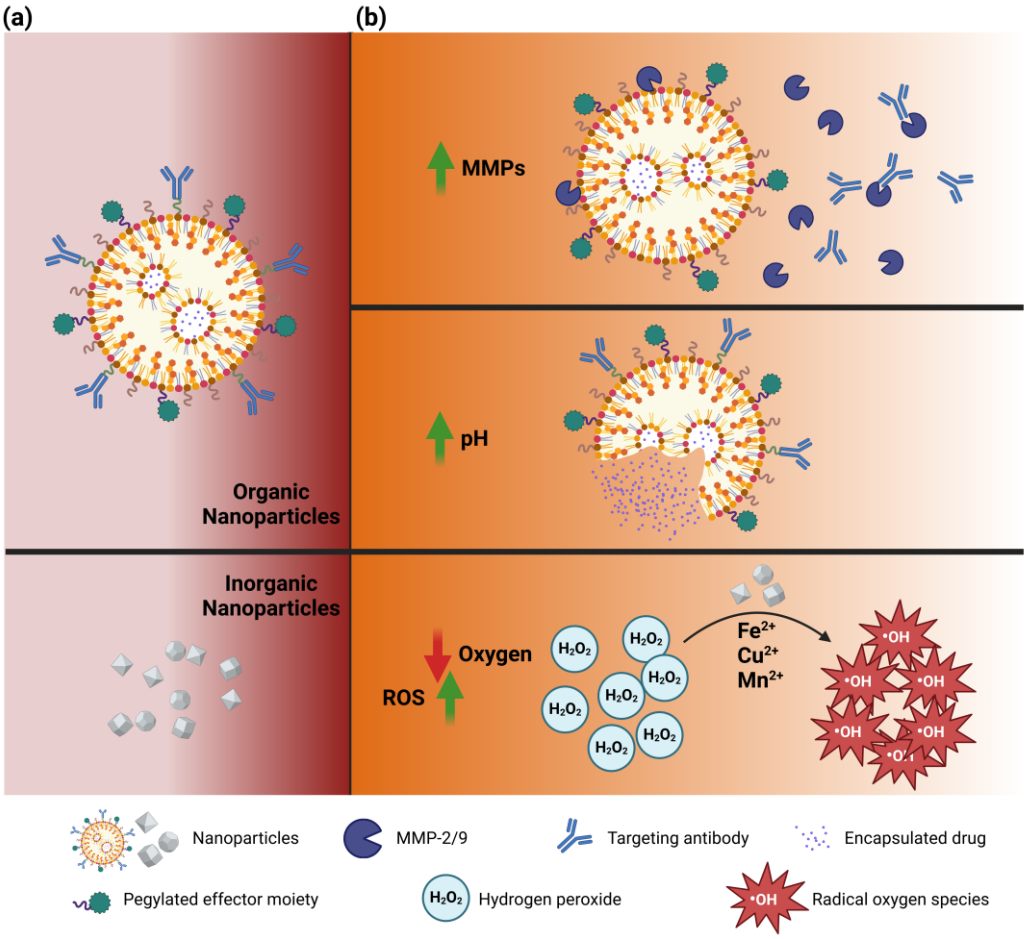

Figure 6. Utilizing ECM physicochemical cues as a nanotechnological strategy. (**a**) Nanoparticles in circulation; (**b**) Nanoparticles upon sensing TME conditional alterations. From top to bottom, an increase in secreted and membrane matrix metalloproteases, an increase in acidity, an increase in hypoxia accompanied by an increase in ROS.

As previously mentioned, MMP-14 is a proteolytic enzyme highly overexpressed in GBs and has been already applied as a microenvironment cue in GB therapy by Mohanty et al. Their work focused on creating a theranostic approach using cross-linked iron oxide nanoparticles, named CLIO-ICT, which combined therapeutic and diagnostic functions to target GB and GSCs. These nanoparticles consisted of cross-linked iron oxide particles conjugated to an azademethylcolchicine (ICT)-peptide prodrug that released the active drug upon cleavage by MMP-14. The study demonstrated that CLIO-ICT selectively targets GB cells and GSCs, disrupting tumor blood vessels and significantly inducing apoptosis

while reducing GSCs populations. In vivo experiments in orthotopic xenografted mice revealed that CLIO-ICT, especially when combined with TMZ, improved survival rates and reduced tumor growth compared to TMZ alone. Additionally, the dual functionality of CLIO-ICT allowed for real-time tumor response monitoring via MRI. [150].

In a similar direction, Gu et al. [139] developed nanoparticles that utilize the up-regulated expression of MMP-2 and MMP-9 in GB [168,184]. These nanoparticles were modified with an activatable cell-penetrating peptide, which is specifically cleaved by MMP-2 and MMP-9, enhancing internalization and enabling targeted PTX delivery within the GB microenvironment. After confirming successful conjugation of the peptide to polyethylene glycol-polycaprolactone (PEG-PCL) nanoparticles, in vitro studies showed significantly increased cellular uptake in GB cells and enhanced penetration in 3D GB spheroids. In vivo studies in intracranial GB xenograft models indicated that the peptide-modified nanoparticles accumulated in tumor tissues, leading to improved survival rates compared to conventional PTX formulations [139].

More recently, Fan et al. engineered MMP-2-activated nanoparticles that combine immunotherapy with ferroptosis induction for GB treatment [151]. These complex nanoparticles consist of bispecific antibodies targeting B7-H3 (associated with poor prognosis in GB) and CD3, along with a dimer of epigallocatechin-3-gallate (dEGCG) linked to HA via an MMP-2-cleavable sequence. dEGCG, on its own, has been shown to provide a myriad of antitumor effects, mainly associated with its production of intracellular ROS and subsequent induction of oxidative damage [185]. This design allowed the nanoparticles to cross the BBB, accumulate in GB tissue, and release their cargo upon MMP-2 cleavage. In vitro studies showed effective targeting of GB cells, T-cell activation, and cytokine release, leading to enhanced anti-tumor effects. In a mouse orthotopic U87 GB xenograft model, the nanoparticles demonstrated significantly higher intracranial accumulation compared to free antibodies or non-targeted formulations. Notably, the treatments resulted in 50% of mice surviving longer than 56 days, indicating a promising strategy for GB therapy that leverages both immune activation and ferroptosis [151].

In addition to MMP-responsiveness, tumor acidosis is a well-studied characteristic of most TMEs [186]. Rapidly proliferating tumor cells often deplete their own oxygen supply, thereby leading to hypoxia, where cells are unable to generate adenosine triphosphate (ATP) through oxidative phosphorylation. In response, the hypoxia-inducible factor (HIF) pathway shifts cellular metabolism towards anaerobic glycolysis, commonly referred to as the Warburg effect, allowing the tumor cells to continue ATP production despite the lack of oxygen. This metabolic adaptation results in the accumulation of lactate and protons as byproducts of fermentation, which alter not only the intracellular pH, but, once expelled, contribute to the characteristic acidification of the TME [94].

To take advantage of the acidic TME in GB, Zhao et al. developed a DOX-loaded liposome that responds to the surrounding pH by incorporating a conjugated peptide, which consists of a cell-penetrating sequence and a pH-sensitive trigger. The liposomes were produced through the common thin-film hydration method followed by the less common remote loading technique of DOX. In vitro experiments showed pH-triggered drug release and specific targeting of C6 and U87 GB cells under acidic conditions caused by the peptide modification. In vivo experiments in C6 subcutaneous and U87 orthotopic tumor-bearing mice demonstrated significant anti-tumor activity and antiangiogenic effects, indicating the liposomes' potential for targeted drug delivery and vascular modulation [152].

In a simpler approach, Sathiyaseelan et al. utilized chitosan as the pH-responsive component in anti-nucleolin aptamer (AS1411)-functionalized gold nanoparticles, biosynthesized from *Gynura procumbens*, and loaded with both 5-fluorouracil (5-FU) and DOX. Chitosan, a cationic polysaccharide, becomes soluble at acidic pH, enhancing the release of

its cargo in such environments. The study demonstrated higher drug release rates under acidic conditions that mimic the GB TME. In vitro experiments on LN229 GB cells showed that the dual-drug-loaded nanoparticles induced greater cell death than single-drug formulations, primarily through G0/G1 phase cell cycle arrest, with transmission electron microscopy (TEM) confirming their internalization in cell organelles [153].

More recently, our group has described an elegant functionalization design that utilizes an acid-cleavable angiopep-2 to functionally create two different nanosystems, a brain-targeting nanoparticle while in circulation that transforms into a GB-accumulating nanoparticle after BBB crossing [154]. In that sense, poly(lactic-*co*-glycolic acid) (PLGA) and PEG based NPs were designed to deliver docetaxel to GB tumors. The polymeric nanoparticles were dual-surface tailored with two key features: (i) a brain-targeted acid-responsive angiopep-2 moiety that triggers a structural rearrangement within BBB endosomal vesicles, and (ii) an L-histidine moiety that provides preferential accumulation into GB cells after BBB crossing. The angiopep-2 peptide targets the low-density lipoprotein receptor (LDLR) overexpressed on the BBB, while L-histidine targets the L-type amino acid transporter 1 (LAT1) overexpressed in GB cells. It is important to note that PEG with different molecular weights were used to create two levels of nanoparticle surface decoration, avoiding intersteric hindrance. In vitro studies using tumor invasive margin patient cells showed that the stimuli-responsive multifunctional nanosystem effectively targeted GB cells, enhancing cell uptake 12-fold and inducing 3 times higher cytotoxicity in both 2D and 3D cell models compared to non-targeting formulations. In vitro BBB permeability was assessed with a hCMEC/D3 transwell model, with the nanosystem demonstrating a threefold increased BBB permeability. An in vivo biodistribution trial confirmed a threefold improvement of nanoparticle accumulation in the brain. The antitumor efficacy was validated in GB orthotopic models following both intratumoral and intravenous administration, with the median survival and number of long-term survivors increasing by 50% compared to control groups. The acid-cleavable properties of the nanoparticles ensure that the long-length PEG-angiopep-2 separates from the main structure after encountering the acidic pH of endosomes during BBB trafficking. This facilitates endosomal escape and nanoparticle expulsion towards the brain. Subsequently, the shorter PEG-L-histidine becomes exposed on the NP surface due to steric deprotection, allowing for GB cell targeting. This study represented the first time that a multi-ligand functionalized NP system was proposed to sequentially target the BBB and GB through the exploitation of a BBB-responsive transport mechanism [154].

Furthermore, as previously noted, hypoxia is a prevalent feature in cancer. The TME often stimulates neoangiogenesis, resulting in the development of aberrant and inefficient blood vessels. This process, paradoxically, intensifies the hypoxic conditions within the tumor. These irregular vessels restrict the delivery of oxygen, drugs, and immune cells, making tumors more resistant to treatment. Hypoxia also induces significant changes in tumor cells, activating pathways such as the previously mentioned HIF pathway, which enables cell adaptation, promoting invasion, therapy resistance, and immune evasion [187]. This is particularly relevant in GB, one of the most hypoxic tumors [188]. Very recently, Qi et al. developed a hypoxia-responsive liposomal system (AMVY@NPs) for GB treatment, designed for stepwise targeting and drug release. This system includes a polymetronidazole core that encapsulates the Yes-associated protein (YAP) inhibitor verteporfin (VP), a cationic lipid layer that adsorbs siRNA targeting YAP (siYAP), and an outer coating with the targeting peptide angiopep-2. The nanoparticles are engineered to cross the BBB, specifically target GB cells, and release their cargo in response to the hypoxic TME. In vitro and in vivo studies demonstrated that AMVY@NPs effectively released siYAP and VP under hypoxic conditions, leading to synergistic inhibition of GB cell growth and pluripotency. In an

orthotopic U87 xenograft mouse model, these nanoparticles significantly inhibited tumor growth and improved survival without noticeable adverse effects [155].

TME hypoxia and acidosis are linked to ROS creation by oxidative stress [189]. In GB, elevated ROS levels are a hallmark of the TME, promoting tumor progression, therapy resistance, genomic instability, and invasion [190]. While therapies such as radiation aim to exploit ROS-induced cell death, GB cells often resist by enhancing antioxidant defenses [191]. Considering this, Yang et al. developed a hollow manganese dioxide (h-MnO_2) nanosystem aimed at alleviating tumor hypoxia by degrading endogenous hydrogen peroxide (H_2O_2) into oxygen and water. The pH-responsive MnO_2 breaks down in the acidic TME. This nanosystem, produced via a silica template method and functionalized with PEG for stability, enables targeted drug delivery, imaging, and TME modulation. It efficiently loaded chlorine e6 (Ce6), a photodynamic agent, and DOX, releasing them in the TME while generating Mn^{2+} ions to enhance MRI contrast. By producing oxygen, the system improves photodynamic therapy efficacy, which relies on oxygen to generate ROS. In vivo studies confirmed effective accumulation of Ce6/DOX-loaded nanoparticles in tumors and kidneys, demonstrating synergistic effects of chemotherapy and photodynamic therapy in reducing tumor mass [156].

Finally, regarding ECM-responsiveness, the interaction between glutathione (GSH) and disulfide (SS) bonds has been exploited [192]. This interaction relies on two characteristics: (i) there is a steep GSH gradient between the extracellular environment (micromolar) and the intracellular tumor environment (millimolar), and (ii) SS bonds can be cleaved by GSH. Therefore, drug delivery systems that incorporate SS bonds can rapidly release their therapeutic agents inside target cells, significantly improving drug efficacy [157,193].

This was explored by Tian et al., who developed a redox-sensitive nanocarrier system for targeted curcumin delivery to GB cells by conjugating HA with curcumin via disulfide bonds. This system takes advantage of the high glutathione levels in TMEs, where GSH can cleave disulfide bonds, leading to rapid drug release inside target cells. Their work explored how the molecular weight (MW) of HA affects the properties and performance of nanocarriers. The HA-curcumin conjugates formed nanoscale micelles, enhancing curcumin's solubility and stability. Low (50 kDa) and medium (200–500 kDa) MW HA-based micelles showed GSH sensitivity and superior cytotoxicity and cellular uptake in G422 mouse GB cells compared to high MW micelles or free curcumin, indicating their effectiveness for intracellular drug delivery [157].

5.3. Enhancing ECM Degradation

The GB ECM, as previously discussed, is notably dense and complex, being comprised of overexpressed components, including HA, specific collagens, laminin, TN-C, and fibronectin, among others (Figure 2). These excessive ECM components make the TME more compact and less flexible, hindering the diffusion of therapeutic agents [194]. Additionally, this dense physical barrier impedes both T cell infiltration and drug or nanosystem penetration, contributing to immunosuppression and drug resistance [195]. Recent studies suggest that breaking down the tumor ECM or inhibiting its formation can enhance the penetration and accumulation of nanotherapeutics, thereby improving the efficacy of nanomedicines [140]. One approach to address this issue involves degrading key ECM components, which loosens the ECM structure and increases tumor tissue permeability, allowing immune cells to better migrate and infiltrate the tumor [196].

To optimize the ECM degradation strategy by targeting the most abundant components of GB ECM, Kiyokawa et al. investigated the role of HA degradation in enhancing the effect of oncolytic adenovirus immunotherapy for GB [158]. They used ICOVIR17, a hyaluronidase-expressing oncolytic adenovirus, to target the HA-rich ECM.

In murine orthotopic GB models, ICOVIR17 increased tumor-infiltrating $CD8^+$ T cells and macrophages, leading to prolonged animal survival compared to the control virus ICOVIR15 (no hyaluronidase). ICOVIR17 also upregulated programmed cell death protein (PD)-ligand 1 (PD-L1) expression on GB cells and macrophages. In vitro experiments showed that high MW HA inhibited adenovirus-induced NF-kB signaling in macrophages, linking HA degradation to macrophage activation. Combining ICOVIR17 with anti-PD-1 antibody therapy further extended survival in GB mice models, with some animals achieving long-term remission. Mechanistic studies revealed that $CD4^+$ T cells, $CD8^+$ T cells, and macrophages all contributed to the efficacy of the combination therapy. This treatment induced pro-inflammatory TAMs and enhanced tumor-specific T cell cytotoxicity both locally and systemically [158].

Similarly, Shukla et al. addressed ECM as barrier to nanoparticle penetration through the functionalization of human serum albumin nanoparticles (HSANPs) with collagenase. These collagenase-modified nanoparticles were loaded with gemcitabine (CG-HSANPs) to overcome the limitations of its short half-life and dose-dependent side effects. In vitro, CG-HSANPs demonstrated comparable cytotoxicity with uncoated NPs or free drug but exhibited improved tumor spheroid penetration. Also, CG-HSANPs induced higher levels of nuclear fragmentation, ROS generation, and mitochondrial membrane potential disruption compared to the native drug, emphasizing the importance of ECM degradation in enhancing drug delivery efficacy [159].

5.4. Preventing ECM Degradation

The invasive nature of GB is closely associated with its ECM, which facilitates tumor cell migration and invasion [176]. As previously elucidated, given the role of MMPs in GB progression, various approaches targeting their inhibition have been explored [197,198]. Synthetic MMP inhibitors such as Batimastat and Marimastat, which bind to the MMPs' zinc atom, have shown promise in reducing MMP activity [199]. However, clinical studies have failed to demonstrate significant improvements in patient progression-free and overall survival, primarily due to the molecules' low aqueous solubility and potential side effects [200]. As a result, research focusing on MMPs and ECM remodeling as actively targeted therapeutic strategies has been relatively limited [201]. Despite these past challenges, recent strategies have sought innovative ways to target MMPs. While traditional hydroxamate-based MMP inhibitors faced clinical setbacks, nanotechnology offers a promising alternative. By improving solubility and minimizing side effects, fields where nanoparticles excel, nanosystems have the potential to reinvigorate these inhibitors and enable more effective ECM-targeted therapies.

The scorpion venom-derived chlorotoxin (CTX) is a more modern and less synthetic alternative for the old hydroxamate-based MMP inhibitors [202] and has demonstrated active targeting of GB cells [203]. Agarwal et al. functionalized PLGA nanoparticles with CTX (with high affinity for MMP-2 and chloride channels overexpressed in GB cells) to deliver morusin, a chemotherapeutic agent with poor bioavailability. These CTX-functionalized nanoparticles (PLGA-MOR-CTX) effectively crossed the BBB and presented anti-cancer effects in U87 and GI-1 human GB cell lines through apoptosis induction, ROS generation, and MMP inhibition, with low toxicity to normal neuronal cells [160].

Islam et al. synthesized amphiphilic peptides containing a brain-targeting ligand (HAIYPRH or CKAPETALC) conjugated with an MMP-9 inhibiting peptide (CTTHWGFTLC), linked by glycine spacers and conjugated to cholesterol at the N-terminus [161]. The amphiphilic peptide-cholesterol (c-GGGCTTHWGFTLCHAIYPRH) formed nanoparticles able to cross an in vitro BBB hCMEC/D3 transwell model while showing low toxicity

in HeLa cells. The authors also demonstrated an efficient inhibition of MMP-9 activity in an acellular in vitro setting [161].

6. Challenges and Future Perspectives

Nanotechnology offers significant promise to address the challenges of GB therapy, particularly in targeting its ECM. However, several hurdles remain to be addressed to achieve its full clinical potential.

The GB ECM is highly complex and heterogeneous, varying between patients and even within the same tumor. This makes it difficult to develop a one-size-fits-all nanoparticle approach. Additionally, the dense and rigid structure of the GB ECM poses a significant barrier to nanoparticle penetration and drug delivery. Current ECM degradation strategies need further enhancement. Additionally, the BBB presents a major obstacle. While some promising nanoparticle targeting strategies have shown promise in preclinical models, translating these results to humans remains challenging due to differences in BBB structure and function.

Current research is exploring innovative alternatives to address these issues. Multifunctional nanoparticles are being designed to simultaneously target GB cells and modulate ECM. For example, particles incorporating MMP inhibitors alongside chemotherapeutic agents aim to remodel the ECM and expose tumor cells to treatment. Stimuli-responsive systems, which activate in response to specific TME cues (e.g., pH, enzyme activity), are another promising avenue. This approach could improve target specificity by guaranteeing that the effect only occurs within the TME and reduce off-target effects. Biomimetic strategies, such as nanoparticles coated with cell membranes or engineered to mimic extracellular vesicles, offer potential to improve BBB crossing and tumor targeting. Combination therapies, like using nanoparticles in conjunction with other treatment modalities, such as focused ultrasound to temporarily disrupt the BBB, could enhance delivery to the tumor site.

Looking forward, several key areas of research are essential for advancing this field. Personalized approaches, such as tailoring NPs based on the ECM of each individual patient, could greatly improve therapeutic outcome by tailoring nanoparticle formulations accordingly. Advanced imaging techniques could enable real-time visualization of nanoparticle distribution and ECM interactions in vivo, optimizing delivery strategies. Robust predictive in vitro and in silico models of the GB ECM and BBB are needed to accelerate nanoparticle design and testing. High-throughput screening of NP formulations generated by these predictive models could identify the most feasible designs. Additionally, long-term safety studies are crucial to evaluate the potential long-term impact of ECM-modulating nanoparticles on healthy brain tissue and tumor recurrence. Ultimately, scalable manufacturing, by developing cost-effective and reproducible methods for large-scale production of complex nanoparticle formulations, will invariably have to be implemented.

In conclusion, nanotechnology offers promising avenues for advancing GB treatment by addressing key challenges such as BBB penetration, targeted drug delivery, and overcoming drug resistance. The ability to modulate the ECM through nanotechnological approaches presents a particularly exciting avenue for therapeutic strategies. While significant hurdles remain, including scale-up optimization and reproducibility, the rapid progress in this field provides cautious optimism for developing more effective GB therapies in the coming decade. As we continue to unravel the complexities of GB biology and refine nanotechnological tools, the potential for significant improvements in patient outcomes becomes ever more tangible.

Author Contributions: M.H., P.S., C.L.P. and R.T.L. contributed to the review conception and design. The original draft of the manuscript was written by M.H., C.L.P. and R.T.L., and all authors reviewed and edited previous versions of the manuscript. The work was supervised by C.L.P. and R.T.L. Funding and resources were obtained by P.S., C.L.P. and R.T.L. All authors have read and agreed to the published version of the manuscript.

Funding: This work was financed by Fundação para a Ciência e Tecnologia (FCT) with the PhD Grant 2020.10014.BD. This research was partly supported by the project "Institute for Research and Innovation in Health Sciences" (UID/BIM/04293/2019) and the project "The Porto Comprehensive Cancer Center" ref. NORTE-01-0145-FEDER-072678—Consórcio PORTO.CCC—Porto. Comprehensive Cancer Center Raquel Seruca. The funders had no role in the study design, data collection, analysis, publication decision, or manuscript preparation.

Institutional Review Board Statement: Not applicable.

Informed Consent Statement: Not applicable.

Data Availability Statement: No new data were created or analyzed in this study. Data sharing is not applicable to this article.

Conflicts of Interest: The authors declare no conflicts of interest.

Abbreviations

The following abbreviations are used in this manuscript:

GB	Glioblastoma
CNS	Central Nervous System
WHO	World Health Organization
IDH	Isocitrate Dehydrogenase
TERT	Telomerase Reverse Transcriptase
EGF	Epithelial Growth Factor
EGFR	Epithelial Growth Factor Receptor
NOS	Not Otherwise Specified
NEC	Not Elsewhere Classified
RT	Radiotherapy
TMZ	Temozolomide
MGMT	Methylguanine Methyltransferase
FDA	Food and Drug Administration
VEGF	Vascular Endothelial Growth Factor
BBB	Blood-Brain Barrier
TTFields	Tumor Treating Fields
TME	Tumor Microenvironment
TCGA	The Cancer Genome Atlas
CDKN2A	Cyclin-Dependent Kinase Inhibitor 2A
TP53	Tumor Protein P53
SMO	Smoothened
GAS1	Growth Arrest-Specific Protein 1
GLI2	GLI family zinc finger 2
NOTCH3	Neurogenic Locus Notch Homolog Protein 3
JAG1	Jagged 1
LFNG	Beta-1,3-*N*-acetylglucosaminyltransferase Lunatic Fringe
NF1	Neurofibromin
PTEN	Phosphatase and Tensin Homolog
PI3K	phosphatidylinositol 3-kinase
CHI3L1	Chitinase-3-Like Protein 1
CD	Cluster of Differentiation
NF-κB	Nuclear Factor Kappa-Light-Chain-Enhancer of Activated B Cells

PDGFRA	Platelet-Derived Growth Factor Receptor A
AC-like	Astrocyte-like
MES-like	Mesenchymal-like
OPC-like	Oligodendrocyte Progenitor-like
NPC-like	Neural Progenitor-like
CDK4	Cyclin-Dependent Kinase 4
GSCs	Glioma Stem Cells
SOX2	Sex Determining Region Y Box 2
DNA	Deoxyribonucleic Acid
ABC	ATP-Binding Cassette
OCT4	Octamer-Binding Transcription Factor 4
IL	Interleukin
TGF-β	Transforming Growth Factor Beta
TAM	Tumor-Associated Macrophage
CSF-1	Colony Stimulating Factor 1
GDNF	Glial Cell Line-Derived Neurotrophic Factor
CCL2	Chemokine (CC Motif) Ligand 2
SFD-1	Stromal Cell-Derived Factor 1
CXCL1	Chemokine (CXC Motif) Ligand 1
GM-CSF	Granulocyte-Macrophage Colony-Stimulating Factor
IGF-1	Insulin-like Growth Factor 1
PDGF	Platelet-Derived Growth Factor
MDSC	Myeloid-Derived Suppressor Cells
NK	Natural Killer
ROS	Reactive Oxygen Species
CAF	Cancer-Associated Fibroblast
ERK	Extracellular Signal-Regulated Kinase
ECM	Extracellular Matrix
HA	Hyaluronic Acid
TN-C	Tenascin-C
MMP	Matrix Metalloproteinase
NP	Nanoparticle
DOX	Doxorubicin
EDB	Extra Domain B
CypA	Cyclophilin A
siRNA	Small Interfering Ribonucleic Acid
EPR	Enhanced Permeability and Retention
PTX	Paclitaxel
PLA	Polylactic Acid
NRP-1	Neuropilin-1
NW	Nanoworm
AgNP	Silver Nanoparticle
NIRF	Near-Infrared Fluorescence
PET	Positron Emission Tomography
MNP	Magnetic Nanoparticle
BSA	Bovine Serum Albumin
MRI	Magnetic Resonance Imaging
CLIO	Cross-Linked Iron Oxide
ICT	Azademethylcolchicine
PEG	Polyethylene Glycol
PCL	Polycaprolactone
dEGCG	Epigallocatechin-3-Gallate Dimer
ATP	Adenosine Triphosphate
HIF	Hypoxia-Inducible Factor

AS1411	Anti-Nucleolin Aptamer
5-FU	5-Fluorouracil
TEM	Transmission Electron Microscopy
PLGA	Poly(Lactic-Co-Glycolic Acid)
LDLR	Low-Density Lipoprotein Receptor
LAT1	L-type Amino Acid Transporter 1
YAP	Yes-Associated Protein
VP	Verteporfin
h-MnO_2	Hollow Manganese Dioxide
H_2O_2	Hydrogen Peroxide
Ce6	Chlorine e6
GSH	Glutathione
SS	Disulfide Bonds
MW	Molecular Weight
PD	Programmed Cell Death Protein
PD-L1	Programmed Death-Ligand 1
CG-HSANP	Collagenase-Modified Human Serum Albumin Nanoparticle
CTX	Chlorotoxin

References

1. Grochans, S.; Cybulska, A.M.; Simińska, D.; Korbecki, J.; Kojder, K.; Chlubek, D.; Baranowska-Bosiacka, I. Epidemiology of Glioblastoma Multiforme-Literature Review. *Cancers* **2022**, *14*, 2412. [CrossRef] [PubMed]
2. Gittleman, H.; Boscia, A.; Ostrom, Q.T.; Truitt, G.; Fritz, Y.; Kruchko, C.; Barnholtz-Sloan, J.S. Survivorship in adults with malignant brain and other central nervous system tumor from 2000–2014. *Neuro-Oncology* **2018**, *20* (Suppl. 7), vii6–vii16. [CrossRef] [PubMed]
3. Ostrom, Q.T.; Gittleman, H.; Truitt, G.; Boscia, A.; Kruchko, C.; Barnholtz-Sloan, J.S. CBTRUS Statistical Report: Primary Brain and Other Central Nervous System Tumors Diagnosed in the United States in 2011–2015. *Neuro-Oncology* **2018**, *20* (Suppl. 4), iv1–iv86. [CrossRef] [PubMed]
4. Reinders, A.N.; Koshy, M.; Korpics, M. The Patterns of Failure and Prognostic Impact of Tumor Location in Patients Undergoing Reirradiation for Glioblastoma. *Cureus* **2024**, *16*, e68820. [CrossRef]
5. Carrano, A.; Juarez, J.J.; Incontri, D.; Ibarra, A.; Guerrero Cazares, H. Sex-Specific Differences in Glioblastoma. *Cells* **2021**, *10*, 1783. [CrossRef]
6. Louis, D.N.; Perry, A.; Wesseling, P.; Brat, D.J.; Cree, I.A.; Figarella-Branger, D.; Hawkins, C.; Ng, H.K.; Pfister, S.M.; Reifenberger, G.; et al. The 2021 WHO Classification of Tumors of the Central Nervous System: A summary. *Neuro-Oncology* **2021**, *23*, 1231–1251. [CrossRef] [PubMed]
7. Li, S.; Wang, C.; Chen, J.; Lan, Y.; Zhang, W.; Kang, Z.; Zheng, Y.; Zhang, R.; Yu, J.; Li, W. Signaling pathways in brain tumors and therapeutic interventions. *Signal Transduct. Target. Ther.* **2023**, *8*, 8. [CrossRef]
8. Gue, R.; Lakhani, D.A. The 2021 World Health Organization Central Nervous System Tumor Classification: The Spectrum of Diffuse Gliomas. *Biomedicines* **2024**, *12*, 1349. [CrossRef]
9. Han, S.; Liu, Y.; Cai, S.J.; Qian, M.; Ding, J.; Larion, M.; Gilbert, M.R.; Yang, C. IDH mutation in glioma: Molecular mechanisms and potential therapeutic targets. *Br. J. Cancer* **2020**, *122*, 1580–1589. [CrossRef] [PubMed]
10. Whitfield, B.T.; Huse, J.T. Classification of adult-type diffuse gliomas: Impact of the World Health Organization 2021 update. *Brain Pathol.* **2022**, *32*, e13062. [CrossRef]
11. Torp, S.H.; Solheim, O.; Skjulsvik, A.J. The WHO 2021 Classification of Central Nervous System tumours: A practical update on what neurosurgeons need to know—A minireview. *Acta Neurochir.* **2022**, *164*, 2453–2464. [CrossRef] [PubMed]
12. Stoyanov, G.S.; Lyutfi, E.; Georgieva, R.; Georgiev, R.; Dzhenkov, D.L.; Petkova, L.; Ivanov, B.D.; Kaprelyan, A.; Ghenev, P. Reclassification of Glioblastoma Multiforme According to the 2021 World Health Organization Classification of Central Nervous System Tumors: A Single Institution Report and Practical Significance. *Cureus* **2022**, *14*, e21822. [CrossRef]
13. Osborn, A.G.; Louis, D.N.; Poussaint, T.Y.; Linscott, L.L.; Salzman, K.L. The 2021 World Health Organization Classification of Tumors of the Central Nervous System: What Neuroradiologists Need to Know. *Am. J. Neuroradiol.* **2022**, *43*, 928–937. [CrossRef]
14. Colman, H.; Zhang, L.; Sulman, E.P.; McDonald, J.M.; Shooshtari, N.L.; Rivera, A.; Popoff, S.; Nutt, C.L.; Louis, D.N.; Cairncross, J.G.; et al. A multigene predictor of outcome in glioblastoma. *Neuro-Oncology* **2010**, *12*, 49–57. [CrossRef]

15. Verhaak, R.G.; Hoadley, K.A.; Purdom, E.; Wang, V.; Qi, Y.; Wilkerson, M.D.; Miller, C.R.; Ding, L.; Golub, T.; Mesirov, J.P.; et al. Integrated genomic analysis identifies clinically relevant subtypes of glioblastoma characterized by abnormalities in PDGFRA, IDH1, EGFR, and NF1. *Cancer Cell* **2010**, *17*, 98–110. [CrossRef] [PubMed]
16. Wang, Q.; Hu, B.; Hu, X.; Kim, H.; Squatrito, M.; Scarpace, L.; deCarvalho, A.C.; Lyu, S.; Li, P.; Li, Y.; et al. Tumor Evolution of Glioma-Intrinsic Gene Expression Subtypes Associates with Immunological Changes in the Microenvironment. *Cancer Cell* **2017**, *32*, 42–56.e6. [CrossRef] [PubMed]
17. Ostrom, Q.T.; Adel Fahmideh, M.; Cote, D.J.; Muskens, I.S.; Schraw, J.M.; Scheurer, M.E.; Bondy, M.L. Risk factors for childhood and adult primary brain tumors. *Neuro-Oncology* **2019**, *21*, 1357–1375. [CrossRef] [PubMed]
18. Smith, C.J.; Perfetti, T.A.; Chokshi, C.; Venugopal, C.; Ashford, J.W.; Singh, S.K. Risk factors for glioblastoma are shared by other brain tumor types. *Hum. Exp. Toxicol.* **2024**, *43*, 09603271241241796. [CrossRef] [PubMed]
19. Gunasegaran, B.; Ashley, C.L.; Marsh-Wakefield, F.; Guillemin, G.J.; Heng, B. Viruses in glioblastoma: An update on evidence and clinical trials. *BJC Rep.* **2024**, *2*, 33. [CrossRef] [PubMed]
20. Tarev, I.; Cekov, A. Cerebellar Glioblastoma: A Literature Review and Case Analysis. *Cureus* **2024**, *16*, e55135. [CrossRef]
21. Alharbi, B.; Alammar, H.; Alkhaibary, A.; Alharbi, A.; Khairy, S.; Alassiri, A.H.; AlSufiani, F.; Aloraidi, A.; Alkhani, A. Primary spinal cord glioblastoma: A rare cause of paraplegia. *Surg. Neurol. Int.* **2022**, *13*, 160. [CrossRef] [PubMed]
22. Valenzuela-Fuenzalida, J.J.; Moyano-Valarezo, L.; Silva-Bravo, V.; Milos-Brandenberg, D.; Orellana-Donoso, M.; Nova-Baeza, P.; Suazo-Santibáñez, A.; Rodríguez-Luengo, M.; Oyanedel-Amaro, G.; Sanchis-Gimeno, J.; et al. Association between the Anatomical Location of Glioblastoma and Its Evaluation with Clinical Considerations: A Systematic Review and Meta-Analysis. *J. Clin. Med.* **2024**, *13*, 3460. [CrossRef] [PubMed]
23. De Luca, C.; Virtuoso, A.; Papa, M.; Certo, F.; Barbagallo, G.M.V.; Altieri, R. Regional Development of Glioblastoma: The Anatomical Conundrum of Cancer Biology and Its Surgical Implication. *Cells* **2022**, *11*, 1349. [CrossRef] [PubMed]
24. Fyllingen, E.H.; Bø, L.E.; Reinertsen, I.; Jakola, A.S.; Sagberg, L.M.; Berntsen, E.M.; Salvesen, Ø.; Solheim, O. Survival of glioblastoma in relation to tumor location: A statistical tumor atlas of a population-based cohort. *Acta Neurochir.* **2021**, *163*, 1895–1905. [CrossRef]
25. Gilard, V.; Tebani, A.; Dabaj, I.; Laquerrière, A.; Fontanilles, M.; Derrey, S.; Marret, S.; Bekri, S. Diagnosis and Management of Glioblastoma: A Comprehensive Perspective. *J. Pers. Med.* **2021**, *11*, 258. [CrossRef]
26. Rodgers, L.T.; Villano, J.L.; Hartz, A.M.S.; Bauer, B. Glioblastoma Standard of Care: Effects on Tumor Evolution and Reverse Translation in Preclinical Models. *Cancers* **2024**, *16*, 2638. [CrossRef]
27. Stupp, R.; Mason, W.P.; van den Bent, M.J.; Weller, M.; Fisher, B.; Taphoorn, M.J.; Belanger, K.; Brandes, A.A.; Marosi, C.; Bogdahn, U.; et al. Radiotherapy plus concomitant and adjuvant temozolomide for glioblastoma. *N. Engl. J. Med.* **2005**, *352*, 987–996. [CrossRef] [PubMed]
28. Rong, L.; Li, N.; Zhang, Z. Emerging therapies for glioblastoma: Current state and future directions. *J. Exp. Clin. Cancer Res.* **2022**, *41*, 142. [CrossRef] [PubMed]
29. Jezierzański, M.; Nafalska, N.; Stopyra, M.; Furgoł, T.; Miciak, M.; Kabut, J.; Gisterek-Grocholska, I. Temozolomide (TMZ) in the Treatment of Glioblastoma Multiforme—A Literature Review and Clinical Outcomes. *Curr. Oncol.* **2024**, *31*, 3994–4002. [CrossRef] [PubMed]
30. Furtak, J.; Kwiatkowski, A.; Śledzińska, P.; Bebyn, M.; Krajewski, S.; Szylberg, T.; Birski, M.; Druszcz, A.; Krystkiewicz, K.; Gasiński, P.; et al. Survival after reoperation for recurrent glioblastoma multiforme: A prospective study. *Surg. Oncol.* **2022**, *42*, 101771. [CrossRef] [PubMed]
31. González, V.; Brell, M.; Fuster, J.; Moratinos, L.; Alegre, D.; López, S.; Ibáñez, J. Analyzing the role of reoperation in recurrent glioblastoma: A 15-year retrospective study in a single institution. *World J. Surg. Oncol.* **2022**, *20*, 384. [CrossRef] [PubMed]
32. Zhao, Y.-H.; Wang, Z.-F.; Pan, Z.-Y.; Péus, D.; Delgado-Fernandez, J.; Pallud, J.; Li, Z.-Q. A Meta-Analysis of Survival Outcomes Following Reoperation in Recurrent Glioblastoma: Time to Consider the Timing of Reoperation. *Front. Neurol.* **2019**, *10*, 286. [CrossRef] [PubMed]
33. Minniti, G.; Niyazi, M.; Alongi, F.; Navarria, P.; Belka, C. Current status and recent advances in reirradiation of glioblastoma. *Radiat. Oncol.* **2021**, *16*, 36. [CrossRef]
34. Christ, S.M.; Youssef, G.; Tanguturi, S.K.; Cagney, D.; Shi, D.; McFaline-Figueroa, J.R.; Chukwueke, U.; Lee, E.Q.; Hertler, C.; Andratschke, N.; et al. Re-irradiation of recurrent IDH-wildtype glioblastoma in the bevacizumab and immunotherapy era: Target delineation, outcomes and patterns of recurrence. *Clin. Transl. Radiat. Oncol.* **2024**, *44*, 100697. [CrossRef] [PubMed]
35. García-Cabezas, S.; Rivin Del Campo, E.; Solivera-Vela, J.; Palacios-Eito, A. Re-irradiation for high-grade gliomas: Has anything changed? *World J. Clin. Oncol.* **2021**, *12*, 767–786. [CrossRef] [PubMed]
36. Bosio, A.; Cerretti, G.; Padovan, M.; Caccese, M.; Denaro, L.; Chioffi, F.; Della Puppa, A.; Aldegheri, V.; Guarneri, V.; Zagonel, V.; et al. Metronomic Temozolomide in Heavily Pretreated Patients with Recurrent Isocitrate Dehydrogenase Wild-type Glioblastoma: A Large Real-Life Mono-Institutional Study. *Clin. Oncol.* **2023**, *35*, e319–e327. [CrossRef] [PubMed]

37. Brandes, A.A.; Tosoni, A.; Cavallo, G.; Bertorelle, R.; Gioia, V.; Franceschi, E.; Biscuola, M.; Blatt, V.; Crinò, L.; Ermani, M. Temozolomide 3 weeks on and 1 week off as first-line therapy for recurrent glioblastoma: Phase II study from gruppo italiano cooperativo di neuro-oncologia (GICNO). *Br. J. Cancer* **2006**, *95*, 1155–1160. [CrossRef] [PubMed]
38. Franceschi, E.; Lamberti, G.; Visani, M.; Paccapelo, A.; Mura, A.; Tallini, G.; Pession, A.; De Biase, D.; Minichillo, S.; Tosoni, A.; et al. Temozolomide Rechallenge in Recurrent Glioblastoma: When is it Useful? *Future Oncol.* **2018**, *14*, 1063–1069. [CrossRef]
39. Weller, M.; Tabatabai, G.; Kästner, B.; Felsberg, J.; Steinbach, J.P.; Wick, A.; Schnell, O.; Hau, P.; Herrlinger, U.; Sabel, M.C.; et al. MGMT Promoter Methylation Is a Strong Prognostic Biomarker for Benefit from Dose-Intensified Temozolomide Rechallenge in Progressive Glioblastoma: The DIRECTOR Trial. *Clin. Cancer Res.* **2015**, *21*, 2057–2064. [CrossRef] [PubMed]
40. Wick, W.; Steinbach, J.P.; Küker, W.M.; Dichgans, J.; Bamberg, M.; Weller, M. One week on/one week off: A novel active regimen of temozolomide for recurrent glioblastoma. *Neurology* **2004**, *62*, 2113–2115. [CrossRef] [PubMed]
41. Brandes, A.A.; Tosoni, A.; Amistà, P.; Nicolardi, L.; Grosso, D.; Berti, F.; Ermani, M. How effective is BCNU in recurrent glioblastoma in the modern era? A phase II trial. *Neurology* **2004**, *63*, 1281–1284. [CrossRef] [PubMed]
42. Herrlinger, U.; Tzaridis, T.; Mack, F.; Steinbach, J.P.; Schlegel, U.; Sabel, M.; Hau, P.; Kortmann, R.-D.; Krex, D.; Grauer, O.; et al. Lomustine-temozolomide combination therapy versus standard temozolomide therapy in patients with newly diagnosed glioblastoma with methylated *MGMT* promoter (CeTeG/NOA–09): A randomised, open-label, phase 3 trial. *Lancet* **2019**, *393*, 678–688. [CrossRef] [PubMed]
43. Brandes, A.A.; Tosoni, A.; Basso, U.; Reni, M.; Valduga, F.; Monfardini, S.; Amistà, P.; Nicolardi, L.; Sotti, G.; Ermani, M. Second-line chemotherapy with irinotecan plus carmustine in glioblastoma recurrent or progressive after first-line temozolomide chemotherapy: A phase II study of the Gruppo Italiano Cooperativo di Neuro-Oncologia (GICNO). *J. Clin. Oncol.* **2004**, *22*, 4779–4786. [CrossRef] [PubMed]
44. Reithmeier, T.; Graf, E.; Piroth, T.; Trippel, M.; Pinsker, M.O.; Nikkhah, G. BCNU for recurrent glioblastoma multiforme: Efficacy, toxicity and prognostic factors. *BMC Cancer* **2010**, *10*, 30. [CrossRef]
45. You, W.-C.; Lee, H.-D.; Pan, H.-C.; Chen, H.-C. Re-irradiation combined with bevacizumab for recurrent glioblastoma beyond bevacizumab failure: Survival outcomes and prognostic factors. *Sci. Rep.* **2023**, *13*, 9442. [CrossRef]
46. Ameratunga, M.; Pavlakis, N.; Wheeler, H.; Grant, R.; Simes, J.; Khasraw, M. Anti-angiogenic therapy for high-grade glioma. *Cochrane Database Syst. Rev.* **2018**, *11*, CD008218. [CrossRef] [PubMed]
47. Fu, M.; Zhou, Z.; Huang, X.; Chen, Z.; Zhang, L.; Zhang, J.; Hua, W.; Mao, Y. Use of Bevacizumab in recurrent glioblastoma: A scoping review and evidence map. *BMC Cancer* **2023**, *23*, 544. [CrossRef]
48. Ranchor, R.; Ramos, M.J.R.G.D.L.; Romao, R.M.; Mendes, A.S.; Pichel, R.C.; Coelho, J.Q.; Rosendo, E.M.; Magalhaes, M.J.; Araújo, A.M.F. 3P Bevacizumab plus irinotecan as second-line treatment of glioblastoma: Real-world evidence. *ESMO Open* **2023**, *8*, 101015. [CrossRef]
49. Alves, B.; Peixoto, J.; Macedo, S.; Pinheiro, J.; Carvalho, B.; Soares, P.; Lima, J.; Lima, R.T. High VEGFA Expression Is Associated with Improved Progression-Free Survival after Bevacizumab Treatment in Recurrent Glioblastoma. *Cancers* **2023**, *15*, 2196. [CrossRef] [PubMed]
50. Chiesa, S.; Mangraviti, A.; Martini, M.; Cenci, T.; Mazzarella, C.; Gaudino, S.; Bracci, S.; Martino, A.; Della Pepa, G.M.; Offi, M.; et al. Clinical and NGS predictors of response to regorafenib in recurrent glioblastoma. *Sci. Rep.* **2022**, *12*, 16265. [CrossRef] [PubMed]
51. Lombardi, G.; De Salvo, G.L.; Brandes, A.A.; Eoli, M.; Rudà, R.; Faedi, M.; Lolli, I.; Pace, A.; Daniele, B.; Pasqualetti, F.; et al. Regorafenib compared with lomustine in patients with relapsed glioblastoma (REGOMA): A multicentre, open-label, randomised, controlled, phase 2 trial. *Lancet Oncol.* **2019**, *20*, 110–119. [CrossRef]
52. Mongiardi, M.P.; Pallini, R.; D'Alessandris, Q.G.; Levi, A.; Falchetti, M.L. Regorafenib and glioblastoma: A literature review of preclinical studies, molecular mechanisms and clinical effectiveness. *Expert Rev. Mol. Med.* **2024**, *26*, e5. [CrossRef] [PubMed]
53. Pearson, J.R.D.; Regad, T. Targeting cellular pathways in glioblastoma multiforme. *Signal Transduct. Target. Ther.* **2017**, *2*, 17040. [CrossRef] [PubMed]
54. Brar, H.K.; Jose, J.; Wu, Z.; Sharma, M. Tyrosine Kinase Inhibitors for Glioblastoma Multiforme: Challenges and Opportunities for Drug Delivery. *Pharmaceutics* **2022**, *15*, 59. [CrossRef]
55. Rahban, M.; Joushi, S.; Bashiri, H.; Saso, L.; Sheibani, V. Characterization of prevalent tyrosine kinase inhibitors and their challenges in glioblastoma treatment. *Front. Chem.* **2024**, *11*, 1325214. [CrossRef] [PubMed]
56. Arrieta, V.A.; Dmello, C.; McGrail, D.J.; Brat, D.J.; Lee-Chang, C.; Heimberger, A.B.; Chand, D.; Stupp, R.; Sonabend, A.M. Immune checkpoint blockade in glioblastoma: From tumor heterogeneity to personalized treatment. *J. Clin. Investig.* **2023**, *133*, e163447. [CrossRef]
57. Ser, M.H.; Webb, M.J.; Sener, U.; Campian, J.L. Immune Checkpoint Inhibitors and Glioblastoma: A Review on Current State and Future Directions. *J. Immunother. Precis. Oncol.* **2024**, *7*, 97–110. [CrossRef]
58. Wang, H.; Yang, J.; Li, X.; Zhao, H. Current state of immune checkpoints therapy for glioblastoma. *Heliyon* **2024**, *10*, e24729. [CrossRef] [PubMed]

59. Schonfeld, E.; Choi, J.; Tran, A.; Kim, L.H.; Lim, M. The landscape of immune checkpoint inhibitor clinical trials in glioblastoma: A systematic review. *Neurooncol. Adv.* **2024**, *6*, vdae174. [CrossRef] [PubMed]
60. Davis, M.E. Glioblastoma: Overview of Disease and Treatment. *Clin. J. Oncol. Nurs.* **2016**, *20* (Suppl. 5), S2–S8. [CrossRef]
61. Kirson, E.D.; Dbalý, V.; Tovarys, F.; Vymazal, J.; Soustiel, J.F.; Itzhaki, A.; Mordechovich, D.; Steinberg-Shapira, S.; Gurvich, Z.; Schneiderman, R.; et al. Alternating electric fields arrest cell proliferation in animal tumor models and human brain tumors. *Proc. Natl. Acad. Sci. USA* **2007**, *104*, 10152–10157. [CrossRef] [PubMed]
62. Stupp, R.; Taphoorn, M.; Dirven, L.; Taillibert, S.; Honnorat, J.; Chen, T.; Sroubek, J.; Paek, S.H.; Bruna Escuder, J.; Easaw, J.; et al. Tumor Treating Fields (TTFields)—A novel cancer treatment modality: Translating preclinical evidence and engineering into a survival benefit with delayed decline in quality of life. *Ann. Oncol.* **2017**, *28*, v112. [CrossRef]
63. Wang, Y.; Pandey, M.; Ballo, M.T. Integration of Tumor-Treating Fields into the Multidisciplinary Management of Patients with Solid Malignancies. *Oncologist* **2019**, *24*, e1426–e1436. [CrossRef] [PubMed]
64. Tan, A.C.; Ashley, D.M.; López, G.Y.; Malinzak, M.; Friedman, H.S.; Khasraw, M. Management of glioblastoma: State of the art and future directions. *CA Cancer J. Clin.* **2020**, *70*, 299–312. [CrossRef]
65. Chang, C.; Chavarro, V.S.; Gerstl, J.V.E.; Blitz, S.E.; Spanehl, L.; Dubinski, D.; Valdes, P.A.; Tran, L.N.; Gupta, S.; Esposito, L.; et al. Recurrent Glioblastoma—Molecular Underpinnings and Evolving Treatment Paradigms. *Int. J. Mol. Sci.* **2024**, *25*, 6733. [CrossRef]
66. Birzu, C.; French, P.; Caccese, M.; Cerretti, G.; Idbaih, A.; Zagonel, V.; Lombardi, G. Recurrent Glioblastoma: From Molecular Landscape to New Treatment Perspectives. *Cancers* **2020**, *13*, 47. [CrossRef] [PubMed]
67. Carpentier, A.; Stupp, R.; Sonabend, A.M.; Dufour, H.; Chinot, O.; Mathon, B.; Ducray, F.; Guyotat, J.; Baize, N.; Menei, P.; et al. Repeated blood–brain barrier opening with a nine-emitter implantable ultrasound device in combination with carboplatin in recurrent glioblastoma: A phase I/II clinical trial. *Nat. Commun.* **2024**, *15*, 1650. [CrossRef] [PubMed]
68. Ling, A.L.; Solomon, I.H.; Landivar, A.M.; Nakashima, H.; Woods, J.K.; Santos, A.; Masud, N.; Fell, G.; Mo, X.; Yilmaz, A.S.; et al. Clinical trial links oncolytic immunoactivation to survival in glioblastoma. *Nature* **2023**, *623*, 157–166. [CrossRef] [PubMed]
69. Barthel, L.; Hadamitzky, M.; Dammann, P.; Schedlowski, M.; Sure, U.; Thakur, B.K.; Hetze, S. Glioma: Molecular signature and crossroads with tumor microenvironment. *Cancer Metastasis Rev.* **2022**, *41*, 53–75. [CrossRef] [PubMed]
70. Himes, B.T.; Geiger, P.A.; Ayasoufi, K.; Bhargav, A.G.; Brown, D.A.; Parney, I.F. Immunosuppression in Glioblastoma: Current Understanding and Therapeutic Implications. *Front. Oncol.* **2021**, *11*, 770561. [CrossRef] [PubMed]
71. Eisenbarth, D.; Wang, Y.A. Glioblastoma heterogeneity at single cell resolution. *Oncogene* **2023**, *42*, 2155–2165. [CrossRef] [PubMed]
72. Huse, J.T.; Phillips, H.S.; Brennan, C.W. Molecular subclassification of diffuse gliomas: Seeing order in the chaos. *Glia* **2011**, *59*, 1190–1199. [CrossRef]
73. Lin, N.; Yan, W.; Gao, K.; Wang, Y.; Zhang, J.; You, Y. Prevalence and Clinicopathologic Characteristics of the Molecular Subtypes in Malignant Glioma: A Multi-Institutional Analysis of 941 Cases. *PLoS ONE* **2014**, *9*, e94871. [CrossRef]
74. Chen, R.; Smith-Cohn, M.; Cohen, A.L.; Colman, H. Glioma Subclassifications and Their Clinical Significance. *Neurotherapeutics* **2017**, *14*, 284–297. [CrossRef] [PubMed]
75. Rodriguez, S.M.B.; Kamel, A.; Ciubotaru, G.V.; Onose, G.; Sevastre, A.S.; Sfredel, V.; Danoiu, S.; Dricu, A.; Tataranu, L.G. An Overview of EGFR Mechanisms and Their Implications in Targeted Therapies for Glioblastoma. *Int. J. Mol. Sci.* **2023**, *24*, 11110. [CrossRef]
76. Lee, Y.-J.; Seo, H.W.; Baek, J.-H.; Lim, S.H.; Hwang, S.-G.; Kim, E.H. Gene expression profiling of glioblastoma cell lines depending on TP53 status after tumor-treating fields (TTFields) treatment. *Sci. Rep.* **2020**, *10*, 12272. [CrossRef] [PubMed]
77. Brennan, C.W.; Verhaak, R.G.; McKenna, A.; Campos, B.; Noushmehr, H.; Salama, S.R.; Zheng, S.; Chakravarty, D.; Sanborn, J.Z.; Berman, S.H.; et al. The Somatic Genomic Landscape of Glioblastoma. *Cell* **2013**, *155*, 462–477. [CrossRef] [PubMed]
78. Zhang, P.; Xia, Q.; Liu, L.; Li, S.; Dong, L. Current Opinion on Molecular Characterization for GBM Classification in Guiding Clinical Diagnosis, Prognosis, and Therapy. *Front. Mol. Biosci.* **2020**, *7*, 562798. [CrossRef] [PubMed]
79. Behnan, J.; Finocchiaro, G.; Hanna, G. The landscape of the mesenchymal signature in brain tumours. *Brain* **2019**, *142*, 847–866. [CrossRef] [PubMed]
80. Azam, Z.; To, S.-S.T.; Tannous, B.A. Mesenchymal Transformation: The Rosetta Stone of Glioblastoma Pathogenesis and Therapy Resistance. *Adv. Sci.* **2020**, *7*, 2002015. [CrossRef] [PubMed]
81. Neftel, C.; Laffy, J.; Filbin, M.G.; Hara, T.; Shore, M.E.; Rahme, G.J.; Richman, A.R.; Silverbush, D.; Shaw, M.L.; Hebert, C.M.; et al. An Integrative Model of Cellular States, Plasticity, and Genetics for Glioblastoma. *Cell* **2019**, *178*, 835–849.e21. [CrossRef]
82. Couturier, C.P.; Ayyadhury, S.; Le, P.U.; Nadaf, J.; Monlong, J.; Riva, G.; Allache, R.; Baig, S.; Yan, X.; Bourgey, M.; et al. Single-cell RNA-seq reveals that glioblastoma recapitulates a normal neurodevelopmental hierarchy. *Nat. Commun.* **2020**, *11*, 3406. [CrossRef] [PubMed]

83. Nikitin, P.V.; Musina, G.R.; Pekov, S.I.; Kuzin, A.A.; Popov, I.A.; Belyaev, A.Y.; Kobyakov, G.L.; Usachev, D.Y.; Nikolaev, V.N.; Mikhailov, V.P. Cell-Population Dynamics in Diffuse Gliomas during Gliomagenesis and Its Impact on Patient Survival. *Cancers* **2022**, *15*, 145. [CrossRef]
84. Gimple, R.C.; Bhargava, S.; Dixit, D.; Rich, J.N. Glioblastoma stem cells: Lessons from the tumor hierarchy in a lethal cancer. *Genes Dev.* **2019**, *33*, 591–609. [CrossRef] [PubMed]
85. Eckerdt, F.; Platanias, L.C. Emerging Role of Glioma Stem Cells in Mechanisms of Therapy Resistance. *Cancers* **2023**, *15*, 3458. [CrossRef]
86. Almairac, F.; Turchi, L.; Sakakini, N.; Debruyne, D.N.; Elkeurti, S.; Gjernes, E.; Polo, B.; Bianchini, L.; Fontaine, D.; Paquis, P.; et al. ERK-Mediated Loss of miR-199a-3p and Induction of EGR1 Act as a "Toggle Switch" of GBM Cell Dedifferentiation into NANOG- and OCT4-Positive Cells. *Cancer Res.* **2020**, *80*, 3236–3250. [CrossRef] [PubMed]
87. Ma, D.K.; Bonaguidi, M.A.; Ming, G.L.; Song, H. Adult neural stem cells in the mammalian central nervous system. *Cell Res* **2009**, *19*, 672–682. [CrossRef]
88. Eramo, A.; Ricci-Vitiani, L.; Zeuner, A.; Pallini, R.; Lotti, F.; Sette, G.; Pilozzi, E.; Larocca, L.M.; Peschle, C.; De Maria, R. Chemotherapy resistance of glioblastoma stem cells. *Cell Death Differ.* **2006**, *13*, 1238–1241. [CrossRef] [PubMed]
89. Auffinger, B.; Spencer, D.; Pytel, P.; Ahmed, A.U.; Lesniak, M.S. The role of glioma stem cells in chemotherapy resistance and glioblastoma multiforme recurrence. *Expert Rev. Neurother.* **2015**, *15*, 741–752. [CrossRef] [PubMed]
90. Hersh, A.M.; Gaitsch, H.; Alomari, S.; Lubelski, D.; Tyler, B.M. Molecular Pathways and Genomic Landscape of Glioblastoma Stem Cells: Opportunities for Targeted Therapy. *Cancers* **2022**, *14*, 3743. [CrossRef]
91. Crivii, C.-B.; Boșca, A.B.; Melincovici, C.S.; Constantin, A.-M.; Mărginean, M.; Dronca, E.; Suflețel, R.; Gonciar, D.; Bungărdean, M.; Șovrea, A. Glioblastoma Microenvironment and Cellular Interactions. *Cancers* **2022**, *14*, 1092. [CrossRef] [PubMed]
92. Liu, S.; Zhang, C.; Wang, B.; Zhang, H.; Qin, G.; Li, C.; Cao, L.; Gao, Q.; Ping, Y.; Zhang, K.; et al. Regulatory T cells promote glioma cell stemness through TGF-β–NF-κB–IL6–STAT3 signaling. *Cancer Immunol. Immunother.* **2021**, *70*, 2601–2616. [CrossRef] [PubMed]
93. Li, X.; Liu, M.; Zhao, J.; Ren, T.; Yan, X.; Zhang, L.; Wang, X. Research Progress About Glioma Stem Cells in the Immune Microenvironment of Glioma. *Front. Pharmacol.* **2021**, *12*, 750857. [CrossRef]
94. Sharma, P.; Aaroe, A.; Liang, J.; Puduvalli, V.K. Tumor microenvironment in glioblastoma: Current and emerging concepts. *Neurooncol. Adv.* **2023**, *5*, vdad009. [CrossRef] [PubMed]
95. Persico, P.; Lorenzi, E.; Dipasquale, A.; Pessina, F.; Navarria, P.; Politi, L.S.; Santoro, A.; Simonelli, M. Checkpoint Inhibitors as High-Grade Gliomas Treatment: State of the Art and Future Perspectives. *J. Clin. Med.* **2021**, *10*, 1367. [CrossRef]
96. Roesch, S.; Rapp, C.; Dettling, S.; Herold-Mende, C. When Immune Cells Turn Bad-Tumor-Associated Microglia/Macrophages in Glioma. *Int. J. Mol. Sci.* **2018**, *19*, 436. [CrossRef]
97. Mi, Y.; Guo, N.; Luan, J.; Cheng, J.; Hu, Z.; Jiang, P.; Jin, W.; Gao, X. The Emerging Role of Myeloid-Derived Suppressor Cells in the Glioma Immune Suppressive Microenvironment. *Front. Immunol.* **2020**, *11*, 737. [CrossRef]
98. Alban, T.J.; Bayik, D.; Otvos, B.; Rabljenovic, A.; Leng, L.; Jia-Shiun, L.; Roversi, G.; Lauko, A.; Momin, A.A.; Mohammadi, A.M.; et al. Glioblastoma Myeloid-Derived Suppressor Cell Subsets Express Differential Macrophage Migration Inhibitory Factor Receptor Profiles That Can Be Targeted to Reduce Immune Suppression. *Front. Immunol.* **2020**, *11*, 1191. [CrossRef] [PubMed]
99. Veglia, F.; Sanseviero, E.; Gabrilovich, D.I. Myeloid-derived suppressor cells in the era of increasing myeloid cell diversity. *Nat. Rev. Immunol.* **2021**, *21*, 485–498. [CrossRef]
100. Gabrilovich, D.I. Myeloid-Derived Suppressor Cells. *Cancer Immunol. Res.* **2017**, *5*, 3–8. [CrossRef] [PubMed]
101. Fares, J.; Davis, Z.B.; Rechberger, J.S.; Toll, S.A.; Schwartz, J.D.; Daniels, D.J.; Miller, J.S.; Khatua, S. Advances in NK cell therapy for brain tumors. *npj Precis. Oncol.* **2023**, *7*, 17. [CrossRef]
102. Galbo, P.M., Jr.; Madsen, A.T.; Liu, Y.; Peng, M.; Wei, Y.; Ciesielski, M.J.; Fenstermaker, R.A.; Graff, S.; Montagna, C.; Segall, J.E.; et al. Functional Contribution and Clinical Implication of Cancer-Associated Fibroblasts in Glioblastoma. *Clin. Cancer Res.* **2024**, *30*, 865–876. [CrossRef] [PubMed]
103. Zuo, M.; Zhang, S.; Chen, S.; Xiang, Y.; Yuan, Y.; Li, T.; Yang, W.; Wang, Z.; He, Y.; Li, W.; et al. Glioma-associated fibroblasts promote glioblastoma resistance to temozolomide through CCL2-CCR2 paracrine signaling. *bioRxiv* **2024**. [CrossRef]
104. Lootens, T.; Roman, B.I.; Stevens, C.V.; De Wever, O.; Raedt, R. Glioblastoma-Associated Mesenchymal Stem/Stromal Cells and Cancer-Associated Fibroblasts: Partners in Crime? *Int. J. Mol. Sci.* **2024**, *25*, 2285. [CrossRef] [PubMed]
105. Zhang, C.; Fei, Y.; Wang, H.; Hu, S.; Liu, C.; Hu, R.; Du, Q. CAFs orchestrates tumor immune microenvironment—A new target in cancer therapy? *Front. Pharmacol.* **2023**, *14*, 1113378. [CrossRef] [PubMed]
106. Randles, A.; Wirsching, H.G.; Dean, J.A.; Cheng, Y.K.; Emerson, S.; Pattwell, S.S.; Holland, E.C.; Michor, F. Computational modelling of perivascular-niche dynamics for the optimization of treatment schedules for glioblastoma. *Nat. Biomed. Eng.* **2021**, *5*, 346–359. [CrossRef] [PubMed]
107. Ahir, B.K.; Engelhard, H.H.; Lakka, S.S. Tumor Development and Angiogenesis in Adult Brain Tumor: Glioblastoma. *Mol. Neurobiol.* **2020**, *57*, 2461–2478. [CrossRef]

108. Hovis, G.; Chandra, N.; Kejriwal, N.; Hsieh, K.J.; Chu, A.; Yang, I.; Wadehra, M. Understanding the Role of Endothelial Cells in Glioblastoma: Mechanisms and Novel Treatments. *Int. J. Mol. Sci.* **2024**, *25*, 6118. [CrossRef] [PubMed]
109. Pacheco, C.; Martins, C.; Monteiro, J.; Baltazar, F.; Costa, B.M.; Sarmento, B. Glioblastoma Vasculature: From its Critical Role in Tumor Survival to Relevant in Vitro Modelling. *Front. Drug Deliv.* **2022**, *2*, 823412. [CrossRef]
110. Maddison, K.; Bowden, N.A.; Graves, M.C.; Tooney, P.A. Characteristics of vasculogenic mimicry and tumour to endothelial transdifferentiation in human glioblastoma: A systematic review. *BMC Cancer* **2023**, *23*, 185. [CrossRef] [PubMed]
111. Zhu, T.S.; Costello, M.A.; Talsma, C.E.; Flack, C.G.; Crowley, J.G.; Hamm, L.L.; He, X.; Hervey-Jumper, S.L.; Heth, J.A.; Muraszko, K.M.; et al. Endothelial Cells Create a Stem Cell Niche in Glioblastoma by Providing NOTCH Ligands That Nurture Self-Renewal of Cancer Stem-Like Cells. *Cancer Res.* **2011**, *71*, 6061–6072. [CrossRef] [PubMed]
112. Lam, D.; Enright, H.A.; Cadena, J.; Peters, S.K.G.; Sales, A.P.; Osburn, J.J.; Soscia, D.A.; Kulp, K.S.; Wheeler, E.K.; Fischer, N.O. Tissue-specific extracellular matrix accelerates the formation of neural networks and communities in a neuron-glia co-culture on a multi-electrode array. *Sci. Rep.* **2019**, *9*, 4159. [CrossRef] [PubMed]
113. Lau, L.W.; Cua, R.; Keough, M.B.; Haylock-Jacobs, S.; Yong, V.W. Pathophysiology of the brain extracellular matrix: A new target for remyelination. *Nat. Rev. Neurosci.* **2013**, *14*, 722–729. [CrossRef] [PubMed]
114. Marino, S.; Menna, G.; Di Bonaventura, R.; Lisi, L.; Mattogno, P.; Figà, F.; Bilgin, L.; D'Alessandris, Q.G.; Olivi, A.; Della Pepa, G.M. The Extracellular Matrix in Glioblastomas: A Glance at Its Structural Modifications in Shaping the Tumoral Microenvironment-A Systematic Review. *Cancers* **2023**, *15*, 1879. [CrossRef]
115. Safarians, G.; Sohrabi, A.; Solomon, I.; Xiao, W.; Bastola, S.; Rajput, B.W.; Epperson, M.; Rosenzweig, I.; Tamura, K.; Singer, B.; et al. Glioblastoma Spheroid Invasion through Soft, Brain-Like Matrices Depends on Hyaluronic Acid–CD44 Interactions. *Adv. Healthc. Mater.* **2023**, *12*, 2203143. [CrossRef] [PubMed]
116. Serres, E.; Debarbieux, F.; Stanchi, F.; Maggiorella, L.; Grall, D.; Turchi, L.; Burel-Vandenbos, F.; Figarella-Branger, D.; Virolle, T.; Rougon, G.; et al. Fibronectin expression in glioblastomas promotes cell cohesion, collective invasion of basement membrane in vitro and orthotopic tumor growth in mice. *Oncogene* **2014**, *33*, 3451–3462. [CrossRef] [PubMed]
117. Wang, C.; Sinha, S.; Jiang, X.; Murphy, L.; Fitch, S.; Wilson, C.; Grant, G.; Yang, F. Matrix Stiffness Modulates Patient-Derived Glioblastoma Cell Fates in Three-Dimensional Hydrogels. *Tissue Eng. Part A* **2021**, *27*, 390–401. [CrossRef] [PubMed]
118. Erices, J.I.; Bizama, C.; Niechi, I.; Uribe, D.; Rosales, A.; Fabres, K.; Navarro-Martínez, G.; Torres, Á.; San Martín, R.; Roa, J.C.; et al. Glioblastoma Microenvironment and Invasiveness: New Insights and Therapeutic Targets. *Int. J. Mol. Sci.* **2023**, *24*, 7047. [CrossRef]
119. Belousov, A.; Titov, S.; Shved, N.; Garbuz, M.; Malykin, G.; Gulaia, V.; Kagansky, A.; Kumeiko, V. The Extracellular Matrix and Biocompatible Materials in Glioblastoma Treatment. *Front. Bioeng. Biotechnol.* **2019**, *7*, 341. [CrossRef]
120. Gupta, R.K.; Niklasson, M.; Bergström, T.; Segerman, A.; Betsholtz, C.; Westermark, B. Tumor-specific migration routes of xenotransplanted human glioblastoma cells in mouse brain. *Sci. Rep.* **2024**, *14*, 864. [CrossRef] [PubMed]
121. Sood, D.; Tang-Schomer, M.; Pouli, D.; Mizzoni, C.; Raia, N.; Tai, A.; Arkun, K.; Wu, J.; Black, L.D., III; Scheffler, B.; et al. 3D extracellular matrix microenvironment in bioengineered tissue models of primary pediatric and adult brain tumors. *Nat. Commun.* **2019**, *10*, 4529. [CrossRef] [PubMed]
122. Ganguly, K.; Adhikary, K.; Acharjee, A.; Acharjee, P.; Trigun, S.K.; Mutlaq, A.S.; Ashique, S.; Yasmin, S.; Alshahrani, A.M.; Ansari, M.Y. Biological significance and pathophysiological role of Matrix Metalloproteinases in the Central Nervous System. *Int. J. Biol. Macromol.* **2024**, *280*, 135967. [CrossRef]
123. Wu, D.; Chen, Q.; Chen, X.; Han, F.; Chen, Z.; Wang, Y. The blood–brain barrier: Structure, regulation and drug delivery. *Signal Transduct. Target. Ther.* **2023**, *8*, 217. [CrossRef] [PubMed]
124. Mărginean, L.; Ștefan, P.A.; Lebovici, A.; Opincariu, I.; Csutak, C.; Lupean, R.A.; Coroian, P.A.; Suciu, B.A. CT in the Differentiation of Gliomas from Brain Metastases: The Radiomics Analysis of the Peritumoral Zone. *Brain Sci.* **2022**, *12*, 109. [CrossRef]
125. Manzarbeitia-Arroba, B.; Hodolic, M.; Pichler, R.; Osipova, O.; Soriano-Castrejón, Á.M.; García-Vicente, A.M. ^{18}F-Fluoroethyl-L Tyrosine Positron Emission Tomography Radiomics in the Differentiation of Treatment-Related Changes from Disease Progression in Patients with Glioblastoma. *Cancers* **2024**, *16*, 195. [CrossRef] [PubMed]
126. Yusuf, A.; Almotairy, A.R.Z.; Henidi, H.; Alshehri, O.Y.; Aldughaim, M.S. Nanoparticles as Drug Delivery Systems: A Review of the Implication of Nanoparticles' Physicochemical Properties on Responses in Biological Systems. *Polymers* **2023**, *15*, 1596. [CrossRef] [PubMed]
127. Yu, W.; Liu, R.; Zhou, Y.; Gao, H. Size-Tunable Strategies for a Tumor Targeted Drug Delivery System. *ACS Cent. Sci.* **2020**, *6*, 100–116. [CrossRef] [PubMed]
128. Ruiz-Molina, D.; Mao, X.; Alfonso-Triguero, P.; Lorenzo, J.; Bruna, J.; Yuste, V.J.; Candiota, A.P.; Novio, F. Advances in Preclinical/Clinical Glioblastoma Treatment: Can Nanoparticles Be of Help? *Cancers* **2022**, *14*, 4960. [CrossRef]
129. Lai, G.; Wu, H.; Yang, K.; Hu, K.; Zhou, Y.; Chen, X.; Fu, F.; Li, J.; Xie, G.; Wang, H.-F.; et al. Progress of nanoparticle drug delivery system for the treatment of glioma. *Front. Bioeng. Biotechnol.* **2024**, *12*, 1403511. [CrossRef] [PubMed]

130. Fabel, K.; Dietrich, J.; Hau, P.; Wismeth, C.; Winner, B.; Przywara, S.; Steinbrecher, A.; Ullrich, W.; Bogdahn, U. Long-term stabilization in patients with malignant glioma after treatment with liposomal doxorubicin. *Cancer* **2001**, *92*, 1936–1942. [CrossRef] [PubMed]
131. Chua, S.L.; Rosenthal, M.A.; Wong, S.S.; Ashley, D.M.; Woods, A.M.; Dowling, A.; Cher, L.M. Phase 2 study of temozolomide and Caelyx in patients with recurrent glioblastoma multiforme. *Neuro-Oncology* **2004**, *6*, 38–43. [CrossRef]
132. Hau, P.; Fabel, K.; Baumgart, U.; Rümmele, P.; Grauer, O.; Bock, A.; Dietmaier, C.; Dietmaier, W.; Dietrich, J.; Dudel, C.; et al. Pegylated liposomal doxorubicin-efficacy in patients with recurrent high-grade glioma. *Cancer* **2004**, *100*, 1199–1207. [CrossRef] [PubMed]
133. Beier, C.P.; Schmid, C.; Gorlia, T.; Kleinletzenberger, C.; Beier, D.; Grauer, O.; Steinbrecher, A.; Hirschmann, B.; Brawanski, A.; Dietmaier, C.; et al. RNOP-09: Pegylated liposomal doxorubicine and prolonged temozolomide in addition to radiotherapy in newly diagnosed glioblastoma—A phase II study. *BMC Cancer* **2009**, *9*, 308. [CrossRef] [PubMed]
134. Ananda, S.; Nowak, A.K.; Cher, L.; Dowling, A.; Brown, C.; Simes, J.; Rosenthal, M.A. Phase 2 trial of temozolomide and pegylated liposomal doxorubicin in the treatment of patients with glioblastoma multiforme following concurrent radiotherapy and chemotherapy. *J. Clin. Neurosci.* **2011**, *18*, 1444–1448. [CrossRef] [PubMed]
135. Clarke, J.L.; Molinaro, A.M.; DeSilva, A.A.; Rabbitt, J.E.; Drummond, D.C.; Chang, S.M.; Butowski, N.A.; Prados, M. A phase I trial of intravenous liposomal irinotecan in patients with recurrent high-grade gliomas. *J. Clin. Oncol.* **2015**, *33* (Suppl. 15), 2029. [CrossRef]
136. Elinzano, H.; Toms, S.; Robison, J.; Mohler, A.; Carcieri, A.; Cielo, D.; Donnelly, J.; Disano, D.; Vatketich, J.; Baekey, J.; et al. Nanoliposomal Irinotecan and Metronomic Temozolomide for Patients with Recurrent Glioblastoma: BrUOG329, A Phase I Brown University Oncology Research Group Trial. *Am. J. Clin. Oncol.* **2021**, *44*, 49–52. [CrossRef] [PubMed]
137. Roque, D.; Cruz, N.; Ferreira, H.A.; Reis, C.P.; Matela, N.; Herculano-Carvalho, M.; Cascão, R.; Faria, C.C. Nanoparticle-Based Treatment in Glioblastoma. *J. Pers. Med.* **2023**, *13*, 1328. [CrossRef]
138. Horta, M.; Soares, P.; Sarmento, B.; Leite Pereira, C.; Lima, R.T. Nanostructured lipid carriers for enhanced batimastat delivery across the blood–brain barrier: An in vitro study for glioblastoma treatment. *Drug Deliv. Transl. Res.* **2025**. *online ahead of print*. [CrossRef]
139. Gu, G.; Xia, H.; Hu, Q.; Liu, Z.; Jiang, M.; Kang, T.; Miao, D.; Tu, Y.; Pang, Z.; Song, Q.; et al. PEG-co-PCL nanoparticles modified with MMP-2/9 activatable low molecular weight protamine for enhanced targeted glioblastoma therapy. *Biomaterials* **2013**, *34*, 196–208. [CrossRef]
140. Xu, X.; Wu, Y.; Qian, X.; Wang, Y.; Wang, J.; Li, J.; Li, Y.; Zhang, Z. Nanomedicine Strategies to Circumvent Intratumor Extracellular Matrix Barriers for Cancer Therapy. *Adv. Healthc. Mater.* **2022**, *11*, 2101428. [CrossRef] [PubMed]
141. Mohiuddin, E.; Wakimoto, H. Extracellular matrix in glioblastoma: Opportunities for emerging therapeutic approaches. *Am. J. Cancer Res.* **2021**, *11*, 3742–3754.
142. Mai, Z.; Lin, Y.; Lin, P.; Zhao, X.; Cui, L. Modulating extracellular matrix stiffness: A strategic approach to boost cancer immunotherapy. *Cell Death Dis.* **2024**, *15*, 307. [CrossRef]
143. Saw, P.E.; Zhang, A.; Nie, Y.; Zhang, L.; Xu, Y.; Xu, X. Tumor-Associated Fibronectin Targeted Liposomal Nanoplatform for Cyclophilin A siRNA Delivery and Targeted Malignant Glioblastoma Therapy. *Front. Pharmacol.* **2018**, *9*, 1194. [CrossRef] [PubMed]
144. Chung, E.J.; Cheng, Y.; Morshed, R.; Nord, K.; Han, Y.; Wegscheid, M.L.; Auffinger, B.; Wainwright, D.A.; Lesniak, M.S.; Tirrell, M.V. Fibrin-binding, peptide amphiphile micelles for targeting glioblastoma. *Biomaterials* **2014**, *35*, 1249–1256. [CrossRef] [PubMed]
145. Kang, T.; Zhu, Q.; Jiang, D.; Feng, X.; Feng, J.; Jiang, T.; Yao, J.; Jing, Y.; Song, Q.; Jiang, X.; et al. Synergistic targeting tenascin C and neuropilin-1 for specific penetration of nanoparticles for anti-glioblastoma treatment. *Biomaterials* **2016**, *101*, 60–75. [CrossRef]
146. Lingasamy, P.; Tobi, A.; Kurm, K.; Kopanchuk, S.; Sudakov, A.; Salumäe, M.; Rätsep, T.; Asser, T.; Bjerkvig, R.; Teesalu, T. Tumor-penetrating peptide for systemic targeting of Tenascin-C. *Sci. Rep.* **2020**, *10*, 5809. [CrossRef] [PubMed]
147. Lingasamy, P.; Põšnograjeva, K.; Kopanchuk, S.; Tobi, A.; Rinken, A.; General, I.J.; Asciutto, E.K.; Teesalu, T. PL1 Peptide Engages Acidic Surfaces on Tumor-Associated Fibronectin and Tenascin Isoforms to Trigger Cellular Uptake. *Pharmaceutics* **2021**, *13*, 1998. [CrossRef] [PubMed]
148. Kasten, B.B.; Jiang, K.; Cole, D.; Jani, A.; Udayakumar, N.; Gillespie, G.Y.; Lu, G.; Dai, T.; Rosenthal, E.L.; Markert, J.M.; et al. Targeting MMP-14 for dual PET and fluorescence imaging of glioma in preclinical models. *Eur. J. Nucl. Med. Mol. Imaging* **2020**, *47*, 1412–1426. [CrossRef] [PubMed]
149. Abakumov, M.A.; Nukolova, N.V.; Sokolsky-Papkov, M.; Shein, S.A.; Sandalova, T.O.; Vishwasrao, H.M.; Grinenko, N.F.; Gubsky, I.L.; Abakumov, A.M.; Kabanov, A.V.; et al. VEGF-targeted magnetic nanoparticles for MRI visualization of brain tumor. *Nanomed. Nanotechnol. Biol. Med.* **2015**, *11*, 825–833. [CrossRef]

150. Mohanty, S.; Chen, Z.; Li, K.; Morais, G.R.; Klockow, J.; Yerneni, K.; Pisani, L.; Chin, F.T.; Mitra, S.; Cheshier, S.; et al. A Novel Theranostic Strategy for MMP-14-Expressing Glioblastomas Impacts Survival. *Mol. Cancer Ther.* **2017**, *16*, 1909–1921. [CrossRef] [PubMed]
151. Fan, R.; Chen, C.; Mu, M.; Chuan, D.; Liu, H.; Hou, H.; Huang, J.; Tong, A.; Guo, G.; Xu, J. Engineering MMP-2 Activated Nanoparticles Carrying B7-H3 Bispecific Antibodies for Ferroptosis-Enhanced Glioblastoma Immunotherapy. *ACS Nano* **2023**, *17*, 9126–9139. [CrossRef]
152. Zhao, Y.; Ren, W.; Zhong, T.; Zhang, S.; Huang, D.; Guo, Y.; Yao, X.; Wang, C.; Zhang, W.-Q.; Zhang, X.; et al. Tumor-specific pH-responsive peptide-modified pH-sensitive liposomes containing doxorubicin for enhancing glioma targeting and anti-tumor activity. *J. Control. Release* **2016**, *222*, 56–66. [CrossRef]
153. Sathiyaseelan, A.; Saravanakumar, K.; Mariadoss, A.V.A.; Wang, M.-H. pH-controlled nucleolin targeted release of dual drug from chitosan-gold based aptamer functionalized nano drug delivery system for improved glioblastoma treatment. *Carbohydr. Polym.* **2021**, *262*, 117907. [CrossRef]
154. Martins, C.; Araujo, M.; Malfanti, A.; Pacheco, C.; Smith, S.J.; Ucakar, B.; Rahman, R.; Aylott, J.W.; Preat, V.; Sarmento, B. Stimuli-Responsive Multifunctional Nanomedicine for Enhanced Glioblastoma Chemotherapy Augments Multistage Blood-to-Brain Trafficking and Tumor Targeting. *Small* **2023**, *19*, e2300029. [CrossRef] [PubMed]
155. Qi, J.; Zhang, L.; Ren, Z.; Yuan, Y.; Yu, J.; Zhang, Y.; Gu, L.; Wang, X.; Wang, Y.; Xu, H.; et al. Stepwise-targeting and hypoxia-responsive liposome AMVY@NPs carrying siYAP and verteporfin for glioblastoma therapy. *J. Nanobiotechnol.* **2024**, *22*, 495. [CrossRef]
156. Yang, G.; Xu, L.; Chao, Y.; Xu, J.; Sun, X.; Wu, Y.; Peng, R.; Liu, Z. Hollow MnO2 as a tumor-microenvironment-responsive biodegradable nano-platform for combination therapy favoring antitumor immune responses. *Nat. Commun.* **2017**, *8*, 902. [CrossRef]
157. Tian, C.; Asghar, S.; Xu, Y.; Chen, Z.; Zhang, M.; Huang, L.; Ye, J.; Ping, Q.; Xiao, Y. The effect of the molecular weight of hyaluronic acid on the physicochemical characterization of hyaluronic acid-curcumin conjugates and in vitro evaluation in glioma cells. *Colloids Surf. B Biointerfaces* **2018**, *165*, 45–55. [CrossRef]
158. Kiyokawa, J.; Kawamura, Y.; Ghouse, S.M.; Acar, S.; Barçın, E.; Martínez-Quintanilla, J.; Martuza, R.L.; Alemany, R.; Rabkin, S.D.; Shah, K.; et al. Modification of Extracellular Matrix Enhances Oncolytic Adenovirus Immunotherapy in Glioblastoma. *Clin. Cancer Res.* **2021**, *27*, 889–902. [CrossRef] [PubMed]
159. Shukla, M.K.; Behera, C.; Chakraborty, S.; Sandha, K.K.; Goswami, A.; Gupta, P.N. Tumor micro-environment targeted collagenase-modified albumin nanoparticles for improved drug delivery. *J. Drug Deliv. Sci. Technol.* **2022**, *71*, 103366. [CrossRef]
160. Agarwal, S.; Mohamed, M.S.; Mizuki, T.; Maekawa, T.; Sakthi Kumar, D. Chlorotoxin modified morusin–PLGA nanoparticles for targeted glioblastoma therapy. *J. Mater. Chem. B* **2019**, *7*, 5896–5919. [CrossRef] [PubMed]
161. Islam, Y.; Khalid, A.; Pluchino, S.; Sivakumaran, M.; Teixidò, M.; Leach, A.; Fatokun, A.A.; Downing, J.; Coxon, C.; Ehtezazi, T. Development of Brain Targeting Peptide Based MMP-9 Inhibiting Nanoparticles for the Treatment of Brain Diseases with Elevated MMP-9 Activity. *J. Pharm. Sci.* **2020**, *109*, 3134–3144. [CrossRef]
162. Ventura, E.; Weller, M.; Macnair, W.; Eschbach, K.; Beisel, C.; Cordazzo, C.; Claassen, M.; Zardi, L.; Burghardt, I. TGF-β induces oncofetal fibronectin that, in turn, modulates TGF-β superfamily signaling in endothelial cells. *J. Cell Sci.* **2018**, *131*, jcs209619. [CrossRef]
163. Lui, B.G.; Salomon, N.; Wüstehube-Lausch, J.; Daneschdar, M.; Schmoldt, H.-U.; Türeci, Ö.; Sahin, U. Targeting the tumor vasculature with engineered cystine-knot miniproteins. *Nat. Commun.* **2020**, *11*, 295. [CrossRef]
164. Spaeth, N.; Wyss, M.T.; Pahnke, J.; Biollaz, G.; Trachsel, E.; Drandarov, K.; Treyer, V.; Weber, B.; Neri, D.; Buck, A. Radioimmunotherapy targeting the extra domain B of fibronectin in C6 rat gliomas: A preliminary study about the therapeutic efficacy of iodine-131-labeled SIP(L19). *Nucl. Med. Biol.* **2006**, *33*, 661–666. [CrossRef] [PubMed]
165. Dzikowski, L.; Mirzaei, R.; Sarkar, S.; Kumar, M.; Bose, P.; Bellail, A.; Hao, C.; Yong, V.W. Fibrinogen in the glioblastoma microenvironment contributes to the invasiveness of brain tumor-initiating cells. *Brain Pathol.* **2021**, *31*, e12947. [CrossRef]
166. Zhang, N.; Ru, B.; Hu, J.; Xu, L.; Wan, Q.; Liu, W.; Cai, W.; Zhu, T.; Ji, Z.; Guo, R.; et al. Recent advances of CREKA peptide-based nanoplatforms in biomedical applications. *J. Nanobiotechnol.* **2023**, *21*, 77. [CrossRef] [PubMed]
167. Brack, S.S.; Silacci, M.; Birchler, M.; Neri, D. Tumor-Targeting Properties of Novel Antibodies Specific to the Large Isoform of Tenascin-C. *Clin. Cancer Res.* **2006**, *12*, 3200–3208. [CrossRef] [PubMed]
168. Zhou, W.; Yu, X.; Sun, S.; Zhang, X.; Yang, W.; Zhang, J.; Zhang, X.; Jiang, Z. Increased expression of MMP-2 and MMP-9 indicates poor prognosis in glioma recurrence. *Biomed. Pharmacother.* **2019**, *118*, 109369. [CrossRef] [PubMed]
169. de Almeida, L.G.N.; Thode, H.; Eslambolchi, Y.; Chopra, S.; Young, D.; Gill, S.; Devel, L.; Dufour, A. Matrix Metalloproteinases: From Molecular Mechanisms to Physiology, Pathophysiology, and Pharmacology. *Pharmacol. Rev.* **2022**, *74*, 714–770. [CrossRef] [PubMed]
170. Ramachandran, R.K.; Sorensen, M.D.; Aaberg-Jessen, C.; Hermansen, S.K.; Kristensen, B.W. Expression and prognostic impact of matrix metalloproteinase-2 (MMP-2) in astrocytomas. *PLoS ONE* **2017**, *12*, e0172234. [CrossRef] [PubMed]

171. Xue, Q.; Cao, L.; Chen, X.Y.; Zhao, J.; Gao, L.; Li, S.Z.; Fei, Z. High expression of MMP9 in glioma affects cell proliferation and is associated with patient survival rates. *Oncol. Lett.* **2017**, *13*, 1325–1330. [CrossRef] [PubMed]
172. Rao, J.S. Molecular mechanisms of glioma invasiveness: The role of proteases. *Nat. Rev. Cancer* **2003**, *3*, 489–501. [CrossRef] [PubMed]
173. Conlon, G.A.; Murray, G.I. Recent advances in understanding the roles of matrix metalloproteinases in tumour invasion and metastasis. *J. Pathol.* **2019**, *247*, 629–640. [CrossRef]
174. Munaut, C.; Noel, A.; Hougrand, O.; Foidart, J.M.; Boniver, J.; Deprez, M. Vascular endothelial growth factor expression correlates with matrix metalloproteinases MT1-MMP, MMP-2 and MMP-9 in human glioblastomas. *Int. J. Cancer* **2003**, *106*, 848–855. [CrossRef]
175. Ulasov, I.; Yi, R.; Guo, D.; Sarvaiya, P.; Cobbs, C. The emerging role of MMP14 in brain tumorigenesis and future therapeutics. *Biochim. Biophys. Acta (BBA) Rev. Cancer* **2014**, *1846*, 113–120. [CrossRef]
176. Niland, S.; Riscanevo, A.X.; Eble, J.A. Matrix Metalloproteinases Shape the Tumor Microenvironment in Cancer Progression. *Int. J. Mol. Sci.* **2021**, *23*, 146. [CrossRef]
177. Hatoum, A.; Mohammed, R.; Zakieh, O. The unique invasiveness of glioblastoma and possible drug targets on extracellular matrix. *Cancer Manag. Res.* **2019**, *11*, 1843–1855. [CrossRef] [PubMed]
178. Zhang, A.B.; Mozaffari, K.; Aguirre, B.; Li, V.; Kubba, R.; Desai, N.C.; Wei, D.; Yang, I.; Wadehra, M. Exploring the Past, Present, and Future of Anti-Angiogenic Therapy in Glioblastoma. *Cancers* **2023**, *15*, 830. [CrossRef] [PubMed]
179. Codrici, E.; Enciu, A.-M.; Popescu, I.-D.; Mihai, S.; Tanase, C. Glioma Stem Cells and Their Microenvironments: Providers of Challenging Therapeutic Targets. *Stem Cells Int.* **2016**, *2016*, 5728438. [CrossRef]
180. Reardon, D.A.; Turner, S.; Peters, K.B.; Desjardins, A.; Gururangan, S.; Sampson, J.H.; McLendon, R.E.; Herndon, J.E., II; Jones, L.W.; Kirkpatrick, J.P.; et al. A review of VEGF/VEGFR-targeted therapeutics for recurrent glioblastoma. *J. Natl. Compr. Cancer Netw.* **2011**, *9*, 414–427. [CrossRef]
181. Wu, Z.; Dai, L.; Tang, K.; Ma, Y.; Song, B.; Zhang, Y.; Li, J.; Lui, S.; Gong, Q.; Wu, M. Advances in magnetic resonance imaging contrast agents for glioblastoma-targeting theranostics. *Regen. Biomater.* **2021**, *8*, rbab062. [CrossRef] [PubMed]
182. Karamanos, N.K.; Theocharis, A.D.; Piperigkou, Z.; Manou, D.; Passi, A.; Skandalis, S.S.; Vynios, D.H.; Orian-Rousseau, V.; Ricard-Blum, S.; Schmelzer, C.E.H.; et al. A guide to the composition and functions of the extracellular matrix. *FEBS J.* **2021**, *288*, 6850–6912. [CrossRef] [PubMed]
183. Hogan, K.J.; Perez, M.R.; Mikos, A.G. Extracellular matrix component-derived nanoparticles for drug delivery and tissue engineering. *J. Control. Release* **2023**, *360*, 888–912. [CrossRef] [PubMed]
184. Karimi, N.; Kheiri, H.; Zarrinpour, V.; Forghanifard, M.M. Bioinformatic analysis of MMP family members in GBM. *Inform. Med. Unlocked* **2023**, *39*, 101240. [CrossRef]
185. Talib, W.H.; Awajan, D.; Alqudah, A.; Alsawwaf, R.; Althunibat, R.; Abu AlRoos, M.; Al Safadi, A.a.; Abu Asab, S.; Hadi, R.W.; Al Kury, L.T. Targeting Cancer Hallmarks with Epigallocatechin Gallate (EGCG): Mechanistic Basis and Therapeutic Targets. *Molecules* **2024**, *29*, 1373. [CrossRef] [PubMed]
186. Bogdanov, A.; Bogdanov, A.; Chubenko, V.; Volkov, N.; Moiseenko, F.; Moiseyenko, V. Tumor acidity: From hallmark of cancer to target of treatment. *Front. Oncol.* **2022**, *12*, 979154. [CrossRef] [PubMed]
187. Chen, Z.; Han, F.; Du, Y.; Shi, H.; Zhou, W. Hypoxic microenvironment in cancer: Molecular mechanisms and therapeutic interventions. *Signal Transduct. Target. Ther.* **2023**, *8*, 70. [CrossRef]
188. Park, J.H.; Lee, H.K. Current Understanding of Hypoxia in Glioblastoma Multiforme and Its Response to Immunotherapy. *Cancers* **2022**, *14*, 1176. [CrossRef]
189. Kuo, C.-L.; Ponneri Babuharisankar, A.; Lin, Y.-C.; Lien, H.-W.; Lo, Y.K.; Chou, H.-Y.; Tangeda, V.; Cheng, L.-C.; Cheng, A.N.; Lee, A.Y.-L. Mitochondrial oxidative stress in the tumor microenvironment and cancer immunoescape: Foe or friend? *J. Biomed. Sci.* **2022**, *29*, 74. [CrossRef]
190. Aggarwal, V.; Tuli, H.S.; Varol, A.; Thakral, F.; Yerer, M.B.; Sak, K.; Varol, M.; Jain, A.; Khan, M.A.; Sethi, G. Role of Reactive Oxygen Species in Cancer Progression: Molecular Mechanisms and Recent Advancements. *Biomolecules* **2019**, *9*, 735. [CrossRef]
191. Olivier, C.; Oliver, L.; Lalier, L.; Vallette, F.M. Drug Resistance in Glioblastoma: The Two Faces of Oxidative Stress. *Front. Mol. Biosci.* **2020**, *7*, 620677. [CrossRef] [PubMed]
192. Ma, W.; Wang, X.; Zhang, D.; Mu, X. Research Progress of Disulfide Bond Based Tumor Microenvironment Targeted Drug Delivery System. *Int. J. Nanomed.* **2024**, *19*, 7547–7566. [CrossRef] [PubMed]
193. Li, J.; Huo, M.; Wang, J.; Zhou, J.; Mohammad, J.M.; Zhang, Y.; Zhu, Q.; Waddad, A.Y.; Zhang, Q. Redox-sensitive micelles self-assembled from amphiphilic hyaluronic acid-deoxycholic acid conjugates for targeted intracellular delivery of paclitaxel. *Biomaterials* **2012**, *33*, 2310–2320. [CrossRef]
194. Henke, E.; Nandigama, R.; Ergün, S. Extracellular Matrix in the Tumor Microenvironment and Its Impact on Cancer Therapy. *Front. Mol. Biosci.* **2020**, *6*, 160. [CrossRef]

195. Abyaneh, H.S.; Regenold, M.; McKee, T.D.; Allen, C.; Gauthier, M.A. Towards extracellular matrix normalization for improved treatment of solid tumors. *Theranostics* **2020**, *10*, 1960–1980. [CrossRef] [PubMed]
196. Zhou, Y.; Chen, X.; Cao, J.; Gao, H. Overcoming the biological barriers in the tumor microenvironment for improving drug delivery and efficacy. *J. Mater. Chem. B* **2020**, *8*, 6765–6781. [CrossRef]
197. Parsons, S.L.; Watson, S.A.; Steele, R.J. Phase I/II trial of batimastat, a matrix metalloproteinase inhibitor, in patients with malignant ascites. *Eur. J. Surg. Oncol.* **1997**, *23*, 526–531. [CrossRef]
198. Groves, M.D.; Puduvalli, V.K.; Hess, K.R.; Jaeckle, K.A.; Peterson, P.; Yung, W.K.; Levin, V.A. Phase II trial of temozolomide plus the matrix metalloproteinase inhibitor, marimastat, in recurrent and progressive glioblastoma multiforme. *J. Clin. Oncol.* **2002**, *20*, 1383–1388. [CrossRef]
199. Boguszewska-Czubara, A.; Budzynska, B.; Skalicka-Wozniak, K.; Kurzepa, J. Perspectives and New Aspects of Metalloproteinases' Inhibitors in the Therapy of CNS Disorders: From Chemistry to Medicine. *Curr. Med. Chem.* **2019**, *26*, 3208–3224. [CrossRef] [PubMed]
200. Cathcart, J.; Pulkoski-Gross, A.; Cao, J. Targeting Matrix Metalloproteinases in Cancer: Bringing New Life to Old Ideas. *Genes Dis.* **2015**, *2*, 26–34. [CrossRef]
201. Sehedic, D.; Chourpa, I.; Tetaud, C.; Griveau, A.; Loussouarn, C.; Avril, S.; Legendre, C.; Lepareur, N.; Wion, D.; Hindre, F.; et al. Locoregional Confinement and Major Clinical Benefit of ^{188}Re-Loaded CXCR4-Targeted Nanocarriers in an Orthotopic Human to Mouse Model of Glioblastoma. *Theranostics* **2017**, *7*, 4517–4536. [CrossRef] [PubMed]
202. Fields, G.B. Mechanisms of Action of Novel Drugs Targeting Angiogenesis-Promoting Matrix Metalloproteinases. *Front. Immunol.* **2019**, *10*, 1278. [CrossRef] [PubMed]
203. Farkas, S.; Cioca, D.; Murányi, J.; Hornyák, P.; Brunyánszki, A.; Szekér, P.; Boros, E.; Horváth, P.; Hujber, Z.; Rácz, G.Z.; et al. Chlorotoxin binds to both matrix metalloproteinase 2 and neuropilin 1. *J. Biol. Chem.* **2023**, *299*, 104998. [CrossRef]

Appendix II

Original article:

Miguel Horta, Paula Soares, Bruno Sarmento, Catarina Leite Pereira* and Raquel T. Lima* **(2025)**. *Nanostructured Lipid Carriers for Enhanced Batimastat Delivery Across the Blood-Brain Barrier: An In vitro Study for Glioblastoma Treatment*. Drug Delivery and Translational Research. DOI: https://doi.org/10.1007/s13346-024-01775-8.

*These authors contributed equally to this work.

Graphical abstract:

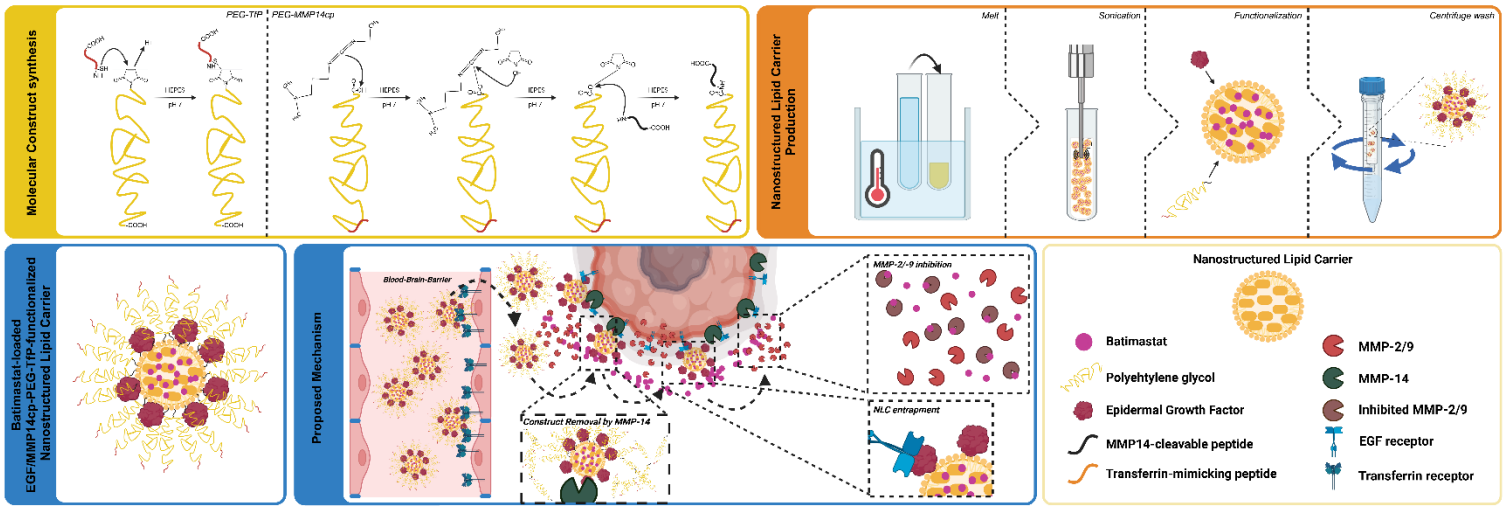

SPRINGER NATURE LICENSE
TERMS AND CONDITIONS

Jan 17, 2025

This Agreement between Miguel Diogo de Freitas Horta ("You") and Springer Nature ("Springer Nature") consists of your license details and the terms and conditions provided by Springer Nature and Copyright Clearance Center.

License Number:	**5951411284341**
License date:	Jan 17, 2025
Licensed Content Publisher:	Springer Nature
Licensed Content Publication:	Drug Delivery and Translational Research
Licensed Content Title:	Nanostructured lipid carriers for enhanced batimastat delivery across the blood–brain barrier: an *in vitro* study for glioblastoma treatment
Licensed Content Author:	Miguel Horta *et al*
Licensed Content Date:	Jan 6, 2025
Type of Use:	Thesis/Dissertation
Requestor type:	Academic/university or research institute
Format:	Print and electronic
Portion:	Full article/chapter
Will you be translating?	No
Circulation/distribution:	1 - 29

Drug Delivery and Translational Research
https://doi.org/10.1007/s13346-024-01775-8

ORIGINAL ARTICLE

Nanostructured lipid carriers for enhanced batimastat delivery across the blood–brain barrier: an in vitro study for glioblastoma treatment

Miguel Horta[1,2,4] · **Paula Soares**[1,2,4] · **Bruno Sarmento**[1,3,5] · **Catarina Leite Pereira**[1,3] · **Raquel T. Lima**[1,2,4]

Accepted: 18 December 2024

Abstract

Glioblastoma presents a significant treatment challenge due to the blood–brain barrier (BBB) hindering drug delivery, and the overexpression of matrix metalloproteinases (MMPs), which promotes tumor invasiveness. This study introduces a novel nanostructured lipid carrier (NLC) system designed for the delivery of batimastat, an MMP inhibitor, across the BBB and into the glioblastoma microenvironment. The NLCs were functionalized with epidermal growth factor (EGF) and a transferrin receptor-targeting construct to enhance BBB penetration and entrapment within the tumor microenvironment. NLCs were prepared by ultrasonicator-assisted hot homogenization, followed by surface functionalization with EGF and the construct though carbodiimide chemistry. The construct was successfully conjugated with an efficiency of 81%. Two functionalized NLC formulations, fMbat and fNbat, differing in the surfactant amount, were characterized. fMbat had a size of 302 nm, a polydispersity index (PDI) of 0.298, a ζ-potential (ZP) of -27.1 mV and an 85% functionalization efficiency (%FE), whereas fNbat measured 285 nm, with a PDI of 0.249, a ZP of -28.6 mV and a %FE of 92%. Both formulations achieved a drug loading of 0.42 µg/mg. In vitro assays showed that fNbat was cytotoxic and failed to cross the BBB, while fMbat showed cytocompatibility at concentrations 10 times higher than the drug's IC50. Additionally, fMbat inhibited MMP-2 activity between 11 and 62% across different cell lines and achieved a three-fold increase in BBB penetration upon functionalization. Our results suggest that the fMbat formulation has potential for enhancing GB treatment by overcoming current drug delivery limitations and may be combined with other therapeutic strategies for improved outcomes.

Keywords Nanostructured Lipid Carrier · Glioblastoma · Batimastat · Extracellular Matrix

Catarina Leite Pereira and Raquel T. Lima co-senior authors that contributed equally to this work.

✉ Catarina Leite Pereira
catarina.pereira@ineb.up.pt

Miguel Horta
mhorta@i3s.up.pt

Paula Soares
psoares@ipatimup.pt

Bruno Sarmento
bruno.sarmento@i3s.up.pt

Raquel T. Lima
rlima@ipatimup.pt

[1] i3S – Instituto de Investigação e Inovação em Saúde, University of Porto, Rua Alfredo Allen 208, 4200-135 Porto, Portugal

[2] IPATIMUP – Instituto de Patologia e Imunologia Molecular, University of Porto, Rua Júlio Amaral de Carvalho 45, 4200-135 Porto, Portugal

[3] INEB – Instituto de Engenharia Biomédica, University of Porto, Rua Alfredo Allen 208, 4200-135 Porto, Portugal

[4] FMUP – Faculty of Medicine, University of Porto, Alameda Prof. Hernâni Monteiro, 4200-319 Porto, Portugal

[5] IUCS-CESPU - Instituto Universitário de Ciências da Saúde, Rua Central de Gandra 1317, 4585-116 Gandra, Portugal

Published online: 06 January 2025

Introduction

Glioblastoma (GB) is the most common and lethal glioma subtype, representing circa 50% of all central nervous system (CNS) malignant tumors [1, 2]. The current standard of care involves the tumor's maximal safe surgical resection, followed by adjuvant chemotherapy (with temozolomide, an alkylating agent) and radiotherapy [3, 4]. Despite this aggressive approach, GB patient prognosis remains poor, with a median survival rate of approximately 15 months and a 5-year survival rate of less than 6% [2, 5].

One of the reasons for the lack of new treatments effectiveness is the poor drug bioavailability in the brain parenchyma limited by the blood–brain barrier (BBB) [6]. The BBB is a specialized barrier formed by a continuous unfenestrated endothelial cell layer that constitutes the blood vessels in the brain, tightly regulating the exchange of molecules between the bloodstream and the CNS [7]. It accomplishes this through a lining of tight junctions between endothelial cells, restricting paracellular flow, and a low rate of transcytosis, restricting transcellular flow [8]. While extremely important to maintain the physiological homeostasis in the brain, it is a difficult hurdle that brain targeting agents must overcome. For this, strategies exploiting the BBB's receptors and transporters have been employed, such as the transferrin receptor [9], insulin receptor [10], low density lipoprotein receptor [11], leptin receptor [12], nicotine acetylcholine receptor [13], diphtheria toxin receptor [12], scavenger receptor [14, 15], glucose transporter [16], and glutathione transporter [14], among others. In the past, our group was able to show a two-fold increase in permeability of siRNA-loaded polymeric nanoparticles when functionalized with a modified transferrin-like peptide (TfP), effectively demonstrating a transferrin receptor-mediated capacity to transcytose the BBB [17].

Nanotechnology offers a unique approach to improve GB prognosis and drug delivery limitations [18]. Through drug encapsulation and surface chemistry modification, nanoparticles (NP) may improve drug bioavailability at the tumor site through improved BBB crossing, controlled drug release, prolonged half-life by avoiding the reticuloendothelial system (RES) uptake, and increased specificity by molecular targeting [19].

Several nanoformulations have been developed for GB, encompassing chemo- [20, 21], photodynamic- [22], sonodynamic- [23], radiotherapy- [21, 24], immune- [25] and hyperthermia-based treatments [26, 27] and magnetic resonance imaging [27, 28]. Some of these formulations, mostly liposomal, have even progressed into clinical trials [29, 30]. Notably, a superparamagnetic iron oxide nanoparticle marketed as NanoTherm™, is the only nano-based therapeutic, indicated for GB treatment, approved by the European Medicines Agency [31, 32]. Despite these advances, there has not been an effective improvement in clinical outcomes.

Among the plethora of NP types available, nanostructured lipid carriers (NLCs) are of special interest as a GB therapeutic vehicle [33, 34]. Synthesized with "generally recognized as safe" (GRAS) lipids and surfactants, NLCs represent an evolution of solid lipid nanoparticles through the inclusion of a liquid lipid in its core [35]. The absence of organic solvents during synthesis provides a greater biocompatibility, while the addition of the liquid lipid bestows a more disorganized matrix, increasing the drug loading capacity [36, 37]. In GB, NLCs have been shown to increase drug bioavailability due to: i) efficient BBB crossing, ii) diminished drug side effects, iii) targeting functionalizations and iv) biocompatibility [37–40].

In addition to the poor drug bioavailability in the brain, another major cause for treatment failure in GB is its extremely aggressive invasion into the surrounding tissue. This invasive capacity is closely associated to the overexpression of various molecules, including the epidermal growth factor receptor (EGFR) and matrix metalloproteinases (MMPs), two hallmarks of GB [41, 42].

Regarding the first, *EGFR* mutations and alterations (usually amplifications) lead to the receptor's overexpression and/or constitutive activation [43, 44]. Abnormal EGFR signaling promotes uncontrolled cell growth, survival, invasion, and angiogenesis, all of which contribute to the aggressive nature of GB [45–49]. Targeting the EGFR pathway has therefore been a major focus of research and therapeutic development for this type of tumor [50, 51].

The second, MMPs, are a family of zinc-dependent enzymes involved in extracellular matrix (ECM) remodeling, which play a vital role in normal physiological processes. However, when physiological equilibrium is disrupted, MMPs contribute to malignancy through increased ECM degradation [52]. Albeit several MMPs have been found overexpressed in GB microenvironment [53], MMP-2 and MMP-9 are the two most extensively studied in gliomas [39, 54–56]. These gelatinases play a crucial role in the degradation of main ECM components, such as collagens, elastin, and fibronectin [57]. By cleaving these components, MMP-2 and −9 facilitate the creation of new pathways that enable tumor cells to migrate and invade surrounding tissues more effectively [58]. In addition to their role in ECM degradation, these MMPs promote the release of sequestered pro-angiogenic factors, such as vascular endothelial growth factor (VEGF). This increases the tumor's resource availability and facilitates GB infiltration to surrounding brain tissue through the chaotic neovasculature [59]. MMP-14, a membrane-anchored member of the MMP family, was also

found to be overexpressed in GB cells [60–62]. Besides having similar proteolytic, angiogenic and immunomodulatory abilities as the above secreted gelatinases, MMP-14 is capable of activating pro-MMP-2 into its active form, further contributing to GB invasiveness [57].

Given the importance of MMPs in GB, various therapies targeting their inhibition have been attempted [63–65]. Several synthetic MMP inhibitors were shown to decrease MMP activity, such as the hydroxamate-based batimastat and marimastat, which bind the MMPs' zinc atom and effectively suppress their functionality [55, 66–69]. Still, clinical studies have failed to demonstrate significant impact of both these molecules on patient progression-free and overall survival. This was attributed to the molecules' low aqueous solubility and potential side effects [57, 70–72]. Consequently, there has been relatively little research focusing on MMPs and ECM remodeling as actively targeted therapeutic strategies [73].

In the present project, we propose the development of a NLC formulation encapsulating batimastat, a highly potent MMP inhibitor, and further functionalized with both EGF and a custom molecular construct, targeting the transferrin receptor at the BBB. This construct is comprised of a 10 kDa polyethyleneglycol (PEG) linker, to sterically impede EGF interactions, and is terminated by TfP, to promote the BBB crossing, and an MMP-14 cleavable peptide (MMP14cp) to cause the construct's removal once it reaches the GB microenvironment, leading to the display of EGF and consequential nanoparticle entrapment. This approach aims to locally inhibit MMPs within the GB microenvironment and consequently hamper tumor proliferation and invasiveness.

Materials and methods

Reagents

Gelucire® 44/14 and Compritol® 888 ATO were bought from Gattefossé (Lyon, France). Miglyol® 810N was acquired from CREMER OLEO (Hamburg, Germany), 1,2-Distearoyl-sn-glycero-3-phosphorylethanolamine (DSPE) from Tokyo Chemical Industry (Zwijndrecht, Belgium), and Tween® 80 from Avantor (Easton, Pennsylvania). TfP (THRPPMWSPVWPC) and MMP14cp (SGRIGFLRTA) were synthesized by Genscript Biotech (Rijswijk, Netherlands). N-(3-Dimethylaminopropyl)-N′-ethylcarbodiimide hydrochloride (EDC), N-Hydroxysuccinimide (NHS), Tris(2-carboxyethyl)phosphine hydrochloride (TCEP), 4-(2-hydroxyethyl)−1-piperazineethanesulfonic acid (HEPES) and batimastat (BB-94) were bought from Sigma-Aldrich (Strasbourg, France). Maleimide-PEG-COOH with 10 kDa was received from RuixiBiotech (Shaanxi, China). The micro-BCA™ protein assay kits and the Spectrum™ Spectra/Por™ 3 RC Dialysis Membrane Tubing 3.5 kDa were bought from ThermoFisher Scientific (Porto Salvo, Portugal). The NHA and T98G cell lines were purchased from ATCC® (Virginia, USA) and the U-87 cell line from Biochrom (Berlin, Germany). The U-251 cell line was kindly provided by the Cell Bank of IPATIMUP (Porto, Portugal) and the hCMEC/D3 cells were purchased from Cedarlane (Burlington, Canada).

Functionalization construct synthesis

The molecular construct synthesis here optimized was adapted from carbodiimide and maleimide-cysteine reactions previously published by our group [74]. TfP and Maleimide-PEG-COOH conjugation was conducted through a thioether bond between TfP's cysteine and the PEG's maleimide moiety with a Michael addition reaction [75]. First, TfP and TCEP (1:10 molar ratio) were left to react at room temperature for 1 h. Then, a freshly prepared PEG solution was added (1:1 molar ratio of PEG:TfP), and the resulting mixture was left overnight at 4 °C. The TfP-PEG-COOH solution was then diluted 1:50 (v/v) to 5 mL in distilled water and purified through dialysis in a 3.5 kDa membrane for 24 h, with a sink volume of 5 L of distilled water and water changes at 2, 4 and 8 h. Purified TfP-PEG-COOH was thereafter subjected to carbodiimide chemistry with EDC and NHS [76, 77]. Briefly, the polymer-peptide molecule, EDC and NHS were mixed at a 1:10:10 molar ratio, respectively, and left to react for 1 h. Then, MMP14cp was added (1:1 molar ratio to TfP-PEG) and left to react overnight at 4 °C. The final molecular construct is again purified by dialyzing against 5 L of distilled water in a 3.5 kDa membrane for 24 h with water changes at 2, 4 and 8 h. All reactions occurred with HEPES buffer at pH 7.00.

Construct conjugation efficiency

PEG-TfP, PEG-MMP14cp and MMP14cp-PEG-TfP conjugation efficiencies were assessed through a micro-BCA™ assay on purified samples following the manufacturer's protocol [78]. Briefly, a 25:24:1 (v/v) ratio of micro-BCA™ reagents A:B:C were combined to create a BCA™ working solution, which was then added to the samples at a 1:1 (v/v) ratio. The resulting mixture was incubated for 2 h at 37 °C and analyzed at 562 nm in a Synergy MX microplate reader (BioTek). To further confirm the conjugation efficiencies, ^{1}H-NMR was conducted for all samples in an Ascend III 400 9.4 T (Bruker). For qualitative validation of the conjugation success, the molecular weight of the conjugates and pure PEG solutions were calculated by gel permeation chromatography/size exclusion chromatography (GPC/SEC). The analysis was performed using a tri-module system: OMNISEC Reveal, OMNISEC Resolve and OMNISEC

Software. Separations were performed at 30 °C in PL aqua gel-OH mixed columns (with porous hydroxy methacrylate polymer). The mobile phase consisted of 0.05 M $NaSO_4$ at a flow rate of 1 mL/min. Samples were filtered through 0.45 µm cellulose acetate filters, and 100 µL of the sample were automatically injected by the autosampler at room temperature. All modules were controlled by the OMNISEC software, which also analyzed sample data.

NLC synthesis

The lipidic NPs were prepared through an ultrasonicator-assisted hot homogenization technique [79]. Briefly, a lipid phase comprised by Gelucire® 44/14, Compritol® 888 ATO, Miglyol® 810N, DSPE and Tween® 80, and an aqueous phase of double-distilled water were separately heated to 80 °C in a water bath. The latter was then vigorously poured into the former, and the resulting microemulsion was homogenized using a probe-sonicator (VC50 50 W model from Vibra-Cell with a 3 mm probe) at 100% for 15 min to obtain a nanodispersion. To synthesize batimastat-encapsulating NLCs, a varied amount of batimastat (dissolved in absolute ethanol at 1 mM) was added to the organic phase during the melting step. All formulations were left to cool down at room temperature and stored at 4 °C. For the optimization process, different formulations were tested, regarding the ratio of solid to liquid lipids, amount of surfactant, amount of DSPE, sonicator tip and sonicated volume, as specified in Table 1. The best formulations, based on average diameter and polydispersity index (PDI), were selected to proceed with functionalization.

NLC physicochemical characterization

NLC formulations' average diameter, PDI and zeta-potential were analyzed using dynamic and electrophoretic light scattering (DLS/ELS) (Zetasizer Nano-ZS ZEN3600 with a DTS1060C cuvette and Zetasizer v7.13 software, all from Malvern Panalytical). All samples were diluted 1:50 (v/v) with distilled water to reach a count rate of 200 k-400 k counts per second. The quantity of available reactive primary amines at the nanoparticle surface was qualitatively evaluated through a fluorescamine assay [80]. Briefly, 100 µL of double-distilled water is inserted into a well of a 96-well plate. Afterwards, 100 µL of the sample and 50 µL of fluorescamine (0.3 mg/mL in DMSO) is added. After 15 min of incubation in the dark, the emitted fluorescence (400/460 nm, excitation/emission) is measured. Size and morphology were further analyzed by transmission electronic microscopy (TEM) at the i3S Histology and Electron Microscopy platform, with a JEM-1400 microscope (JEOL) at an accelerating voltage of 120 kV. Briefly, samples were prepared by pipetting 10 µL of an NLC formulation onto a

Table 1 Summary of the iterative optimization process for blank NLCs. Nanoparticles were optimized by varying their components and relative ratios, and characterized regarding their average diameter, polydispersity index and zeta potential, assessed with a Zetasizer, and relative surface amines, evaluated by fluorescamine assay. Results are represented as the mean ± SD of at least 3 independent characterizations. Formulations in bold were selected for functionalization

Formulation ID	Gelucire 44/14 (mg)	Compritol 888 ATO (mg)	Miglyol 810N (mg)	Tween 80 (mg)	DSPE (mg)	Solid:Liquid lipid ratio	Average diameter (nm)	Polydispersity Index	Zeta potential (mV)	Surface amines (RFU)
A	70	6	10	12	2	0.13	179 ± 59	0.260 ± 0.018	−19.7 ± 1.3	2412 ± 330
B	70	6	10	12	5	0.12	311 ± 77	0.277 ± 0.033	−19.6 ± 2.2	1606 ± 452
C	70	6	10	12	10	0.12	209 ± 35	0.286 ± 0.030	−18.9 ± 1.9	2059 ± 189
D	70	6	10	12	15	0.11	218 ± 123	0.280 ± 0.095	−20.6 ± 0.9	2514 ± 357
F	70	0	10	12	5	0.13	313 ± 240	0.300 ± 0.179	−20.1 ± 2.0	3293 ± 770
G	70	0	10	12	10	0.13	376 ± 277	0.440 ± 0.195	−18.8 ± 6.2	4504 ± 531
H	70	0	10	12	15	0.12	144 ± 45	0.313 ± 0.189	−25.6 ± 3.8	4468 ± 1602
J	0	70	10	12	10	0.13	223 ± 27	0.321 ± 0.047	−18.3 ± 0.9	1144 ± 8
K	70	6	20.25	10	5	0.25	217 ± 57	0.284 ± 0.052	−21.0 ± 2.0	2282 ± 234
L	70	6	20.25	5	5	0.25	324 ± 130	0.312 ± 0.134	−22.9 ± 4.2	520 ± 13
M	**70**	**6**	**40.5**	**10**	**5**	**0.50**	**160 ± 46**	**0.147 ± 0.040**	**−20.6 ± 1.8**	**6078 ± 1203**
N	**70**	**6**	**40.5**	**5**	**5**	**0.50**	**191 ± 39**	**0.125 ± 0.039**	**−20.3 ± 2.4**	**6769 ± 543**

300-mesh nickel grid, using uranyl acetate to increase contrast. Batimastat was quantified by high performance liquid chromatography (HPLC) to assess the encapsulation efficiency (EE%) and loading degree (LD) [81]. The chromatography was performed by reverse-phase HPLC (Hitachi 7000 from Merck), with a Nova-Pak C18 4 µm column (Waters) as the stationary phase and 50% water 50% acetonitrile as the mobile phase, at a flow rate of 1 mL/min. The analyte was measured at a wavelength of 256 nm and was injected at a volume of 50 µL per sample. The NLC stability over time was analyzed by DLS/ELS up to 2 months.

NP functionalization

Nanoparticle functionalization with the construct and EGF was achieved with a carbodiimide reaction in a similar manner as described for the construct synthesis [74]. Briefly, the carboxylic acids of both MMP14cp-PEG-TfP and EGF (1:1 molar ratio) were activated with EDC and NHS at a 1:10:10 molar ratio for 1 h, after which the aminated NLCs were added, reacting overnight at 4 °C. The functionalized suspensions were washed with double-distilled water in an Amicon® Ultra 15 mL centrifugal filter. The reactions occurred with HEPES buffer at pH 7.00. The functionalization efficiency was quantified by both micro-BCA™, with samples in a 2% sodium dodecyl sulfate (SDS) solution [82], and ^{1}H-NMR, as previously explained for MMP14cp-PEG-TfP conjugation efficiency (Construct conjugation efficiency). Functionalized NLCs were physicochemically characterized in the exact same manner as their non-functionalized counterparts.

Cell culturing

The glioblastoma cell lines, U-87, U-251 and T98G and the non-tumor astrocytic cell line NHA were routinely maintained in Dulbecco's modified Eagle's medium (DMEM) high-glucose (4.5 g/L) with stable glutamine and sodium pyruvate, supplemented with Gibco™ heat-inactivated fetal bovine serum (FBS, 10% v/v), penicillin–streptomycin (1% v/v) and amphotericin B (0.5% v/v). hCMEC/D3 cells were cultured in endothelial basal medium-2 (EBM-2) supplemented with FBS (5% v/v), penicillin–streptomycin (1% v/v), hydrocortisone (1.4 µM), ascorbic acid (5 µg/mL), chemically defined lipid concentrate (1% v/v), 4-(2-hydroxyethyl)−1-piperazineethanesulphonic acid (10 mM) and basic fibroblast growth factor (1 ng/mL). This last supplement was added extemporaneously in the culture medium. Cells were maintained in a humidified incubator at 37 °C with 5% CO_2 and 95% relative humidity. Cell culture medium was changed every 2 to 3 days, depending on cell confluence.

Cell viability assays

Cells (5×10^3 /well) were plated on a 96-well transparent plate and allowed to adhere for 24 h at 37 °C. Cells were then treated for 24, 48 or 72 h with supplemented media (untreated control), free batimastat in concentrations ranging from 0 to 100 nM, or NLC formulations at concentrations equivalent to batimastat at 0 to 100 nM. To evaluate cell response to the treatments, PrestoBlue™ cell viability assay was conducted as previously described by our group [83]. Briefly, cells were washed three times with the non-supplemented media and then incubated with PrestoBlue™ reagent diluted in supplemented medium (10% v/v) for 45 min at 37 °C in the dark. Fluorescence was then measured at 560 nm and 590 nm excitation and emission wavelengths in a SpectraMax iD3 multi-detection microplate reader (Molecular Devices, USA) in five technical replicates, excluding the background.

BBB permeability assay

The methodology for establishing an in vitro BBB model was adapted from a previously published protocol [17]. Prior to cell seeding, 24-well Transwell inserts were treated with 50 µL of rat tail collagen type I solution (50 µg/mL in 20 mM acetic acid) for 60 min at 37 °C, followed by two Phosphate Buffered Saline washes. hCMEC/D3 cells were plated onto the apical chamber of the inserts at a density of 7.5×10^3 cells per well in 400 µL of EBM-2 medium and the basolateral chamber was filled with 1 mL of medium. The model was incubated at 37 °C for 8 days, with media replacement every 48 h. By day 8, the hCMEC/D3 cells formed a confluent monolayer, at which point the permeability study was initiated. The integrity of the cellular barrier was assessed every 48 h by measuring the transepithelial electrical resistance (TEER) using a Millicell ERS-2 endothelial Volt-Ohm meter (Merck Millipore, USA). The resistance of a cell-free insert in the same conditions was subtracted from each measurement to obtain the true TEER value. The permeability assay was conducted in the apical-to-basolateral direction, as DiO-labeled NPs, either functionalized or unfunctionalized, suspended in Hanks' balanced salt solution (HBSS, 400 µL at 600 µg/mL) were introduced to the apical compartment. The experiment was performed at 37 °C in an orbital shaker incubator set to 100 rpm. At specific time points (1, 4, 12 and 24 h), 200 µL aliquots were collected from the basolateral chamber and replaced with 200 µL of pre-heated HBSS. The fluorescence intensity of these samples was quantified using a SpectraMax iD3 multi-detection microplate reader (Molecular Devices, USA) at excitation and emission wavelengths of 471 nm and 511 nm, respectively. All experiments were conducted in triplicate.

Collection of conditioned media

Cells (3×10^5 /well) were plated on a 6-well transparent plate, with 3 mL of supplemented medium, and allowed to adhere for 48 h at 37 °C. Cells were then treated for 24, 48 or 72 h with 1.5 mL of non-supplemented media (untreated control), NLC formulations at a concentration equivalent to 50 nM of batimastat, or free batimastat (50 nM), after which the media was collected. Following a centrifugation at 13,000 rpm for 10 min, the pellet was discarded, and the supernatant concentrated tenfold by centrifugation at 3500 rpm for 10 min, at 4 °C, in an Amicon® Ultra 4 mL centrifugal filter (30 kDa molecular weight cutoff). The conditioned media (secretomes) were then stored at −80 °C.

Gelatin zymography

Total protein content of each secretome was quantified with a DC™ protein assay kit (Bio-Rad, USA). 15 µg of protein was mixed with sample loading buffer (10% Sodium dodecyl sulfate (SDS), 4% sucrose and 0.03% bromophenol blue in 0.5 M Tris-HCl pH 6.8) at a 2:1 (v/v) ratio. Separation was achieved through electrophoresis with a 10% polyacrylamide gel, containing 0.1% gelatin as substrate, at 80 V for 2 h, as previously described [84, 85]. The gels were then washed twice with 2% Triton X-100 for 30 min to remove the SDS, washed with ddH2O, and further incubated for 16 h at 37 °C with MMP substrate buffer (10 mM $CaCl_2$, 0.5% NaN_2 in 50 mM Tris-HCL pH 7.5). Lastly, the gels were stained with Coomassie Blue for 30 min and destained until the bands were clear. Gel images and band density calculations were obtained with a GS-900 Calibrated Densitometer and the Image Lab 6.1 software (Bio-Rad, USA).

Statistical analysis

The results are presented as the mean ± standard deviation from at least three independent experiments. Statistical analyses were conducted using a one-way analysis of variance (ANOVA) followed by Holm-Sidak's multiple comparison test or Kruskal–Wallis test followed by Dunn's post hoc test to compare the experimental groups. Differences were deemed statistically significant at *$p < 0.05$, **$p < 0.01$, ***$p < 0.005$ or ****$p < 0.001$. All statistical analyses were carried out using GraphPad Prism 8.0.1 software (GraphPad Software, USA).

Results and discussion

Chemical synthesis of the targeting molecular construct

The molecular construct, MMP14cp-PEG-TfP, was designed to provide a cleavable moiety in its link to the nanoparticle (MMP14cp) and to permeate the BBB, through its transferrin-mimicking moiety (TfP). Binding both peptides, the COOH-PEG-maleimide molecule was designed to have a molecular weight (MW) of 13 kDa, in order to conceal the functionalization of EGF, which has a lower MW (6.4 kDa). First, the PEG-maleimide was chemically conjugated with the cysteine-terminated TfP (Fig. 1a) following a common thiol-maleimide click chemistry. The addition of TCEP, a reducing agent, ensured that no disulfide bridge cross-linking was present between the peptides. The conjugation's efficiency, assayed through micro-BCA™, was 66 ± 20%, presenting a high variability between replicates. As the room temperature under which the reactions occurred was not controlled, its variability could have led to different rates of maleimide hydrolysis, which degrades the maleimide and prevents its reaction with thiols [86]. Nonetheless, this efficiency was considered to be acceptable since its upper limit was very close to other optimized thiol-maleimide reactions described in the literature, between 70 to 90% [74, 86]. Additionally, GPC analysis showed a reproducible increase in molecular weights after the conjugation reaction, consistent with the expected peptide MW of 1.6 kDa (Fig. 1b). To further confirm the conjugation, an ^{1}H-NMR analysis was conducted on both the reagents and the dialyzed conjugate (Fig. 1c). The NMR chemical shifts between $\delta = 2.9$ ppm and 3.1 ppm, which are attributed to a carbon linked to another carbon and to an aromatic ring [87, 88], exhibited low intensity in the pure PEG sample and high intensity in the dialyzed conjugate. This indicates the presence of the peptide's aminoacid side chains in the final product (conjugate). Before proceeding with the full construct conjugation, the PEG-MMP14cp bound was also characterized, following a typical NHS-assisted carbodiimide reaction strategy. The conjugation efficiency could not be assessed with micro-BCA™ due to the unexpected interference of undialyzed NHS, which reacted colorimetrically with the assay's copper-based agents. Nevertheless, similarly to PEG-TfP, GPC analysis of the conjugate showed a molecular weight increase compared to the pure polymer, consistent with the MMP14cp's molecular weight of 1.1 kDa (Fig. 1b). Additionally, ^{1}H-NMR analysis of the dialyzed conjugate showed an increase in chemical shift at an identical $\delta = 2.9$–3.1 ppm, suggesting the presence of the aromatic rings of MMP14cp in the final product (Fig. 1c). The final construct was prepared following the same reaction procedure using PEG-TfP instead of PEG. The conjugation efficiency, assessed using micro-BCA™, was 81 ± 4%, which is at the reported upper limits of carbodiimide chemistry [74, 89, 90]. GPC analysis showed an increase in molecular weight consistent with the presence of both peptides, totaling a MW of 2.7 kDa (Fig. 1b). The analysis of the ^{1}H-NMR spectra of the dialyzed conjugate indicated the previously stated presence of histidine, tryptophan and phenylalanine residues in the molecular construct, evidenced by the increased chemical shift at $\delta = 2.9$–3.1 ppm (Fig. 1c).

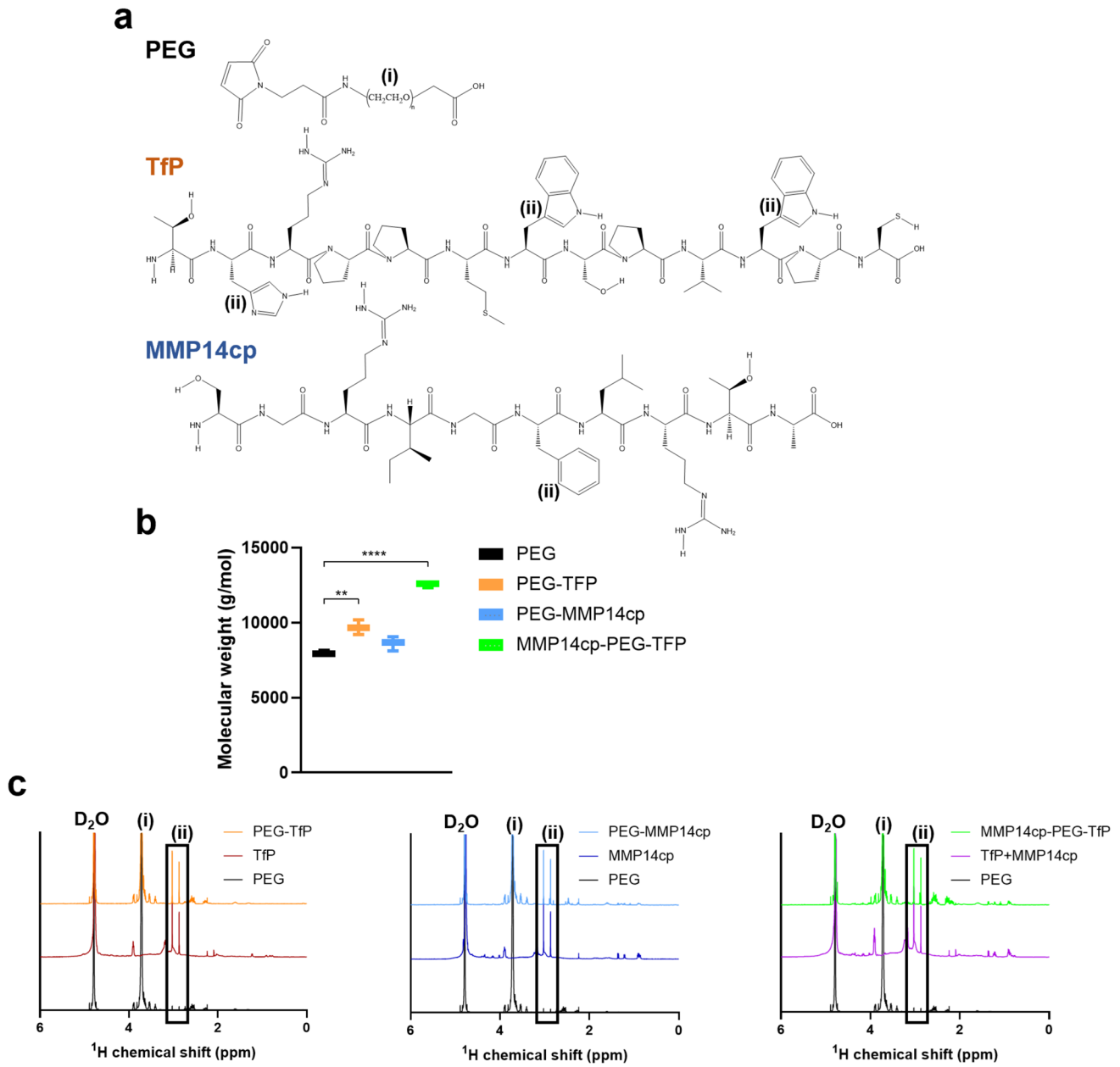

Fig. 1 Conjugation and characterization of the molecular construct for NP functionalization. **a** Chemical structure of PEG, TfP and MMP14cp. **b** Molecular weight of MMP14cp-PEG-TfP reaction steps, determined by GPC analysis. Results are expressed as mean ± SD of 3 independent experiments. $^{**}p < 0.005$, $^{****}p < 0.0001$. **c** ^{1}H-NMR spectra of PEG, peptide(s) and purified PEG-peptide(s) for the molecular construct conjugations, PEG-TfP, PEG-MMP14cp and MMP14cp-PEG-TfP. Experiments were conducted in triplicate. D_2O – deuterium oxide, (i) C–C-O at 4.7 ppm, (ii) C–C-C-aromatic ring at 2.9–3.1 ppm

Nanostructured lipid carrier production and characterization

All NLC formulations were synthesized following an ultrasound-assisted hot homogenization technique (Fig. 2) [79]. During initial optimization, different combinations and quantities of solid and liquid lipids, surfactant, and the phospholipid DSPE (required for further functionalization) were tested, as depicted in Table 1. Ideal benchmarks for average diameter and polydispersity index were chosen as 200 nm, considered to be the standard for blood-to-brain delivery, and < 0.2, respectively, to maximize efficient load delivery potential [91, 92]. Zeta potential was optimized to be distant from neutral, as neutral dispersions tend to aggregate due to Wan-der-Walls hydrophobic interactions [93]. Surface amine concentration was intended to be as

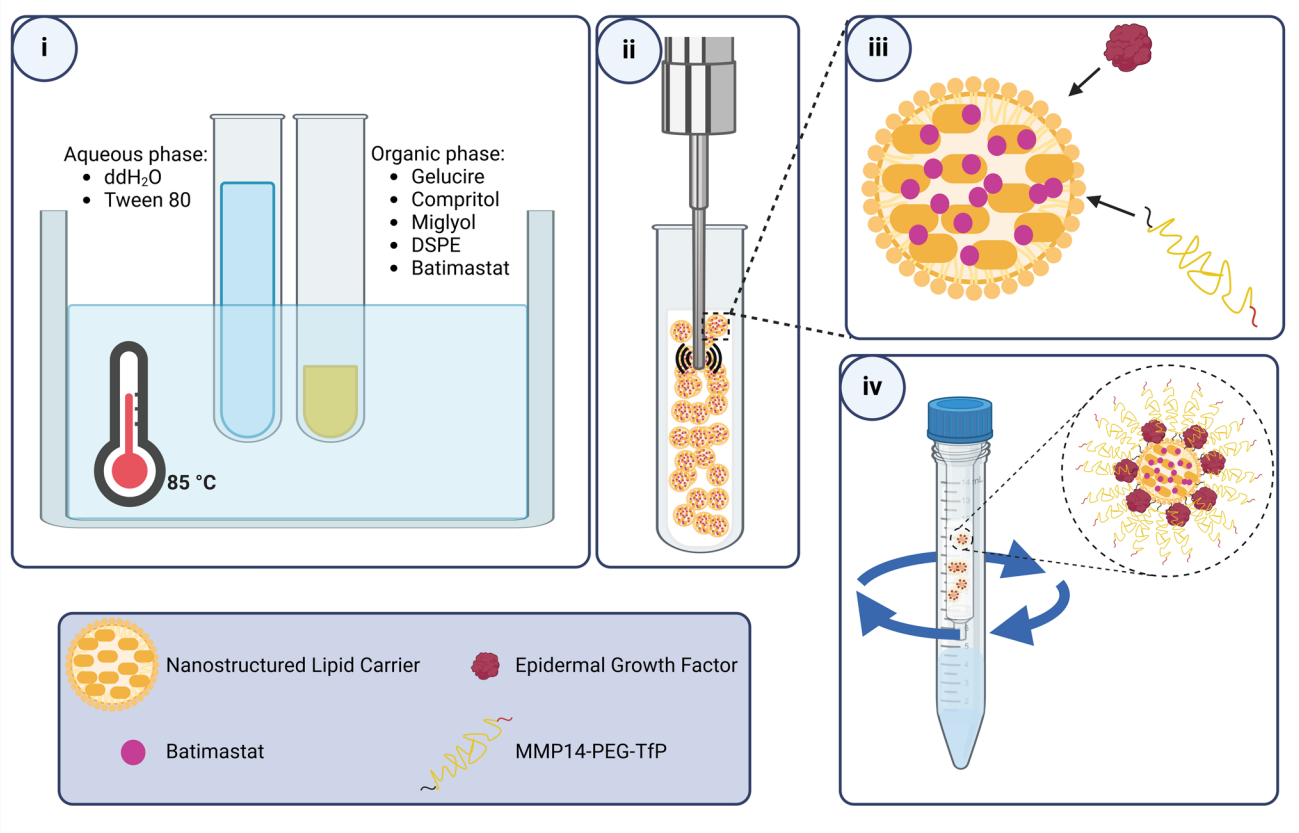

Fig. 2 Batimastat-loaded EGF/MMP14cp-PEG-TfP-functionalized Nanostructured Lipid Carrier production methodology. (i) Melting; (ii) Sonication; (iii); Functionalization; (iv) Centrifugation wash

high as possible, in order to achieve a comprehensive functionalization.

To encapsulate batimastat, 100 µL of the inhibitor (1 mM) dissolved in absolute ethanol were added to the melted lipidic phase prior to sonication (Fig. 2i). This quantity was chosen to balance batimastat's high inhibitory potential (IC50 described as being between 4–10 nM for most MMPs), and the need to minimize the amount of ethanol introduced to the production process [94, 95]. Evaluation of the encapsulation efficiency and drug loading followed a direct method and were carried out by HPLC. Results showed that both formulations presented an equal capacity for batimastat encapsulation, of 30.5% for Mbat and 30.4% for Nbat. We were also able to observe that an additional 20% of batimastat was lost during the functionalization process, as the formulations fMbat and fNbat presented efficiencies of 10.1% and 10.2%, respectively. These values correspond to a drug loading of 0.42 µg/mg, which is equivalent to 1000 times the reported IC50 of batimastat (Fig. 3a). Nasoudi et al. reported 4–5000 greater drug loading percentages in polymeric NPs than our lipidic ones but did not provide encapsulation efficiency data [96], while Zhang et al. managed to encapsulate 56.72%, without specifying the method used, of the similar compound marimastat in liposomes [97]. In our work, despite the relatively low encapsulation efficiency, the amount of encapsulated drug is enough to provide a biological effect, according to previously reported data [94]. Moreover, regarding physicochemical characteristics, the batimastat-encapsulating formulations showed no significant difference compared to empty NLCs, maintaining the behavior between M and N formulations (Fig. 3b).

NLC functionalization was obtained through the previously described carbodiimide strategy, conjugating the DSPE amines on the NLC surface to the carboxylic terminus of both the molecular construct and EGF (Fig. 2c) [98]. Physicochemical characteristics were assayed in a Zetasizer for all the functionalizations carried out on both formulations M and N, with and without batimastat (Fig. 4a and Fig. 4b). Results showed that the average sizes varied significantly between different functionalizations (Fig. 4a), albeit there were no significant alterations to the non-functionalized suspensions. The polydispersity indexes mostly remained slightly above 0.2, indicating almost monodisperse formulations [91]. Most importantly, however, all zeta-potentials were altered, becoming more negative, evidencing that the functionalization had an impact on nanoparticle

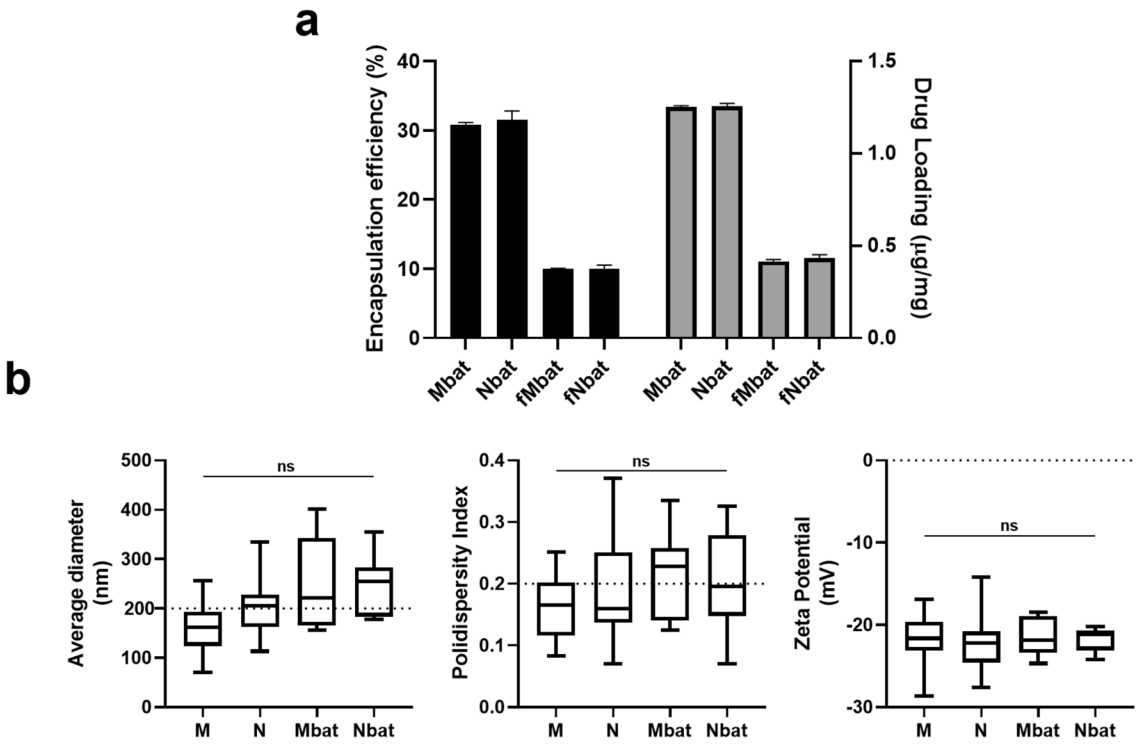

Fig. 3 Encapsulation of batimastat and its effect on the physicochemical characteristics of the NPs. **a** Encapsulation efficiency and drug loading of formulations M, N and their functionalized variants, fM and fN, as assessed through the direct method using HPLC. Results are represented as the mean ± SD of 3 independent experiments. **b** Physicochemical characteristics of empty formulations (M and N) and NLCs loaded with batimastat (Mbat and Nbat), determined with a Zetasizer. Results are shown as the mean ± SD of at least 5 independent characterizations. Dotted lines represent ideal characteristic benchmarks for NP brain delivery, average size below 200 nm and PDI below 0.2

surface charge (Fig. 4b) [99, 100]. As the zeta-potential is a characterization of the interface between the NP and the surrounding fluid, a change in this interface is expected to induce an alteration in electrical potential [101]. In a previous study, Han et al. demonstrated a similar decrease in zeta potential upon functionalizing their NLCs with transferrin [99]. More specifically, our group has previously reported that functionalization of lipidic NPs with the same transferrin peptide here utilized provoked a small decrease in zeta potential [100]. The efficiency of the functionalization procedure was assessed through a modification of the previously described micro-BCA™ technique, where the addition of a 2% SDS solution was used to mask the lipids' colorimetric influence [82]. The efficiency of fMbat, 85 ± 15%, was expectedly lower than that of fNbat, 92 ± 6%, as the first contained a higher amount of surfactant, resulting in less accessible surface compared to the second. A direct comparison with data reported in the literature is complex owing to the multiple parameters involved, such as the lipids and surfactants utilized, their ratios, the conjugation reaction itself, the molecules being attached, among others. Kebebe et al. successfully conjugated cyclic-RGD tumor-targeting peptides to the surface of a gamboic acid-loaded NLC, with the help of EDC/NHS, at a near 100% efficiency [76]. In another study, Du and Li utilized carbodiimide chemistry in an optimization process to functionalize an NLC containing DNA and doxorubicin with bombesin, achieving between 85 to 95% conjugation efficiencies [102]. More recently, a similar conjugation to the one used in this study was conducted by Teixeira et al., achieving 95% functionalization efficiency in a carbodiimide bond between lactoferrin and stearic acid present in NLCs [103]. Overall, our degree of functionalization is mostly in the range of those described in the aforementioned studies.

Previously synthesized and characterized NLC formulations were further analyzed for morphology using transmission electron microscopy (TEM) at all stages of encapsulation and functionalization (Fig. 5). The TEM images revealed that the NPs were generally spherical but displayed slight distortions. This was probably due to the accumulation of smaller NPs around them, which pressed against the inherently labile nature of the lipidic matrices. The formulations tended to aggregate under vacuum but seemed homogenous. Interestingly, two different populations were observed, a larger one with sizes of approximately 300 nm and a smaller one with diameters below 100 nm.

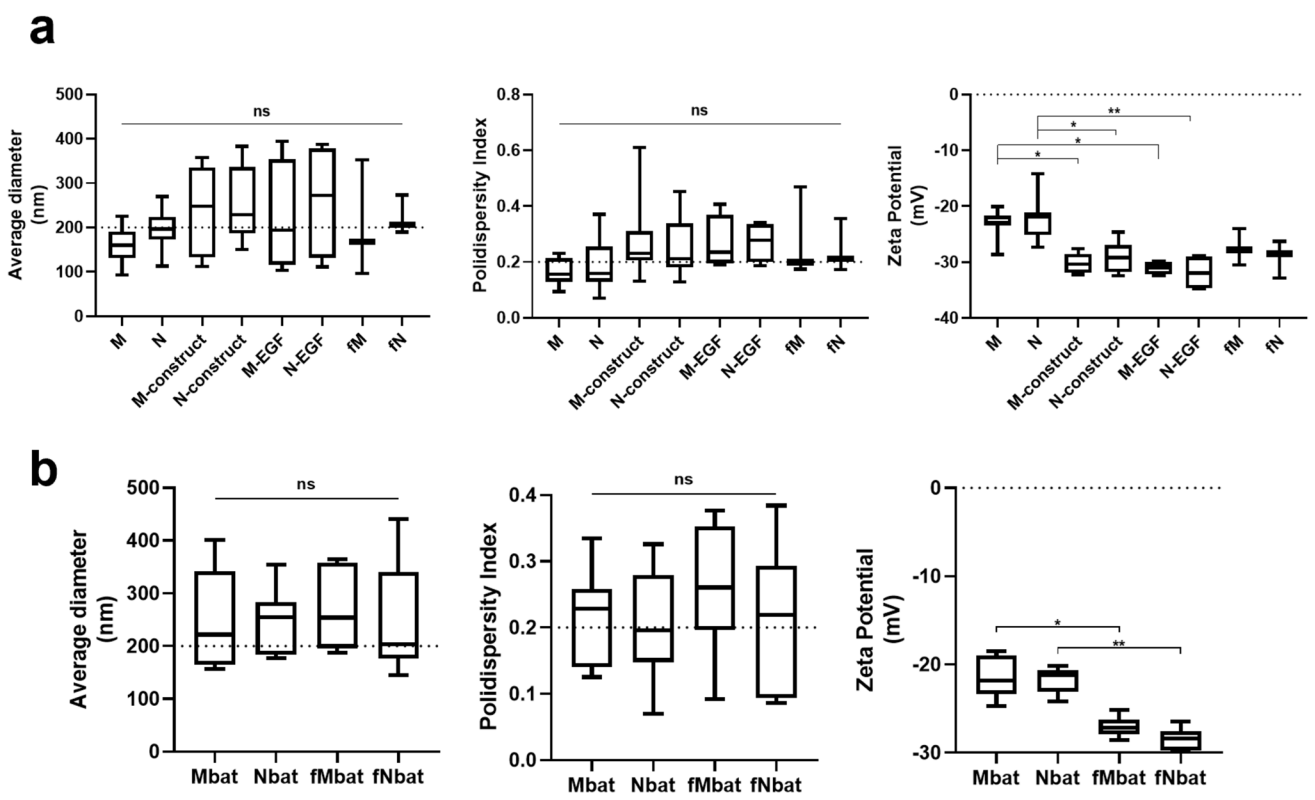

Fig. 4 Functionalization of EGF and MMP14cp-PEG-TfP and its effect on the physicochemical properties of the NPs. All dotted lines represent ideal property benchmarks for NP brain delivery, average size below 200 nm and PDI below 0.2. **a** Physicochemical characteristics of empty NLC formulations at different functionalization stages, as measured in a Zetasizer. Results are represented as the mean ± SD of at least 3 independent experiments. *$p < 0.05$, **$p < 0.01$. M-construct and N-construct – formulations M and N functionalized with the molecular construct; M-EGF and N-EGF – formulations M and N functionalized with EGF; fM and fN – formulations M and N functionalized with both the construct and EGF; Mbat, Nbat, fMbat and fNbat – formulations M and N encapsulating batimastat and their functionalized variants. **b** Physicochemical characteristics of batimastat-encapsulating NLCs before and after functionalization. Results are shown as the mean ± SD of at least 3 independent experiments. *$p < 0.05$

The possibility of such a bimodal size distribution to occur has been stated in a comprehensive review by the NLC's inventor Professor R. H. Müller [104]. The presence of these smaller NPs can explain the lower than expected encapsulation efficiencies previously detected, as their small diameter may result in their removal during the centrifugation washing procedure.

The NLC formulations exhibited a good shelf stability in terms of particle size, PDI, and zeta potential over a 30-day storage period at 4 °C (Fig. 6). The initial average particle size ranged from 200 to 350 nm, which is close to the optimal range for BBB-crossing nanostructured lipid carriers [91, 92]. Excluding the Nbat formulation, particle size showed minimal variation, with a relative deviation consistently below 15%, reflecting good batch uniformity and stability during storage. Although the percentual PDI values appeared highly variable, due to their small absolute values, they remained consistently low, starting between 0.1 and 0.2, and staying below 0.3 throughout the storage period. This suggests that the NLC formulations maintained their homogeneous nature with no significant particle aggregation or size alterations. Similarly, zeta potential measurements exhibited robust stability characteristics, maintaining a negative charge of −25 to −30 mV with negligible variation. This magnitude of zeta potential is considered optimal for maintaining electrostatic repulsion between particles, thereby preventing aggregation and ensuring physical stability [105]. The complete formulations, fMbat and fNbat, were also further assessed for stability in different physiologically relevant fluids, including 0.09% NaCl, phosphate buffered saline (PBS), DMEM and DMEM supplemented with 10% FBS. Both formulations were found to be stable over 28 days. As shown in Fig. S1, the formulations presented no variation in zeta potential, regardless of the fluid. While diameter measurements remained largely consistent, a slight increase in size (although not statistically significant) was observed starting in the third week. Lastly, the PDI values were, again, varying by less than 0.05 units between each assessed timepoint. Overall, the developed NLC formulations exhibited suitable physicochemical characteristics

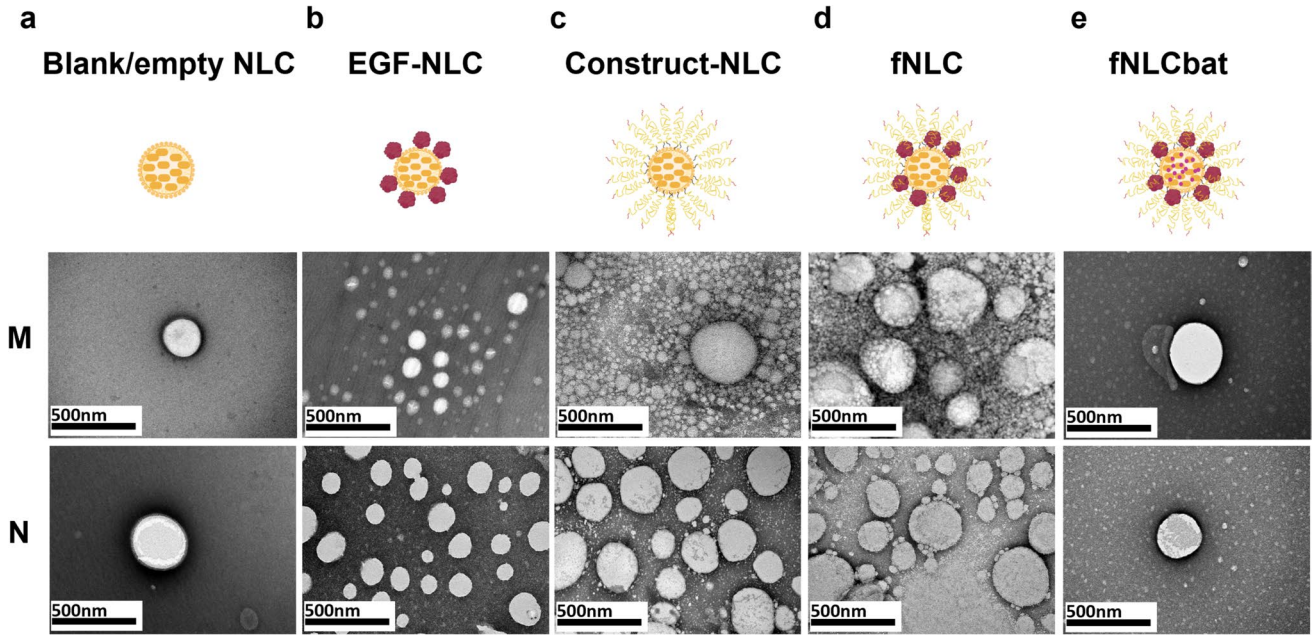

Fig. 5 TEM images of NLC formulations M and N on the different production steps. **a** Initial NLCs. **b** Construct-functionalized empty NLCs. **c** EGF-functionalized empty NLCs. **d** Empty NLCs functionalized with both EGF and MMP14cp-PEG-TfP. **e** Batimastat-encapsulating construct/EGF-functionalized NLCs

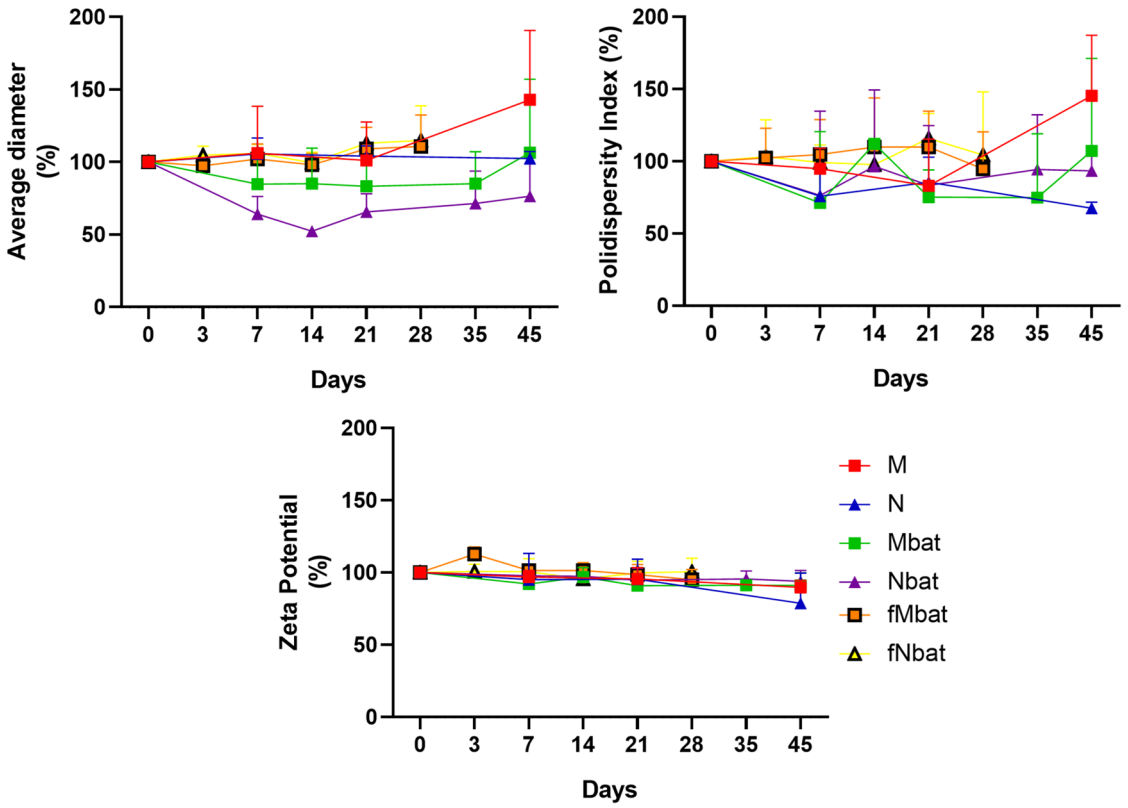

Fig. 6 Physicochemical stability of NLC suspensions M, N, Mbat, Nbat, fMbat and fNbat when stored at 4 °C. All NLC properties were measured periodically with a Zetasizer, for up to 45 days. Results are represented as the mean ± SD of 3 independent experiments

for potential pharmaceutical applications, with promising stability under normal storage conditions. The maintenance of critical quality attributes over the studied period indicates successful formulation development and appropriate selection of lipid matrices, stabilizers and surface chemistry.

In vitro permeability across the BBB of DiO-labeled NPs

To assess the ability of the NLC nanoparticles to permeate through the BBB, a highly hampering therapeutical barrier, we employed a widely recognized in vitro model, previously established by our team [17, 74, 100]. This model, which utilizes a monolayer of the hCMEC/D3 cell line, offers several benefits compared to alternative in vitro BBB models, including: i) the consistent preservation of BBB-specific characteristics across multiple passages; ii) ease of maintenance and cost-effective reproduction; and iii) the capability to form functional barriers featuring essential tight junction proteins [106]. Moreover, these endothelial cells overexpress the transferrin receptor, the mediator of our NPs' BBB crossing (Fig. S2a). This model allows for the in vitro evaluation of nanoparticle permeability across a simulated BBB environment under controlled laboratory conditions [107].

Prior to the permeability assays, the NLCs were labeled with DiO, a highly lipophilic fluorescent dye, to allow their measurement [108]. The previously assessed physicochemical characteristics of average size, polydispersity index and zeta-potential were again measured for the fluorescent NLCs, in order to guarantee that the addition of DiO would not alter the final NP properties. As shown in Fig. 7a, no statistically significant alterations were observed.

As expected, due to the surface functionalization with the transferrin-mimicking peptide-terminated molecular constructs, we observed a significant increase in permeability of the fMbat formulation. Indeed, following 24 h, the permeated mass nearly tripled (Fig. 7b). In contrast, the functionalization presented no effect on fNbat, which was unexpected. Given its higher functionalization efficiency, resulting from lower surfactant surface coverage, the fNbat was expected to be more permeable [109]. One limitation of using peptide quantification to assess the functionalization efficiency of a dual-functionalized NP is that this technique can not differentiate between the two molecules being measured. Therefore, despite its higher efficiency, formulation fNbat might actually have a lower amount of the molecular construct on its surface compared to fMbat. Another possibility is that a higher surface coverage of such long molecules might have a deleterious effect due to steric hindrance, contrary to the expected beneficial impact [110]. Interestingly, the unfunctionalized Mbat formulation demonstrated superior permeability compared to the fNbat formulation. This unexpected result is likely attributed to the higher surfactant content in Mbat, which may enhance the nanoparticle's interaction with the cellular membranes of the BBB endothelium.

Overall, our results align with existing reports on nanoparticles coopting the transferrin pathway for brain delivery [109, 111]. Moura et al., utilizing the same transferrin-mimicking peptide on a lipid nanocapsule, described a similar increase in permeability from 0 to 3% [100]. In a similar study, Gomes and colleagues, using the same peptide, showed a three-fold increase in interaction between solid lipid nanoparticles and hCMEC/D3 cells [112].

NLC cytotoxicity assessment

To evaluate the cytotoxicity of the developed NLCs, the heterogeneous nature of GB was considered, and various cell lines were used to represent distinct molecular and genetic profiles [53, 113–116]. As such, the widely utilized cell lines U-87, U-251, and T98G were selected to screen the efficacy of our nano based approach to GB. In addition to the above, normal human astrocytes (NHA) were used to mimic a healthy glia and serve as a critical control to evaluate the nanoparticle's selectivity and potential off-target effects [117].

As shown in Fig. S2b, all the aforementioned cell lines exhibit elevated expression levels of the EGF receptor, which serves as the target for our NPs to accumulate within the tumor microenvironment. To further assess the cytotoxicity of the accumulation of NPs in non-brain tissue, which frequently occurs in an in vivo setting, we conducted viability assays on the endothelial hCMEC/D3 cell line, as a model for the BBB, and HEPG2 cells, as a model of hepatotoxicity [106, 118].

Cell viability was evaluated after treatment of all the cells lines with fMbat, fNbat or free batimastat at concentrations ranging from 0 to 100 nM for 24, 48 or 72 h (Fig. 8). Free batimastat showed no significant effect on cell viability at increasing concentration across all cell lines and treatment durations, suggesting that any cytotoxicity present is likely due to the vehicle and not batimastat itself. This is consistent with previous studies reporting similar findings in various cell types and viability assays [119–122]. Regarding the nanoparticle formulations, fNbat induced a significant decrease in cell viability across all timepoints and concentrations in all cell lines, except in U-87. With the fMbat formulation, the NHA cell line showed a decrease in viability only at the highest concentrations, particularly at the 72 h timepoint. In contrast, the U-87 cell line, which appeared more resistant than the others (as observed with fNbat), presented a slight decrease in viability initially, which became less noticeable over time. Moreover, fMbat appeared to have a more pronounced cytotoxic effect on the U-251 cell line than on the others cell lines, with a significant decrease in viability at concentrations above 5 nM. For the T98G cell line, fMbat induced a progressive, albeit small, increase in toxicity as concentrations increased.

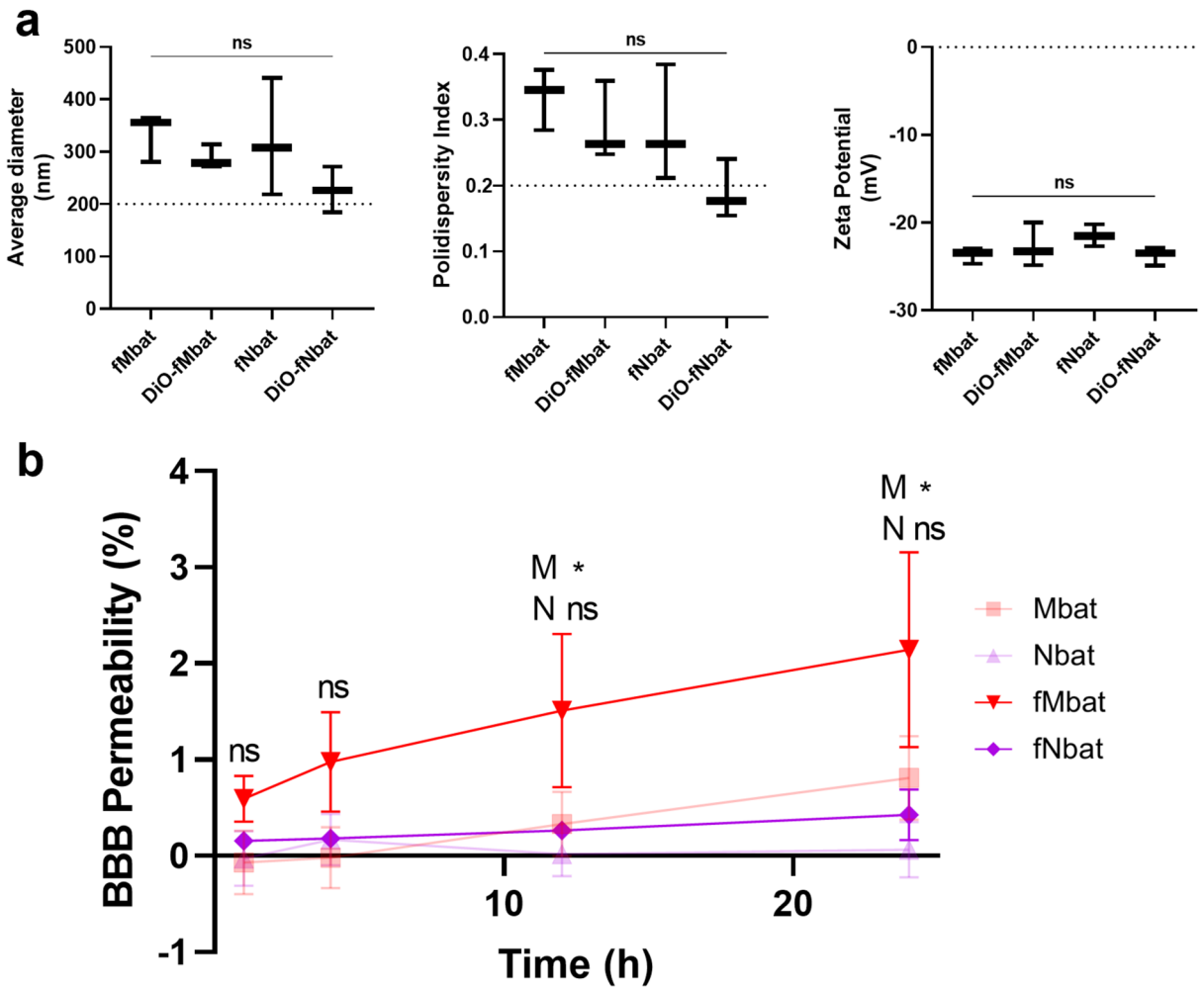

Fig. 7 BBB permeability of DiO-labeled functionalized NLC formulations compared to unfunctionalized DiO-NLCs and their physicochemical characterization. **a** Physicochemical characteristics of functionalized formulations fMbat and fNbat produced with and without DiO, measured with a Zetasizer. Results are shown as the mean ± SD of 3 independent characterizations and the dotted lines represent ideal characteristic benchmarks for BBB crossing, average size below 200 nm and PDI below 0.2. **b** Assessment of DiO-labeled NP transport across an in vitro BBB Transwell model over 24 h. Results are expressed as the percentage of NP mass that traversed a hCMEC/D3 endothelial cell monolayer to the basolateral compartment, relative to the initial NP mass in the apical chamber. Values represent the mean ± SD of 3 independent experiments. Statistical comparisons were made between each experimental group and the non-functionalized NP control counterpart. *$p < 0.05$

Lastly, the cytotoxicity profiles of fMbat and fNbat were evaluated in non-brain tissues, using liver HEPG2 cells and endothelial hCMEC/D3 cells. In HEPG2 cells, both formulations demonstrated a generally safe profile, with fNbat exhibiting a minor increase in cytotoxicity at 72 h (Fig. S3a). The endothelial hCMEC/D3 cells, however, showed different responses to the two formulations. fNbat displayed cytotoxicity starting at 48 h, which became more pronounced at 72 h, particularly at the 100 nM concentration. In contrast, fMbat maintained a safe profile up to 72 h, at which point some cytotoxic effects were observed (Fig. S3b). These results suggest that fMbat has a more favorable safety profile in non-brain tissues compared to fNbat.

The observed difference in cytotoxicity between the two formulations may be attributed to their surfactant content. fMbat contains twice the amount of surfactant compared to fNbat, which likely contributes to its increased stability. The lower surfactant content in fNbat may have led to faster degradation and potential destabilization of cell membranes. Despite the formulations differing only in surfactant amount and having a small disparity in functionalization efficiency, the substantial difference in cytotoxicity between the two formulations was unexpected. Based on these results, fMbat appears to be the better candidate for our therapeutic approach, as it demonstrated lower cytotoxicity, particularly in NHA cells, suggesting a potentially reduced risk of side effects. Nevertheless, while both formulations were designed to target GB cells, their effect on astrocytes became significant at higher concentrations

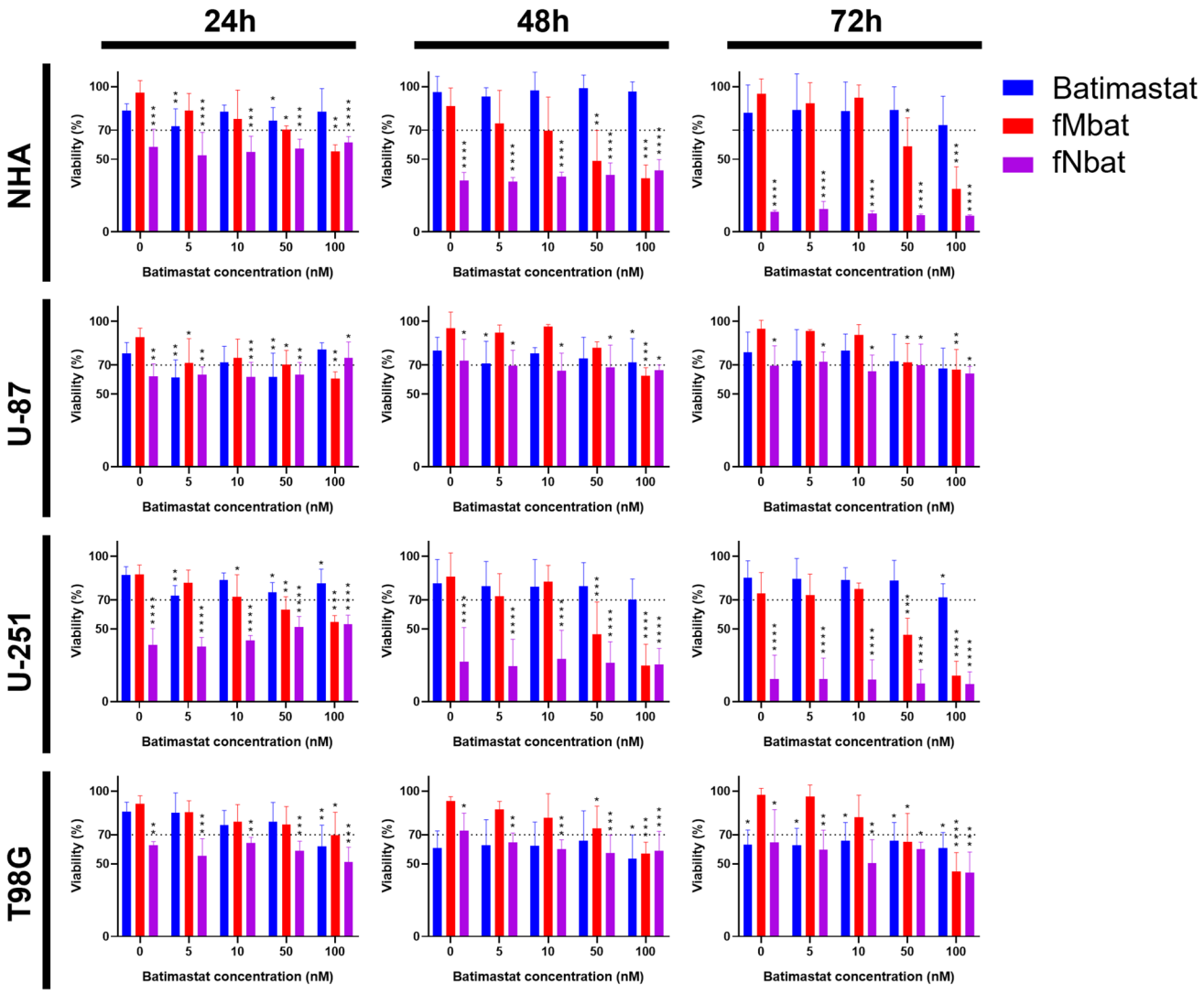

Fig. 8 Evaluation of the cell viability of NHA, U-87, U-251 and T98G cell lines following treatment with free batimastat, batimastat-loaded functionalized NLC M (fMbat) or batimastat-loaded functionalized NLC N (fNbat). Concentrations of 0 nM represent treatments with the empty NLCs fM and fN. Viability was analyzed with PrestoBlue™ assay at 24, 48 or 72 h and is represented as a percentage relative to cells treated with culture medium (untreated control). Results represent the mean ± SD of at least 3 independent experiments. Dotted line represents 70% of cell viability, the cytotoxicity benchmark referenced by the ISO 10993–5 (in vitro cytotoxicity test standardization for medical devices). Statistical comparisons were conducted between each experimental group and the untreated control. *$p < 0.05$, **$p < 0.01$, ***$p < 0.005$, ****$p < 0.001$

and this cannot be ignored. As such, to combine both a low cytotoxicity and a high MMP inhibitory potential, the 50 nM concentration of batimastat, which is ten-fold higher than its reported IC50 [94], was chosen to continue the in vitro assays.

NLC MMP inhibitory potential evaluation

The potential of the batimastat-loaded NPs to inhibit MMPs' activity was examined via gel zymography using the secretome of all cell lines tested. Initially, the basal levels of active MMPs, MMP-2 and MMP-9, was assessed in all 4 cell lines. Although several studies have shown MMPs expression on each of these cell lines [53], to the best of our knowledge, none of them presented a simultaneous comparative zymography between all the different cell types and GB cell lines. Nevertheless, some comparisons have determined the relative gelatinase secretion profile between some of them. Bao and colleagues reported that, as expected, U-87 cells secrete both MMP-2 and MMP-9 in much higher amounts than NHA cells [123]. In a different study, Liu et al. compared the U-251 and T98G cell lines, demonstrating that T98G cells produce MMP-2 at a higher concentration when compared to U-251. Nevertheless, the

U-251 cells secrete MMP-9 at much higher amounts, with analysis of T98G secretome staying below their zymography sensitivity limit [124]. More recently, Ferreira et al. compared the effects of cyclooxygenase inhibitors on U-251, U-87 and T98G cell lines, albeit only performing zymographies of the last two. They demonstrated that, despite having similar pro-MMP-2 activities, U-87 cells have much larger MMP-2 concentrations than T98G cells. Again, the authors were unable to detect any MMP-9 activity [125]. Lastly, Souza et al. were able to compare the U-87 and U-251 cell lines, finding that U-87 secretes much more active MMP-2 than U-251. Interestingly, they were also unable to observe any MMP-9 activity [126]. Therefore, from the available data in the literature, the order of active MMP-2 secretors is U-87 > T98G > U-251 > NHA, and T98G is, seemingly, the only cell line capable of secreting active MMP-9 in measurable quantities. Our results further support these findings (Fig. 9a). As expected, the NHA cell line presented an MMP-2 activity (62 kDa [127]) four-fold lower than the U-87 cell line, while the U-251 cell line was only 20% lower than U-87. Unexpectedly, T98G cells presented similar MMP activity to U-87 cells. Additionally, and also contrary to the literature, this cell line was the one with the most noticeable activity of MMP-9 (82 kDa [127]), as opposed to U-251. These discrepancies could be attributed to inherent variability in cell line behavior [128], potentially influenced by factors such as differences in experimental conditions, culture protocols, or intrinsic cellular heterogeneity.

Regarding the effect of the developed NLC formulations on these cell lines (Fig. 9b and Fig. 9c), we observed that the unloaded N formulation led to an overall MMP-2 inhibition in all cell lines: 25% for NHA, 14% for U-87,

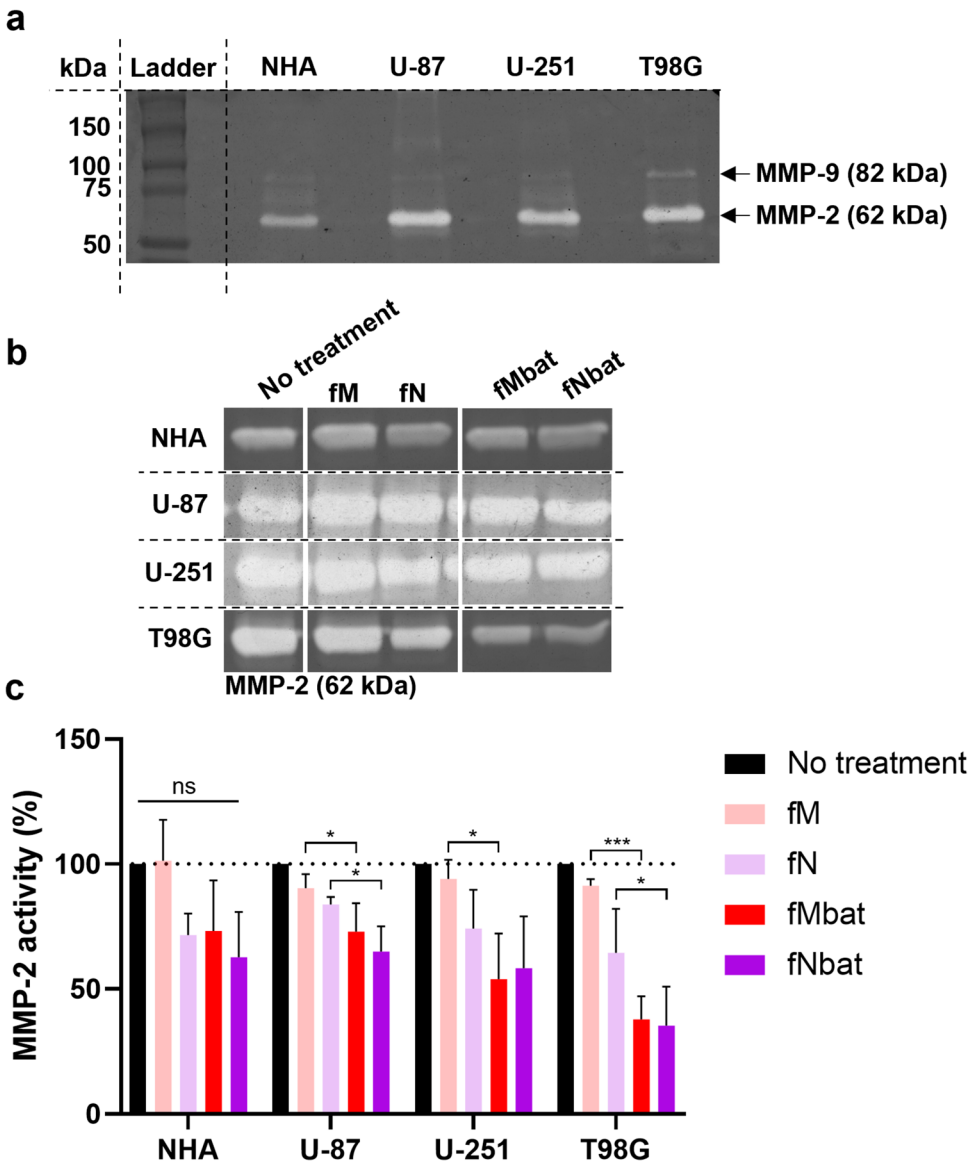

Fig. 9 Assessment of MMP-2 and MMP-9 activity and their inhibition by the NPs on NHA, U-87, U-251 and T98G cell lines, evaluated by gelatin zymography. **a** Relative gelatinase activity between the concentrated secretomes. **b** MMP-2 activity on concentrated secretomes collected from all the cell lines following treatment with complete media (positive control), empty functionalized NLCs, fM and fN, and batimastat-loaded functionalized NLCs, fMbat and fNbat. **c** Densitometry analysis of the gel bands in (b). Density is shown as a percentage relative to the untreated control. The results represent the mean ± SD of 3 independent experiments. Statistical comparisons were made between each experimental group and the empty NP counterpart. *$p < 0.05$, ***$p < 0.005$

19% for U-251 and 41% for T98G. This inhibition could be due to the previously observed cytotoxicity, which may lead to increased cell death and a higher presence of non-proteolytic proteins in the secretomes. As all samples were normalized for total protein content, the secretomes contained a relatively lower percentage of MMPs. In contrast, the batimastat-loaded M formulations achieved a higher MMP-2 inhibition of: 32% in NHA, 11% in U-87, 27% in U-251 and 62% in T98G. Although, this increased efficacy could be associated with higher drug loadings, the fact that the encapsulation efficiency of M and N formulations was nearly identical might indicate that the enhanced effect of the M formulation is more likely due to its improved stability and controlled release. [129]. We could also observe that the NHA and U-87 cell lines showed the least effect of the NLC formulations. For U-87, the higher overall MMP activity may dilute the effect that this concentration of batimastat can provide. To overcome this limitation, the NPs would need to be loaded with a higher amount of the inhibitor, as the 50 nM utilized was evidently not enough to overcome the MMP activity and an increase in NLC concentration is impractical due to the consequent increase in cytotoxicity. Regarding NHA, while literature on batimastat's effect is scarce, Ulasov and colleagues showed that marimastat, a similar compound, presented an MMP inhibitory and growth inhibiting effect on U-87 and U-251 but did not affect NHA cells [130]. Similarly, Alves et al. found that batimastat had the same inhibiting effect on models of hematological tumors, which could indicate that it may also possesses the same lower efficiency on the NHA cell line [131].

Interestingly, T98G appears to have a particularly high sensitivity to batimastat. Since, to the best of our knowledge, there are no previous studies on batimastat's effect on T98G cells, this is a promising avenue for further mechanistic research. It is, however, important to note that the MMP activity profile of T98G cells observed in this work was slightly different from the previously reported behaviors [124, 125].

Conclusions

In this study, dual-functionalized NLCs for the delivery of the MMP inhibitor batimastat to GB were developed. The molecular construct, a pegylated MMP-14-cleavable transferrin mimicking molecule, was successfully synthesized and purified with high efficiency. Two NLC formulations, fMbat and fNbat, were produced with physicochemical parameters suitable for a GB therapy, namely a very negative and slightly polydisperse suspension averaging 300 nm, loaded with batimastat at concentrations 1000-fold higher than its reported IC50 and covered with a mixture of EGF and the developed molecular construct. In vitro assays to evaluate the effect of both formulations in different GB cell lines and a non-tumoral astrocytic cell line demonstrated a schism between the two nanodispersions. On the one hand, formulation fNbat was shown to be cytotoxic on all tested cell lines and, disappointingly, presented no BBB permeability. On the other hand, formulation fMbat showed great potential owning to: i) the demonstrated cytocompatibility at concentrations 10 times higher than their load's IC50, ii) MMP-2 inhibition ranging from 11 to 62%, and iii) three-fold improved BBB crossing comparing to its unfunctionalized counterpart. Overall, the nanosystem here developed targeting the GB tumor microenvironment holds great promise in GB therapy. Moreover, it may offer the potential to be further combined with other strategies to improve treatment outcomes. Theranostifying fMbat through the co-encapsulation of superparamagnetic iron oxide nanoparticles (SPIONs) would further provide both imaging and hyperthermia capabilities, while combination with other molecules, cytotoxic or cytostatic, will potentially create more effective ways to attack GB and its microenvironment. Future work will explore this nanosystem's potential in vivo, using animal models, regarding its BBB penetration effectiveness, biodistribution and tumor invasiveness inhibition.

Finally, it is important to highlight the versatility of the functionalization strategy herein described – while it is proving promisingly effective for GB invasiveness hampering, they can also be useful as carriers for other compounds, such as chemo-, photo- or immunotherapeutics, targeting the GB microenvironment.

Supplementary Information The online version contains supplementary material available at https://doi.org/10.1007/s13346-024-01775-8.

Acknowledgements This work was supported by FCT—Fundação para a Ciência e a Tecnologia in the framework of the PhD grant of Miguel Horta (2020.10014.BD). This research was partly supported by the project "Institute for Research and Innovation in Health Sciences" (UID/BIM/04293/2019) and the project "The Porto Comprehensive Cancer Center" ref. NORTE-01-0145-FEDER-072678—Consórcio PORTO.CCC—Porto. Comprehensive Cancer Center Raquel Seruca. The funders had no role in the study design, data collection, analysis, publication decision, or manuscript preparation. The authors would also like to extend their acknowledgements to the i3S Scientific Platforms Histology and Electron Microscopy (HEMS), Biochemical and Biophysical Technologies (b2Tech), and Biointerfaces and Nanotechnology (BN). Centro de Materiais da Universidade do Porto (CEMUP), particularly Mariana Andrade, is also acknowledged for the 1H-NMR analysis. Lastly, the authors acknowledge the assistance of Instituto de Investigação em Ciências da Vida e Saúde (ICVS) for providing the non-tumor astrocytic cell line, and Instituto Superior Técnico (IST) for gifting the T98G cell line.

Author's contributions MH, PS, CLP and RTL contributed to the study conception and design. Material preparation, method validation, data collection and data analysis were performed by MH, CLP and RTL. The original draft of the manuscript was written by MH, CLP and RTL, and all authors reviewed and edited previous versions of the manuscript. The work was supervised by CLP and RTL. Funding and resources were acquired by PS, BS, CLP and RTL. All authors have read and approved the final manuscript.

Funding This work was financed by Fundação para a Ciência e Tecnologia (FCT) with the PhD Grant 2020.10014.BD. This research was partly supported by the project "Institute for Research and Innovation in Health Sciences" (UID/BIM/04293/2019) and the project "The Porto Comprehensive Cancer Center" ref. NORTE-01–0145-FEDER-072678—Consórcio PORTO.CCC—Porto. Comprehensive Cancer Center Raquel Seruca.

Data availability All data generated or analysed during this study are included in this publication and its supplementary information files.

Declarations

Competing interests The authors have no relevant financial or non-financial interests to disclose.

References

1. Rajaratnam V, et al. Glioblastoma: Pathogenesis and Current Status of Chemotherapy and Other Novel Treatments. Cancers. 2020;12(4):937. https://doi.org/10.3390/cancers12040937.
2. Jezierzański M, et al. Temozolomide (TMZ) in the Treatment of Glioblastoma Multiforme—A Literature Review and Clinical Outcomes. Curr Oncol. 2024;31(7):3994–4002. https://doi.org/10.3390/curroncol31070296.
3. Davis ME. Glioblastoma: Overview of Disease and Treatment. Clin J Oncol Nurs. 2016;20(5 Suppl):S2-8. https://doi.org/10.1188/16.CJON.S1.2-8.
4. Martins C, et al. Glioblastoma immuno-endothelial multicellular microtissue as a 3D in vitro evaluation tool of anti-cancer nanotherapeutics. J Control Release. 2023;353:77–95. https://doi.org/10.1016/j.jconrel.2022.11.024.
5. Zhao M, et al. Nanocarrier-based drug combination therapy for glioblastoma. Theranostics. 2020;10(3):1355–72. https://doi.org/10.7150/thno.38147.
6. Shergalis A, et al. Current Challenges and Opportunities in Treating Glioblastoma. Pharmacol Rev. 2018;70(3):412–45. https://doi.org/10.1124/pr.117.014944.
7. Serlin Y, et al. Anatomy and physiology of the blood-brain barrier. Semin Cell Dev Biol. 2015;38:2–6. https://doi.org/10.1016/j.semcdb.2015.01.002.
8. Daneman R, Prat A. The blood-brain barrier. Cold Spring Harb Perspect Biol. 2015;7(1): a020412. https://doi.org/10.1101/cshperspect.a020412.
9. Dixit S, et al. Transferrin receptor-targeted theranostic gold nanoparticles for photosensitizer delivery in brain tumors. Nanoscale. 2015;7(5):1782–90. https://doi.org/10.1039/c4nr04853a.
10. Ulbrich K, Knobloch T, Kreuter J. Targeting the insulin receptor: nanoparticles for drug delivery across the blood-brain barrier (BBB). J Drug Target. 2011;19(2):125–32. https://doi.org/10.3109/10611861003734001.
11. Zhang B, et al. LDLR-mediated peptide-22-conjugated nanoparticles for dual-targeting therapy of brain glioma. Biomaterials. 2013;34(36):9171–82. https://doi.org/10.1016/j.biomaterials.2013.08.039.
12. Tosi G, et al. Can leptin-derived sequence-modified nanoparticles be suitable tools for brain delivery? Nanomedicine (Lond). 2012;7(3):365–82. https://doi.org/10.2217/nnm.11.98.
13. You L, et al. Targeted Brain Delivery of Rabies Virus Glycoprotein 29-Modified Deferoxamine-Loaded Nanoparticles Reverses Functional Deficits in Parkinsonian Mice. ACS Nano. 2018;12(5):4123–39. https://doi.org/10.1021/acsnano.7b08172.
14. Gaillard PJ, et al. Enhanced brain drug delivery: safely crossing the blood-brain barrier. Drug Discov Today Technol. 2012;9(2):e71–174. https://doi.org/10.1016/j.ddtec.2011.12.002.
15. Ashizawa AT, Steindler D. Et-61 * Novel Lipid Nanoparticles for the Delivery of Nucleic Acids to Glioblastoma. Neuro Oncol. 2014;16(suppl 5):v92–v92. https://doi.org/10.1093/neuonc/nou255.58.
16. Gromnicova R, et al. Glucose-coated gold nanoparticles transfer across human brain endothelium and enter astrocytes in vitro. PLoS ONE. 2013;8(12): e81043. https://doi.org/10.1371/journal.pone.0081043.
17. Gomes MJ, et al. Delivery of siRNA silencing P-gp in peptide-functionalized nanoparticles causes efflux modulation at the blood-brain barrier. Nanomedicine (Lond). 2017;12(12):1385–99. https://doi.org/10.2217/nnm-2017-0023.
18. ter Linden E, et al. Overcoming Barriers in Glioblastoma—Advances in Drug Delivery Strategies. Cells. 2024;13(12):998. https://doi.org/10.3390/cells13120998.
19. Janjua TI, et al. Frontiers in the treatment of glioblastoma: Past, present and emerging. Adv Drug Deliv Rev. 2021;171:108–38. https://doi.org/10.1016/j.addr.2021.01.012.
20. Gregory JV, et al. Systemic brain tumor delivery of synthetic protein nanoparticles for glioblastoma therapy. Nat Commun. 2020;11(1):5687. https://doi.org/10.1038/s41467-020-19225-7.
21. He Z, et al. A Catalase-Like Metal-Organic Framework Nanohybrid for O(2) -Evolving Synergistic Chemoradiotherapy. Angew Chem Int Ed Engl. 2019;58(26):8752–6. https://doi.org/10.1002/anie.201902612.
22. Zhang H, et al. Second near-infrared photodynamic therapy and chemotherapy of orthotopic malignant glioblastoma with ultrasmall Cu(2–x)Se nanoparticles. Nanoscale. 2019;11(16):7600–8. https://doi.org/10.1039/c9nr01789e.
23. Zhu P, Chen Y, Shi J. Nanoenzyme-Augmented Cancer Sonodynamic Therapy by Catalytic Tumor Oxygenation. ACS Nano. 2018;12(4):3780–95. https://doi.org/10.1021/acsnano.8b00999.
24. Bhattarai SR, et al. Gold nanotriangles: scale up and X-ray radiosensitization effects in mice. Nanoscale. 2017;9(16):5085–93. https://doi.org/10.1039/c6nr08172j.
25. Kadiyala P, et al. High-Density Lipoprotein-Mimicking Nanodiscs for Chemo-immunotherapy against Glioblastoma Multiforme. ACS Nano. 2019;13(2):1365–84. https://doi.org/10.1021/acsnano.8b06842.
26. Jiang H, et al. Silver nanocrystals mediated combination therapy of radiation with magnetic hyperthermia on glioma cells. J Nanosci Nanotechnol. 2012;12(11):8276–81. https://doi.org/10.1166/jnn.2012.6626.
27. Dadfar SM, et al. Iron oxide nanoparticles: Diagnostic, therapeutic and theranostic applications. Adv Drug Deliv Rev. 2019;138:302–25. https://doi.org/10.1016/j.addr.2019.01.005.
28. Gao Z, et al. Polypeptide-Based Theranostics with Tumor-Microenvironment-Activatable Cascade Reaction for Chemoferroptosis Combination Therapy. ACS Appl Mater Interfaces. 2020;12(18):20271–80. https://doi.org/10.1021/acsami.0c03748.
29. Kumthekar P, et al. A first-in-human phase 0 clinical study of RNA interference-based spherical nucleic acids in patients with recurrent glioblastoma. Sci Transl Med. 2021;13(584):eabb3945. https://doi.org/10.1126/scitranslmed.abb3945.
30. Beier CP, et al. RNOP-09: pegylated liposomal doxorubicine and prolonged temozolomide in addition to radiotherapy in newly diagnosed glioblastoma–a phase II study. BMC Cancer. 2009;9:308. https://doi.org/10.1186/1471-2407-9-308.
31. Maier-Hauff K, et al. Efficacy and safety of intratumoral thermotherapy using magnetic iron-oxide nanoparticles combined with external beam radiotherapy on patients with recurrent glioblastoma multiforme. J Neurooncol. 2011;103(2):317–24. https://doi.org/10.1007/s11060-010-0389-0.

32. Rodríguez F, et al. Nano-Based Approved Pharmaceuticals for Cancer Treatment: Present and Future Challenges. Biomolecules. 2022;12(6):784. https://doi.org/10.3390/biom12060784.
33. Song S, et al. Novel RGD containing, temozolomide-loading nanostructured lipid carriers for glioblastoma multiforme chemotherapy. Drug Deliv. 2016;23(4):1404–8. https://doi.org/10.3109/10717544.2015.1064186.
34. Chen Y, et al. Nanostructured lipid carriers enhance the bioavailability and brain cancer inhibitory efficacy of curcumin both in vitro and in vivo. Drug Deliv. 2016;23(4):1383–92. https://doi.org/10.3109/10717544.2015.1049719.
35 Khan S, Sharma A, Jain V. An Overview of Nanostructured Lipid Carriers and its Application in Drug Delivery through Different Routes. Adv Pharm Bull. 2023;13(3):446–60. https://doi.org/10.34172/apb.2023.056.
36. Mura P, et al. Evaluation and Comparison of Solid Lipid Nanoparticles (SLNs) and Nanostructured Lipid Carriers (NLCs) as Vectors to Develop Hydrochlorothiazide Effective and Safe Pediatric Oral Liquid Formulations. Pharmaceutics. 2021;13(4):437. https://doi.org/10.3390/pharmaceutics13040437.
37. Zwain T, et al. Tailoring functional nanostructured lipid carriers for glioblastoma treatment with enhanced permeability through in-vitro 3D BBB/BBTB models. Mater Sci Eng C Mater Biol Appl. 2021;121: 111774. https://doi.org/10.1016/j.msec.2020.111774.
38. Di Filippo LD, et al. Glioblastoma multiforme targeted delivery of docetaxel using bevacizumab-modified nanostructured lipid carriers impair in vitro cell growth and in vivo tumor progression. Int J Pharm. 2022;618: 121682. https://doi.org/10.1016/j.ijpharm.2022.121682.
39. Zhou Z, Sun T, Jiang C. Recent advances on drug delivery nanocarriers for cerebral disorders. Biomed Mater. 2021;16(2):024104. https://doi.org/10.1088/1748-605X/abdc97.
40. Shirazi AS, et al. SN38 loaded nanostructured lipid carriers (NLCs); preparation and in vitro evaluations against glioblastoma. J Mater Sci Mater Med. 2021;32(7):78. https://doi.org/10.1007/s10856-021-06538-2.
41. Demuth T, Berens ME. Molecular mechanisms of glioma cell migration and invasion. J Neurooncol. 2004;70(2):217–28. https://doi.org/10.1007/s11060-004-2751-6.
42. Hatoum A, Mohammed R, Zakieh O. The unique invasiveness of glioblastoma and possible drug targets on extracellular matrix. Cancer Manag Res. 2019;11:1843–55. https://doi.org/10.2147/CMAR.S186142.
43. Gan HK, Cvrljevic AN, Johns TG. The epidermal growth factor receptor variant III (EGFRvIII): where wild things are altered. FEBS J. 2013;280(21):5350–70. https://doi.org/10.1111/febs.12393.
44 Wee P, Wang Z. Epidermal Growth Factor Receptor Cell Proliferation Signaling Pathways. Cancers. 2017;9(5):52. https://doi.org/10.3390/cancers9050052.
45. Paw I, et al. Mechanisms regulating glioma invasion. Cancer Lett. 2015;362(1):1–7. https://doi.org/10.1016/j.canlet.2015.03.015.
46. Saadeh FS, Mahfouz R, Assi HI. EGFR as a clinical marker in glioblastomas and other gliomas. Int J Biol Markers. 2018;33(1):22–32. https://doi.org/10.5301/ijbm.5000301.
47. Li J, et al. Prognostic significance of epidermal growth factor receptor expression in glioma patients. Onco Targets Ther. 2018;11:731–42. https://doi.org/10.2147/OTT.S155160.
48. Rutkowska A, et al. EGFR(vIII): An Oncogene with Ambiguous Role. J Oncol. 2019;2019:1092587. https://doi.org/10.1155/2019/1092587.
49. Sareen H, et al. Molecular Biomarkers in Glioblastoma: A Systematic Review and Meta-Analysis. Int J Mol Sci. 2022;23(16):8835. https://doi.org/10.3390/ijms23168835.
50. Maya S, et al. Chitosan cross-linked docetaxel loaded EGF receptor targeted nanoparticles for lung cancer cells. Int J Biol Macromol. 2014;69:532–41. https://doi.org/10.1016/j.ijbiomac.2014.06.009.
51. Xu W, et al. Combination of an anti-EGFRvIII antibody CH12 with Rapamycin synergistically inhibits the growth of EGFRvIII+PTEN-glioblastoma in vivo. Oncotarget. 2016;7(17):24752–65. https://doi.org/10.18632/oncotarget.8407.
52. de Almeida LGN, et al. Matrix Metalloproteinases: From Molecular Mechanisms to Physiology, Pathophysiology, and Pharmacology. Pharmacol Rev. 2022;74(3):714–70. https://doi.org/10.1124/pharmrev.121.000349.
53. Hagemann C, et al. A complete compilation of matrix metalloproteinase expression in human malignant gliomas. World J Clin Oncol. 2012;3(5):67–79. https://doi.org/10.5306/wjco.v3.i5.67.
54. Rao JS. Molecular mechanisms of glioma invasiveness: the role of proteases. Nat Rev Cancer. 2003;3(7):489–501. https://doi.org/10.1038/nrc1121.
55. Xue Q, et al. High expression of MMP9 in glioma affects cell proliferation and is associated with patient survival rates. Oncol Lett. 2017;13(3):1325–30. https://doi.org/10.3892/ol.2017.5567.
56. Ramachandran RK, et al. Expression and prognostic impact of matrix metalloproteinase-2 (MMP-2) in astrocytomas. PLoS ONE. 2017;12(2): e0172234. https://doi.org/10.1371/journal.pone.0172234.
57. Conlon GA, Murray GI. Recent advances in understanding the roles of matrix metalloproteinases in tumour invasion and metastasis. J Pathol. 2019;247(5):629–40. https://doi.org/10.1002/path.5225.
58. Erices JI, et al. Glioblastoma Microenvironment and Invasiveness: New Insights and Therapeutic Targets. Int J Mol Sci. 2023;24(8):7047.
59 Munaut C, et al. Vascular endothelial growth factor expression correlates with matrix metalloproteinases MT1-MMP, MMP-2 and MMP-9 in human glioblastomas. Int J Cancer J Int du Cancer. 2003;106(6):848–55. https://doi.org/10.1002/ijc.11313.
60 Thome I, et al. Neoplastic Cells are the Major Source of MT-MMPs in IDH1-Mutant Glioma, Thus Enhancing Tumor-Cell Intrinsic Brain Infiltration. Cancers. 2020;12(9):2456. https://doi.org/10.3390/cancers12092456.
61. Mohanty S, et al. A Novel Theranostic Strategy for MMP-14-Expressing Glioblastomas Impacts Survival. Mol Cancer Ther. 2017;16(9):1909–21. https://doi.org/10.1158/1535-7163.MCT-17-0022.
62. Kasten BB, et al. Targeting MMP-14 for dual PET and fluorescence imaging of glioma in preclinical models. Eur J Nucl Med Mol Imaging. 2020;47(6):1412–26. https://doi.org/10.1007/s00259-019-04607-x.
63. Levin VA, et al. Randomized, double-blind, placebo-controlled trial of marimastat in glioblastoma multiforme patients following surgery and irradiation. J Neurooncol. 2006;78(3):295–302. https://doi.org/10.1007/s11060-005-9098-5.
64. Groves MD, et al. Phase II trial of temozolomide plus the matrix metalloproteinase inhibitor, marimastat, in recurrent and progressive glioblastoma multiforme. J Clin Oncol. 2002;20(5):1383–8. https://doi.org/10.1200/JCO.2002.20.5.1383.
65. Parsons SL, Watson SA, Steele RJ. Phase I/II trial of batimastat, a matrix metalloproteinase inhibitor, in patients with malignant ascites. Eur J Surg Oncol. 1997;23(6):526–31. https://doi.org/10.1016/s0748-7983(97)93077-8.
66. Brown PD. Matrix metalloproteinase inhibitors in the treatment of cancer. Med Oncol. 1997;14(1):1–10. https://doi.org/10.1007/BF02990939.
67. Mannello F, Tonti G, Papa S. Matrix metalloproteinase inhibitors as anticancer therapeutics. Curr Cancer Drug Targets. 2005;5(4):285–98. https://doi.org/10.2174/1568009054064615.
68. Boguszewska-Czubara A, et al. Perspectives and New Aspects of Metalloproteinases' Inhibitors in the Therapy of CNS

Disorders: From Chemistry to Medicine. Curr Med Chem. 2019;26(18):3208–24. https://doi.org/10.2174/0929867325666180514111500.
69. Pijet B, et al. The matrix metalloproteinase inhibitor marimastat inhibits seizures in a model of kainic acid-induced status epilepticus. Sci Rep. 2020;10(1):21314. https://doi.org/10.1038/s41598-020-78341-y.
70. Mentlein R, Hattermann K, Held-Feindt J. Lost in disruption: role of proteases in glioma invasion and progression. Biochem Biophys Acta. 2012;1825(2):178–85. https://doi.org/10.1016/j.bbcan.2011.12.001.
71 Cathcart J, Pulkoski-Gross A, Cao J. Targeting Matrix Metalloproteinases in Cancer: Bringing New Life to Old Ideas. Genes Dis. 2015;2(1):26–34. https://doi.org/10.1016/j.gendis.2014.12.002.
72. Quesnel A, Karagiannis GS, Filippou PS. Extracellular proteolysis in glioblastoma progression and therapeutics. Biochim Biophys Acta Rev Cancer. 2020;1874(2): 188428. https://doi.org/10.1016/j.bbcan.2020.188428.
73. Sehedic D, et al. Locoregional Confinement and Major Clinical Benefit of (188)Re-Loaded CXCR4-Targeted Nanocarriers in an Orthotopic Human to Mouse Model of Glioblastoma. Theranostics. 2017;7(18):4517–36. https://doi.org/10.7150/thno.19403.
74. Martins C, et al. Stimuli-Responsive Multifunctional Nanomedicine for Enhanced Glioblastoma Chemotherapy Augments Multistage Blood-to-Brain Trafficking and Tumor Targeting. Small. 2023;19(22): e2300029. https://doi.org/10.1002/smll.202300029.
75. Esfandyari-Manesh M, et al. S2P peptide-conjugated PLGA-Maleimide-PEG nanoparticles containing Imatinib for targeting drug delivery to atherosclerotic plaques. Daru. 2020;28(1):131–8. https://doi.org/10.1007/s40199-019-00324-w.
76. Kebebe D, et al. Dimeric c(RGD) peptide conjugated nanostructured lipid carriers for efficient delivery of Gambogic acid to breast cancer. Int J Nanomed. 2019;14:6179–95. https://doi.org/10.2147/IJN.S202424.
77. Gao L, et al. Tumor-penetrating Peptide Conjugated and Doxorubicin Loaded T(1)-T(2) Dual Mode MRI Contrast Agents Nanoparticles for Tumor Theranostics. Theranostics. 2018;8(1):92–108. https://doi.org/10.7150/thno.21074.
78. Smith PK, et al. Measurement of protein using bicinchoninic acid. Anal Biochem. 1985;150(1):76–85. https://doi.org/10.1016/0003-2697(85)90442-7.
79. Ferreira M, et al. Optimization of nanostructured lipid carriers loaded with methotrexate: A tool for inflammatory and cancer therapy. Int J Pharm. 2015;492(1–2):65–72. https://doi.org/10.1016/j.ijpharm.2015.07.013.
80. Udenfriend S, et al. Fluorescamine: A Reagent for Assay of Amino Acids, Peptides, Proteins, and Primary Amines in the Picomole Range. Science (New York, N.Y.), 1972. 178(4063): p. 871–872. https://doi.org/10.1126/science.178.4063.871
81. Cao Z, et al. Bioorthogonal in situ assembly of nanomedicines as drug depots for extracellular drug delivery. Nat Commun. 2022;13(1):2038. https://doi.org/10.1038/s41467-022-29693-8.
82. Morton RE, Evans TA. Modification of the bicinchoninic acid protein assay to eliminate lipid interference in determining lipoprotein protein content. Anal Biochem. 1992;204(2):332–4. https://doi.org/10.1016/0003-2697(92)90248-6.
83. Peixoto J, et al. Using a Dual CRISPR/Cas9 Approach to Gain Insight into the Role of LRP1B in Glioblastoma. Int J Mol Sci. 2023;24(14):11285. https://doi.org/10.3390/ijms241411285.
84. Ferreira LB, et al. Osteopontin-a splice variant is overexpressed in papillary thyroid carcinoma and modulates invasive behavior. Oncotarget. 2016;7(32):52003–16. https://doi.org/10.18632/oncotarget.10468.
85. Cardoso AP, et al. Macrophages stimulate gastric and colorectal cancer invasion through EGFR Y1086, c-Src, Erk1/2 and Akt phosphorylation and smallGTPase activity. Oncogene. 2014;33(16):2123–33. https://doi.org/10.1038/onc.2013.154.
86. Martinez-Jothar L, et al. Insights into maleimide-thiol conjugation chemistry: Conditions for efficient surface functionalization of nanoparticles for receptor targeting. J Control Release. 2018;282:101–9. https://doi.org/10.1016/j.jconrel.2018.03.002.
87. Van Koninckxloo A, et al. NMR chemical shift study of the interaction of selected peptides with liposomal and micellar models of apoptotic cells. J Biol Inorg Chem. 2014;19(8):1367–76. https://doi.org/10.1007/s00775-014-1195-5.
88. Kumar S, Hause G, Binder WH. Thio-Bromo "Click" Reaction Derived Polymer-Peptide Conjugates for Their Self-Assembled Fibrillar Nanostructures. Macromol Biosci. 2020;20(6): e2000048. https://doi.org/10.1002/mabi.202000048.
89. Gurer F, et al. Water-based carbodiimide mediated synthesis of polysaccharide-amino acid conjugates: Deprotection, charge and structural analysis. Carbohyd Polym. 2021;267: 118226. https://doi.org/10.1016/j.carbpol.2021.118226.
90. Wickramathilaka MP, Tao BY. Characterization of covalent crosslinking strategies for synthesizing DNA-based bioconjugates. J Biol Eng. 2019;13(1):63. https://doi.org/10.1186/s13036-019-0191-2.
91. Danaei M, et al. Impact of Particle Size and Polydispersity Index on the Clinical Applications of Lipidic Nanocarrier Systems. Pharmaceutics. 2018;10(2):57. https://doi.org/10.3390/pharmaceutics10020057.
92. Furtado D, et al. Overcoming the Blood-Brain Barrier: The Role of Nanomaterials in Treating Neurological Diseases. Adv Mater. 2018;30(46):1801362. https://doi.org/10.1002/adma.201801362.
93. Doane TL, et al. Nanoparticle zeta -potentials. Acc Chem Res. 2012;45(3):317–26. https://doi.org/10.1021/ar200113c.
94. Chang M. Matrix metalloproteinase profiling and their roles in disease. RSC Adv. 2023;13(9):6304–16. https://doi.org/10.1039/d2ra07005g.
95. Anchan A, et al. Melanoma Mediated Disruption of Brain Endothelial Barrier Integrity Is Not Prevented by the Inhibition of Matrix Metalloproteinases and Proteases. Biosensors (Basel). 2022;12(8):660. https://doi.org/10.3390/bios12080660.
96. Nosoudi N, et al. Prevention of abdominal aortic aneurysm progression by targeted inhibition of matrix metalloproteinase activity with batimastat-loaded nanoparticles. Circ Res. 2015;117(11):e80–9. https://doi.org/10.1161/CIRCRESAHA.115.307207.
97. Zhang K, et al. Dual Targeting of Cancer Cells and MMPs with Self-Assembly Hybrid Nanoparticles for Combination Therapy in Combating Cancer. Pharmaceutics. 2021;13(12):1990. https://doi.org/10.3390/pharmaceutics13121990.
98. Marques AC, et al. Functionalizing nanoparticles with cancer-targeting antibodies: A comparison of strategies. J Control Release. 2020;320:180–200. https://doi.org/10.1016/j.jconrel.2020.01.035.
99. Han Y, et al. Transferrin-modified nanostructured lipid carriers as multifunctional nanomedicine for codelivery of DNA and doxorubicin. Int J Nanomed. 2014;9:4107–16. https://doi.org/10.2147/ijn.S67770.
100. Moura RP, et al. Functionalized retinoic acid lipid nanocapsules promotes a two-front attack on inflammation and lack of demyelination on neurodegenerative disorders. J Control Release. 2023;358:43–58. https://doi.org/10.1016/j.jconrel.2023.04.034.
101. Cho W-S, et al. Surface functionalization affects the zeta potential, coronal stability and membranolytic activity of polymeric nanoparticles. Nanotoxicology. 2014;8(2):202–11. https://doi.org/10.3109/17435390.2013.773465.
102. Du J, Li L. Which one performs better for targeted lung cancer combination therapy: pre- or post-bombesin-decorated

nanostructured lipid carriers? Drug Delivery. 2016;23(5):1799–809. https://doi.org/10.3109/10717544.2015.1099058.
103. Teixeira MI, et al. Formulation, Characterization, and Cytotoxicity Evaluation of Lactoferrin Functionalized Lipid Nanoparticles for Riluzole Delivery to the Brain. Pharmaceutics. 2022;14(1):185. https://doi.org/10.3390/pharmaceutics14010185.
104. Muller RH, Radtke M, Wissing SA. Solid lipid nanoparticles (SLN) and nanostructured lipid carriers (NLC) in cosmetic and dermatological preparations. Adv Drug Deliv Rev. 2002;54(Suppl 1):S131–55. https://doi.org/10.1016/s0169-409x(02)00118-7.
105 Azhar Shekoufeh Bahari L, Hamishehkar H. The Impact of Variables on Particle Size of Solid Lipid Nanoparticles and Nanostructured Lipid Carriers; A Comparative Literature Review. Adv Pharm Bull. 2016;6(2):143–51. https://doi.org/10.15171/apb.2016.021.
106. Weksler B, Romero IA, Couraud P-O. The hCMEC/D3 cell line as a model of the human blood brain barrier. Fluids Barriers CNS. 2013;10(1):16. https://doi.org/10.1186/2045-8118-10-16.
107. Chaulagain B, et al. Experimental Models of In Vitro Blood-Brain Barrier for CNS Drug Delivery: An Evolutionary Perspective. Int J Mol Sci. 2023;24(3):2710. https://doi.org/10.3390/ijms24032710.
108. de Barros DPC, et al. Design of Quercetin-Loaded Natural Oil-Based Nanostructured Lipid Carriers for the Treatment of Bacterial Skin Infections. Molecules (Basel, Switzerland). 2022;27(24):8818. https://doi.org/10.3390/molecules27248818.
109 Thomsen MS, et al. Blood-Brain Barrier Transport of Transferrin Receptor-Targeted Nanoparticles. Pharmaceutics. 2022;14(10):2237. https://doi.org/10.3390/pharmaceutics14102237.
110. Beard R, et al. Chemical biology tools for probing transcytosis at the blood–brain barrier. Chem Sci. 2019;10(46):10772–8. https://doi.org/10.1039/C9SC04024B.
111. Johnsen KB, et al. Targeting the transferrin receptor for brain drug delivery. Prog Neurobiol. 2019;181: 101665. https://doi.org/10.1016/j.pneurobio.2019.101665.
112. Gomes MJ, et al. Tailoring Lipid and Polymeric Nanoparticles as siRNA Carriers towards the Blood-Brain Barrier - from Targeting to Safe Administration. J Neuroimmune Pharmacol. 2017;12(1):107–19. https://doi.org/10.1007/s11481-016-9685-6.
113. Perrin SL, et al. Glioblastoma heterogeneity and the tumour microenvironment: implications for preclinical research and development of new treatments. Biochem Soc Trans. 2019;47(2):625–38. https://doi.org/10.1042/BST20180444.
114. Hagemann C, et al. Comparative expression pattern of Matrix-Metalloproteinases in human glioblastoma cell-lines and primary cultures. BMC Res Notes. 2010;3:293. https://doi.org/10.1186/1756-0500-3-293.
115. Li H, et al. Differences in Protein Expression between the U251 and U87 Cell Lines. Turk Neurosurg. 2017;27(6):894–903. https://doi.org/10.5137/1019-5149.JTN.17746-16.1.
116. Motaln H, et al. Heterogeneous glioblastoma cell cross-talk promotes phenotype alterations and enhanced drug resistance. Oncotarget. 2015;6(38):40998–1017. https://doi.org/10.18632/oncotarget.5701.
117. Eldridge BN, et al. Photothermal therapy of glioblastoma multiforme using multiwalled carbon nanotubes optimized for diffusion in extracellular space. ACS Biomater Sci Eng. 2016;2(6):963–76. https://doi.org/10.1021/acsbiomaterials.6b00052.
118. Vilas-Boas V, Vinken M. Hepatotoxicity induced by nanomaterials: mechanisms and in vitro models. Arch Toxicol. 2021;95(1):27–52. https://doi.org/10.1007/s00204-020-02940-x.
119 Tonn JC, et al. Effect of synthetic matrix-metalloproteinase inhibitors on invasive capacity and proliferation of human malignant gliomas in vitro. Int J Cancer J Int Du Cancer. 1999;80(5):764–72. https://doi.org/10.1002/(sici)1097-0215(19990301)80:5%3c764::aid-ijc22%3e3.0.co;2-j.
120. Layfield HJ, et al. Repurposing Cancer Drugs Batimastat and Marimastat to Inhibit the Activity of a Group I Metalloprotease from the Venom of the Western Diamondback Rattlesnake, Crotalus atrox. Toxins (Basel). 2020;12(5):309. https://doi.org/10.3390/toxins12050309.
121. Jimenez RE, et al. Effect of matrix metalloproteinase inhibition on pancreatic cancer invasion and metastasis: an additive strategy for cancer control. Ann Surg. 2000;231(5):644–54. https://doi.org/10.1097/00000658-200005000-00004.
122. Tian K, et al. p53 modeling as a route to mesothelioma patients stratification and novel therapeutic identification. J Transl Med. 2018;16(1):282. https://doi.org/10.1186/s12967-018-1650-0.
123. Bao G, et al. Glycoprotein non-metastaticmelanoma protein B promotes glioma motility and angiogenesis through the Wnt/β-catenin signaling pathway. Exp Biol Med. 2016;241(17):1968–76. https://doi.org/10.1177/1535370216654224.
124. Liu Q, et al. IL-6 promotion of glioblastoma cell invasion and angiogenesis in U251 and T98G cell lines. J Neurooncol. 2010;100(2):165–76. https://doi.org/10.1007/s11060-010-0158-0.
125. Ferreira MT, et al. Cyclooxygenase Inhibition Alters Proliferative, Migratory, and Invasive Properties of Human Glioblastoma Cells In Vitro. Int J Mol Sci. 2021;22(9):4297. https://doi.org/10.3390/ijms22094297.
126 Souza FDC, Ferreira MT, Colquhoun A. Influence of Lipoxygenase Inhibition on Glioblastoma Cell Biology. Int J Mol Sci. 2020;21(21):8395. https://doi.org/10.3390/ijms21218395.
127. Toth M, Sohail A, Fridman R. Assessment of Gelatinases (MMP-2 and MMP-9) by Gelatin Zymography, in Metastasis Research Protocols, M. Dwek, S.A. Brooks, and U. Schumacher, Editors. 2012, Humana Press: Totowa, NJ. p. 121–135. https://doi.org/10.1385/1-59259-136-1:163
128. Torsvik A, et al. U-251 revisited: genetic drift and phenotypic consequences of long-term cultures of glioblastoma cells. Cancer Med. 2014;3(4):812–24. https://doi.org/10.1002/cam4.219.
129. Moore TL, et al. Nanoparticle colloidal stability in cell culture media and impact on cellular interactions. Chem Soc Rev. 2015;44(17):6287–305. https://doi.org/10.1039/C4CS00487F.
130. Ulasov I, et al. Inhibition of MMP14 potentiates the therapeutic effect of temozolomide and radiation in gliomas. Cancer Med. 2013;2(4):457–67. https://doi.org/10.1002/cam4.104.
131. Alves R, et al. Batimastat Induces Cytotoxic and Cytostatic Effects in In Vitro Models of Hematological Tumors. Int J Mol Sci. 2024;25(8):4554. https://doi.org/10.3390/ijms25084554.